Diagnosis of heel pad injuries

Matteoli, Sara; Wilhjelm, Jens E.; T. Torp-Pedersen, Søren

Publication date:
2012

Document Version
Publisher's PDF, also known as Version of record

Technical University of Denmark

Sara Matteoli

Diagnosis of heel pad injuries

PhD thesis, December 2011

DTU Electrical Engineering
Department of Electrical Engineering

Technical University of Denmark
DTU Elektro, Biomedical Group
DK-2800 Kgs. Lyngby
Denmark

Submitted in partial fulfillment of the requirements for the degree of Doctor of Philosophy at the Technical University of Denmark.

We beat prisoners beneath the foot,
we are not crazy enough to hit the whole body
because that can be used against us in court.
(Zimbabwean police officer, [1])

PREFACE

The work presented in this dissertation has been carried out at the section of Biomedical Engineering, Department of Electrical Engineering, Technical University of Denmark from January 2009 to December 2011, and supervised by Prof. Jens E. Wilhjelm from the Department of Electrical Engineering (DTU Elektro), Technical University of Denmark, and Dr. Søren T.Torp-Pedersen from the Parker Institute, Frederiksberg Hospital. This dissertation includes 1 submitted review paper, 1 accepted co-authored journal paper, 6 conference contributions, and 1 journal paper ready-to-be-submitted within February 2012.

This PhD dissertation summarizes three years of research, during which I had the great opportunity to explore the biomechanics field - that has always fascinated me- as well as to enlarge my engineering background bringing my knowledge to higher level.
During these three years I had the possibility to collaborate with different research groups (both in Denmark and in Italy), and to travel through Europe, USA and South America where I had the opportunity to present my work at conferences and workshops. These experiences have been invaluable in terms of confrontations and personal enrichment.
For one year I had the privilege to stay at the Department of Mechanics and Industrial Technologies (DMTI), University of Florence, and conduct research under the supervision of Prof. Andrea Corvi, and the precious help of PhD Antonio Virga.
I also had the pleasure to advise 15 students during their BSc., Msc. and Special projects. The student meetings planned every two weeks had been a very fruitful mean of exchange and I really appreciated all the work done by the students involved in projects related to the heel pad. Their contributions have been important for my research.

Sara Matteoli
Lyngby 31-12-2011

ACKNOWLEDGMENTS

This dissertation represents not only the end of three years of research, but also the end of a stage of my life which has been tough but also full of precious experiences. As it will be too long and not appropriate to describe all of them, I would rather use this opportunity to thank all the people who were always beside me giving a strong shoulder and believing in me during this adventure.

First of all, I am very grateful for the support I have received from my advisor Professor Jens E. Wilhjelm, who has given me the opportunity to come back and work at the department after my thesis. He has always trusted me, demonstrating a fully availability during my research by infusing courage in difficult moments. Thanks for his patience, for the many fruitful discussions about different aspects of the project and life, and for all the suggestions. I really appreciated all his support.
My gratitude extends also to my advisor Dr. Søren T. Torp-Pedersen who has supported and guided me in the medical field. I am also very grateful to Else M. Bartels, Robin Christensen, and Claus Bomhoff from Parker Institute, Frederiksberg Hospital for the fruitful collaboration.

I would like also to thank all the people working with me at the department and the students I supervised. Thanks to all of them for being also tasters of my baking creations. A particular thought to my office-mate Marie, especially for her patience during my Skype-Italian-calls, and for our fruitful conversations.

The collaboration with the Department of Mechanics and Industrial Technologies (DMTI), University of Florence, played a fundamental role for the research. For this reason I would like to express my gratitude to Professor Andrea Corvi who gave me the opportunity to stay for one year at his department and to start the fruitful collaboration with Professor Arturo Natali and his students from the Center of Mechanics of Biological Materials, University of Padua. At this regards I am very thankful towards Chiara Giulia for the industriousness and devotion she put in her work. I really enjoyed working with her, and I hope the collaboration will continue in the future.
A special thank to PhD Antonio Virga from DMTI who has always been a huge reference point during

the last two years. I will never finish to thank him as he had a key-role for the progress of the research. Thanks also to Federica, Altibano, Lorenzo, Teo, Filippo and Carlo for all laughs and chats as well as the fruitful exchange of ideas we had during my staying at DMTI.

Many thanks to all volunteers (from DMTI, DTU, and Parker Institute) who kindly participated to the heel pad investigations. Their availability was crucial for the experimental part of the research. Thanks also to the students who collaborated with me for being a precious source of inspiration.

My gratitude goes also to workshop HPCC System S.r.l. in Florence for building some of the components of the device in a short time, and to both Andrea Meini (from DMTI) and Jens Chr. Jensen (from DTU Elektro) for their availability and efficiency. Many thanks to photographer Ehrhorn & Hummerston for the pictures taken at the department, some of those used in this dissertation.

I would like also to give my warmest thanks to Cecilia and Anna who helped me in settling down in Copenhagen and were close to me even in very difficult moments. I hope our friendship will last forever. Thanks to Michela for all laughs and travels we shared, Francesca for her precious English conversations, and all my Italian friends.

Last but not least my deepest gratitude goes to my family and Marco for their precious support and patience, for always believing in me and my dreams, and for being able to shorten distances.

ABSTRACT

The biomechanics of *in vivo* heel pads has been investigated for more than 30 years, but unfortunately numerical results from the many individual investigators cannot be compared due to the different methodologies used, and the sometimes modest number of subjects investigated. The overall aim of the present thesis is to obtain a thorough understanding of the mechanical properties of *in vivo* human heel pad by studying the anatomical and physiological structure of healthy and diseased tissue, and to develop quantitative methods for diagnosing injuries.

A compression device was built in order to record load-displacement curves from in vivo heel pads. To ensure applicability also for pathological feet, the device uses force levels lower than those needed to reproduce the physiological conditions of walking. One hundred twenty seven healthy volunteers were enrolled for compression tests and ultrasound investigation of heel pad thickness, so that three biomechanical parameters could be investigated: Heel Pad Compressibility Index (HPCI), Elastic modulus (E), and Energy Dissipation Ratio (EDR). Statistical analysis, based on linear regression models, showed that intrinsic subject factors such as age, weight, height and gender did influence HPCI, E and EDR, and that there was a significant statistically difference between males and females in E, but not in EDR and HPCI.

In order to attempt a verification of the method used above, compression tests and ultrasound investigations on *artificial* heel pad models were conducted in two additional studies. In vivo experimental tests were used to validate a numerical 3D subject-specific heel pad model subjected to an external compression, and to further investigate the visco-elastic nature of the heel pad. Ultrasound distance measurements were compared with corresponding distance measurements with MRI and true values in order to assess its reliability in heel pad thickness measurements. The latter study confirmed the need to investigate the real speed of sound for the heel pad tissues, in order to obtain realistic measurements when dealing with human heel pad.

RESUMÈ

Den humane hælpudes biomekanik er blevet undersøgt i mere end 30 år, men desværre er det ikke muligt at sammenligne de kvantitative resultater fra de mange individuelle undersøgelser på grund af de forskellige metoder, som er blevet benyttet, og det begrænsede antal testpersoner. Nærværende afhandlings hovedmål er at opnå et indgående kendskab til de mekaniske egenskaber af *in vivo* hælpuder ved at undersøge den anatomiske og den fysiologiske struktur på rask og sygt væv og at udvikle kvantitative metoder til at diagnostisere skader på hælpuden.

I projektet er et stempelbaseret kompressionsapparat blevet konstrueret for at kunne registrere sammenhængen mellem sammenpresning og stempelkraft fra *in vivo* hælpuder. For at sikre anvendelighed på syge hæle bruger apparatet kraftpåvirkningsniveauer, som er lavere end de, som skal bruges for at gengive de fysiologiske betingelser ved normal gang. 127 raske frivillige testpersoner deltog i kompressionstest og måling af hælpudens tykkelse (diagnostisk ultralyd) således at tre biomekaniske parametre kunne undersøgs: Heel Pad Compressibility Index (HPCI), Elastic modulus E, og Engergy Dissipation Ratio (EDR). Statistiske analyser, som er baseret på lineære regressionsmodeller viser, at faktorer som alder, vægt, højde og køn påvirker HPCI, E og EDR og at der var en signifikant forskel mellem kvinder og mænd i E, men ikke i EDR og HPCI.

Med henblik på at vurdere ovennævnte metoder blev kompressionstest og ultralydsundersøger på kunstige hælpuder udført i to supplerende undersøgelser. *In vivo* eksperimentelle undersøgelser blev benyttet til at underbygge en numerisk 3D person-specific hælpudemodel, som blev udsat for et ydre tryk og for at undersøge hælpudens visko-elasticitet yderligere. Afstandsmålinger med ultralyd blev sammenlignet med tilsvarende afstandsmålinger med MRI og disse blev holdt op mod sande værdier med henblik på at vurdere pålideligheden af tykkelsesmålinger med billeddiagnostiske metoder.

ABBREVIATION

US	= Ultrasound
MRI	= Magnetic Resonance Imaging
CT	= Computed Tomography
UHPT	= Unloaded Heel Pad Thickness
LHPT	= Loaded Heel Pad Thickness
HPCI	= Heel Pad Compressibility Index
BMI	= Body Mass Index
S	= Stiffness
E	= Elastic Modulus
EDR	= Energy Dissipation Ratio
SD	= Standard Deviation
3D	= Three Dimensional
LVDT	= Linear Variable Displacement Transducer
TE	= Echo Time
TR	= Relaxation Time
TA	= Acquisition Time
PVA	= PolyVinyl Alcohol
DTU	= Technical University of Denmark
DMTI	= Department of Mechanics and Industrial Technologies

Contents

CHAPTER

ONE

INTRODUCTION

The overall aim of the present research is to obtain a thorough understanding of the mechanical properties of the *in vivo* human heel pad by studying the anatomical and physiological structure of healthy and diseased tissue, and to develop quantitative methods for diagnosing injuries.

Damage of the intricate septation of the heel pad is a severe condition which implies the loss of the shock absorbing feature of the heel pad, causing great pain for the subject, when trying to stand and walk. The structural change of the heel pad might be a consequence of severe trauma such as fall accidents [2], falanga torture [3], or due to a gradual deterioration with age [2]. Especially for falanga torture - which consists in repeatedly beating the soles of the feet including the heel pads leaving relatively few objective findings despite the severe chronic physical disability - there is a need for validated examination methods to be used for medico-legal purposes (such as dealing with refugees, alleged torture victims, insurance cases, etc.) and as important tools in the prevention of torture. Indeed, the aetiology and pathogenesis of the chronic pain and disability seen after falanga torture is still not clear [4], and the positive confirmation of alleged act of torture is still difficult for the medico-legal investigators especially in those cases which are assessed several months after the trauma [5]. Furthermore, knowledge of the mechanical properties of the tissue may be used in tools for screening patients for the purpose of preventing further complications in the foot (*e.g.* ulcerations may be prevented in diabetics [6]).

Palpation is presently the only method for diagnosing falanga torture, in which the physician tries to assess how the heel bone (calcaneus) is felt under the skin [4, 7, 8]. Such examination is subjective and depends on the experience of the individual investigator, as already shown in previous studies [4, 7]. Moreover, results obtained by palpation are not completely reliable due to a number of confounding factors. One of the most important confounding factor is the natural variation of skin-to-calcaneus distance (heel pad thickness), which highly influences the elastic properties of the heel pad [9, 10]. Ultrasound is the clinical imaging technique used most for heel pad thickness investigations being cheap, portable, fast and completely safe. However, it is strongly operator-dependent [12], and the unknown speed of sound in a given soft tissue gives high uncertainty to the results.

Therefore, there is a need of developing an accurate, reliable, robust, non-invasive equipment that can be used to investigate changes in the architecture of the heel pad tissue by describing its behavior in a numerical and objective way [4, 7].

The heel pad was first investigated by Steinbach and Russell [11] in 1964 to diagnose acromegaly. For more than 25 years the thickness of *in vivo* heel pads and its mechanical properties (Heel Pad Compressibility Index, Elastic modulus, Energy Dissipation Ratio, etc) have been investigated in healthy individuals as well as in subjects with diabetes, obesity, heel pain, acromegaly and calcaneal fractures. Unfortunately, studies investigating the same biomechanical property of the heel pad differed both in terms of method applied and population studied, and it is not feasible to compare the numerical results.

The majority of this PhD project focuses on the development and the application of a compression device for investigating the mechanical properties of the heel pad (study I). Since patients (especially survivors of falanga torture) are not readily available for recording experimental data, physical models and computer heel pad models might be needed as well (study II and III). The heel pad models would also allow assessment of performance of the equipment to be developed. In particular, for the physical models PVA-cryogel is used for mimicking the artificial heel pad tissue, as its reliability has been proved by mechanical compression test [7]. In order to investigate whether there are any differences between healthy and diseased heel pads when dealing with their biomechanics, it is necessary to establish first a ”normal” range of such biomechanical parameters. Thus, the equipment developed will first be applied on a group of healthy volunteers, so that a bank of normal data can be collected.

The flow diagram in Figure 1.1 illustrates the main studies conducted during the three years of research. The human heel pad is the key-point which leads to three directions (each one identified by a number and on a specific color in Figure 1.1).

This dissertation is divided into four parts (chapters) as follows:

Chapter 2 describes both the anatomy and biomechanics of healthy and injured heel pads as well as the clinical imaging techniques used for diagnosis. Much of the knowledge, used to deeply understand the behavior under compression of such a complicated structure, derives from a literature study done throughout books and articles.

Chapter 3 presents in details the development of the compression device intended to be a possible clinical device for future investigation on survivors of falanga torture. It also describes all the procedures applied for the heel pad investigations as well as the results achieved. This part of the project was performed in collaboration with PhD Antonio Virga from the Department of Mechanics and Industrial Technologies, University of Florence, and BSc. students Maja M. Madsen and Sabrina U. Hjørringgaard.

Chapter 4 presents a combined research which involves experimental tests carried on an *in vivo* human heel pad, and numerical modeling and simulations. The research was carried on thanks to the fruitful collaboration with the Center of Mechanics of Biological Materials, University of Padua, as well as PhD

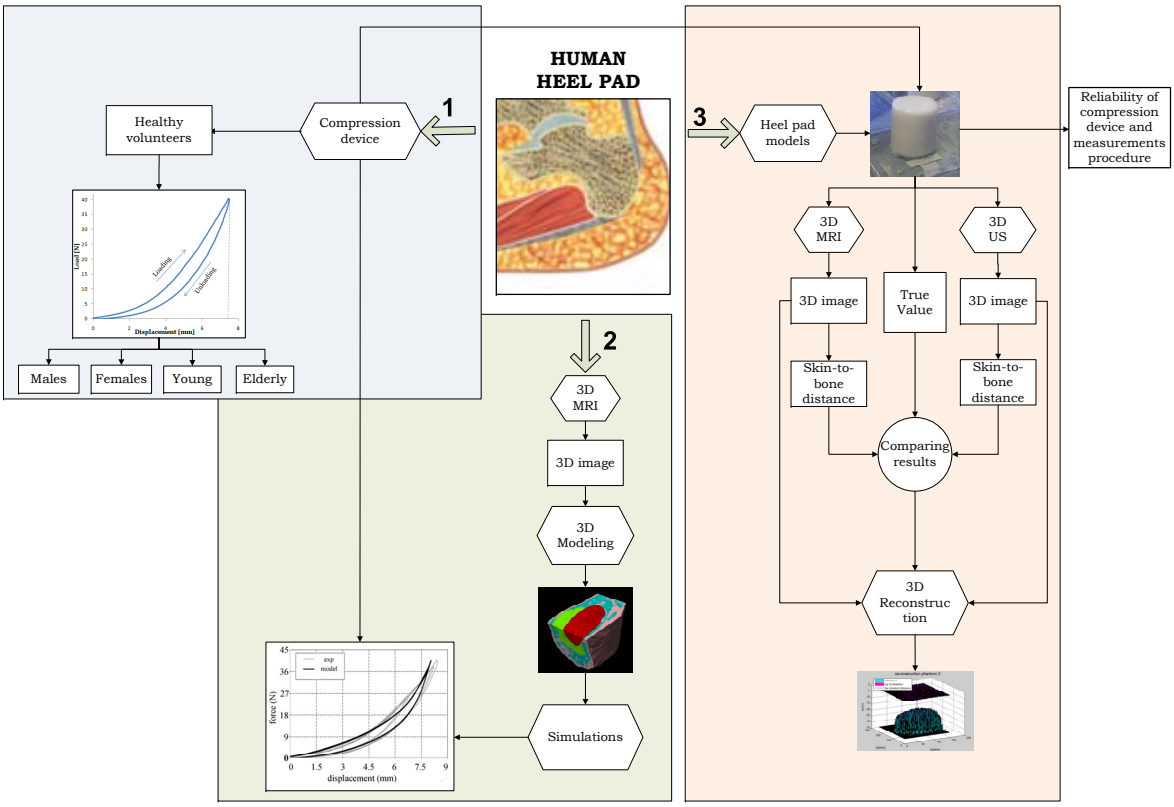

Figure 1.1: Research carried out during the PhD. The human heel pad is the key-point which leads to different studies. The numbers on the grey thick arrows indicate the the order on which the studies are described in this dissertation.

Antonio Virga and BSc. student Nadège Corbin.

Chapter 5 presents the preliminary research which aims to investigate the reliability of the clinical imaging modalities used nowadays for heel pad thickness measurements. The software development work and data analyses were mainly performed by BSc. student Nadège Corbin during her summer internship at the Department of Electrical Engineering, DTU.

The contributions to the field of the heel pad biomechanics developed during my PhD project cover one submitted journal review, one accepted co-authored paper, and six conference contributions (some of them published in proceeding books). All conference contributions as well as journal papers are included in Appendix E. The contributions are listed as follows:

Journal papers

Matteoli S, Wilhjelm JE, Bartels ME, Christensen R, Torp-Pedersen ST. *Intrinsic factors influencing biomechanical measures of in vivo human heel pad: A systematic review.* [sent to the editor of

Journal of Applied Biomechanics on the 28^{th} November 2011]

Matteoli S, Fontanella CG, Carnel EL, Wilhjelm JE, Virga A, Corbin N, Corvi A, Natali AN. *Investigation on the visco-elastic behavior of a human healthy heel pad:* in vivo *compression data compared to numerical results.* [to be submitted to Computer Methods in Biomechanics and Biomedical Engineering within February 2012]

Co-authored journal papers

Fontanella CG, Matteoli S, Carnel EL, Wilhjelm JE, Virga A, Corvi A, Natali AN. *Investigation on the load-deformation curves of a human healthy heel pad: in vivo compression data compared to numerical results.* Medical Engineering & Physics [available online from the 19^{th} January 2012]

Abstract and Conference contributions

Matteoli S, Madsen MM, Virga A, Wilhjelm JE, Torp-Pedersen ST. *Investigation on* in vivo *human heel pad thickness.*, European Society of Biomechanics, 2012, Lisbon, Portugal. [abstract]

Matteoli S, Corbin N, Wilhjelm JE, Torp-Pedersen ST. *On the comparison between MRI and US imaging for thickness measurements.*, Proceedings of International Tissue Elasticity Conference, 2011, Arlington, Texas, USA. [oral contribution]

Matteoli S, Wilhjelm JE, Virga A, Corvi A, Torp-Pedersen ST. *Initial studies on the variations of load-displacements curves of in vivo human healthy heel pads.* Proceedings of 15. Nordic-Baltic Conference on Biomedical Engineering and Medical Physics, 2011, Aalborg, Denmark. [oral contribution]

Matteoli S, Wilhjelm JE, Corvi A, Torp-Pedersen ST. *On heel pad modeling.* Proceedings of Second National Congress of Bioengineering, 2010, Turin, Italy. [poster contribution]

Matteoli S, Corvi A, Wilhjelm JE. *Modeling the human heel pad.* Simpleware's Users Meeting, 2010, Solihull, UK. [abstract for oral contribution]

Matteoli S, Wilhjelm JE, Torp-Pedersen ST. *Some of the factors influencing the Heel Pad Compressibility Index (HPCI): a literature search.* Proceedings of International Conference on the Ultrasonic Measurement and Imaging of Tissue Elasticity, 2009, Vlissingen, Holland. [poster contribution]

CHAPTER

TWO

HUMAN HEEL PAD

This chapter gives an overview of the anatomy and biomechanics of the human heel pad, as well as the injuries which affect its functionality and the clinical imaging modalities used for diagnosis.

2.1 Anatomy of healthy heel pad

The human **heel fat pad**, also known as *corpus adiposum*, is a portion of the plantar foot tissues located between the heel bone (calcaneus) and the skin on the rear part of the foot, as shown in Figure 2.1. It has a high specialized and unique anatomic configuration which works as a shock-absorber able to catch and dampen the impact of the weight on the foot during locomotion and standing. Indeed, the heel fat pad consists of a very complex structure made of neuronal, vascular, fibrous and elastic components which are intertwined with fat cells [13]. The thickness of the normal heel pad, defined as the shortest distance between the heel skin and the calcaneus, as shown in Figure 2.2, ranges between 14.4 mm and 24.5 mm with an average value of 18 mm [14]. In this dissertation the term heel pad will indicate the whole made of heel fat pad and skin.

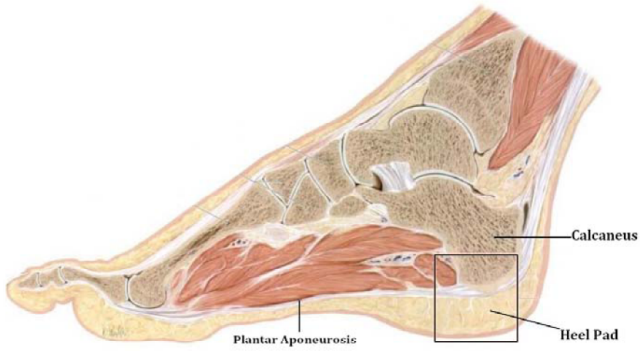

Figure 2.1: Anatomical representation of the foot: lateral section. From [15].

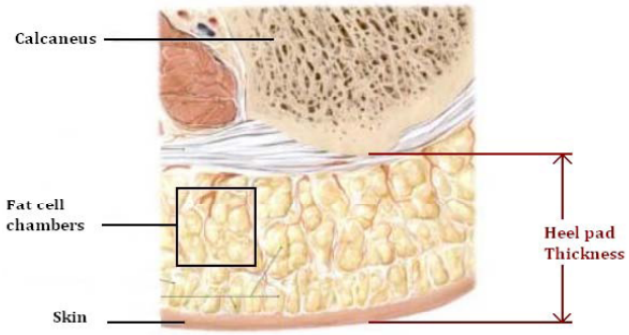

Figure 2.2: Close up image of the heel fat pad showing its peculiar structure. From [15].

The adipose tissue of the heel pad, due to the compressive stresses during locomotion and standing, has very strong connective tissue strands that tether the skin and limit the displacement of the fat, thus augmenting rather than impeding its resilient cushioning effect [16].

The skin overlying the heel pad consists of a very thick epidermis which is characterized by numerous ridges on its underside that extend into the dermis [16]. The dermis consists of two layers: a papillary dermis which contains elastic (5-10%) and collagen fibres (90-95%), and a reticular dermis which contains substantially more elastic tissue (40-50%) [17]. Both layers have the elastic and collagen fibers randomly intertwined with a higher concentration of collagen found in the periphery of these bundles [17]. The dermis is then bound by thick fibrous strands (or septa) which enclose compartments of adipose tissue [16]. Such compartments were found [14] to be spherical to ellipsoidal in shape, with a dimension in diameter which varied between 0.6 to 10 mm. The strands merge with a horizontal septum - composed of transverse and longitudinal bundles of collagen and elastic fibres in almost the same amount- which divides the subcutis into two strata: a superficial stratum and a deep stratum [16]. The superficial subcutis stratum is made of compartments of adipose tissue limited by fibrous strands. The individual compartments (or chambers) are divided into smaller compartments by several septa containing a large amount of elastic septa [16]. The deep stratum is a much thicker subcutaneous layer and it is separated from the muscular compartment by the plantar aponeurosis located just superficial to the calcaneus. Like the superficial subcutis stratum, the tissue components of the deep stratum are divided into connective septa which contain slightly more elastic fibers (50-60%) than collagen fibers [17], and adipose compartments. Figure 2.3 illustrates a section of the sole of the foot from the lateral margin showing the septal framework and the structure of the different layers [16].

The architecture of the heel pad shows a very characteristic honeycomb configuration with a complete apposition of adjacent cell walls which results in apparent absence of intercellular spaces [13], as visible in Figure 2.4. Individual spherical fat cells, so-called *adypocites* with diameters ranging between 100 and 200 μm [18], and fat globules are sealed by delicate membranes. It is indeed such honeycomb configuration which combines elastic fibres, collagen fibres and adipose tissue, that makes the heel pad be

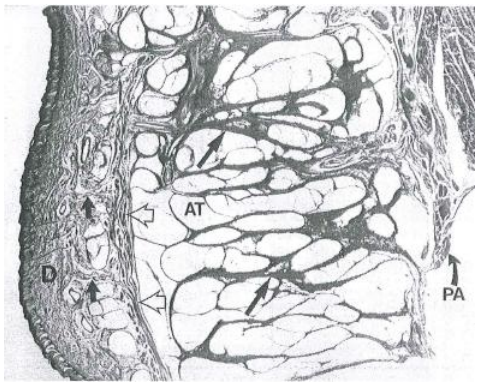

Figure 2.3: Thick section of the sole of the foot from the lateral margin showing the septal framework and the structure of the different layers. The long black arrows indicate the broad septa located in the subcutis that surround the adipose tissue (AT). The subcutis is divided into superficial and deep strata by a fibrous septum (white arrows). The dermis (D) consists of several fibrous strands (short black arrows). From [16]

such a delicate and peculiar anatomical structure able to resist compressive loads. Specifically, collagen fibres provide rigid constrains limiting the deformation, thus have mainly a protective role, whereas elastic fibres due to their reversible extendibility maintain a continuous and smoothly graded deformation of the adipose tissue when subjected to compressive forces [16]. The energy of recoil inherent in the elastic fibres may facilitate the return of the tissue compartments to the normal resting state [16]. That is why elastic fibres are found more in the papillary dermis and in the septal framework of the subcutis, which are repeatedly subjected to shearing and compressive forces during locomotion and standing [16].

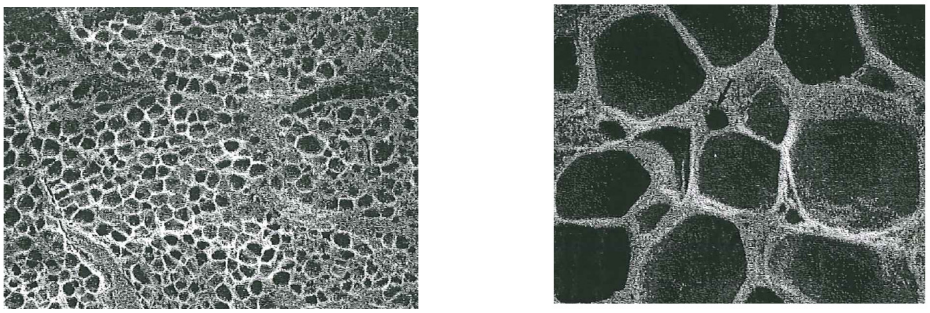

Figure 2.4: Heel pad section showing the septal walls and closed fat cell chambers (on the left). Detail of fat cell chambers (on the right). From [13].

The heel fat pad can be seen as anatomically divided into a superficial microchambers and a deep macrochambers layers, as shown in Figure 2.5. The fibrous septa within the human heel fat pad contain predominantly elastic fibers in the thin microchambers layer and roughly an equal amount of collagen and

elastic fibers in the thick macrochambers layer [19]. Thus different biomechanical behaviors between the two subcutaneous compartments can be anticipated based on the different tissue compositions [19].

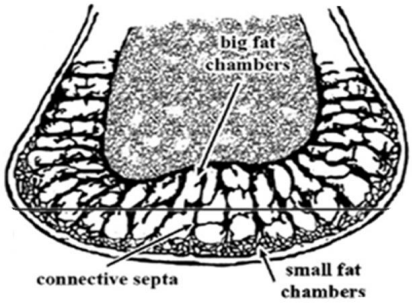

Figure 2.5: Transversal section of the heel pad: microchambers are close to the skin, while macro chambers are close to the bone. From [110]

The fibrous septa extend from the skin to the calcaneal perichondrium following a very complex orientation. Near the sole of the foot the septa are almost transverse, then they arrange spirally among the fat cells extending from the subcutaneous tissue to the calcaneus [2]. The septa are usually U-shaped, with the open end of the U pointing toward the calcaneus [2], as shown in Figure 2.6.

Figure 2.6: Spiral orientation of septa. From [20]

The orientation of both septa and fat chambers play a fundamental role in the behavior of the heel fat pad during weight-bearing. In fact, during the weight-bearing the calcaneus treads deeper, while the fat pad flattens out toward the side and at the same tome bulges laterally [20]. In a non weight-bearing state the septa stands rather vertically to the skin, whereas in weight-bearing the chambers are not compressed despite the reduction of the distance skin-calcaneus [20]. This phenomenon is illustrated in Figure 2.7. The pressure inside the fat pad is distributed irregularly in the center of the fat pad and below the deepest point of the calcaneus it reaches the highest level [20]. Then the pressure decreases towards the medial edge.
The honeycomb configuration indicates that despite what a water cushion might do, a flow off of fat cannot occur in the heel fat pad, and that high fluctuations of pressure must be maintained in weight-bearing state [20].

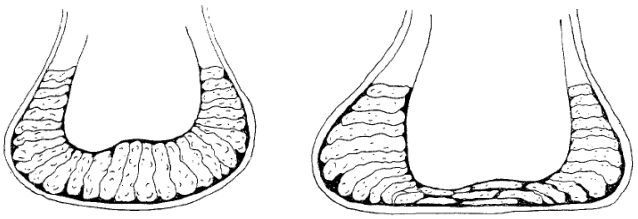

Figure 2.7: Illustrations of the coronal section of a normal heel pad. Non weight-bearing (on the left). Weight-bearing (on the right). From [21].

The mechanical integrity of the heel fat pad as a whole depends on the integrity of the septa that enclose each independent unit within this closed-cell structure [13]. However neuronal and vascular supply play also an important role in maintaining the correct function of the heel fat pad.

The principle of springs in the connective tissue is viewed in the arrangement of the elastic fibres [22]. Elastic fibres are numerous around the vessels, so when the tissue is compressed it can bounce back as soon as the load is removed [22]. An adequate blood supply and fast restoration of the blood flow when the decompression occurs, are at the basis of the biomechanics of the heel fat pad [22].
Histological sections of the heel fat pad made by [13] indicate that the vascular trees run in the septa and eventually supply the dermis, the blood supply to the fat itself seems sparse, and the capillaries are present in association with free nerve endings in the fat, as well as independently without nerves. Dissection of the heel region made by [14] demonstrated that the upper dermis was well vascularized by a subpapillary plexus (Figure 2.8, on the left), and that the heel pad was vascularized by a subdermal plexus and periosteal plexus with vessels traveling between the two within fibrous septa. These septa created isolated compartments containing avascular fat [14], as shown in Figure 2.8, on the right.
The heel fat pad receives its blood supply from the anterior tibial, posterior tibial and peroneal arteries [13]. The vessels travel in the septa to supply the skin, and the fat pad has its own blood supply made of capillaries lying free within the fat [13]. In the heel fat pad everything is built towards elasticity and prepared for a quick recover of the tissue that has been compressed.

The heel fat pad contains also several innervations, as described by [13]. Anatomic dissections shows that the nerves penetrate the fibrous septa between the fat globules along with the vascular bundles [13]. The nerves are quite large as they enter the deep surface of the fat pad [13]. As they penetrate deeper into the fat pad toward the dermis the nerves become smaller in diameter [13]. Terminal branches exist just under the dermis and within the dermis [13]. Vater-Pacini nerve corpuscles are located in both superficial and deep layers of the heel fat pad, but they are not seen in the dermis [13].

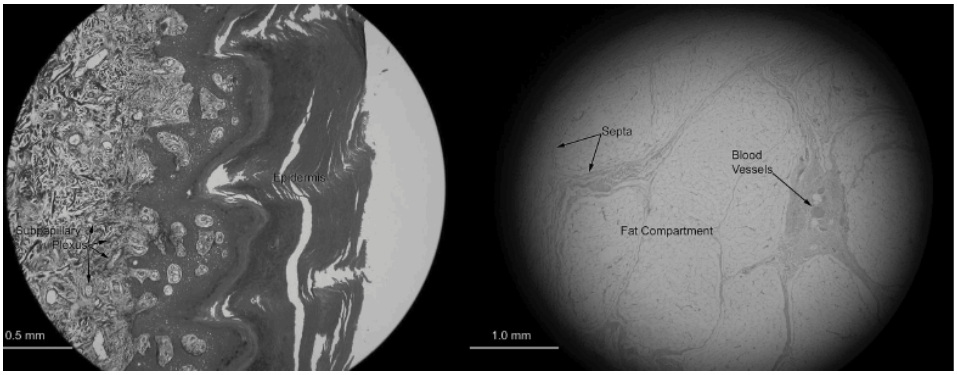

Figure 2.8: The upper dermis is well vascularized by a subpapillary plexus and is protected from external trauma by a thick layer of dermis (on the left). The fibrous septa create avascular compartments of fat within the subcutaneous tissue (on the right). From [14]

2.2 Anatomy of diseased and injured heel pads

The whole purpose of the heel pad is to sustain strain and pressure through fat chambers and elastic tissue. However, the heel pad may lose its compressibility by rupture of the fibrous septa (due to a severe trauma) or thinning of the fat pad [23]. Moreover, the heel fat pat shows a gradual deterioration with age [2]. A gradual loss of collagen, a decrease in elastic fibrous tissue as well as a decrease of water content are the most constant finding related to the increase of age [2]. A loss of heel pad substance, whether due to atrophy or a previous injury, will not enable the heel pad to respond to stress or persistent pressure [23]. Whereas in other parts of the body there is a remodeling of the tissue and restoration of the original structure even after a severe trauma, it does not happen for the heel pad [2, 23]. Once the trauma involves the breaking of the honeycomb structure, lateral tearing, compression of the elastic adipose tissue and bloody supply [2], the heel pad will forever lose its natural defence against any dynamic pressure [23]. This is a crucial point when dealing with injured heel pads.

Atrophic heel pad

The heel fat atrophy is a well known clinical entity which is often associated with senescence, peripheral neuropathy, diabetes, dysvascular diseases, and collagen disorders [17].
The histology and the histomorphometric of atrophic heel fat pads were investigated by [17] and [13]. The adypocites in the superficial subcutaneous layers were found 25% smaller in mean cell area than normal heel fat pads, and 10% smaller in mean maximum diameter [17]. In the deep subcutaneous layers instead the adypocites were found 45% smaller in mean cell area and 25% smaller in maximum diameter than in normal heel fat pads [17]. Furthermore, in atrophic heels the epidermal reticular layer was found 25% thicker than in normals, but containing septa whose ratio of collagen to elastic tissue did not differ from

that of normals [13]. The overall decrease in volume in the atrophic heels resulted in a thinner superficial layer [13]. Septa in the superficial and deep subcutaneous layers were found up to be 25% thicker than in normals and to contain higher percentage of elastic tissue (60-70%) which appeared fragmented in some cases [13]. [24] reported also a significant change in the composition of satured fatty acids in heels of patients with rheumatoid arthritis. This would lead to an increased fat viscosity, which decreases the shock absorbency of the heel pad during walking and/or standing. This factor can be seen as another cause of degeneration of the septal system with resulting heel fat pad atrophy [24]. Figure 2.11 shows the difference between a normal (on the left), and dysvascular senescent heel fat pad (on the right). In the normal case the fat cells are round and very well surrounded by fibroelastic tissue, whereas there are some dark stains and fragmented fibroelastic tissue (indicated by the black arrows) in the dysvascular foot.

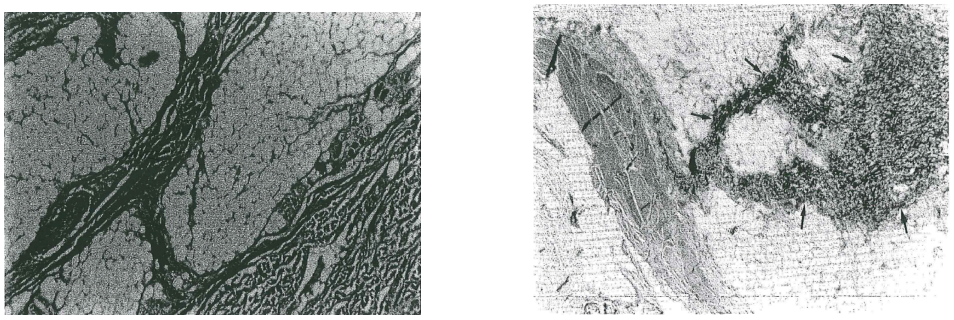

Figure 2.9: Comparison between a normal heel fat pad (on the left), and a dysvascular senescent heel fat pad (on the right). From [13].

Pain and burning in the subcutaneous region of the heel after prolonged standing or walking are common discomforts in soreness heels. These symptoms are associated with degenerative changes in the calcaneal area. As described in the previous section, a normal heel pad shows a smooth undersurface of the calcaneus and, beneath the bone, an area of dense fibrous adipose tissue with regular and parallel strands and chambers similar in size [2]. A soreness heel instead presents bony irregularity, less dense layers of elastic adipose tissue, thinner fibrous strands (often irregular and broken in outline), not parallel and sometimes confluent strands [2]. Such changes are visible after 40 years, in case of obesity of after severe trauma [2].

Diabetic heel pad

As already mentioned before, collagen septa in diabetic heel fat pads are found to be thicker and the adipose cells smaller than in normal heel fat pads [17, 25]. It is also known that diabetes is associated with an increase of fragmentation [13]. These changes indicate that diabetes may affect the microscopic and macroscopic composition of the plantar soft tissues, making them more vulnerable to mechanical stresses which would lead to ulcerations [25]. Indeed, the diabetic fat pad is reported to be less elastic

and less able to distribute pressure, leading to an impaired cushioning effect [25]. The higher energy dissipated in diabetic heel pad during weight-bearing might increase the risk of ulceration [25]. In fact, it is not senseless to think that a stiffer tissue would be more fragile and more prone to damage by an excessive force than an healthy elastic tissue [26]. The stiffening and thinning of diabetic heel pad might be also explained by the skin condition. In fact, most diabetics have a dry skin due to problem of glucose regulation which might make the tissue harder and more brittle, and the skin less flexible [27].

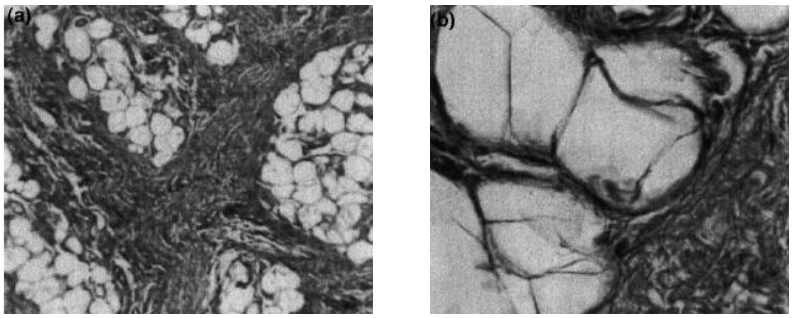

Figure 2.10: Histology of the fat pad belonging to a neuropathic diabetic foot. Disorganized fat globules separated by coarse septa fat pad (on the left). Misshapen fat cells compressed by fibrosis (on the right). From [28].

Heel pain and sport injuries

The risk of suffering disorders of the soft tissue of the foot is one of the few adverse effects of having a physically active lifestyle. Engagement in a physically challenging sport, demanding and repetitive physical activity or high-impact exercising has particularly been linked to heel pain due to cumulative microtrauma caused by cyclical overuse. Indeed, sports that involve running and jumping place repetitive stresses on the heel pad resulting in a slow degeneration or displacement of the heel pad which may cause a greater degree of the forces of impact transmitted to the calcaneus.

Fat pad inflammation associated with edematous changes in heel pad has been reported to caused by sport injuries in young persons [29, 30], even thought the authors did not report the kind of physical activity nor the specific age groups. MR investigations demonstrated that there was significant increase of calcaneal marrow edema in young healthy runners [31, 32]. Biological adaption might occur in subjects with overuse injuries [33]. In everyday running activity the heel pad acts as a fluid filled cushion where the volume has to remain constant with the increase of stresses. Microtrauma would lead the biological response of increasing the heel pad thickness in order to reduce the maximum impact force and increase the deceleration time [34]. The inflammatory edema may be an indication of the architectural changes of the heel pad due to a decrease of the shock absorbency capability at the heel strike [35]. The decrease in stiffness of the heel pad might be due to a breakdown in the balance between fatigue damage and routine repair [33, 35].

Painful heel pad is often confused with plantar fasciitis, even though it is characterized by tenderness of the posterior weight-bearing portion of the calcaneus, in contrast to the more anterior region associated with fasciitis [36].

Falanga torture

Falanga torture is one the most traumatic and tragic way to get the heel pad injured. Falanga torture is a corporal punishment which consists of beating repetitively the soles of feet - especially the heel and the ball of the foot - with objects like sticks and canes. This punishment, originated in the Middle-East and nowadays spread worldwide, represents a prolonged repetitive high-energy injury to the heel [3].

Figure 2.11: Falanga torture. Painting by the Kurdish artist Arif Serving [37].

The degree of injury depends on a number of obvious factors: the instrument used, the force that is applied (*e.g.* whipping versus beating), and the length of time that force is applied [1]. The effects related to this kind of torture are very difficult to identify medically, even though the permanent damage of the soft tissue would lead to chronic pain and impaired gait [38, 39], with both walking speed and walking distance being reduced. Typically the victim will only be able to walk a short distance before the increasing pain will stop this activity [1]. Obviously, this has profound impact on future life of the survivor of the torture. The immediate acute signs, such as tissue swelling and internal hemorrhage, disappear spontaneously after one-two weeks, once the hemorrhage resolves [3, 40] leaving very few clinical signs. The most severe complication of falanga torture is the closed compartment syndrome, which can cause muscle necrosis, vascular obstruction or gangrene of the distal portion of the foot or toes [38]. Further, the connective tissue strands connecting the skin to the calcaneus are torn and the cushioning effect is lost for ever [38]. Clinical examinations based on palpation [8, 39] reported reduced elasticity in the heel pads, loosening of the skin, thickened and uneven plantar fascia (aponeurosis). The prevalence of clinical finding after falanga, however, is unknown [40]. Imaging modalities such as MRI, ultrasound and bone scintigraphy

were also used for clinical diagnosis and documentation of falanga torture [3, 5, 41]. Those investigations showed morphological changes involving the full length of plantar fascia which were not seen in normal heel pads [3, 41].
However, the aetiology and pathogenesis of the chronic pain and disability seen after falanga torture is still not clear [4], and the positive confirmation of alleged act of torture is still difficult for the medico-legal investigators especially in those cases which are assessed several months after the trauma [5].

2.3 Biomechanics of healthy and unhealthy heel pads

The heel pad is the most distal part of the human locomotion system, hence it is subjected to ground reaction forces during locomotion [42]. Biomechanically the heel pad acts as an efficient shock absorber to attenuate the peak of dynamic forces and to dampen the vibrations during the gait [43]. The honeycomb arrangement of the fibrous-elastic tissue in the plantar fat has a definite significance, regardless of the explanation of mechanical law [22]. In fact, the strong accumulation and the branching of the connective tissue is more present on the lateral side (where the pressure is applied) than the medial side.
The elastic adipose tissue of the heel pad has the characteristic of resuming its original shape as soon as the excessive pressure has been removed [2]. This unique function of sustaining hydraulic pressure, is obtained by its highly specialized architecture, made of macro and micro chambers, as described in section 2.1, that facilitates the transmission of the weight to the ground during the gait cycle and protects the rear foot and lower extremity at the initiation of the support phase during the locomotion [42]. Hsu et al. [19] reported that the macrochambers layer deform immediately after compression and rebound quickly once loading is released. Under the same loading condition, the microchambers layer deform faster, but the change in thickness is much less than the macrochambers layer [19]. These findings were considered to be associated with the difference in stiffness between the two layers (microchambers layer 10 times stiffer than macrochambers layer), and to the role of such layers [19]. Indeed, the macrochambers layer which contains approximately an equal amount of collagen and elastic fibers, plays a major role in the heel-pad tissue resiliency and may be responsible for the cushioning effect in the heel pad during walking [19]. The microchambers layer - containing predominantly elastic fibers - seems to function as an inherent heel cup that maintains most of the macrochambers layer beneath the calcaneus and prevents excessive macrochambers layer deformation [19].

The heel pad shows non-linear viscous-elastic characteristics, like most of of the human body soft tissues does. The term ”viscous” implies the resistance of the tissue to be deformed when subjected to an external force, whereas the term ”elastic” indicates the property of the tissue to return to the original shape once the force is removed. In the heel pad the viscous and elastic features correspond to the fat cells and septa, respectively. When an external compression is applied to the heel pad and then is removed, a typical load-displacement curve (hysteresis) is obtained, as shown in Figure 2.12.

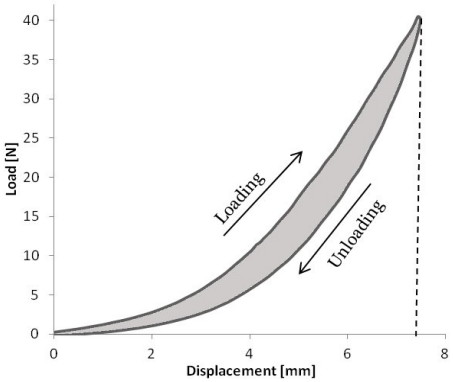

Figure 2.12: Typical load-displacement curve of an *in vivo* heel pad.

From a clinical standpoint, one of the most important properties of viscoelastic materials is the ability to reduce the magnitude of impact forces. Such reduction is achieved in two different ways: by extending the time course of the impact event (with respect to the impact force which occurs during the heel-strike) and by absorbing energy [44]. The **Energy Dissipation Ratio** (EDR) is one of the mechanical properties of the heel pad measuring the quantity of energy lost by viscous friction within the tissue. The greater the EDR, the more energy is absorbed and the more resilient the heel pad is.
With reference to the Figure 2.12, the area under the loading curve, A_l, represents the energy used to compress the heel pad, while the area under the unloading curve, A_u, shows the energy returned during the elastic restitution of the heel pad [45]. The area inside the loop represents the energy absorbed by the heel pad (converted to heat) during the impact. The EDR in percentage can be expressed as [46]:

$$EDR = \frac{A_l - A_u}{A_l} \tag{2.1}$$

A simple representation of the heel pad and the calcaneus, with or without the application of a load, is shown in Figure 2.13. The Unloaded Heel Pad Thickness (UHPT) is defined as the shortest distance between the lowest part of the plantar tuberosity of the calcaneus and the skin (unloaded condition, Figure 2.13, (a)). The Loaded Heel Pad Thickness (LHPT) is defined the same way, but with a load F applied (loaded condition, Figure 2.13, (b)).

The **Heel Pad Compressibility Index** (HPCI), expressed in percentage, is defined as the ratio of the heel pad thickness in loaded conditions to unloaded conditions. It is expressed as [26, 43, 43, 47, 48, 49, 50, 51, 52]:

$$HPCI = \frac{LHPT}{UHPT} * 100 \tag{2.2}$$

HPCI shows the ability of the heel pad to be compressed, thus an index value approaching 100% means a lack of elasticity [48, 49]. Tong et al. [26] considered HPCI a more significant parameter than UHPT when investigating the health of the heel pad, as they found a significant difference in HPCI between heel pain subjects and controls, whereas the thickness was similar between those groups.

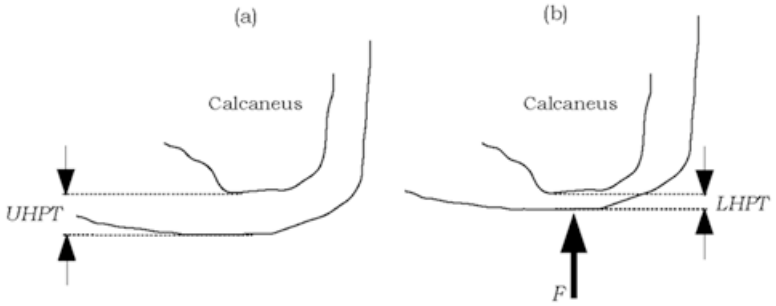

Figure 2.13: Schematic illustration of unloaded (a) and loaded (b) heel pad.

The **Displacement** (δ) indicates the difference between the initial position and the final position of the heel pad when a load (Fmax) is applied. Using the notation illustrated in Figure 2.13, the displacement can be expressed as:

$$\delta = LHPT - UHPT \tag{2.3}$$

In principle, the mechanical properties of the heel pad, like those for other human soft tissues, can be entirely described by load-displacement curves. However, the load-displacement characteristics depend not only on the behavior of the internal tissues, but also on geometry and loading protocol [53]. It is known that UHPT is highly variable even within an healthy population, and this may affect the load-displacement curves. Indeed, as show in Figure 2.14 a thick layer exhibits lower peak stresses in contrast to a thin layer when considering the same area of compression [13].

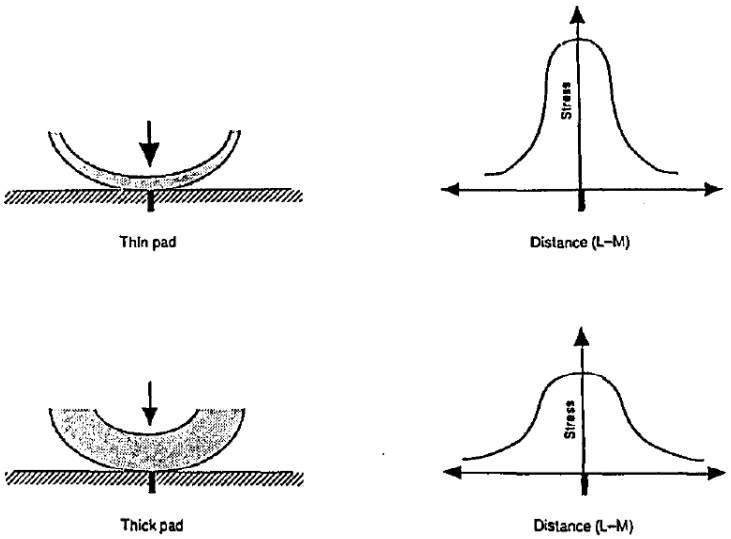

Figure 2.14: Effect of thickness on loading. From [21]

As it is not possible to control such geometric boundary in a clinical setting, it is reasonable to use a

geometry-independent method for quantifying the mechanical properties of the heel pad [53]. It has been to express such properties in terms of stress-strain [54]. Specifically, stress (σ) represents the normalized force (force per unit of area), while strain (ε) indicates the normalized displacement (change from the original shape) [55]. Using the notation illustrated in Figure 2.13, the strain in percentage can be expressed as:

$$\varepsilon = \frac{LHPT - UHPT}{UHPT} * 100 \tag{2.4}$$

The gradients of stress-strain curves represent the most common measure of the heel pad stiffness [53]. Indeed, the **Stiffness** (S) is a measure of the resistance of an elastic body to a deformation.
The slope of the load-displacement curve - and the corresponding stress-strain curve - changes during one loading-unloading cycle, as shown in Figure 2.15.

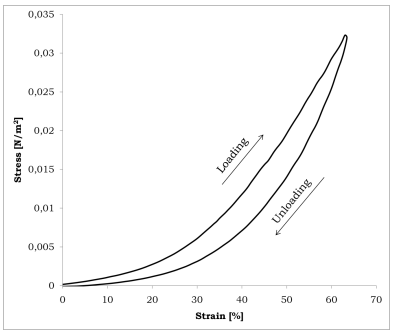

Figure 2.15: Typical stress-strain curve of an *in vivo* heel pad.

The first part of the loading curve might be related to the compressibility of the adipose tissue, while the last part to the fibrous strands [56]. This kind of behavior has been reported to be highly functional in allowing good contact between the foot and the ground during the gait where the heel pad initially deforms quite easily and then reaches a level where further compression does not occur [57]. The histological structure of the fatty heel tissue can be related to sudden increase in stiffness during compression of the heel pad [57]. Under compression the volume of the liquid filling chambers (formed by collagen and septa) has to remain constant and deformation by an external force, applied in a normal direction, implies a sideways displacement of the tissue [57]. Thompson [58] demonstrated that after a low initial stiffness, the collagen septa come under tension, limiting abruptly the deformability of the patty heel tissue and giving a high final stiffness.

Diabetic plantar soft tissue have been found to be stiffer, absorb more energy (higher EDR), recover more slowly, and be harder and thinner than healthy one. These macroscopic characteristics are expression of changes at microscopic level, as mentioned before. These alteration might lead to aberrant distribution of force beneath the foot [59].
In case of falanga torture the cushioning effect is lost and the heel pad does not work as a shock absorber reducing the stresses produced by walking or standing [38]. It might be, thus, reasonable to think that

this would reflect in a higher stiffness of the fat pad tissues.

The heel pad functions are not only straightly related to its histological composition (*e.g.* size, location and integrity of the septa; thickness of fat pad and skin; constituents of the fat itself) [42], but are also influenced by individual factors such as age, body-weight, height, gender and other boundary conditions (such as the individual health, physical activities, etc.). Due to all these confounding factors, it has always been quite difficult to obtain precise values of the heel pad mechanical properties although the biomechanical aspects of *in vivo* healthy and unhealthy heel pads have been investigated for more than 25 years. Unfortunately, different methods as well as different number of subjects vary a great deal, thus the results (in terms of UHPT, LHPT, HPCI, Stiffness and EDR) are not comparable, as shown in the review paper (Paper I) in Appendix E. In such review, results obtained from 50 studies that investigated the biomechanical properties of *in vivo* heel pads were reported as a tendency. In order to indicate whether there was a correlation between a particular intrinsic factor and the biomechanical parameter investigated, the symbols -1, 0 and 1 indicating that there was a negative, null or positive correlation between the intrinsic factor (age, weight, height, gender. etc), and the biomechanical measure taken into consideration, respectively.

When considering the effect of age on UHPT, seven studies out of 15 demonstrated a positive correlation [43, 48, 49, 52, 60, 61, 62], while the remaining eight studies demonstrated no statistical significant effect [11, 60, 63, 64, 65, 66, 67, 68]. Among those, [60] considered only acromegalic patients, while [65, 66] considered only subjects of African origin. The effect of weight on UHPT was considered positive in five studies out of seven [52, 60, 64, 65, 69], whereas the other two studies [67, 70] demonstrated no statistically significant effect. One of the studies showing a positive correlation [70] considered only obese subjects. The effect of height on UHPT is considered to be positive even though only one study [64] investigated this intrinsic factor. When considering the effect of gender on UHPT, seven studies out of 12 indicated a positive correlation [48, 49, 52, 60, 65, 67, 69]. Among those, [65] considered only people of African origin, [60] investigated only acromegalic patients. The remaining five studies demonstrated no difference between males and females [11, 60, 63, 66, 71]. Among the latter studies, [66, 71] considered only subjects of African origin. The effect of race on UHPT is also considered to be positive even though only one study [63] investigated this intrinsic factor. When considering the effect of physical activity on UHPT two studies out of three [34, 51] demonstrated no statistically significant effect, while the remaining study [72] demonstrated a positive correlation. Among those, [34] considered only runners, while [72] indicated that cyclists had a higher UHPT than runners. When taking the effect of diabetes on UHPT into consideration, four studies out of eight demonstrated no statistical significant change [26, 47, 73, 74], two studies demonstrated a positive correlation [75, 76], while the remaining two studies indicated a negative correlation [77, 78]. Eight studies out of 11 demonstrated that there is no correlation between heel pain and UHPT [26, 52, 56, 79, 80, 81, 82, 83], while the remaining two studies reported a positive correlation [34, 49]. Among those, [34] included only runners. Three studies out of five [11, 66, 71] demonstrated that acromegaly has a positive effect on UHPT, while the remaining two studies [64, 84] demonstrated no

statistical significant change. Among those studies demonstrating a positive correlation considered only subjects of African origin [66, 71]. The effect of Rheumatoid Arthritis (RA) and SpondyloArthropathies (SpA) on UHPT was shown to be positive, even though only one study investigated these two intrinsic factor [85]. Two studies out of three reported no statistical significant effect on UHPT after fractures [86, 87], while a study demonstrated a positive correlation [88].

Considering the effect of age on LHPT, three studies out of four demonstrated that there is a positive correlation [48, 52, 61], while the remaining study [67] demonstrated no statistically significant change. When considering the effect of weight on LHPT, one study out of two demonstrated a positive correlation [52], while the remaining study demonstrated no statistically significant change [67]. The effect of gender on LHPT is considered positive, as three studies out of three demonstrated a positive correlation [48, 52, 67]. The effect of physical activity on LHPT is considered to be of no statistical significance, although only one study demonstrated such tendency [51]. The effect of diabetes and heel fractures on LHPT is reported to be positive, even though only one study investigated each intrinsic factor [26, 86]. When looking at the effect of heel pain on LHPT, five studies out of seven demonstrated no statistically significant effect [50, 52, 79, 82, 83], while the remaining two studies demonstrated a positive correlation [26, 49].

When considering the effect of age on HPCI, five studies out of six demonstrated a positive correlation [43, 48, 49, 52, 67], while the remaining study indicated no statistically significant effect [61]. The effect of weight on HPCI is considered positive as all three studies reported a positive correlation [48, 52, 67]. When considering the effect of gender on HPCI, three studies out of four demonstrated no statistically significant difference [48, 49, 52], while the remaining study demonstrated a positive correlation [67]. The effect of physical activity on HPCI is shown to be of no statistical significance, although only one study showed such tendency [51]. The effect of diabetes on HPCI is not clear since one study demonstrated a positive correlation [26], while the other reported no statistically significant difference [47]. The effect of heel pain on HPCI is also not clear, as three studies out of six reported no statistically significant difference [26, 52, 56], while the remaining three studies demonstrated a positive correlation [26, 49, 79].

Two studies out of three demonstrated no significant correlation between age and Stiffness [61, 89], while the other study demonstrated a positive correlation [62]. Only one study investigated the effect of weight on heel pad Stiffness, and it demonstrated a negative correlation [89]. When looking at the effect of gender findings are contrasting as one study reported that males had lower heel pad stiffness than females, [90], while another study reported the opposite result [89]. Only one study investigated the effect of physical activity on heel pad Stiffness, and it demonstrated a positive correlation [72]. This study compared runners vs. cyclist, and the positive correlation indicates that cyclists have higher Stiffness than runners. Four studies out of six investigating the effect of diabetes on Stiffness demonstrated no statistically significant effect [47, 74, 91, 92], while the remaining two studies reported a positive correlation [76, 78]. When looking at the effect of heel pain on Stiffness, two studies out of three demonstrated no statistically significant effect [82, 83], while the other study indicated a negative correlation [35]. It has to be said that

this study the subjects were only runners with heel pain.

When considering the effect of age on EDR, two studies out of five demonstrated a negative correlation [45, 69], one study reported a positive correlation [43], and the remaining two studies demonstrated no statistically significant effect [61, 89]. The effect of weight on EDR was considered positive even though only a study investigated on that parameter [89]. When looking at the effect of gender on EDR, two studies out of three reported that men had lower EDR than women [69, 90], while the other study reported the opposite result [89]. The effect of physical activity is investigated, but only in one study which demonstrated no statistically significant difference [72]. In particular, this study reported that there was no difference between runners and cyclists when comparing EDR values. Diabetes is considered to have a positive effect on EDR, but only one study looked at this intrinsic factor [93]. Two studies out of three looking at effect of heel pain demonstrated a negative correlation [82, 83], while the remaining study reported no statistically significant effect [56].

Understanding the mechanical properties of the heel pad is of fundamental importance in the prevention of disease. Specifically, the soft tissue stiffening and the loss of thickness may be causes of the common location of ulcerations in diabetic feet [77, 94]. Furthermore, knowledge of the influence of age on the biomechanics of the heel pad is helpful for designing footwear and preventing injuries in the elderly [62]. An increase in the distribution of the body fat may be the cause of the increased thickness of the fat pad and may lead to increased pressure in the sealed fibrous compartment, resulting in the stiffer soft tissue found in the elderly [48]. Further, the change in thickness and compressibility could be the main reasons of developing heel pain [95]. The altered mechanical properties might lead to shock absorbency injuries as Achilles tendinitis [43].

2.4 Imaging techniques for human heel pad investigations

The last half of the 20^{th} century saw the development and refinement of several significant medical imaging technologies, including digital X-ray, nuclear medicine, ultrasound (US), positron emission tomography (PET), Magnetic Resonance Imaging (MRI) and computed tomography (CT) for soft tissues investigations. Each technique is characterized by advantages and disadvantages which make one preferable than another depending on the application. In this PhD research both US and MRI have been used to investigate the thickness of *in vivo* heel pads, while CT has been used for heel pad models investigations. Hereafter a brief description of each technique.

Ultrasound

Ultrasonography can be used to measure directly the dimensions of the soft tissue and also to evaluate its internal structure.

There is no ionizing radiation and magnification as inherent in planar X-rays, but it is a strongly operator-dependent imaging modality [12]. It has been used effectively in patients with heel pain. Indeed, inflammations, calcification, partial or complete ruptures of the plantar fascia, calcaneal spurs can be detected sonographically in patients with heel pain [12]. It was also reported by Rome et al. [96] that the thickness of heel pad measured with weight-bearing may reliably be measured by high resolution ultrasonography in normal feet.

Even thought ultrasound is a cheap, fast and portable technique, the precise speed of sound in a given soft tissue remains unknown and not accounted for. In fact, the geometry of the ultrasound image is built on the assumption that the ultrasound pulse travels with a speed of 1540 m/s, which is the average sound velocity in soft tissues. However, cartilage and fat are known outliers with reported velocities of 1892 m/s and 1450 m/s, respectively [97, 98]. With the known high fatty contents of the heel pad it is to be expected that US will overestimate the heel pad thickness. This may to some extent be counteracted by a higher sound velocity in the thick horn layer of the skin and the plantar fascia covering the bone.

The thickness of the heel pad has to be measured both in unloaded and loaded conditions in order to measure its elastic properties. The heel pad thickness is, indeed, one of the subject confounding factors which needs to be taken into consideration when comparing the heel pad mechanical properties of a group of people.

Magnetic Resonance Imaging

MRI has emerged as an important non invasive diagnostic tool for assessment of foot conditions with multiplanar imaging capability [99]. MRI is distinguished in its superior capacity to resolve soft tissue details. No other technique, short of physical dissection, affords clinicians the opportunity to visualize morphology and pathology with such exquisite spatial resolution. Structures and detail as small as a few tenths of millimeters in size can be distinguished, a critical benefit in helping physicians detect incipient disease. MRI also helps clinicians differentiate normal tissues from pathology based on disparate soft tissue relaxation rates or even based on functional variations between tissues. Furthermore, MRI is the modality of choice in followup examinations to visualize disease recurrence or in monitoring the impact of interventions. Importantly, MRI is not a static technology, particularly as it pertains to soft tissue imaging [100].

X-rays and Computed Tomography

Roentgenographic measurements of the heel pad thickness were made first by Steinbach and Russell [11] for diagnosis of acromegaly. Since then X-rays have been used [] to investigate both unloaded and loaded (weight-bearing) heel pad thickness beneath the plantar tuberosity of the calcaneus by measuring the vertical distance between the calcaneus and the skin. Unfortunately, the accuracy of the measurements

obtained with these techniques strongly depends on the orientation of the foot during the examination, which is not usually strictly constrained, thus making the repeatability of the approaches doubtful and there ported heel pad thickness easily overestimated [101]. In addition, measuring heel pad thickness at only one point does not provide a complete knowledge of the heel pad 3D morphology [101]. Such knowledge can be achieved by using Computed Tomography (CT), a medical imaging technique which permits to obtain a volumetric representations of structures from a large series of two-dimensional X-ray images taken around a single axis of rotation. The main disadvantage is the risk of radiation exposure which make this technique be not the preferable choice when dealing with healthy subjects.

CHAPTER

THREE

STUDY I: Compression tests and US investigations

This chapter describes the procedures adopted to investigate the heel pad biomechanics by using a new apparatus (so-called compression device) and 3D ultrasound. The compression device is a prototype, built following specific requirements that make it be usable on heel pads of survivors of falanga torture in the next future.
Papers III and IV in Appendix E describe some of the procedures and results related to the *in vivo* heel pad investigations.

3.1 Background

The interest in quantifying the mechanical properties of human soft tissues is an important aspect of diagnosing diseased tissues. Knowledge of the mechanical properties of heel pad tissue may be used in tools for screening patients for the purpose of preventing further complications in the foot (*e.g.* ulcerations may be prevented in diabetics [6]), as well as of obtaining validated examination methods for medico-legal purposes.
In order to investigate whether there are any differences between healthy and diseased heel pads when dealing with their biomechanics it is first necessary to establish a ”normal” range of biomechanical parameters. Even though the heel pad biomechanics has been investigated for more than 25 years in healthy individuals as well as in subjects with pathological conditions, studies differed both in terms of method applied and population studied, and it is not feasible to compare the numerical results. Thus, the aim of this study is, thus, to collect a bank of ”normal” data characterizing the heel pad biomechanics of a group of healthy people, as the literature cannot be used as a reference.
Heel pad models were used in order to assess both the functionality and reliability of the compression

device. The load-displacement curves recorded for each model were investigated, and then the results were compared with those obtained on the same models in a previous study [102]. Compression tests as well as ultrasound heel pad thickness investigations were then performed on *in vivo* healthy heel pads, so that Heel Pad Compressibility Index (HPCI), Elastic modulus (E), and Energy Dissipation Ratio (EDR) are calculated. Statistical analyses were conducted in order to investigate whether intrinsic factors such as age, weight, height, hour of physical activity influence HPCI, E and EDR, and whether there is a statistical significant difference between males and females in all three parameters.

3.2 Investigations with compression device

3.2.1 Equipment

The measurement part of the compression device consisted of a load cell (model 31, RDP Electronics Ltd., UK), a linear transducer (LVDT, RDP Electronics Ltd., UK) and two amplifiers (E725, RDP Electronics Ltd, UK). The load cell and the linear transducer were both assembled in a cylindrical aluminium body, as shown in Figure 3.1. One end of the cylindrical body was fixed to a Plexiglas vertical plate, while the other end consisted of a threaded shaft which was connected to a stepper motor (PK245-03A, Oriental motor, Japan) by a shaft and a flexible joint (Figure 3.1). The more the threaded shaft was tightened by the stepper motor, the more compression was applied to the heel pad by a piston (diameter of 40mm). A hole in the vertical plate allowed the piston to be in contact with the heel pad. The mechanical drawings of the main components of the device can be found in Appendix B.

The load cell and the linear transducer were each connected to an amplifier which displayed the value of the force or displacement. The stepper motor and the two amplifiers were connected to PC through a digital acquisition board (NI USB-6009, National Instruments). The equipment used for the compression test is shown in Figure 3.2. The sampling frequency was 10 Hz.

3.2.2 Heel pad models and compression tests

Two sets of heel pad models (each containing nine models) were investigated. Each heel pad model consisted of a plastic calcaneus (actually only the part of the calcaneus which faces the load in normal standing position) fixed to a Plexiglas support and surrounded by a heel pad mimicking tissues. A typical mould used to create the heel pad model is shown in Figure 3.3, on the left.
The heel pad tissues were modeled by using a particular viscous liquid composed of 10% of Polyvinyl Alcohol cryogel (PVA-C) dissolved in water-based material. Such material provides an excellent model of the human soft tissue since its elasticity is controllable by varying the number of freeze/thaw cycles to be applied to the material. All these models underwent 2 to 4 freeze/thaw cycles, thus they were characterized by three different elastic modulus (E_2, E_3 and E_4). Specifically:

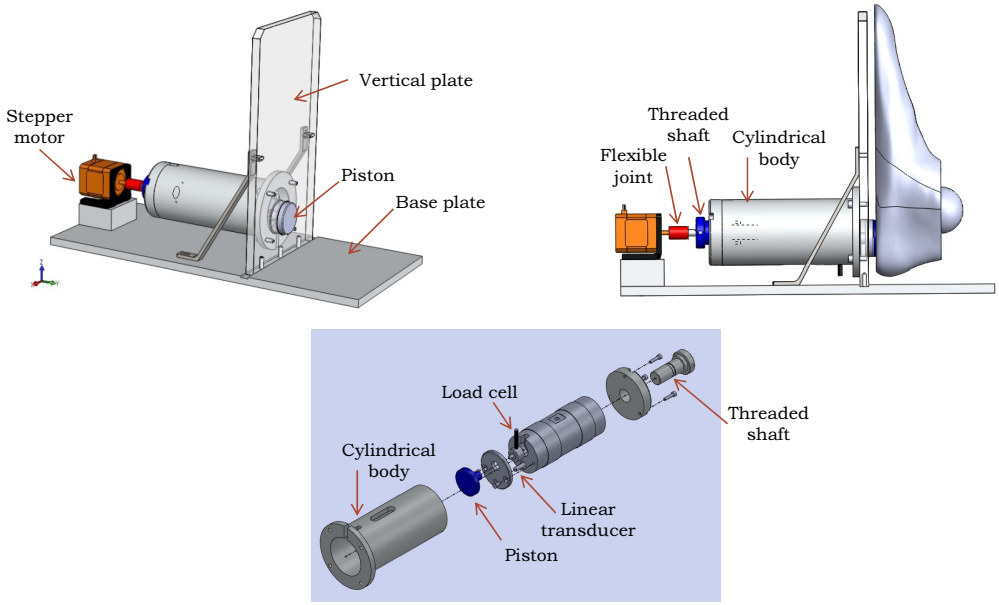

Figure 3.1: The compression device consists of a stepper motor connected to threaded shaft trough a shaft and flexible joint.

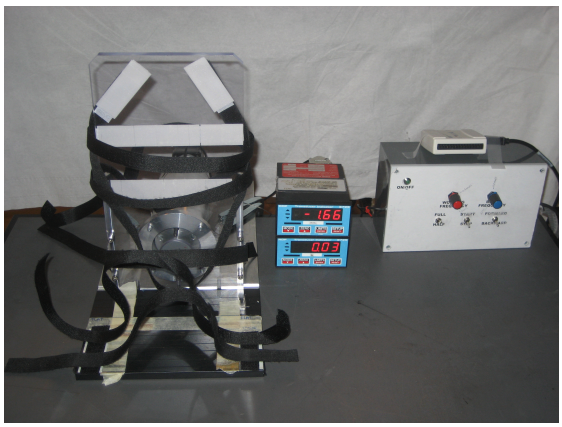

Figure 3.2: Equipment used for the compression test. Starting from the left: the compression device, two amplifiers, digital acquisition board placed on top of the control box.

- E_2=64 kPa, E_3=127 kPa and E_4=161 kPa for the first set.
- E_2=84 kPa, E_3=139 kPa and E_4=181 kPa for the second set.

Once the heel pad model was ready and removed from the mould, it appeared as a white cylinder, as shown in Figure 3.3, on the right. A realistic variation of the heel pad thickness (skin-to-bone distances) was obtained by adjusting the height of the Plexiglas support on which the plastic calcaneus was fixed.

Thus, the models had 9 different known skin-to-bone distances combined with the three elasticities, as shown in Figure 3.4. The first set of models was made in a previous study [102], while the second set was made during this research following the recipe described in [7].

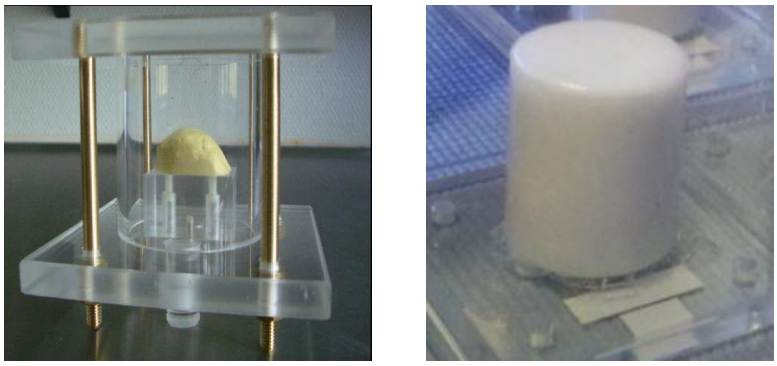

Figure 3.3: Typical mould used to create the heel pad phantom (on the left). Typical heel pad phantom removed from the mould (on the right).

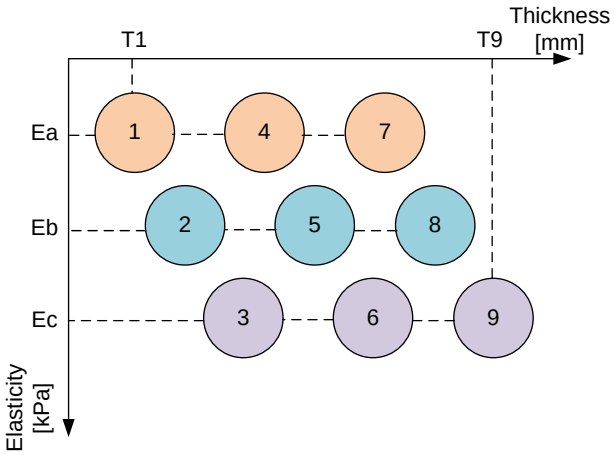

Figure 3.4: Scheme of the heel pad models, illustrating their characteristics in terms of thickness and elasticity.

Both sets of models were investigated with the compression device by applying the same procedure to each heel pad model. The surface of the phantom was covered with a transparent foil in order to prevent it from sticking on the surface of the piston during the test. The square Plexiglas pedestal of the phantom was fixed with two clamps on a heavy metal support and then was positioned in front of the vertical plate in such a way that the center of the cryogel cylinder was coincident with the center of the piston, as shown in Figure 3.5, on the left. Once the model was well positioned, the metal support was also fixed with two clamps on the table, as shown in Figure 3.5, on the right.

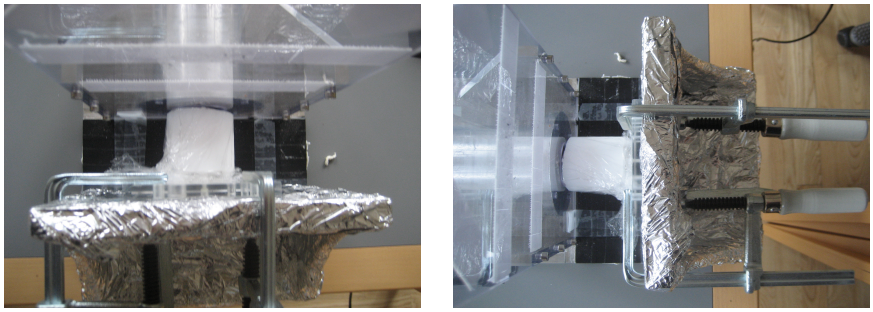

Figure 3.5: Position of the heel pad model in front of the vertical plate, on the left. Fixation of the metal support, on the right.

A program made with LabView (version 2009, National Instruments), visible in Appendix A1, was used to control the entire setting (on/off of system, start/stop of stepper motor, direction of rotation of the stepper motor). The average strain rate used for applying the compression was 1.7 mm/s. Before starting the compression test, an idling test was done in order to verify the system functionality.
For each phantom the compression test was repeated 7 times with a one-minute break between each trial, to allow the material returning to its initial shape.
The value of the displacement determining the point of inversion of rotation of the stepper motor was fixed at 9 mm to avoid arriving at the end of the thread of the shaft that guides the piston, while the superior limit of the force was set to 40 N.
A program made with LabView (version 2009, National Instruments), visible in Appendix A2, was used to visualize and extract all the load-displacement curves recorded.

3.2.3 Subjects

One hundred and twenty seven healthy subjects (63 females, 64 males) were enrolled. Tables 3.1 shows the anthropometric characteristics grouped according to the gender. All values are given as mean $\pm$ one standard deviation.
Only the dominant foot was tested, *i.e.* the foot normally used to hit the ball when playing football. All subjects declared to be in healthy conditions, and to have never had injuries/trauma to any of the feet. The enrolled subjects had different lifestyles, including some being sporty and some following a more sedentary routine. Subjects engaged in professional sport were not included in this study.
All participants were volunteers and were informed about the conditions of the test that involved no harmful procedures or physical pain. The weight and height of each subject were measured, and the footprint of the selected foot was drawn in order to measure both the foot length and the heel pad width. Before starting the compression test the volunteer was asked to give information about age, nature of physical activity and hours per week, as well as size of shoe.

Table 3.1: Anthropometric characteristics of volunteers grouped according to the gender given as mean ± one standard deviation.

	All	Females	Males
Subjects	127	63	64
Age (years)	36.6±14.6	36.7±14.4	36.6±14.7
Weight (kg)	71.7±13.5	64.2±9.2	79.2±12.8
Height (m)	173.6±9.8	166.8±5.7	180.4±8.3
BMI (kg/m^2)	23.7±3.1	23.0±2.7	24.3±3.3
Physical activity (hours/week)	4.0±3.9	4.7±4.1	3.3±3.6

3.2.4 Procedure for compression test on volunteers

The same procedure was applied to each volunteer. Both shoe and sock were removed, and then the subject laid in a supine position with both legs completely straight and relaxed on a table. Such table was covered with a rubber mattress, so that the volunteer had no discomfort during the testing session. Further, a pillow was positioned under the head in order to maintain a neutral cervical spine. The compression device was fixed on the extremity of the same table, as shown in Figure 3.6.

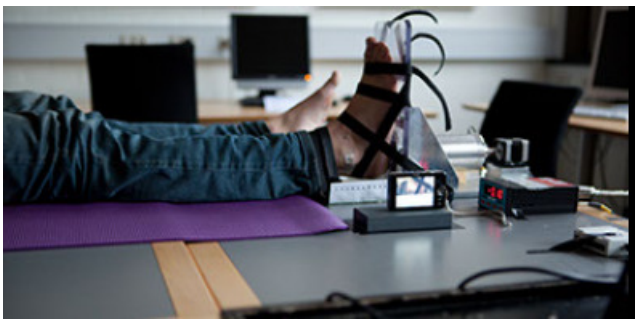

Figure 3.6: Location of the compression device and its equipment. The volunteer lies in a supine position with both legs straight and relaxed.

The foot was positioned in such a way that the anterior part touched the vertical plate, with the heel pad in front of the piston. Specifically, the heel pad was placed in such a way that the longitudinal axis of the foot was passing on the center of the indenter, as shown in Figure 3.7, on the right. Once the foot was well positioned, it was blocked with six Velcro fasteners (two to strap down the anterior part of the foot, one to keep the heel in front of the cylinder, one to stabilize the ankle, and the last two straps to stabilize the lower part of the leg), as shown in Figure 3.7, on the center and left. When necessary, a cushion was positioned under the calf in order to better position the heel pad in front of the piston. The subject was asked to maintain the foot in the same position for the duration of the test and remain as relaxed as possible in order not to influence the measurements with voluntary muscular tension.

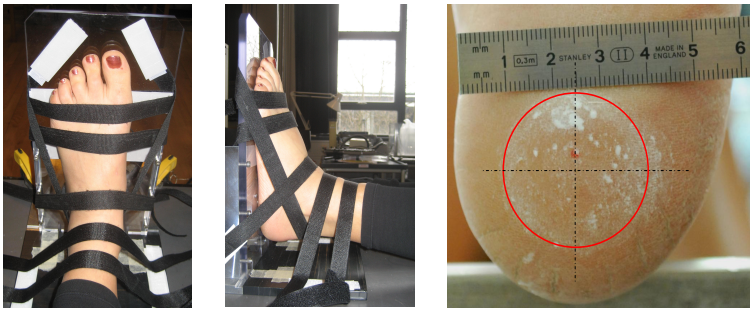

Figure 3.7: Top down and lateral view of the foot positioned on the vertical plate with the six Velcro straps (on the left and center). Position of the cylinder on the heel pad (on the right). The print of the cylinder is made by placing some talcum powder on its surface during the compression.

A program made with LabView (version 2009, National Instruments), visible in Appendix A1, was used to control the entire setting (on/off of system, start/stop of stepper motor, direction of rotation of the stepper motor). The strain rate used for applying the compression was 1.7 mm/s. Before starting the compression test on the heel pad, an idling test was done in order to verify the system functionality.
As soon as the subject was completely relaxed and ready to be tested, the examiner ran the LabView program controlling each step of the measurement procedure. For each subject, the compression test was repeated 7 to 10 times with a one-minute break between each trial, to allow the heel pad tissue returning to its initial shape. Data were saved as text file.
The flow diagram of Figure 3.8 shows in detail the procedure applied for each compression test.

The value of the displacement determining the point of inversion of rotation of the stepper motor was fixed at 9 mm to avoid arriving at the end of the thread of the shaft that guides the piston, while the superior limit of the force was set to 40 N.
Figure 3.9 on the left, shows the typical box to be filled with the subject information before starting the compression test, while on the right it shows the control panel which permits to visualize the zero setting, hysteresis, and average velocity during each test.

The entire approach was not intended to reproduce any physiological condition of walking and/or running, but it was designed to minimize any discomfort and any sensation of being strapped in order to be a possible clinical device applicable on survivors of torture. This explains the relative low strain rate applied during the compression/decompression of the heel pad. Furthermore, due to the weak physical and physiological conditions of patients and their difficulty of movements, especially survivors of falanga torture, the compression device should be portable. Figure 3.10 shows an example of portability which was developed during the research. The cover box is made from Polyester with the lid furnished of a grid in order to dissipate the heat generated by the electrical components. The weight of the equipment might be reduced by replacing, where it is possible, some of the aluminium parts with plastic/Plexiglas (*e.g.* base plate, the cylindrical body, the pedestal of the stepper motor).

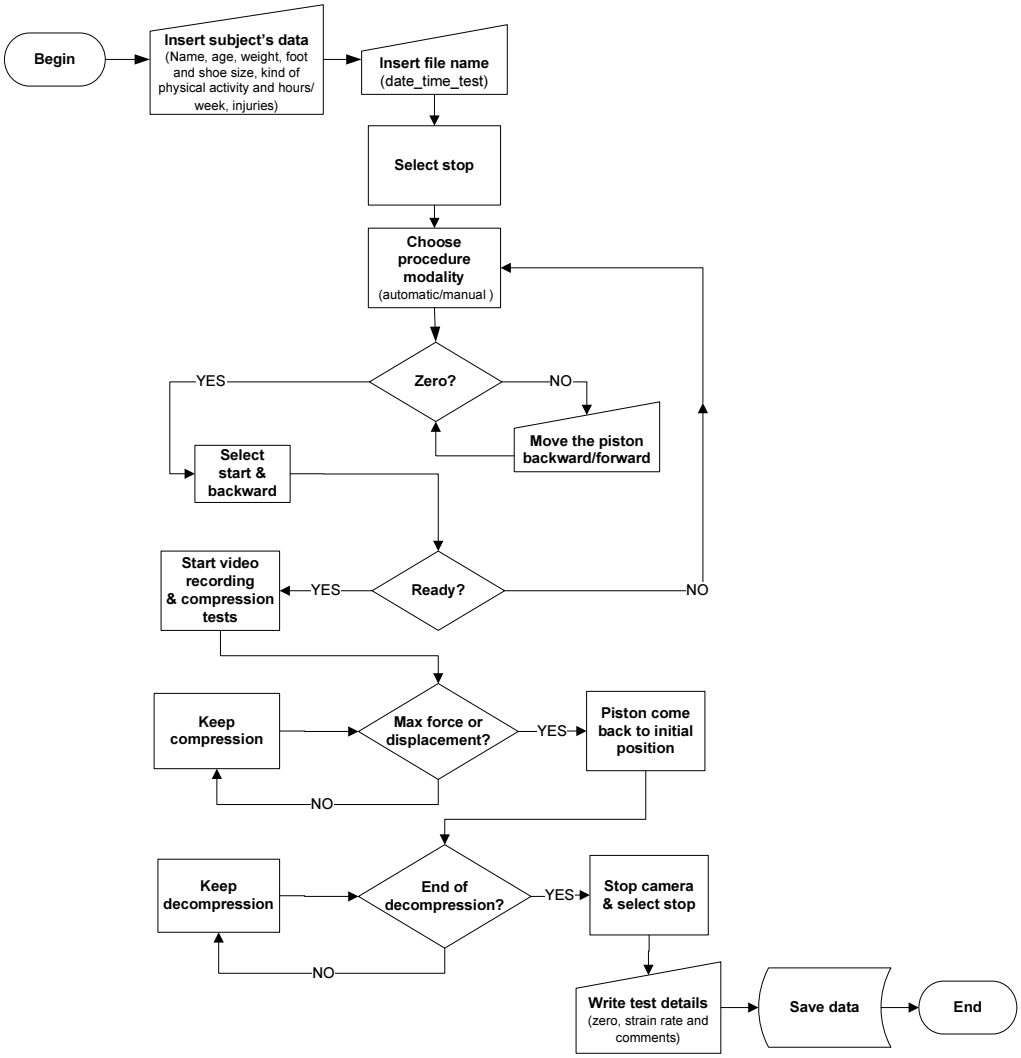

Figure 3.8: Flow diagram illustrating the procedure applied for the compression test. For each subject the cycle is applied 7≤M≤ times.

3.2.5 Procedure for video-processing

Due to the main requirement of the compression device to be a clinical device usable on survivors of falanga torture, the foot cannot be completely fixed. Therefore, involuntary muscular and neuronal movements and/or tensions may occur during the entire procedure, even though the volunteer was asked to remain relaxed. In fact, as the compressions/decompression are made on *in vivo* heel pads, it is almost impossible to consider the foot completely still. The most critical part is the ankle joint because it is only stabilized by using two straps on the lower part of the leg. In order to verify and quantify the involuntary movements of the ankle during the entire duration of the test, a fiducial marker was attached on the skin of

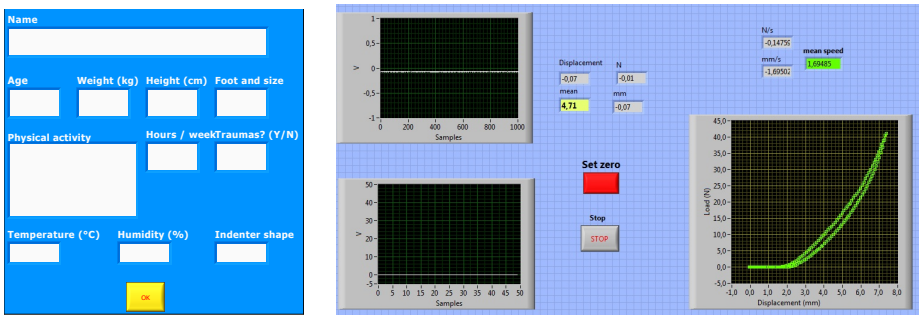

Figure 3.9: Typical box (LabView 2009, National Instruments) to be filled with the subject information before starting the compression test (on the left). Control panel (LabView 2009, National Instruments) which permits to visualize the zero setting, hysteresis, and average velocity during each compression test (on the right).

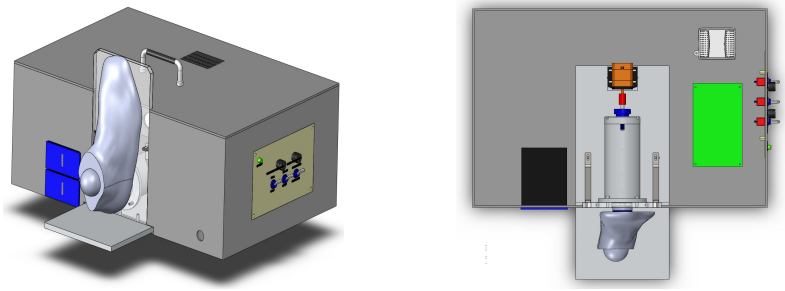

Figure 3.10: Example of portability for the compression device. The box cover is made from Polyester

the ankle bone (malleolus) with a transparent tape, as shown in Figure 3.11, on the left. A video-camera was placed in front of the marker (Figure 3.11, in the center) at a fixed distance, so that videos were recorded during all trials. The video-camera was positioned on the right or left of the compression device depending on which foot (right or left) was investigated.
The aim of this marker-video-procedure was to calculate the movement of the ankle in order to correct the hysteresis obtained from the compression test. Specifically, the displacement of the ankle would be subtracted with a proper procedure from the displacement of the piston. This correction should allow narrowing the spread in data which was visible on a group of healthy young subjects investigated in a preliminary study. The analysis of videos could also be used to discard compression tests that were affected by a very high and irregular ankle displacement (when compared to the others).
In order to find the conversion between pixels and millimeters, a calibration was necessary. Specifically, before starting the compression test a short video was recorded showing two markers placed on the same plane of the ankle and separated by a known distance (19 mm), as shown in Figure 3.11, on the right.

All videos were processed with the MATLAB code `videocode_interpolation.m` (Appendix A4) whose main requirements were: easy-to-be-used and fast processing. Both requirements were necessary

Figure 3.11: Typical marker position (on the left). Location of the camera in front of the ankle (in the center). Sheet of markers used for calibration (on the right).

due to the large number of volunteers and thus a large number of videos to be analyzed.
The use of the code, allowed saving and visualizing the displacement of the ankle by applying a simple procedure. After entering the name of the subject and selecting the folder containing the videos, only two steps were necessary:

1. Calibration: two center points of two markers are selected, as shown in Figure 3.12 (on the left).
2. Limitation of the window: the center of the marker is selected in order to create the boundary of the window on which the movement is analyzed, as shown in Figure 3.12 (on the right).

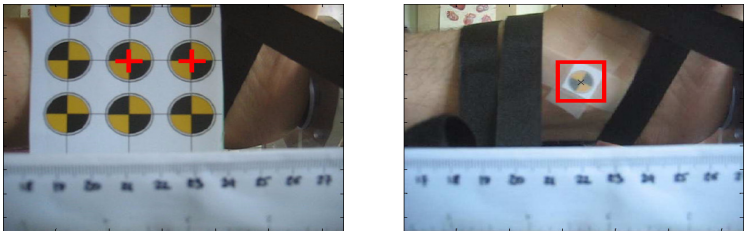

Figure 3.12: Selection of the two center point of the two markers in order to have the calibration (on the left). Selection of the center of the marker located on the malleolus, in order to create the boundary of the window on which the movement is analyzed (on the right).

The code was developed on the basis of 2D cross-correlation. Each video consisted of about 350 frames, therefore, the cross-correlation was applied 350 times. In the present study the vertical displacement was considered negligible, as the piston is pushing the heel pad in the horizontal direction. With such assumption, the correlation works like having a single pixel, and only the profile of the middle horizontal line of the cross-correlation image was treated. Figure 3.13 shows an example of cross-correlation. For each image of cross-correlation, the x-coordinate of the highest point represented the displacement of the foot at this time in term of pixel. In order to find the maximum between two pixels with a better resolution the curves of profiles were interpolated.
For each video the movement of the fiducial marker during compression and decompression of the was interpolated with a 3^{rd} degree polynomial curve. The coefficients of the two polynomial curves were

used for the correction of the hysteresis curves.

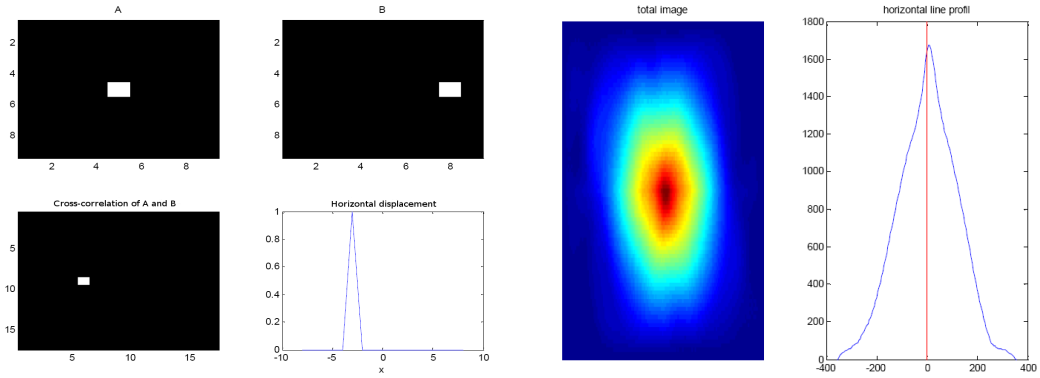

Figure 3.13: Example of horizontal displacement measured by cross-correlation (on the left). Result of cross-correlation between two images (on the right).

For each volunteer the maximum horizontal and vertical displacements of the ankle calculated were plotted (Figure 3.14). In the present study, the vertical movement appeared to be negligible, so only the horizontal one was used for the correction procedure. Furthermore, for each video the function interpolating the displacement of the fiducial marker (3^{rd} degree polynomial curve) was displayed (Figure), and its coefficients were used for the correction of the hysteresis with the procedure explained before.

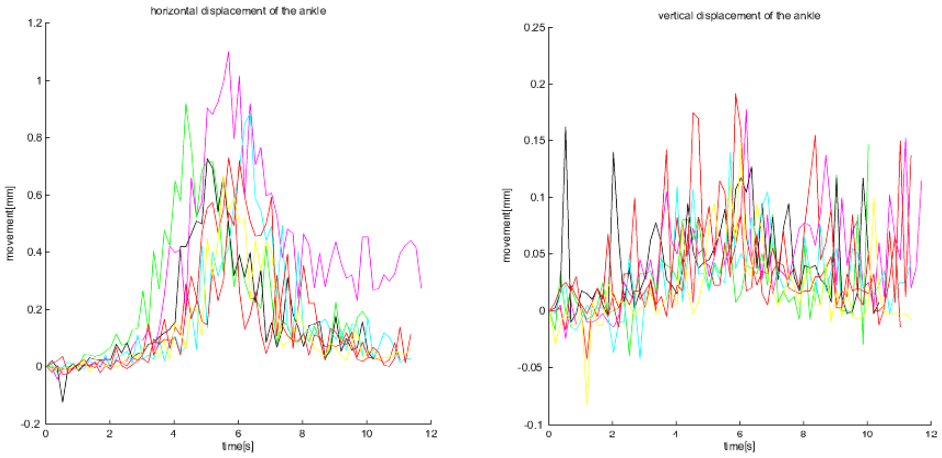

Figure 3.14: Typical plots obtained from the video processing procedure. Maximum horizontal (on the left) and vertical (on the right) displacement of the ankle.

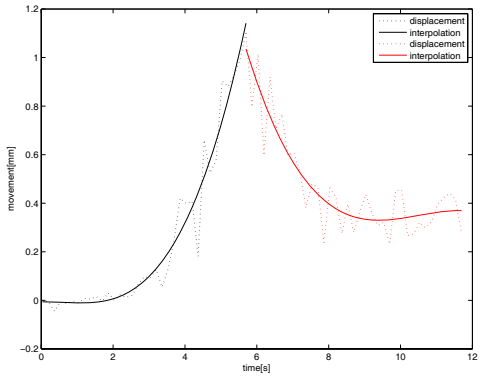

Figure 3.15: Typical 3^{rd} degree polynomial interpolating the movement of the ankle.

3.2.6 *In vivo* heel pads data analysis

A program made with LabView (version 2009, National Instruments), shown in Appendix A3, was used to calculate E and EDR for each volunteer from the data obtained from both compression tests and video processing. The flow diagram illustrated in Figure 3.16 shows in detail the procedure applied for each volunteer.

The control panel shown in Figure 3.17 is the interface which allows the data analysis for each volunteer. Data obtained from the compression tests were loaded as text files for one volunteer at a time. Then, a threshold of 0.3 N was applied, so that all curves started from the same zero and the empty stroke of the piston was removed.

From the video processing both the maximum horizontal displacement and the coefficients had to be inserted in the lower part of the panel shown in Figure 3.17. If the foot investigated was the left one, the sign of the coefficients had to be inverted, just clicking with the mouse on the button shaped as tumbler switch (above the coefficients table of Figure 3.17). The maximum horizontal displacement calculated with MATLAB, was assumed to be coincident with the maximum displacement of the piston. Such assumption allowed synchronizing the time of the video-camera and compression device, as the two devices were not driven by the same control box.

Figure 3.18 illustrates the procedure applied for the correction of each hysteresis.
The generic point P placed on the loading curve of Figure 3.18 indicates the displacement D_p of the piston at a given force L_p. D_p should also indicate the displacement of the heel pad if the foot were completely fixed. Actually, it moves of a certain quantity, ΔD, which was measured from the video-processing. For this reason, the displacement of the heel pad is represented by the point P'', that can be found as follows. Knowing ΔD the point P' can be easily found, as illustrated in Figure 3.18. The corresponding point placed on the unloading at the same load L_p is the point R. Such point is used to draw the tangent (t') to the unloading curve. Specifically, the tangent representing the stiffness of the heel pad at that precise

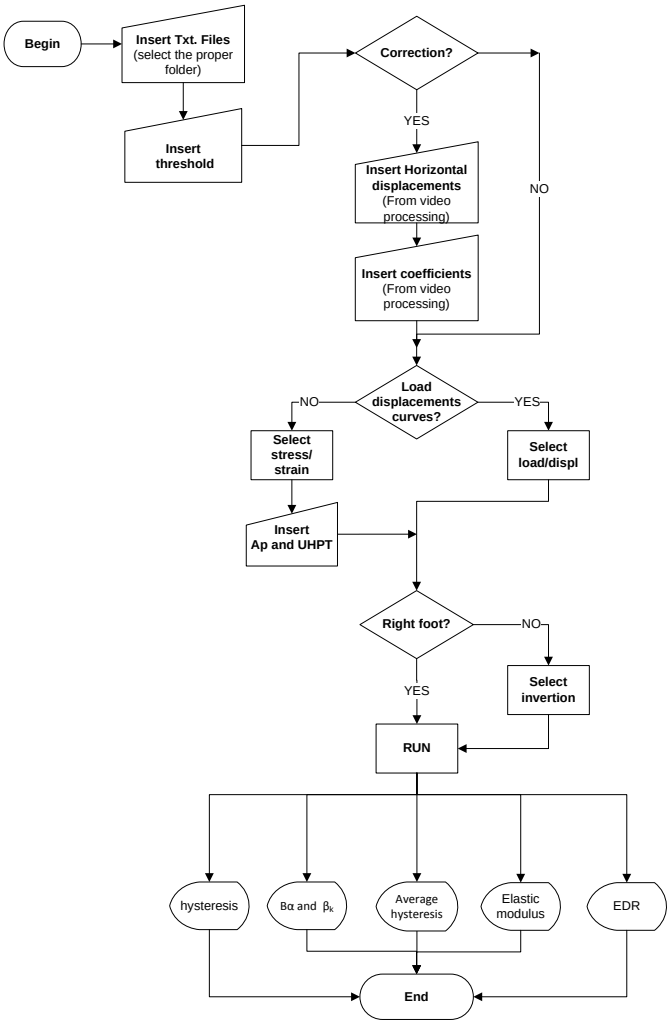

Figure 3.16: Flow diagram illustrating the procedure applied for the analysis of data obtained from both compression tests and video processing for each volunteer.

point, is used to find the point P'' indicating the real displacement of the heel pad at a given load. In fact, the parallel to this tangent (t'') passing from P' can be drawn as well. Thus, the point P'' can be found as the intersection between such straight line and the vertical line passing from P. The point P'' is characterized by a higher value of load at a given displacement D_p. This is due to the movement of the foot which can be interpreted as a separation of the foot from the piston. Indeed, if the foot were fixed, it would have been possible to compress the heel pad with more force.

After applying this correction the maximum load for each volunteer would be higher than 40 N and different for each volunteer (depending on the maximum movement). In order to have comparable curves, the correction was applied limiting the curves to 40 N or the corresponding value in term of stress.

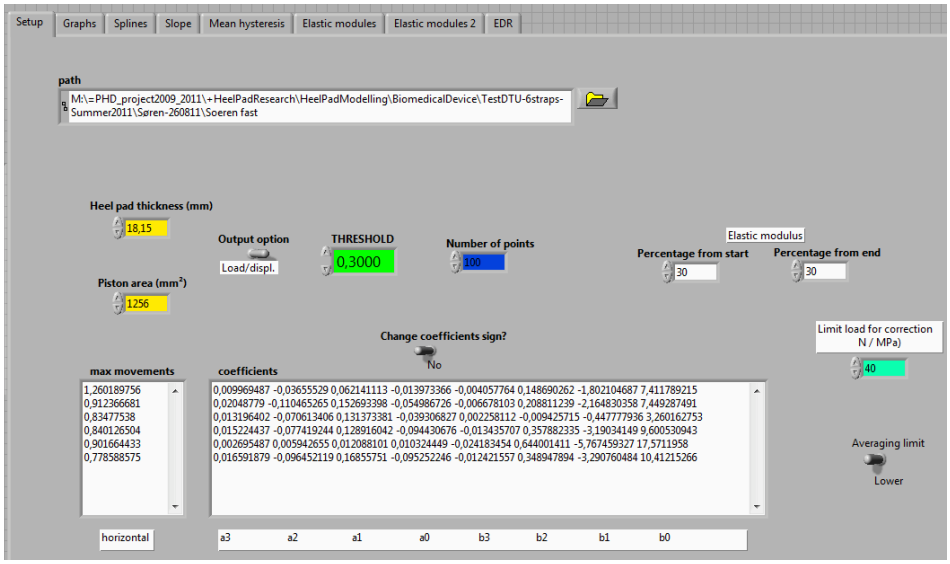

Figure 3.17: Control panel (LabView 2009, National Instruments) which permits the data analysis for each volunteer.

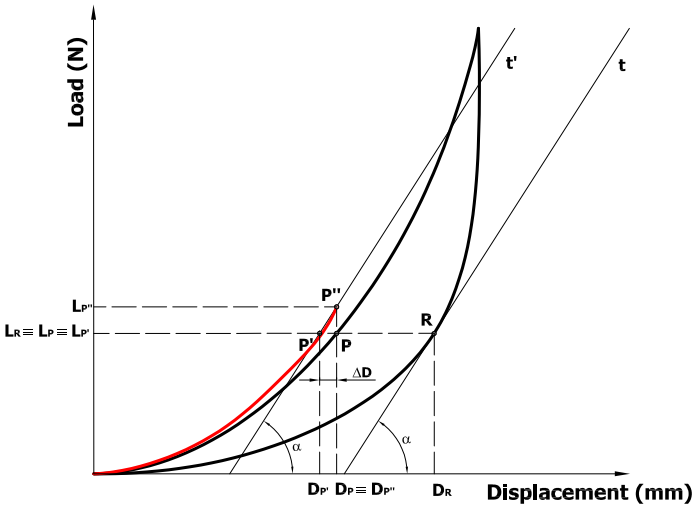

Figure 3.18: Correction procedure.

Once all the numerical information were inserted and the switches positioned on the preferred method (load-displacement or stress-strain), the program was run and the following outputs were extracted.

1. Load-displacement or stress-strain curves.
   The output option (load-displacement or stress strain curves) was chosen by clicking on the tumbler switch. In case of stress-strain curves, the area of the piston (A_p=1256 mm^2) as well as the unloaded

heel pad thickness (UHPT) were inserted. The calculation of UHPT will be explained in the next section. The curves will then be displayed with and without threshold, so that a comparison could be made for each volunteer. Figure 3.19 shows clearly how the application of a threshold can reduce the spread of the hysteresis due to the different starting point (zeros) and the empty stroke of the piston.

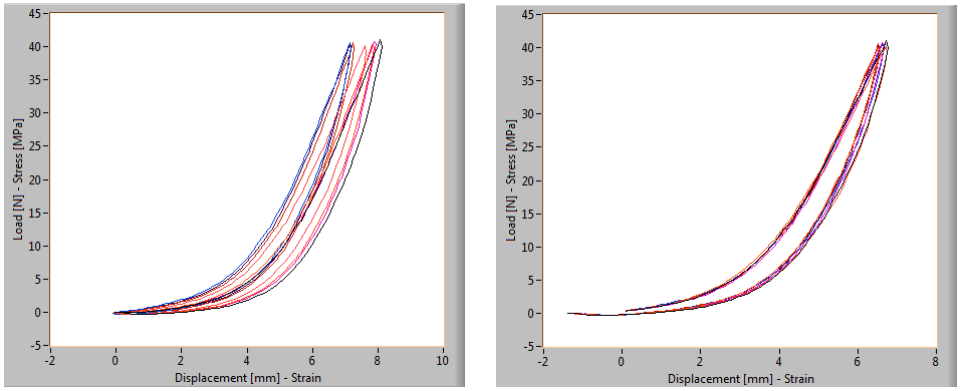

Figure 3.19: Typical load-displacement without threshold (on the left) and with a threshold of 0.3 N (on the right).

2. Splines for all curves.
   A spline function was used to interpolate the data coming from experimental tests. The advantage of working with splines instead experimental points is that they are continuous functions. The calculations of the parameters such as elastic modulus and energy dissipation ratio are thus easier to make.

3. Slope and average curvature of the curves.
   In order to analyze the variation in the data of each subject, the best fit to a 3^{rd} degree polynomial curve, *y*, was calculated for each load-displacement curve, *F(x)*, of each volunteer:

$$y = ax^3 + 2x^2 + cx + d \tag{3.1}$$

   where *x* is the displacement, *y* is the force, *a*, *b*, *c* are coefficients, and *d* is a constant. The polynomial is exemplified in Figure 3.20. In this study, the curves started at very near (0 mm, 0 N). Any distance interval where the load was not increasing, was subtracted from all measurement points, so that *F(x)* starts at x=0 (*d* = 0 in (3.1)). For each 3^{rd} degree polynomial curve two parameters were chosen to describe the load-displacement curves. The slope, $\alpha_{n,m}$, representing the inclination of the straight line connecting the two extremes of the polynomial curve:

$$\alpha_{n,m} = \frac{y(x_{max})}{x_{max}} \tag{3.2}$$

where *n* is the subject number, *m* is the measurements number for subject *n* and x_{max} is the value of *x* corresponding to the maximum of the polynomial curve. The other parameter is the average curvature, $\overline{k}_{m,n}$, obtained by averaging the local curvatures ($k_{m,n,q}$). The latter was calculated by dividing the polynomial curve into *Q* equidistant intervals. At each interval, an expression for the curvature was found by:

$$k_{m,n,q} = \frac{1}{R_q} = \frac{|\frac{d^2y}{dx^2}|}{\left[1 + \left(\frac{dy}{dx}\right)^2\right]^{\frac{3}{2}}} \tag{3.3}$$

where R_q is the radius of the local curvature. $Q \approx$ 80 - 90 intervals.

For each parameter ($\alpha_{n,m}$ and $\overline{k}_{m,n}$) the tendency line could be drawn as well. Specifically, the tendency lines for all 127 volunteers were next analyzed to see if there was a prevailing slope. The slope of the tendency line of $\alpha_{n,m}$ is denoted β_α while the one of $\overline{k}_{m,n}$, is denoted β_k.

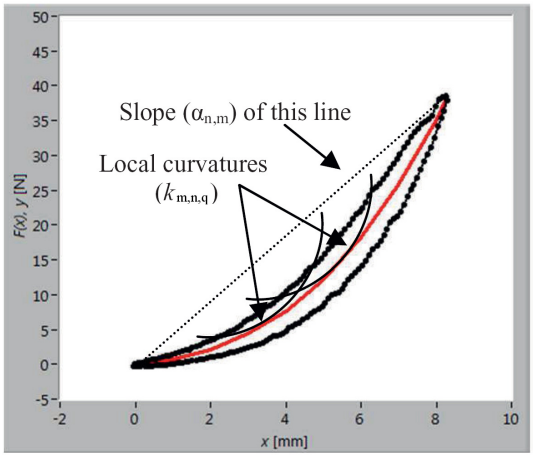

Figure 3.20: Typical load-displacement curve of an *in vivo* heel pad with inside its best fitting 3^{rd} degree polynomial curve.

4. Average hysteresis.
   The average hysteresis was calculated, so that it could be used to compare volunteers. The method consisted in averaging both coordinates (x and y) of the splines. The average process was done separately on the loading and unloading curve, and then the entire curve was displayed.

5. Elastic modulus (E).
   This parameter was calculated as the average between E_1 and E_2. Specifically, E_1 was the elastic modulus calculated on of the initial 30% of the loading curve, while E_2 was calculate on the final 30% of the loading curve. Figure 3.21 shows the initial and final parts of the loading curve on

which E was calculated. Indeed, these two parts can be considered linear and E can be found as:

$$E = \frac{\sigma}{\varepsilon} = \frac{L}{A_p} * \frac{d}{UHPT} \tag{3.4}$$

where L is the load applied on the heel pad during the compression, A_p is the area of the piston, d is the displacement of the heel pad and *UHPT* is unloaded heel pad thickness. The elastic modulus is calculated only from stress-strain curves. Indeed the heel pad thickness has to be taken into account when dealing with the elasticity of the material.

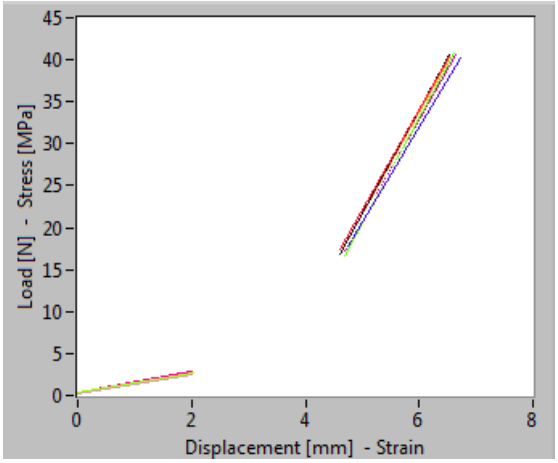

Figure 3.21: Initial and final parts of the loading curve on which the elastic modulus was calculated.

6. Energy Dissipation Ratio (EDR).
   The EDR, representing the energy dissipated as heat of the heel pad during compression/decompression, was calculated by using equation 2.1. The areas were estimated by numerical integration.

3.3 Ultrasound investigations

3.3.1 Heel pad thickness measurements

All 127 volunteers that underwent compression tests, were also enrolled for the heel pad thickness investigations. A 3D high-resolution 14MHz US transducer (Logiq9-GE Healthcare, Angle=29deg) was used to scan the dominant heel of each subject in both unloaded and loaded conditions. Specifically, in unloaded condition the subject was laying down on a medical bed with both legs straight and relaxed, as shown in Figure 3.22, on the left. In order to facilitate the work of the investigator a cushion may have positioned under the calf. The loaded condition was defined by the weight-bearing. Indeed, the subject was standing

on a Plexiglas platform, as shown in Figure 3.22, on the right, transferring all bodyweight on the dominant foot. In both conditions two images were recorded with the US transducer placed longitudinally and transversally to the middle of the heel pad.

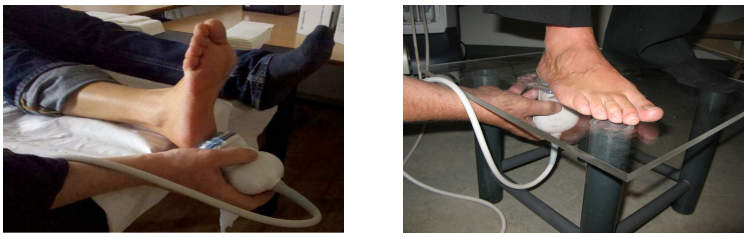

Figure 3.22: Typical US scans in unloaded (on the left) and loaded conditions (on the right).

For each volunteer the unloaded and loaded heel pad thickness were measured from the 3D-block (in the acquisition plane, A).

In order to find the shortest distance between the skin and the calcaneus (as the heel pad thickness is defined), the heel pad was visualized in the three planes A, B and C, as shown in Figure 3.23. The calcaneus was first visualized on plane A and a yellow mark was placed on its top (Figure 3.23, upper left). Then the position of the calcaneus was checked in plane B, so that the red point (Figure 3.23, upper right) was also placed on the highest position of the bone. The image in plane C was used for visual inspection. The optimal distance was found once the images in the three planes matched.

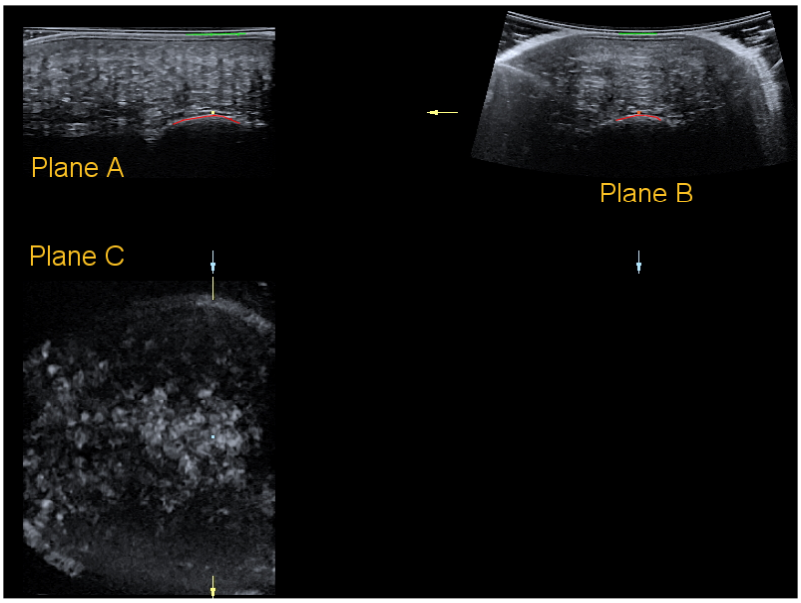

Figure 3.23: Typical US visualization of the heel pad in the three planes (A, B and C). The skin layer and calcaneus are outlined in green and red, respectively.

Figure 3.24 shows two typical US images recorded in unloaded (on the left) and loaded conditions (on the right).

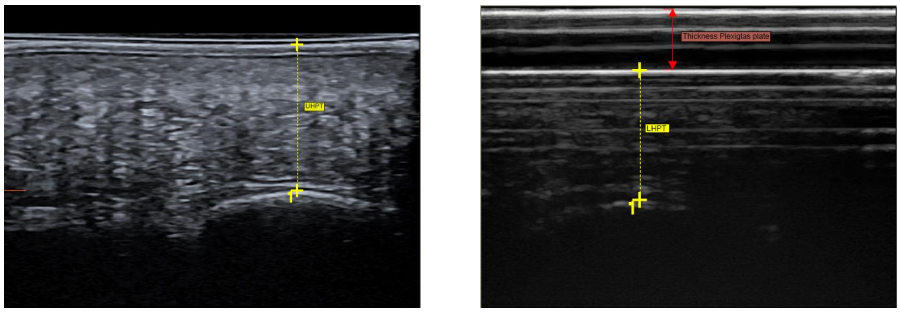

Figure 3.24: Typical heel pad thickness measurements in unloaded (on the left), and loaded conditions (on the right).

The values of UHPT and LHPT were used to calculate the Heel Pad Compressibility Index (HPCI) by using equation 2.2.

3.4 Statistical analysis

Statistical analyses were performed by using the software package R Project for Statistical Computing [103].
Linear regression models were fitted to the data in order to investigate whether there was a statistically significant correlation between HPCI, E and EDR, and intrinsic factors such as age, gender, weight, height, duration of physical activity and heel pad thickness.
When making a linear regression model, as described in Equation 3.5, the goal is to identify the coefficients of the explanatory variables (α_i) and possibly to predict the behavior of the response variable (Y) by the development of explanatory variables (x_i). In the present study HPCI, E and EDR were the response variables, while age, weight, height, gender, duration of physical activity and heel pad thickness were the explanatory variables.

$$Y = \alpha_1 x_1 + \alpha_2 x_2 + ... + \alpha_n x_n + \beta \tag{3.5}$$

In a linear model with many explanatory variables, as in this case, it is rare that all explanatory variables are significant according to the response variable. As there are many explanatory variables incorporated in the model, the system of the linear regression model is filled with a lot of noise from the insignificant variables. In order to find the most precise linear regression, model with as little noise as possible, a step-by-step analysis was done. The approach was to remove the explanatory variable with the highest P-value (indicating the least significant variable) and create a new linear regression model without this variable. This procedure was continued until the highest R^2 was achieved and the best possible regression model

was found. Indeed, the coefficient of determination, R^2, indicates how well the current model is able to predict future results. In relation to linear regression modeling, R^2 indicates how large a percentage of the variation of the data that can be explained by the found model is. If R^2 is close to 1 the linear regression model fits very well the data, whereas if R^2 is close to zero the found linear model does not describe with accuracy the variation in the data [105].
When considering two groups (*e.g.* males and females), it is possible to include interactions between a certain explanatory variable and the other variables in the regression model. As gender is a factorial explanatory variable, its value can be either "male" or "female" without any values in between. Thus, it makes sense to include the interaction between gender and another explanatory variable. Specifically, the interaction between age and gender is included as an explanatory variable in the regression model for all volunteers in order to make the group of subjects as homogeneous as possible.

In order to investigate whether there was a statistically significant difference between males and females for each biomechanical parameter, the Welch Two Sample t-test (used when testing two data sets with possible unequal variances) was applied. The mean value found for males was tested against that obtained for females. The t-test will then take the possible different variances into account and will test whether difference in the means is statistically significant or not [104].

In a statistical analysis the first step is to get an idea about how the raw data is behaving. Therefore, graphs with the chosen response variable plotted against all other explanatory variables were made. These plots would help to understand which of the possible explanatory variables could have a correlation with the response variable. All of these plots are shown in Appendix D.

In this study a confidence interval of 95% as well as a P-value less than 0.05 were chosen to indicate a statistically significant difference. In the step-by-step modeling some of the included explanatory variable may not be statistically significant but still included in the model. Indeed, the explanatory variable is not negligible for the response variable when the P-Value ranges between 0.05 and 0.10.

3.5 Results

3.5.1 Heel pad models

Compression tests were applied on the first set of heel pad models used also in a previous study [102] where their stiffness was investigated. Holst et al. [102] found that the thicker and the softer the heel pad model is, the less force is needed to achieve the same displacement. Thus, the thickness plays the role of confounding factor when trying to classifying the material, as already shown by [7] and confirmed by the present investigation (see Figure 3.25, on the left). The slopes of the force-displacement curves, plotted as a function of thickness (Figure 3.25, on the right), showed the same behavior described previously [102]. The present investigation also confirms that the heel pad models 6 and 5 are difficult to be distinguished.

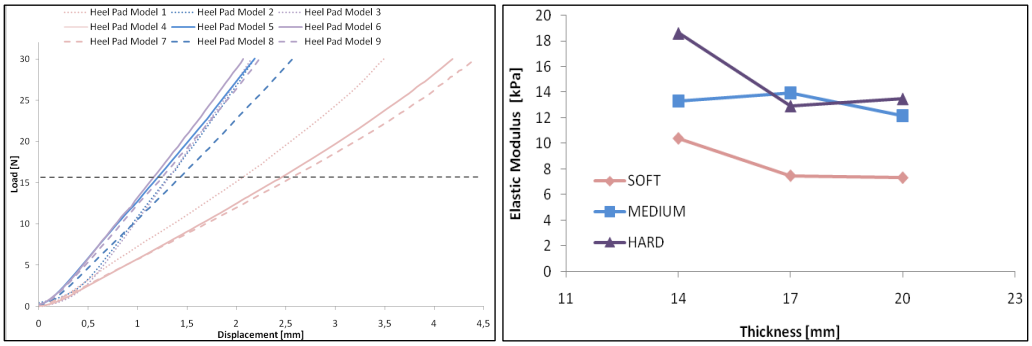

Figure 3.25: Loading curves obtained from the compression test applied on all heel pad models of the first set (on the left). Slopes of the force-displacement curves of the heel pad models plotted as a function of thickness. The dashed line represents the maximum load used in [102] (on the right)

.

Figure 3.26, on the left, shows the typical load-displacements curves obtained by applying the compression test on one of the nine heel pad models of the first set. All models were tested twice with a break of some days in order to investigate the repeatability of the measurements. The load-displacement curves obtained from these two investigations are shown in Figure 3.26, on the right.
Compression tests were also performed on all nine models of the second set. Once again the device demonstrates the repeatability of the measurements and its reliability, as shown in Figure 3.27 where the typical load-displacements curves of one of the heel pad models are completely overlapped.

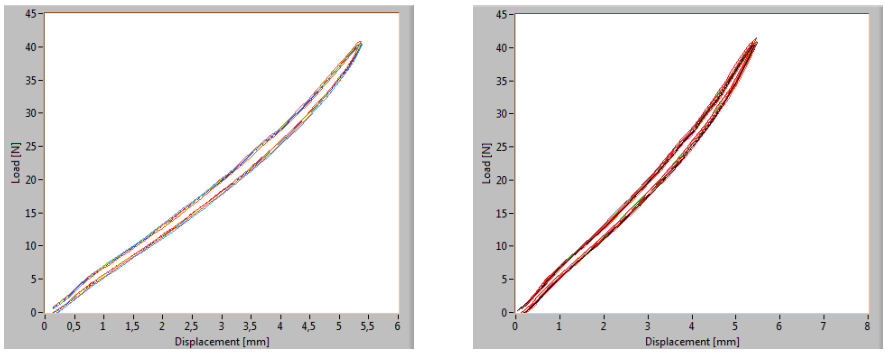

Figure 3.26: Typical load-displacement curves obtained for on the nine heel pad models belonging to the first set (on the left). Load-displacement curves obtained testing twice the same heel pad model with a break of some days (on the right).

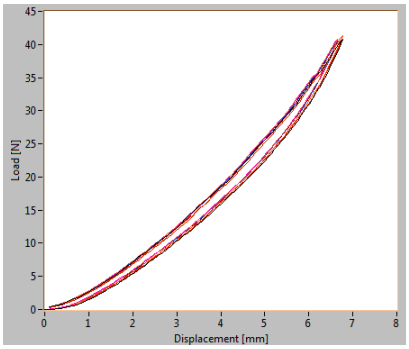

Figure 3.27: Typical load-displacement curves of one of the nine heel pad models of the second set.

3.5.2 In vivo human heel pads

Repeatability and reliability of *in vivo* measurements

Typical load-displacement curves obtained from the compression test applied on *in vivo* heel pad are shown in Figure 3.28, (a). As expected, once the correction was done according to the video-processing data, the maximum value of the load was higher than 40 N (Figure 3.28, (b)). In order to make comparisons among all volunteers, the corrected hysteresis where limited to 40 N (or 0.032 N/mm^2 when considering stress-strain curves), as shown in Figure 3.28, (c).

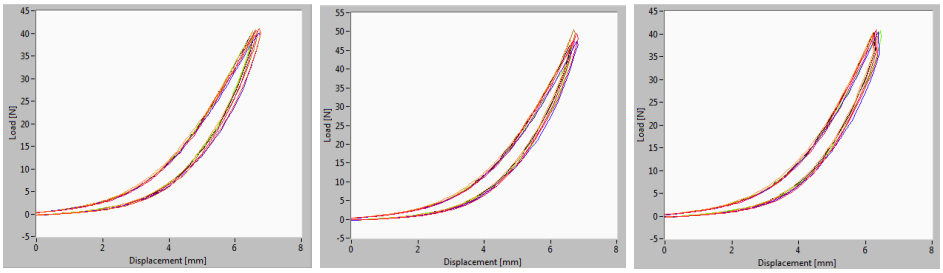

(a) (b) (c)

Figure 3.28: Typical load-displacement curves obtained from the compression test without correction (a), with correction (b), and with correction and limit to 40 N (c).

In order to assess the repeatability of the measurements applied on each heel pad, the trend of both $\alpha_{n,m}$ and $\overline{k}_{m,n}$ of the polynomial curves calculated for each volunteer was plotted together with the tendency lines (Figure 3.29). Then, β_α and β_k (slopes of the two tendency lines) were calculated and plotted to see whether there was a prevailing slope (tendency). A preliminary study conducted on 23 volunteers (Paper III in Appendix E) showed that no statistically significant tendency was identified.

β_α and β_k were calculated and plotted for all 127 volunteers participating to the compression test (Figure 3.30). A qualitative analysis of such plot did not show any tendency, as the values oscillated around

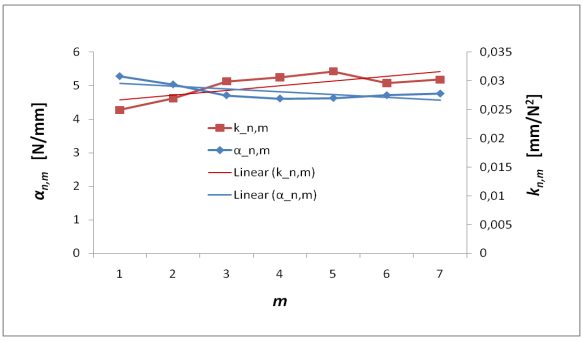

Figure 3.29: Trend of $\alpha_{n,m}$ and $\overline{k}_{m,n}$ of all 7 polynomial curves for a typical subject. The tendency lines are drawn for each parameter.

zero. The measurements showed thus their repeatability. It was, however, necessary to perform statistical analyses in order to investigate whether there were statistically significant difference among volunteers.

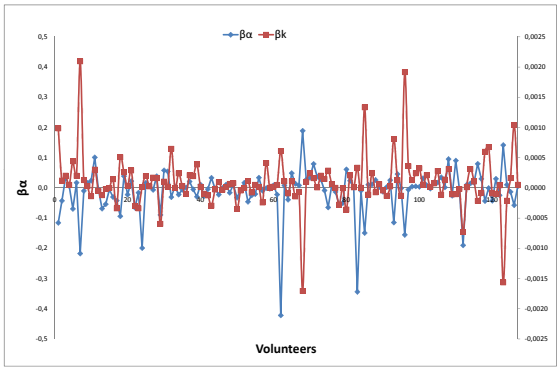

Figure 3.30: Trend of β_α and β_k for all 127 volunteers.

Biomechanical parameters and statistical analysis

Statistical analyses were performed in order to investigate whether intrinsic factors such as age, weight, height, hour of physical activity influenced HPCI, E and EDR, and whether there was a statistical significant difference between males and females in all three biomechanical parameters. Values of E and EDR are considered when calculated without and with correction.

The best fitted regression model for all volunteers with HPCI as response variable included age, gender and the interaction between age and gender as explanatory variables. This model showed that gender (P-value = 0.0476) and interaction between gender and age (P-value = 0.0293) were statistically significant, while age was not a significant variable (P-value = 0.3468).
The fitted regression model for all males included age (P-value $<$ 0.001) as the only statistically sig-

nificant explanatory variable, while that one for all females included none of the intrinsic factors as explanatory variables but only a constant.
Plots of HPCI as a function of subject factors are shown in Appendix D1. Table 3.2 shows results of UHPT, LHPT and HPCI grouped according to the gender. A statistically significant difference between males and females was found in UHPT and LHPT (P-value = 0.000286 and P-value = 0.00721, respectively), while no statistically significant difference was found in HPCI (P-value = 0.8883).

Table 3.2: Results for UHPT, LHPT and HPCI grouped according to the gender given as mean $\pm$ one standard deviation.

	All	Females	Males
UHPT (mm)	15.20$\pm$2.03	14.59$\pm$1.99	15.80$\pm$1.88
LHPT (mm)	8.99$\pm$1.56	8.61$\pm$1.55	9.35$\pm$1.47
HPCI (%)	59.21$\pm$7.20	59.08$\pm$6.98	59.30$\pm$7.38

The best fitted regression model for all volunteers, with E calculated from stress-strain curves without correction as response variable, included age (P-value = 0.0335) and weight (P-value = 5.65e^{-10}) as explanatory variables.
For all males the best fitted linear regression model included age (P-value = 0.0768) and weight (P-value = 0.00274) as explanatory variables. For all females the model included only weight (P-value$<$0.001) as explanatory variable.

The best fitted linear regression model for all volunteers, with E calculated from stress-strain curves with correction as response variable, included only weight (P-value = 3.63e^{-7})as an explanatory variable.
For all males as well as for all females the best fitted linear regression models included only weight, and it was statistically significant for both groups (P-value = 0.0174 and P-value = 0.0021, respectively).

Plots of E as a function of subject factors are shown in Appendix D2. Table 3.3 shows results of E, grouped according to the gender. A statistically significant difference between males and females was found in E calculated without and with correction (P-value = 1.073e^{-5} and P-value = 0.0003156, respectively).

Table 3.3: Results for elastic modulus grouped according to the gender and given as mean $\pm$ one standard deviation.

Elastic modulus (N/mm^2)		
	Females	Males
no correction	0.066$\pm$0.012	0.077$\pm$0.015
correction	0.076$\pm$0.012	0.085$\pm$0.015

The best fitted linear regression model for all volunteers, with EDR calculated from load-displacement

curve without correction as response variable, included age, weight, height and interaction between age and gender. This model showed that age (P-value = $1.51e^{-6}$) and interaction between age and gender (P-value = 0.000529) were statistically significant, while weight (P-value=0.0735) and height (P-value = 0.101) were not statistically significant.
When considering all males, the linear regression model included age (P-value < 0.001) and weight (P-value = 0.0241) as explanatory variables, while for all females included age (P-value = 0.0822) and height (P-value = 0.0350).

The best fitted linear regression model for all volunteers, with EDR calculated from load-displacement curve with correction as a response variable and age, gender, height, UHPT and interaction between the age and gender as explanatory variables. This model showed that age (P-value = $3.07e^{-7}$), height (P-value = 0.0124), UHPT (P-value = 0.0154) and the interaction between age and gender (P-value = 0.00103) were all statistically significant.
For all males the linear regression model included age (P-value < 0.001) and weight (P-value < 0.001) as explanatory variables, while for all females included age (P-value = 0.00786) and height (P-value = 0.04979).

Plots of EDR as a function of subject factors are shown in Appendix D3. Table 3.4 shows results of EDR grouped according to the gender. No statistically significant difference between males and females was found in EDR calculated without and with correction (P-value = 0.4923, and P-value = 0.5052, respectively).

Table 3.4: Results for Energy Dissipation Ratio grouped according to the gender and given as mean $\pm$ one standard deviation.

Energy Dissipation Ratio (%)		
	Females	Males
no correction	29.4$\pm$3.4	29.8$\pm$3.9
correction	29.7$\pm$3.9	30.2$\pm$4.1

3.6 Discussion

The compression device developed in this study allowed investigating the biomechanical properties of *in vivo* human heel pads in order to create a database for healthy heel pads. This device as well as the procedure applied were not intended to reproduce the conditions of walking and/or running, but rather to minimize any discomfort and sensation of being strapped in order to be usable on survivors of falanga torture.

In order to assess the repeatability and reliability of the measurements, compression tests were first made

on heel pad models. Such tests gave a positive response in terms of both repeatability and reliability, and allowed applying the device on a group of *in vivo* human healthy heel pads. The recorded load-displacement curves exhibited the hysteretic behavior, typical for a visco-elastic tissue. For some of the volunteers these curves were not completely overlapping, even after applying a threshold. The spread in data might be due to:

- rotation and translation of the structure consisting of the heel pad tissue and its support apparatus (the calcaneus and the soft tissue surrounding the heel pad tissue). The support apparatus cannot be completely fixed relatively to the measurement device, thus both rotation and translation of the heel pad tissue might occur;
- muscles in the leg might not be completely relaxed during all measurements. An unconscious pressure against *e.g.* the approaching piston, cannot be completely ruled out.

The two points above could theoretically be further reduced by *e.g.* a vacuum cushion, but the effect on the tissue by a more tight support is unknown. On a more speculative basis, it is not known if the individual components of the heel pad tissue returns exactly to the same position after every trial and neither are the influence of possible variations in liquid content (*e.g.* blood perfusion) known. In order to take into account the involuntary movement of the foot/ankle, a video-processing procedure was developed. This procedure allowed correcting the hysteresis curves and having the effective displacement of the heel pad. Results indicate that no remarkable systematic errors took place during the seven individual recordings, and that the variation among the individual hysteresis curves was smaller than among those of all volunteers. A certain range of variability is, however, unavoidable when investigating *in vivo* tissues, due to the natural variation among people. Furthermore, calculation of both E and HPCI can be affected by uncertainties related to the ultrasound measurements of skin-to-bone distance. It was also not possible to verify whether the volunteer put all bodyweight on the selected heel during the loaded conditions, thus the LHPT might reflect this inaccuracy.
Statistical analyses were necessary in order to evaluate whether subject factors such as age, weight, height, gender, duration of physical activity and heel pad thickness influence the mechanical properties of the heel pad (HPCI, E and EDR).
Literature shows discordant results when dealing with *in vivo* heel pad biomechanics, due to the different methodologies applied as well as the different populations investigated. The present study points out that:

- gender as well as interaction between gender and age play a significant role on HPCI, as indicated by [67];
- weight plays a significant role on E, as indicated by [89];
- age, height, UHPT as well as interaction between age and gender play a significant role on EDR, as indicated by [69];

Furthermore, a statistically significant difference between males and females was found in E (males had higher E than females), but not for EDR nor HPCI.

The group of volunteers, made of 127 subjects, was not numerous enough or scattered enough to make investigations that would clarify whether the difference between males and females was caused by the difference in weight/height or gender. Indeed, weight and height of males and females were statistically different (P-value < 0.001). Such kind of investigations would divide the volunteers into weight-groups (*e.g.* 50 kg vs. 80 kg), but it would be necessary to have a number of males and females with exactly the same weight. This is not an impossible request, but in order to use the results as a representation of all normal healthy people, the sample pool should be more than 100 volunteers for each weight-groups. However, it is biologically not "normal" that males and females have the same weight, so it is uncertain whether results from such a test could really be used to represent the normal healthy population.

This study represents a preliminary analysis applied to healthy subjects, which might be extended to subjects with pathology and, in the present form, can be interpreted as a validation of the overall procedure.

Contributions

This study is the sum of the works carried on by several people. Specifically:

- PhD Antonio Virga from DMTI developed all LabView procedures.
- BSc. students Maja M. Madsen and Sabrina U. Hjørringgaard applied the compression device on the first set of heel pad models and the first group of healthy young volunteers.
- BSc. student Nadège Corbin developed the MATLAB procedure for the video processing.
- MSc. student Maja M. Madsen gave help for the compression tests and carried on the statistical analyses.

CHAPTER

FOUR

STUDY II: Experimental vs. numerical procedure

This chapter describes in details the procedures adopted to deeply investigate the visco-elastic properties of the heel pad by comparing *in vivo* experimental data obtained by using the compression device described in Chapter 3 with finite element analyses conducted on a 3D numerical model.
Papers V, VI, VII and VIII in Appendix E describe the work done on heel pad modeling as well as the comparison between experimental and numerical data.

4.1 Background

The collection of data from compression tests on *in vivo* heel pads might be very useful in order to provide the basis for simulation studies and to have a set of data that can be used as a reference when trying to make conclusions on similar data recorded from diseased heel pads. Load-displacement curves do not give the constitutive law of the material, but only the relationship between the applied force and the corresponding displacement. Therefore, the experimental approach can be investigated and integrated with a computational model of the heel pad. Such a model would allow a better understanding of the stress-strain relationship of the tissues, in order to evaluate phenomena that are not measurable with sufficient accuracy by means of experimental tests. Finite element modeling of the soft tissues of the foot would pave the way for understanding stress-related injuries (*e.g.* plantar fasciitis and diabetic ulceration [6, 106]), as well as improve orthotics and footwear design, considering the stress induced in the plantar region, (*e.g.* distribution of the plantar pressure [72, 92, 107, 108]).
Since the human heel pad is a non-linear visco-elastic tissue, its biomechanical behavior under compression depends on how the load is applied, *i.e.* depends on the strain rate and time [53]. Thus, a 3D simulation of the heel pad combined with the compression test can be used not only to calculate stress

and strain of the material, but also to define the proper load and velocity at which the load must be applied for real investigations. It is important to be aware of the fact that results obtained with the simulations and experimental compression tests may differ; the real compression is indeed applied not only on the heel pad, but the entire foot is involved. Thus, when modeling it is important to analyze very carefully the boundary conditions.
The aims of the present study are:

- to build a three-dimensional quantitative subject-specific heel pad model on the basis of MRI data;
- to compare the load-displacement curves and stress relaxation characteristics obtained by applying a compression device on an *in vivo* healthy heel pad with those obtained from the finite element analysis representing the mechanical behavior of the model when subjected to an external compression.

4.2 Experimental and Numerical procedures

4.2.1 Subject

A 30-year-old European female (body weight=54 kg, height=165 cm) was enrolled. Her left foot underwent both MRI and compression tests. She declared to be in healthy condition, to have an active lifestyle, and to have never had injuries/trauma to any of the feet. She was informed that the test did not involve any harmful procedures or physical pain.

4.2.2 MRI and 3D subject-specific heel pad model

A 3D model of the left heel was built on the basis of the MRI data [3T Siemens Magnetom Trio, Fat-suppressed 3D dual echo steady state (DESS) sequence with $(0.7\ mm)^3$ isotropic resolution, size matrix 320x576x104. TE/TR=5.5/13 ms, flip angle 25°, TA=5 min]. The DICOM images were processed using Simpleware, an imaging density segmentation software that allows obtaining 3D CAD solid model by applying density segmentation techniques (Figure 4.1, on the left). The 3D CAD solid model of the heel region, composed of calcaneus, muscles and plantar fascia, fat pad and skin, was meshed by four hundred thousand tetrahedral elements [109], using the software MSC-Patran (MSC.Software Corporation, Santa Ana, CA), as shown in Figure 4.1, on the right.

4.2.3 Compression device and test procedure

The compression device used for the experimental tests was the same described in Section 3.2. Two sets of measurements were done on the same heel pad:

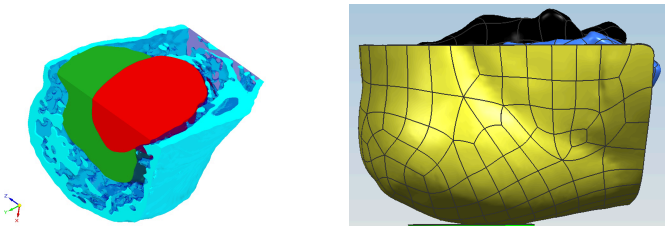

Figure 4.1: 3D model of the heel pad obtained form the segmentation process in Simpleware (on the left). Calcaneus, muscle, fat and skin are in red, green, dark blue and light blue, respectively. 3D CAD solid model obtained in MSC-Patran (on the right).

1. 5 loading/unloading cycles by using a piston of 40 mm in diameter with strain rates of 0.8 mm/s and 1.96 mm/s. Load-displacement curves were recorded by applying experimental and numerical methods (Appendix B, Paper VIII).

2. 5 loading/unloading cycles by using three pistons with diameter of 15, 20 and 40 mm (Figure 4.2), and with a strain rate of 1.73 mm/s. Load-displacement curves and stress relaxation characteristics were recorded by applying experimental and numerical methods (Appendix B, Paper IX).

In the first set of measurements the heel pad was investigated by following the same procedure described in Section 3.2. In the second set of measurements, the heel pad was firstly investigated with three pistons of different diameter (15, 20 and 40 mm) with the same procedure described in Section 3.2, and then stress relaxation characteristics were recorded with all three pistons by applying a specific procedure. Specifically, once one of the two superior limits was reached (40 N for the load, or 9 mm for the displacement), the pistons had a pause of 40 s remaining in contact with the heel pad, and then the decompression started.

Figure 4.2: The three different pistons used for the compression test. From the left, diameter of 15, 20 and 40 mm.

In order to compensate for possible movements of the foot, a video was recorded during each trial of the second set of tests. For the load-displacement curves, the video-processing procedure was the same as described in Section 3.2. In case of stress relaxation characteristics, the procedure was defined after observing that the movement occurred only during the stroke of the piston (either during loading and

unloading), while was negligible during the pause. A 3^{rd} degree polynomial correlation for the movement as a function of time was obtained, both for loading and unloading phase. After synchronizing the video with the load-displacement signal acquired with the maximum horizontal movement, the correction of the loading curve was done by using, as best estimation, the load-displacement characteristic recorded during unloading, since such movement implied a decrease in a load. The same procedure was applied to correct movements during unloading by using the load-displacement characteristic recorded during loading. No correction was necessary during the pause of 40 s, due to the negligible movement of the foot revealed by the recorded videos.
The program made with LabView described in Section 3.2 was used to calculate the EDR from each load-displacement curve as well as stress relaxation characteristics.

4.2.4 Constitutive formulation of the heel pad model

A linear elastic model was adopted to describe the mechanical properties of the bone [110], while the muscles and plantar fascia were described using a hyperelastic formulation [107]. Specific constitutive models were adopted for calcaneal fat pad and skin. Taking into account the typical features of fat pad tissue mechanical response, such as the material and geometric non-linearity, as well as the almost incompressible behavior and time dependent response [109, 111] a specific visco-hyperelastic constitutive model was considered. According to experimental and histological evidence, a fiber-reinforced hyperelastic model was adopted to interpret the mechanical behavior of heel skin tissues, which accounts for different contributions from isotropic ground matrix and fibers. A transversally isotropic material scheme was assumed. The constitutive parameters of the fat pad tissues and skin were found by analyzing in vitro and in vivo tests developed by [112] and [113] such as described in [109, 111]. Detailed information about the constitutive analysis of different tissues can be found in Paper VII of Appendix E.
The numerical analyses were developed in order to investigate the visco-elastic phenomena within the heel tissues, according to the experimental conditions performed in both sets of tests. Three numerical models of the pistons (40, 20 and 15 mm in diameter) were developed and positioned under the heel skin as done in the experimental tests. The superior surface of the calcaneus was fully fixed and the piston was moved upward to the plantar skin. The contact between heel skin and indenter was modeled by a standard coulomb algorithm, according to a friction coefficient of 0.42 [114, 115].
In order to match the conditions of the experimental tests, the numerical analyses were computed considering a strain rate of 0.80 mm/s and 1.96 mm/s for the first set of measurements, while 1.73 mm/s for the second one. When the stress-relaxation phenomena were investigated (second set of tests), the piston remained in contact with the heel pad for 40 s once it reached the displacement of 9 mm, and then the decompression started. Further numerical analyses were computed to measure the viscous recovery phenomena of the heel pad after a simple loading-unloading cycle. The numerical analyses were developed considering the three pistons (40, 20, and 15 mm in diameter). After the loading-unloading cycle, strain recovery phenomena were investigated for one minute time.

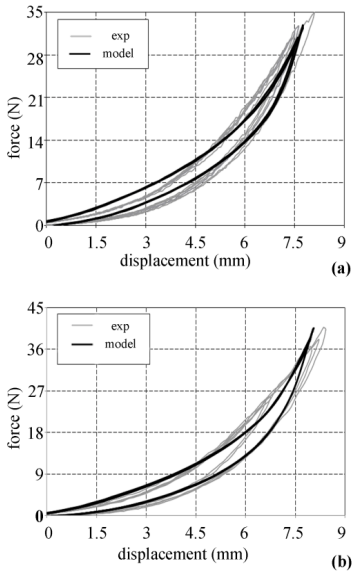

Figure 4.3: Compression tests with a 1 minute-break between each cycle. Comparison of experimental (grey lines) and model (black lines) hysteresis for five cycles of loading and unloading compression tests with cylindrical piston: (a) 0.80 mm/s strain rate tests and (b) 1.96 mm/s strain rate tests.

4.3 Results

First set of measurements

Figure 4.3 shows the experimental load-deformation curves compared with those obtained from the finite element analyses. Specifically, the hysteresis obtained by applying five loading-unloading cycles on the heel pad with a velocity of 0.80 mm/s (Figure 4.3 (a), grey lines) and 1.96 mm/s (Figure 4.3 (b), grey lines), were compared to those of the computational model (Figure 4.3 (a) and (b), black lines). The discrepancy between the experimental data and model results is reported as the mean absolute percentage error in terms of loads. The value of the discrepancy at 0.80 mm/s was 0.39%, while at 1.96 mm/s was 0.28%. For the experimental tests, the EDR for the loading rate of 0.80 mm/s and 1.96 mm/s were 25.0 ± 2.0 and 26.0 ± 3.0, respectively. For the finite element analyses, the EDR for the loading rate of 0.80 mm/s and 1.96 mm/s were 23.0 ± 1.0 and 25.0 ± 1.0, respectively. The values were calculated considering the mean of the EDR found for each of the five trials.

Figure 4.4 (a-b) shows the numerical models of heel region and piston. This figure illustrates the details of the proposed numerical model and the initial position of the piston, matching the experimental condition. Deformed configurations of the heel region after compression are reported with regard to minimum principal stretch (Figure 4.4 (c)) and stress fields (Figure 4.4 (d)) for the strain rates of 1.96 mm/s. All contours are reported over a transverse section of the fat pad, reported in Figure 4.4 (a)), and pertain to

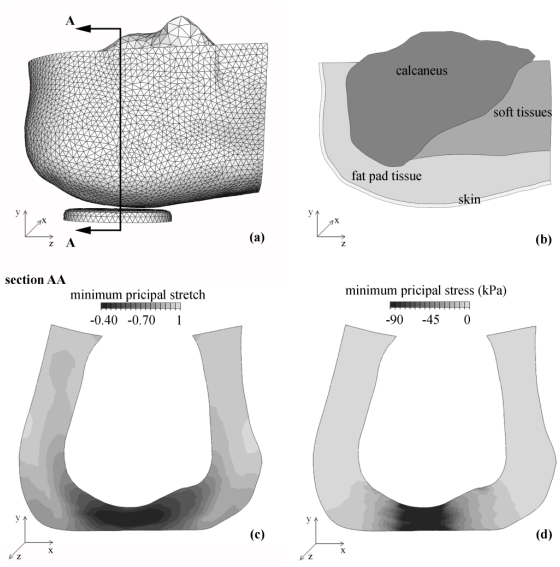

Figure 4.4: (a) Numerical model of heel region with indication of sagittal section AA and (b) longitudinal section to show calcaneus, soft tissues, fat pad tissue and skin. Results from the numerical analysis of compression test on section AA after the first loading: contours of minimum principal stretch field at 1.96 mm/s strain rate (c) and of minimum principal stress fields at 1.96 mm/s strain rate (d).

the configuration achieved when a compression of 8.2 mm is imposed.

Figure 4.5 shows the deformed configuration of fat pad after the first loading-unloading cycle. The minimum principal stretch fields for the analysis with a velocity of 0.80 mm/s (Figure 4.5 (a)) and 1.96 mm/s (Figure 4.5 (b)) are compared. These figures allow evaluation of residual deformation after the loading condition.

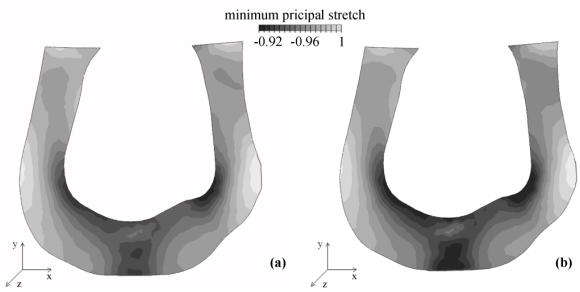

Figure 4.5: Results from the numerical analysis of compression test at (a) 0.80 mm/s and (b) 1.96 mm/s strain rate. Contours of minimum principal stretch in the deformed configuration of heel pad structure after the first cycle of loading-unloading. Contours are reported over a sagittal section AA of heel pad structure (as in Figure 4.4).

Second set of measurements

Figure 4.6 shows the results obtained from experimental tests and numerical analyses. The experimental load-deformation (Figure 4.6(a)) and load-time curves (Figure 4.6(b)), obtained by applying five loading-stress relaxation-unloading cycles on the heel pad with a velocity of 1.73 mm/s (grey lines), are compared with the curves obtained from the numerical analyses (black lines), considering the three different pistons.

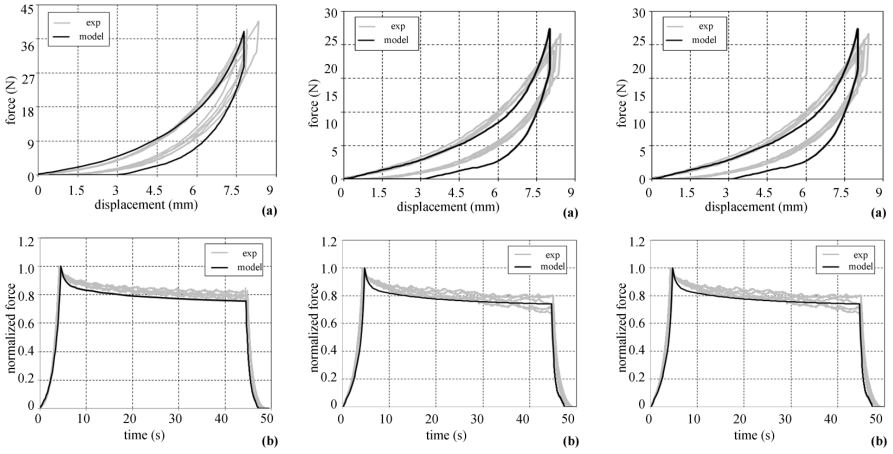

Figure 4.6: From the left, stress relaxation tests done with a piston of 40, 20 and 15 mm in diameter: (a) force vs. displacement and (b) force vs. time.

Figure 4.7 (a) shows the numerical models of heel region and piston and illustrates the details of the proposed numerical model and the initial position of the piston, which is the same for all the pistons. Deformed configurations of the heel region with the piston of 40mm diameter are reported with regard to minimum principal stress (Figure 4.7 (b)) after compression and (Figure 4.7 (c)) after the relaxation period. All contours are reported over a transverse section of the fat pad, reported in Figure 4.7 (a).

Figure 4.8 shows the experimental load-deformation curves compared with the curves obtained from the numerical analyses. Specifically, hysteresis curves obtained by applying five loading-unloading cycles on the heel pad with a velocity of 1.73 mm/s by using the piston with diameter of 40 mm (Figure 4.8 (a), grey lines), 20 mm (Figure 4.8 (b), grey lines) and 15 mm (Figure 4.8 (c), grey lines), were compared to those of the computational model (Figure 4.8 (a), (b) and (c), black lines). The discrepancy between the experimental data and model results is reported as the mean absolute percentage error in terms of loads. The values of the discrepancy by using the piston with diameter of 40 mm, 20 mm and 15 mm were 0.72%, 0.50% and 0.74%, respectively. In order to evaluate the hysteretic response, the energy dissipation ratio (EDR) was calculated for both the experimental and numerical method. Tables 4.1 and 4.2 show the EDR values, expressed as the average plus/minus one standard deviation, calculated for all pistons from the hysteresis and stress relaxation characteristics, respectively.

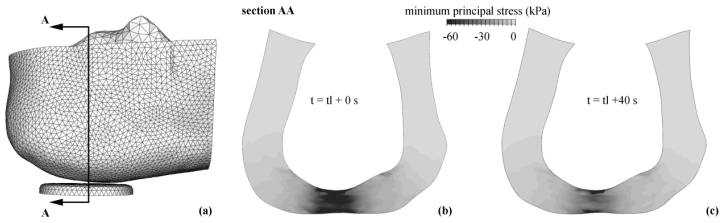

Figure 4.7: (a) Numerical model of heel region with indication of sagittal section AA. Results from the numerical analysis of compression test at 1.73 mm/s strain rate with a piston of 40 mm diameter. Contours of minimum principal stress in the deformed configuration of heel pad structure after a loading: stress relaxation time t=tl+0 seconds (b) and t=t_l+40 s (c), where t_l is the time of loading. Contours are reported over a transversal section AA of heel pad structure.

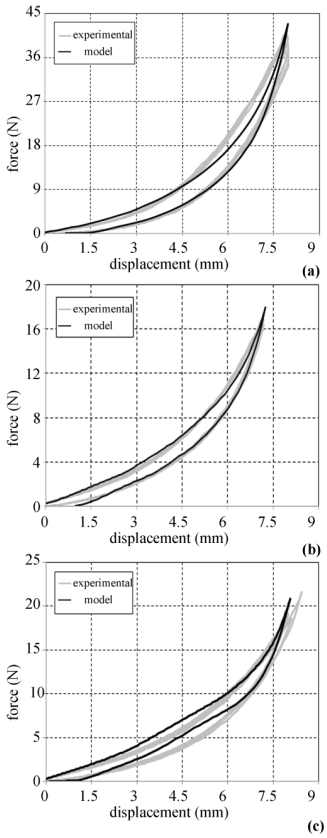

Figure 4.8: Compression tests conducted at 1.73 mm/s of strain rate: force vs. displacement (a) done with a piston of diameter (a) 40 mm (b) 20 mm and (c) 10 mm.

Table 4.1: Energy Dissipation Ratio calculated from the hysteresis obtained from both the experimental and numerical tests by using all pistons (15, 20 and 40 mm in diameter).

	Energy Dissipation Ratio (%)	
Piston Diameter (mm)	Experimental method	Numerical method
15	24.1±1.1	21.6±1.0
20	22.5±1.8	23.0±1.0
40	27.1±2.1	26.0±1.0

Table 4.2: Energy Dissipation Ratio calculated from the stress relaxation obtained from both the experimental and numerical tests by using all pistons (15, 20 and 40 mm in diameter).

	Energy Dissipation Ratio (%)	
Piston Diameter (mm)	Experimental method	Numerical method
15	40.8±3.4	45.6±1.0
20	46.3±3.1	61.0±1.0
40	40.4±4.2	56.4±1.0

Figure 4.9 reports the deformed configurations of the heel region with the piston of 40 mm in diameter. These contours illustrate the viscous recovery phenomena with regard to the minimum principal stretch after a cycle of loading-unloading. The calcaneal fat pad tissues is able to recover the residual deformation in 60 seconds, with a sharp decrease of the stretch in the initial phase.

4.4 Discussion

In this research a healthy subject-specific computational model of the heel pad was developed. The procedure adopted for the definition of constitutive formulation and the evaluation of the constitutive parameters followed the procedure adopted in previous works [109, 110, 111]. The anisotropic characteristics of skin tissues induced by collagen fibers were considered with a fiber-reinforced constitutive model. The visco-hyperelastic model was used for representing calcaneal fat pad tissues with regard to the material and geometric non-linearity, the almost incompressible behavior and time dependent response. These formulations made the model capable of interpreting the typical hysteretic curve of the heel pad under loading/unloading condition. Experimental compression tests and computational simulations followed the same trend, highlighting the reliability of the computational model developed.
Some observations must be made with regard to the experimental procedure. The developed compression device used strain rates as well as loads lower than the peak load present in locomotion (2-3 times the bodyweight), but the 5 seconds of loading are far longer than the duration of the heel pad compression in the gait cycle (0.6 seconds). Furthermore, the foot was stabilized only by using six Velcro straps which

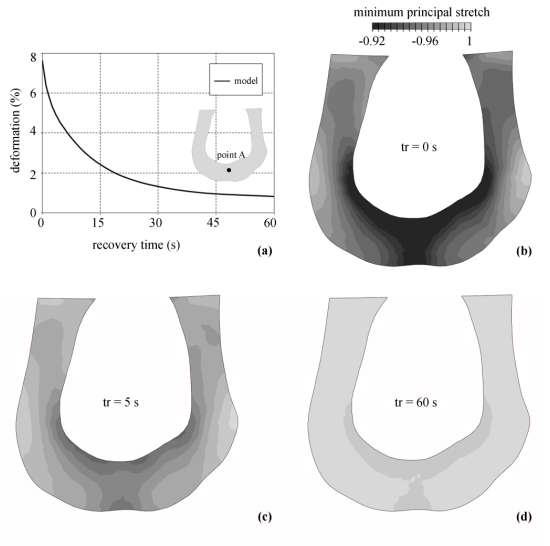

Figure 4.9: Results from the numerical analysis of compression test at 1.73 mm/s strain rate with a piston of 40 mm diameter. Contours of minimum principal stretch in the deformed configuration of heel pad structure after a loading-unloading cycle: viscous recovery time tr=0 seconds (a), tr= 5 s (b) and tr=60 s. Contours are reported over a transversal section AA of heel pad structure.

did not guarantee the immobility of the foot. These features are requirements necessary to make the device be used in clinical setting involving diseased heel pads which cannot necessarily tolerate high loads nor fix the foot.

The experimental load-displacement curves exhibited the hysteresis behavior, typical for a visco-elastic tissue. The five curves recorded in the first set of measurements were not completely overlapping which might be mainly due to the involuntary movement of the foot during each loading/unloading. On the contrary, the finite element analysis is not influenced by these external conditions and the five curves overlap. Some small differences between the five numerical/experimental curves must be associated to the not complete recovery of the stretches.

In the second set of measurements the visco-elastic nature of the *in vivo* human heel pad was investigated. Even in this case, experimental compression tests and computational simulations followed the same trend, highlighting the reliability of the computational model developed. In order to investigate the involuntary movements of the foot and compensate for those, videos were recorded during each compression test and a marker-video-procedure was applied to calculate the ankle movements. Such procedure allowed correcting both load-displacement curves and stress relaxation characteristics obtained, and having a more precise and realistic comparison with the curves obtained from the finite element analyses which are not influenced by these external conditions.
In literature, few experimental tests investigated on the stress relaxation response of heel pad tissues.

Some notes are reported with regard to experimental tests developed on in vitro calcaneal fat pad specimen [112, 116, 117] in order to quantify the visco-elastic tissue properties. These results show the capability of the tissue to recover the stress quickly. However, these results are specific of the fat pad tissue and do not involve the whole structure of heel region. Furthermore, it is well known that there is a big variation among results obtained from *in vivo* and *in vitro* investigations [113].

The numerical model developed in this study might be used for evaluating loading conditions which are not possible with experimental tests. For example, a small recovery time between each trial or different displacements and forces imposed, allowing for a more detailed evaluation of the mechanical behavior of heel pad tissues under loading. Moreover, the numerical results allow for the investigation of the mechanical response of the calcaneal fat pad after a cycle of loading/unloading. The results showed a distribution of residual stretches and stresses, pointing out the visco-elastic response.

The Energy Dissipation Ratio (EDR) is a measure of the energy lost by viscous friction within the tissue [83]. The higher the EDR, the more energy is absorbed by the heel pad. Few studies [43, 45, 56, 61, 69, 72, 82, 83, 89, 90, 93] investigated on EDR of the *in vivo* heel pads in both healthy and diseased conditions, but unfortunately the numerical results are not comparable due to the different number of subjects investigated and methods used. Within these studies the percentage energy dissipation ratio ranged between from 23.7±6.9 [43, 61] and 84.6±6.2 [89]. In the present study percentage energy dissipations for the experimental tests, at the loading rate of 0.80 mm/s and 1.96 mm/s were 25.0±2.0 and 26.0±3.0, respectively. For the finite element analyses, the EDR at the loading rate of 0.80 mm/s and 1.96 mm/s were 23.0±1.0 and 25.0±1.0, respectively. When using different pistons, the EDR for the experimental procedure ranged between 22.5±1.8 (diameter piston of 20 mm) and 27.1±2.1 (diameter piston of 40 mm) for load-displacement curves, while between 40.4±4.2 (diameter piston of 20 mm) and 46.3±3.1 (diameter piston of 40 mm) for the stress relaxation characteristics, all recorded with a strain rate of 1.73 mm/s. The percentage energy dissipations for the numerical simulations ranged between 21.6±1.0 (diameter piston of 15 mm) and 26.0±1.0 (diameter piston of 40 mm) for the load-displacement curves, while between 45.6±1.0 (diameter piston of 15 mm) and 61.0±1.0 (diameter piston of 20 mm) for the stress relaxation characteristics. Due to the complexity of the structure under investigation, it would not be accurate to correlate the dimension of the diameter with the EDR, even though the results obtained from the finite element analyses would suggest that the larger the diameter, the higher the EDR. The lack of correlation in case of experimental investigations might be due to the inhomogeneous structure of the *in vivo* heel pad, as it is made of neuronal, vascular, fibrous and elastic components which are intertwined with fat cells [13]. Consequently, large piston may be used to analyze the mechanical properties of whole structure of heel pad and the results are determined predominantly by the least stiff material within the structure, i.e. calcaneal fat pad. On the contrary, small piston allows the identification of the mechanical properties of limited region and the affected tissues, i.e. calcaneal fat pad and skin. A study [53] report similar considerations, saying that the large probe loading process may be likened to uniaxial bulk compression, while the small probe loading process may cause localized deformation of the superficial region

of the heel and could be likened to indentation.

The discrepancy between the experimental data and finite element analyses is reported as the mean absolute percentage error in terms of loads. In the first study, the discrepancy at 0.80 mm/s was 0.39%, while at 1.96 mm/s was 0.28%. in the second study, the values of discrepancy were 0.72%, 0.50% and 0.74% by using pistons with diameter of 40 mm, 20 mm and 15 mm, respectively.

Numerical analyses allowed for the quantification of viscous recovery after a specific loading condition. Indeed, in this study results show the capability of the heel region to recovery completely the residual deformation in one minute. This confirms that the one-minute-break applied between each trial of the experimental tests is a reasonable choice.

This research represents a preliminary analysis applied to a healthy subject, which can be extended to patients with a pathology and, in the present form, can be interpreted as validation of the overall procedure. This analysis may be useful for patients, firstly evaluating the mechanical properties of the heel pad tissues using experimental tests and successfully implementing a numerical model capable of interpreting the mechanical response of the tissues by means of a damage model accounting for degenerative processes.

Contributions

This study is the sum of the works carried on by several people. Specifically:

- PhD student Chiara Giulia Fontanella from the Center of Mechanics of Biological Materials, University of Padua, developed the numerical model of the heel pad on the basis of MR images recorded at Hvidovre Hospital, Copenhagen, and conducted all the finite element analyses.
- PhD Antonio Virga developed all the procedures in LabView.
- BSc. student Nadège Corbin developed the procedure in MATLAB to be used for the video-processing.

CHAPTER

FIVE

STUDY III: US and MRI investigations

Ultrasound and Magnetic Resonance Imaging are the two imaging techniques most used for soft tissue investigations. This chapter focuses on the comparison between these two clinical imaging modalities in order to investigate their reliability when dealing with heel pad thickness measurements. Both *in vivo* human heel pads and heel pad models have been investigated.
Paper IX in Appendix E describes part of procedures and results presented in this chapter.

5.1 Background

The human heel pad thickness, defined as the shortest distance between the calcaneus and heel skin, is one of the intrinsic factor that must be taken into account when investigating the biomechanics of the heel pad [9, 10]. Indeed, heel pad thickness has been reported to be an important factor in determining stresses observed in healthy as well as pathological feet [9, 10]. Ultrasound (US), Magnetic Resonance Imaging (MRI), Computer Tomography (CT), and X-ray can be used to measure the heel pad thickness. Among those, US (portable, fast scanning time, ionizing-free radiations, low expense), and MRI (ionizing-free radiations) are preferable choices. For US however, measurement errors may occur due to the operator-dependability, the uncertainty of the speed of sound in heel pad tissues as well as the presence of artifacts and angle-dependence. It is, thus necessary to verify the reliability of the measurements by comparing results with a true value. The biggest challenge is related to the *in vivo* human heel pads, as it is not possible to obtain an *in vivo* true value. In principle, CT examinations might be used to find such true value, but due to the ionizing radiations they cannot be considered especially when dealing with healthy subjects. For this reason, PVA-cryogel, a suitable material for mimicking the human soft tissues and compatible to both MRI and US imaging [118], was chosen to build artificial heel pad phantoms.

5.2 *In vivo* investigations

5.2.1 Subjects

Two healthy subjects (one male and one female) were enrolled. Their anthropometric characteristics are shown in Table 5.1. Both subjects were volunteers with an active life style, and with a history of no injuries on their feet. Their left foot was investigated with both US and MRI.

Table 5.1: Anthropometric characteristics of the two subjects under investigation.

	Female	Male
Age (years)	30	48
Weight (kg)	54	70
Height (m)	1.65	1.82
BMI (kg/m^2)	19.85	21.14
Physical activity (hours/week)	7	4

5.2.2 Imaging processing

US measurements

The heel pad of both volunteers was scanned by an experienced doctor with a 3D US transducer (LOQIQE9-GE Healthcare, 14MHz). The procedure used for recording the UHPT was the same as described in Section 3.3. Figure 5.1 shows the heel pad in the three planes acquired by the 3D transducer (a) transverse, b) coronal and c) sagittal). All US images were saved in DICOM format and processed with MATLAB.

The codes `Load3DUSData.m` and `ViewImages.m`, developed by GE Healthcare, were used to extract and visualize the results. The heel pad thickness was calculated by using the relation between the penetration depth (a measure of how deep the ultrasound beam can penetrate into a material) and pixel values. The penetration depth was extracted from the images and was used to calculate the UHPT as follows:

$$UHPT = \frac{l * d}{p} \tag{5.1}$$

where l is the length of the measured dotted line in pixel, d is the penetration depth and p is the total pixel depth value.

US images were analyzed firstly in the transverse plane, where the peak of the calcaneus was located and marked with a green circle, as shown in Figure 5.2 (lower image). This peak-point indicated the coordinates in both coronal and sagittal planes, so that the calcaneus could be located with accuracy in all

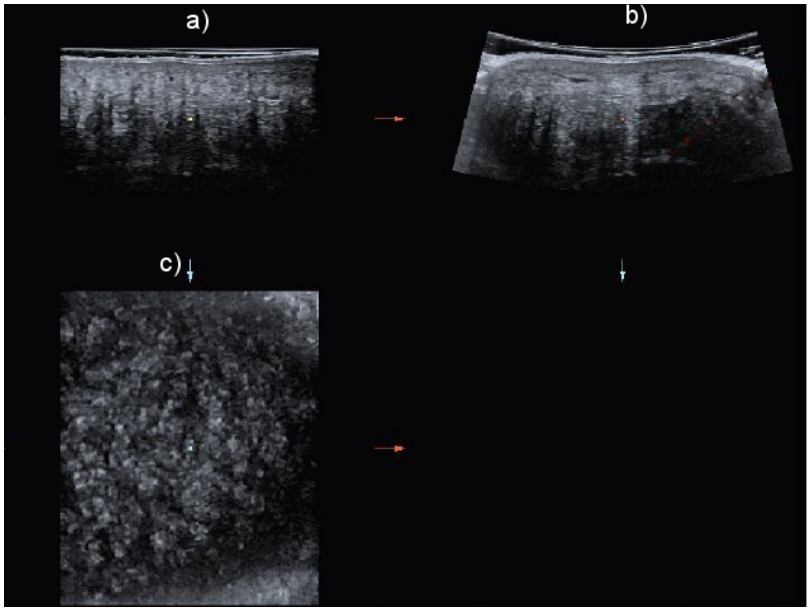

Figure 5.1: 3D US images of the heel pad in the three planes: a) transverse, b) coronal and c) sagittal)

three planes. The upper green circles of Figure 5.2 (top images) indicated the skin, while the lower green circles located the peak of the calcaneus. The dotted line connecting the two circles represented the heel pad thickness.
Due to MATLAB reconstruction, the images exhibited some deformations. However, the heel pad thickness measurements were not influenced as the ratio between the vertical pixel depth and penetration depth was unchanged.

MRI measurements

The two heel pads were also scanned with a 3T Siemens Magnetom Trio scanner. Each volunteer laid down with the heel pad completely relaxed and raised with a proper support, in order to avoid any compression on the heel pad. Two different sequences were applied on the heel pads:

- Female: Fat-suppressed 3D dual echo steady state (DESS) sequence with 0.7 mm^3 isotropic resolution, size matrix 320x576x104. TE/TR=5.5/13 ms, flip angle 25°, TA=5 min.
- Male: T1-weighted 3D gradient echo sequence (FLASH) with 0.7 mm^3 isotropic resolution, size matrix 320x576x104. TE/TR=4.7/14.7 ms, flip angle 25°, TA= 5 min.

For both sequences the slice thickness was 0.52 mm, while the Voxel size in-plane was $(0.65\ mm)^2$.

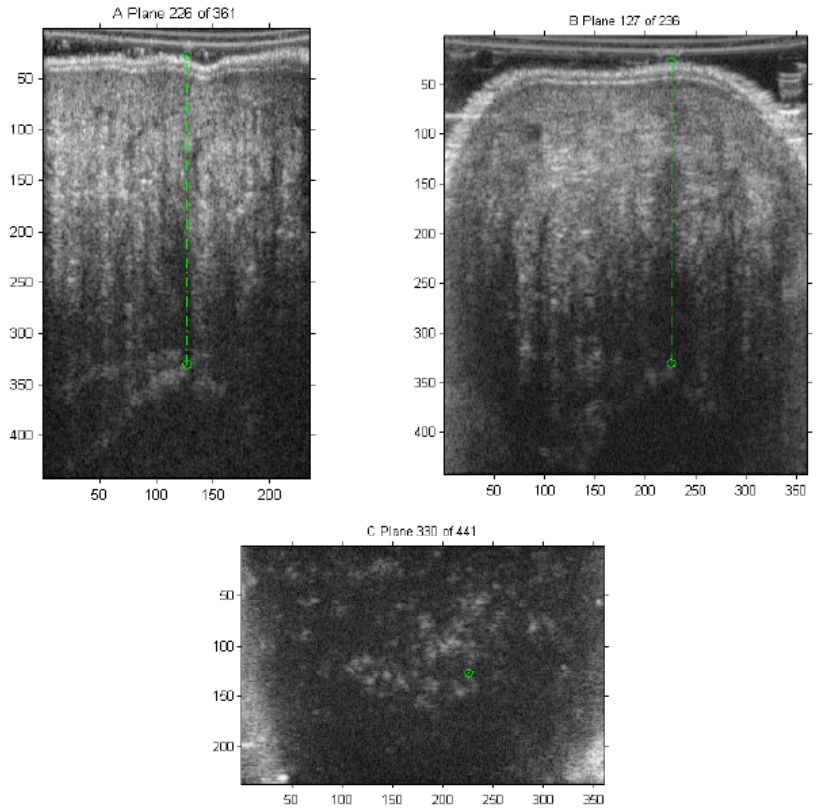

Figure 5.2: Images selected to measure the heel pad thickness of female subject. Planes A, B and C indicate the sagittal, coronal and transverse planes, respectively. The upper green circles indicated the skin, while the lower green circles located the peak of the calcaneus. The dotted line segment between circles represented the heel pad thickness.

The foot of one of the volunteers is shown in Figure 5.3 in the three planes extracted from the 3D images (from left: sagittal, transverse and coronal plane). All 3D MR images, saved in DICOM format, were processed with MATLAB SIS toolbox developed by J.E. Wilhjelm [119], in order to calculate the heel pad thickness.

All images were rotated 130°anti-clockwise (in order to have the calcaneus in the same position of US images), and zoomed (in order to locate with higher accuracy the peak of the calcaneus), as shown in Figure 5.4. The two yellow crosses indicate the skin surface and the peak of the calcaneus, respectively.

In order to really get the shortest distance between skin and bone, the images were analyzed also in all three planes. The peak of the calcaneus, marked by the yellow cross in Figure 5.5, was located after observation slice by slice in the transverse plane. The coordinates of this point determined the position of the peak of the calcaneus also in the coronal and sagittal planes, so that the skin-to-bone could be measured.

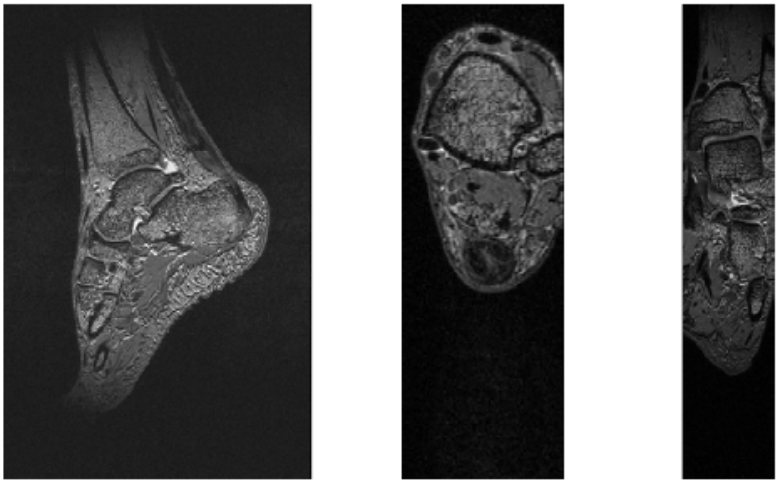

Figure 5.3: MR images of the human foot of one of the volunteer (from left: sagittal, transverse and coronal plane)

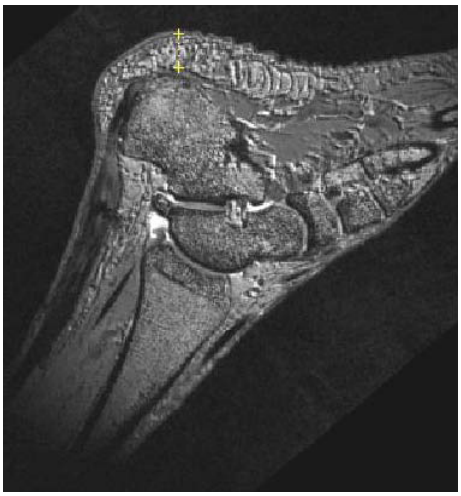

Figure 5.4: Close up image of the heel pad in the sagittal plane. The two yellow crosses indicate the peak of the calcaneus and the skin, respectively.

5.2.3 Results

Results of the measurements for both volunteers are shown in Table 5.2. The heel pad thickness calculated from US images was smaller than the one calculated from MRI. Specifically, the difference between US and MRI was 13.4% and 13.1% for the male and female, respectively.

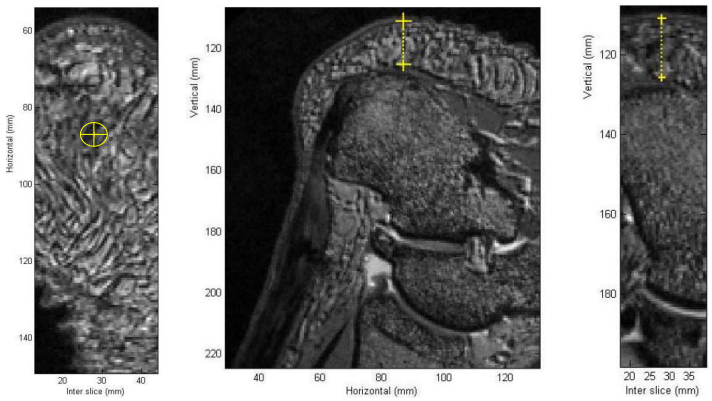

Figure 5.5: Images selected to measure the heel pad thickness in the transversal (on the left) and coronal plane (on the right).

Table 5.2: Heel pad thickness calculated from MRI and US images for both volunteers.

	UHPT (mm)	
	Female	Male
US	14.6	14.9
MRI	16.8	17.2

5.3 Heel pad models investigations

5.3.1 Heel pad models and true value

The first set of heel pad models described in Section 3.2 was investigated. A typical transversal section of the heel pad model is represented in the drawing of Figure 5.6.

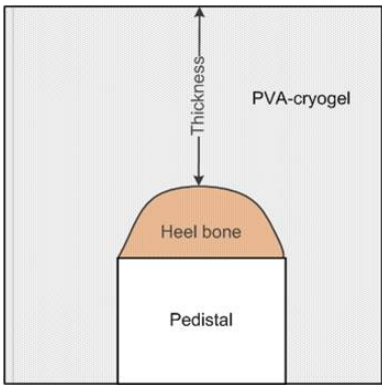

Figure 5.6: Drawing showing a transversal section of the heel pad model.

As already mentioned, the skin-to-bone distance of each model was controlled by adjusting the height of the Plexiglas pedestal on which the plastic calcaneus bone was fixed. However, by increasing the number of freeze/thaw cycles the material becomes stiffer and shrinks. In order to have a true value (TV) of the thickness to be used as a reference when comparing with MRI and US measurements, it was necessary to measure the thickness for each model. Specifically, the skin-to-bone distance was calculated from the physical dimensions of the mould and the phantom, as the difference between the height of the PVA-cryogel cylinder (H2) and the distance bone-pedestal (H1), as shown in Figure 5.7.

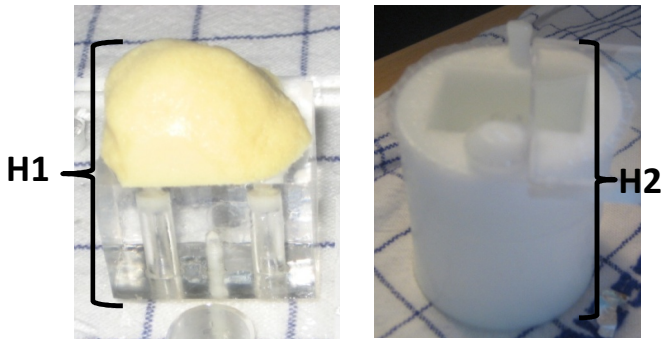

Figure 5.7: Measurement of the distance bone-pedestal (H1) on the left, and the height of the PVA-cryogel cylinder (H2) on the right. The thickness of the model is the difference between H2 and H1.

.

5.3.2 US and MRI

Each heel pad model was scanned from the top by using a high-resolution 3D US transducer (LOGIQE9-GE Healthcare, 12MHz). A water-soluble acoustic gel was spread on top of the model and two images were recorded, with the transducer in both longitudinal and transversal direction, as shown in Figure 5.8. All US images were stored in DICOM format.

All the heel pad models underwent also 3D MRI [3T Siemens Magnetom Verio, T1 Vibe isotropic sequence. TE/TR=5.41/12.4 ms, flip angle 10°, TA=5 min, slice thickness=0.60 mm]. Figure 5.9 shows one of the models placed at the entrance of the MRI scanner. All MR images were stored in DICOM format.

5.3.3 Imaging processing

US images

All US images were processed by using the MATLAB codes `Load3DUSData.m` and `ViewImages.m`, developed by GE Healthcare, in order to extract 3D data and visualize the images. The transverse planes

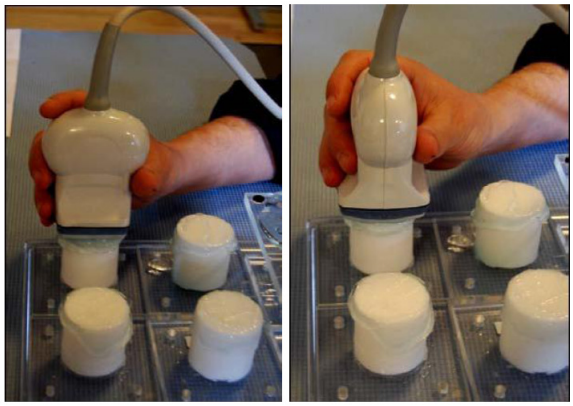

Figure 5.8: US scans on the heel pad models with the transducer in longitudinal (on the left) and transversal position (on the right).

Figure 5.9: One of the heel pad model (marked by the red circle) placed at the entrance of the MRI scanner

(C-planes) were visualized one by one starting by the highest, until the very first image of the top of the calcaneus was visible, as shown in Figure 5.10, on top. The peak coordinates (X and Y) in terms of plane number were found by using the cursor. The thickness of the model, Z_{top}, had to be identified on the images of the planes B and A corresponding to the X and Y coordinates, as shown in Figure 5.10.

The distance between two transverse planes was found as:

$$p = \frac{r}{d} \tag{5.2}$$

where *r* is the penetration depth (available from the output of the function *Load3DUSData*), and *d* is the total number of transverse planes.

These measurements were performed twice for each DICOM file, therefore four measurements were available for each heel pad model. The high cost of the procedure in terms of time (about 30 minutes for

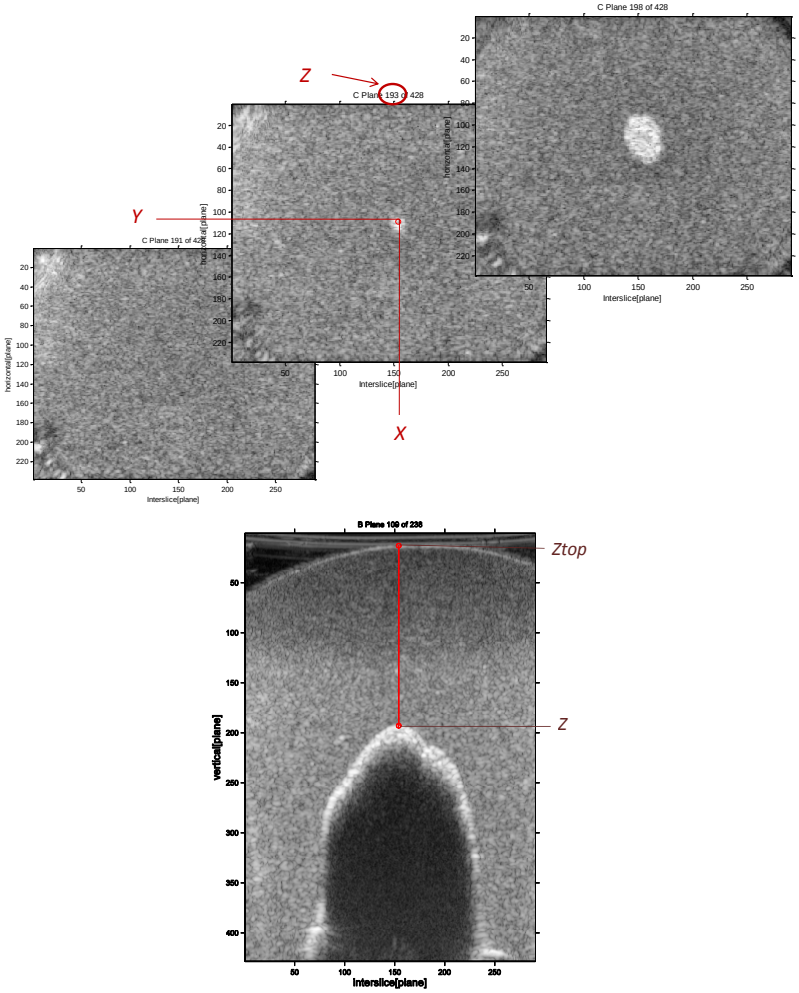

Figure 5.10

each model) and the operator-dependance of the measurements made this manual procedure be replaced by an automatic one. The principle was to obtain a 3D reconstruction of the heel pad model from US images by using the pixel values. Indeed, each image corresponds to a matrix of pixel values (from 0 to 1), which determines the contours of calcaneus and the top of model. Specifically, the calcaneus was represented by pixels with values higher than 0.9, whereas the top of the model by pixels with values higher than 0.6. Each column of each image was read starting by the top, and the first pixels superior to those thresholds were stored. The bone was, thus, reconstructed in a 3D mesh grid and the coordinates of the highest point of calcaneus were found automatically. The skin-to-bone distance was then calculated automatically.

MR images

All MR images were processed in MATLAB following the same procedure explained for US images (manual and automatic methods). Figure 5.11 shows an example of MR images of one of the heel pad models.
In the manual procedure, transverse planes were visualized one by one starting by the highest until the first peak of calcaneus was visible. The scale was in this case directly in millimeter (information available in the DICOM files). Both coordinates of the peak of the calcaneus and the top of the heel pad model were found by visualizing the peak in the three planes.
For MR images the automatic procedure was easier than for US. Indeed, only the PVA-cryogel was white, whereas everything else was black. Therefore, each column of each image was read by starting from the top, and the first and last white pixel were stored.

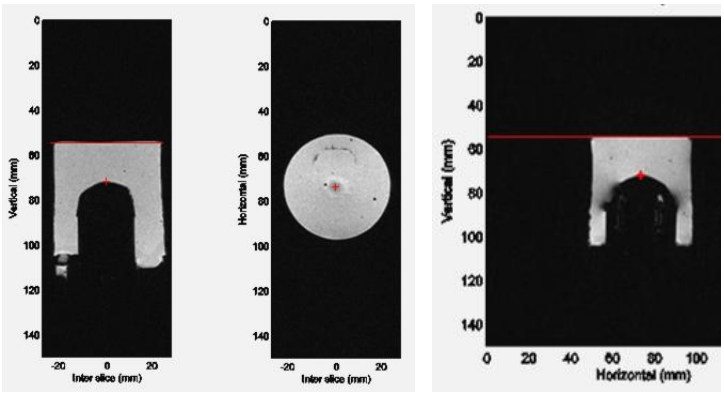

Figure 5.11: Example of MR images of one of the heel pad model. The red line and the red cross indicates the top of the PVA-cryogel and the peak of the calcaneus, respectively.

5.3.4 Statistical analysis

Paired t-test was chosen for statistical analyses, in order to:

- investigate whether there was a significant statistically difference between the two methods (manual and automatic) for both MRI and US images,
- investigate whether there was a significant statistically difference between results obtained from the US/MR technique and the True Value

A P-value$<$0.05 was chosen to indicate a significant statistical difference.

5.3.5 Results

Manual vs. automatic procedure

The manual procedure was applied twice on both US and MR images by the same operator. Specifically, for US the measurements were done twice for both the transversal and longitudinal images. For each model the thickness was calculated as the average between the two measurements. Table 5.3 and Table 5.4 show the thickness measured for each heel pad model from US and MR images, respectively.

Table 5.3: Results obtained by applying the manual method on US images.

	Thickness (mm)						
Heel pad model	US_{T1}	US_{T2}	$Average_T$	US_{L1}	US_{L2}	$Average_L$	$Average_{US}$
1	13.05	13.05	13.05	13.29	13.21	13.25	13.25
2	13.14	13.14	13.14	13.14	13.07	13.11	13.11
3	13.00	12.92	12.96	13.14	13.14	13.14	13.14
4	17.36	17.36	17.36	17.36	17.36	17.36	17.36
5	15.73	15.73	15.73	15.73	15.73	15.73	15.73
6	15.58	15.58	15.58	15.73	15.81	15.77	15.77
7	18.77	18.68	18.73	19.19	19.11	19.15	19.15
8	18.45	18.45	18.45	18.62	18.62	18.62	18.62
9	17.27	17.11	17.19	17.50	17.5	17.50	17.50

US_{T1} and US_{T2} indicate the transversal measurements US_{L1} and US_{L2} indicate the longitudinal measurements

Table 5.4: Results obtained by applying the manual method on MR images.

	Thickness (mm)		
Heel pad model	MRI_1	MRI_2	Average
1	12.59	12.50	12.55
2	12.59	12.60	12.60
3	12.60	12.60	12.60
4	17.28	17.29	17.29
5	15.23	15.23	15.23
6	15.24	14.92	15.08
7	18.74	19.04	18.89
8	17.58	17.86	17.72
9	17.28	17.58	17.40

The nine averages of the thickness calculated from US and MR images from the manual procedure were compared to the nine results returned by the automatic method (shown in Table 5.5). One of the advan-

tages of the automatic procedure was to enable the 3D visualization of both the bone and the top of the model. Figure 5.12 and Figure 5.13 show a typical 3D reconstruction obtained by US and MR images, respectively.

Table 5.5: Results obtained by applying the automatic procedure on both US and MR images.

	Thickness (mm)	
Heel pad model	US	MRI
1	13.01	12.89
2	13.14	12.89
3	13.32	12.30
4	17.29	17.29
5	15.89	15.23
6	15.58	15.53
7	18.86	19.04
8	18.45	18.16
9	17.27	17.58

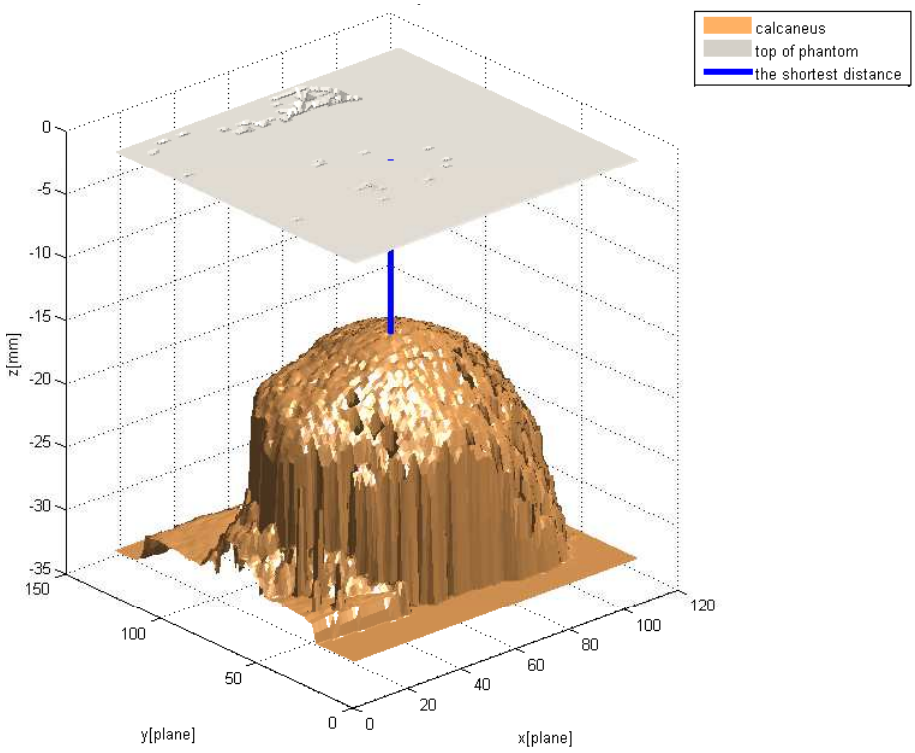

Figure 5.12: Typical 3D reconstruction obtained from US images.

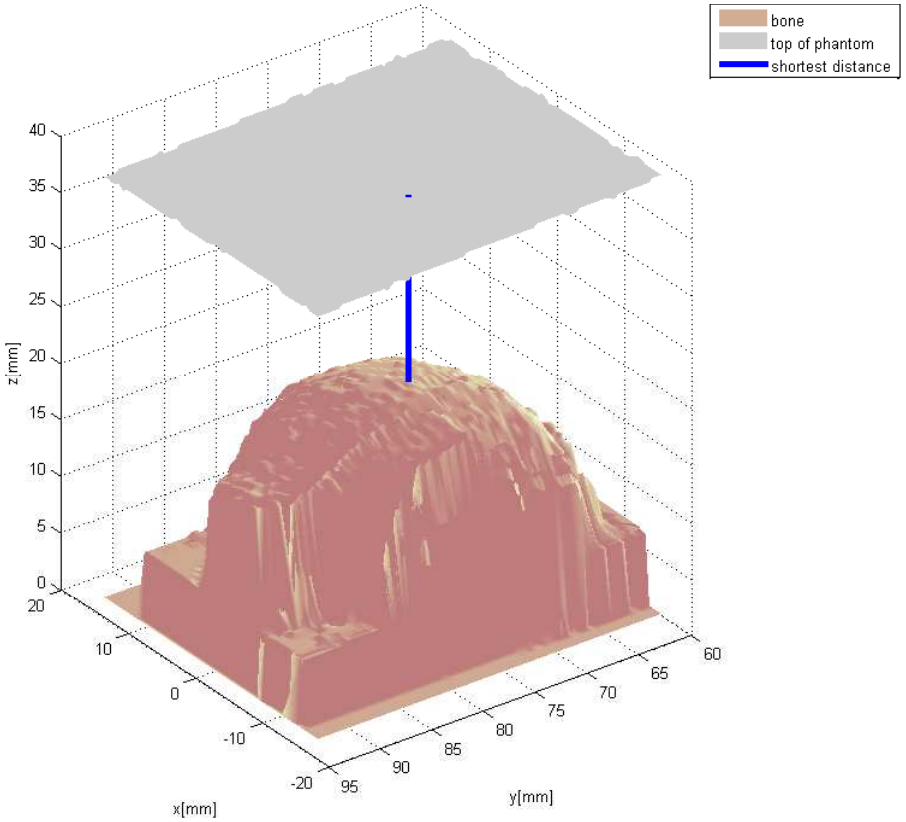

Figure 5.13: Typical 3D reconstruction obtained from MR images.

For both imaging techniques, there was no significant statistically difference between the manual and automatic methods (P-value=0.784 and P-value=0.065, respectively). Thus, the automatic procedure was confirmed to be a reliable method and results obtained were taken into consideration for the comparison with the true values. The automatic measurements, in fact, had the advantages of giving the results in few seconds, and avoiding the operator-dependence.

MRI and US vs. True Value

Once the automatic procedure was validated, it was possible to compare results obtained from both MRI and US images with the True Value (TV). The standard value of the speed of sound used by the ultrasound scanner for human tissue is 1540 m/s, but for PVA-cryogel it ranges from 1520 m/s to 1540 m/s [118]. Therefore, for each heel pad model the thickness was calculated also by using a speed of sound of 1530 m/s. Table 5.6 shows the thickness of all 9 heel pad models measured from US_{1540}, US_{1530}, MRI and TV. Figure 5.14 plots with histograms the values reported in Table 5.6. Figure 5.15 shows for each model the difference (so called error) between the true values and the clinical imaging measurements. It

is clearly visible that MRI overestimated the thickness for five heel pad models out of nine, while US_{1540} overestimated for seven heel pad models out of nine. Furthermore, the thickness calculated with US_{1530} was always lower than US_{1540}, as was expected.

In order to verify whether there was a linear correlation between the clinical imaging measurements and the true values, the error made by US and MRI was plotted as a function of the true values, as shown in Figure 5.16. The statistical analysis showed that there was a statistically significant difference between US_{1540} and TV (P-value=0.008). Furthermore, results showed that there was no statistically significant difference between US_{1530} or MRI and TV (P-value=0.759 and P-value=0.703, respectively) and between MRI and US_{1540} (P-value=0.167).

From Figure 5.16 it can be seen that there was no linear correlation between clinical imaging measurements and the true values.

Table 5.6: Thickness of the heel pad models measured with the automatic procedures, and True values.

	Thickness (mm)			
Heel pad model	US_{1540}	US_{1530}	MRI	TV
1	13.01	12.93	12.89	12.61
2	13.14	13.05	12.89	12.63
3	13.32	13.23	12.30	13.14
4	17.29	17.18	17.29	16.74
5	15.89	15.79	15.23	15.56
6	15.58	15.48	15.53	15.59
7	18.86	18.73	19.04	18.54
8	18.45	18.33	18.16	18.18
9	17.27	17.15	17.58	17.41

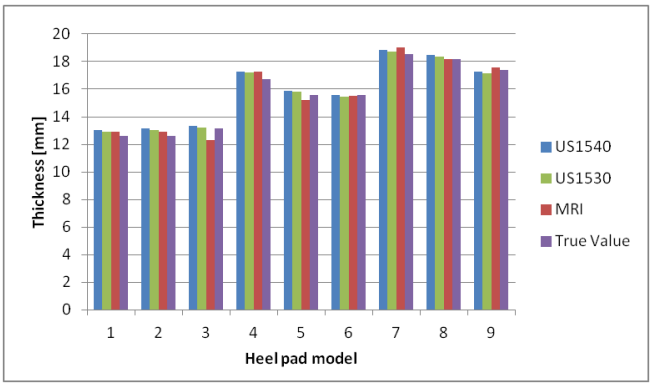

Figure 5.14: Thickness of all 9 heel pad models measured from each technique.

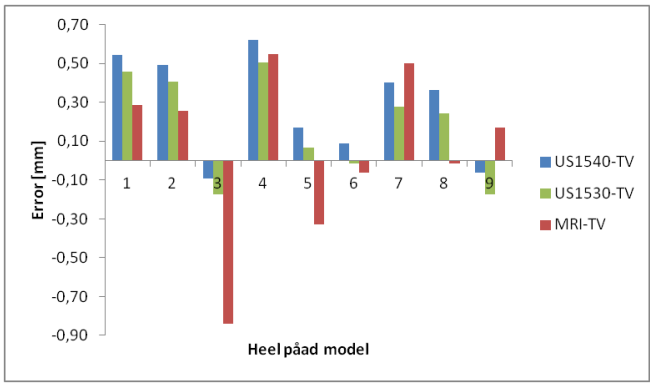

Figure 5.15: Difference of measurements between US or MRI and the true value (TV)

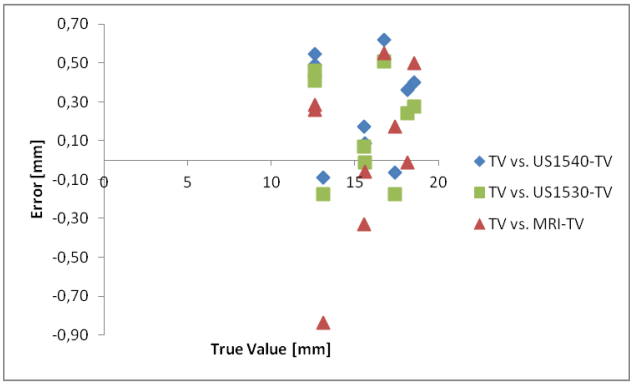

Figure 5.16: The difference of the measurement between the true value and imaging technique (MRI and US) is plotted as a function of the True Value.

5.4 Discussion

The measurements of the thickness of two human *in vivo* heel pads pointed out a discrepancy between US and MRI. Indeed, there was a difference between these two clinical imaging techniques of 13.4% for the female, and 13.1% for the male. Unfortunately, it is not possible to compare such results with a true value nor with CT, so it is difficult to conclude on the measurements reliability. However, some observations must be made. For both heel pads the thickness calculated from US images was smaller than the one obtained from MRI. Two main factors may have played a role in such difference: the uncertainty of the speed of sound in human heel pad tissue as well as the reconstruction of 3D images. Specifically, the surfaces of both heel skin and calcaneus obtained from MRI may not fit those reconstructed from US images leading to a difference between the two measurements.

In MRI, the surfaces are generally problematic as there are susceptibility differences between tissue and air, and between tissue and bone. On the surfaces, signal loss and small distortion could emerge. Since

it is known that heel skin and calcaneus have irregular surfaces, the influence of the signal loss and the distortion at the two surfaces could contribute to the inaccuracy of the measurement. Furthermore, the chemical shift artifact which may cause lipids and water to be displaced in images (amount and directions depend on specific acquisition parameter). Furthermore, MR images were rotated of 130°and some data may have been lost during this process.

Due to all these uncertainties and the lack of a true value, heel pad models needed to be investigated. Even though Figure 5.16 shows that there is no linear correlation between the clinical imaging measurements and the true values, this does not imply the absence of any systematic errors. For US measurements the main uncertainty seems the average speed of sound assumed by the scanner (1540m/s). Error measurements for TV might be reduced by using a true value extracted from μ-CT images by applying the same 3D estimation procedure. In this case 3D reconstruction obtained from MRI, US and μ-CT images should be overlapped in order to verify whether the measurements are done at the same place of the calcaneus. Finally, the error measurements for MRI might be due to the sequence applied, and thus the optimization of it might reduce the uncertainty of the measurements.

The investigations performed on the heel pad models confirms the necessity, once minimized the error measurement before mentioned, to investigate on the real speed of sound for the heel pad tissues, in order to have realistic measurements when dealing with human heel pad.

Contributions

This study is the sum of the works carried on by several people. Specifically:

- Ass. Prof. Lars G. Hanson from Hvidovre Hospital performed MRI on *in vivo* feet.
- Dr. Rasmus Bouert from Frederiksberg Hospital performed both MRI and CT scans on all models.
- BSc. students Ye Liu and Yuqiao Zheng developed the procedures in MATLAB to be used for the manual calculation of the thickness from US and MRI applied on two *in vivo* heel pads.
- BSc. student Nadège Corbin developed the procedures in MATLAB to be used for manual and automatic calculations of the thickness of heel pad models from US and MRI.

CHAPTER

SIX

PROJECT CONCLUSIONS

A new apparatus capable of investigating the mechanical properties of *in vivo* human heel pads was developed, and presented in Chapter 3. This apparatus, a so-called compression device, allowed obtaining load-displacement curves which exhibited the characteristic hysteretic behavior typical for visco-elastic materials. The entire approach was not intended to reproduce the physiological condition of walking and/or running, but it was designed to minimize any discomfort and any sensation of being strapped in order to be a clinical device applicable on pathological feet (*e.g.* survivors of falanga torture). This explains the relative low strain rate applied during the compression/decompression of the heel pad as well as the use of Velcro straps to stabilize the foot and lower part of the leg. As the foot was not completely blocked during the test, involuntary muscular and neuronal movements and/or tensions could not be avoided during the entire procedure, even though the volunteer was asked to remain relaxed. A proper procedure based on video processing was developed in order to calculate the maximum movement of the ankle and to correct the hysteresis curves taking into account such movement.

The reliability of the compression device as well as the repeatability of the measurements were confirmed by results obtained from compression tests applied on heel pad models. Furthermore, a preliminary study conducted on 23 *in vivo* heel pads (Paper III in Appendix E) showed that there was no statistically significant tendency among the individual load-displacement curves, confirming the repeatability of compression tests.

One hundred and twenty seven healthy volunteers (64M-63F) were, thus, enrolled for both compression tests and ultrasound heel pad thickness investigations, so that three biomechanical parameters could be calculated: Heel pad Compressibility Index (HPCI), Elastic modulus (E) and Energy Dissipation Ratio (EDR). The creation of a ”normal” range of biomechanical parameters was necessary in order to investigate in future studies whether there are any differences between healthy and diseased heel pads when dealing with their biomechanics. Indeed, the literature could not be used as a reference for healthy subjects. Even though the heel pad biomechanics has been investigated for more than 25 years in healthy individuals as well as in subjects with diabetes, obesity, heel pain, acromegaly and calcaneal fractures, studies differed both in terms of method applied and population studied, and it is not feasible to compare

the numerical results. In the present study statistical analyses showed that there was a statistically significant difference between males and females in E (males had higher E than females) as reported by [89], but not in EDR nor in HPCI as described by [48, 49, 52]. Furthermore, age, weight, height, gender and UHPT were shown to influence significantly the three biomechanical parameters.
This study represents a preliminary analysis applied to healthy subjects, which might be extended to subjects with pathology and, in the present form, can be interpreted as a validation of the overall procedure. However, some improvements might be carried on before investigating pathological heel pads, such as synchronizing the video-camera with the compression device, *i.e.* using the same control box to drive the entire equipment, and refining the procedure developed to correct the hysteresis.

The compression device was also used to collect *in vivo* experimental data that were compared with results obtained from finite element analyses carried on a 3D subject specific heel pad model, as described in Chapter 4. The geometry of the numerical 3D heel pad model was built on the basis of MRI of the same foot that underwent compression tests, while constitutive parameters describing the fat pad tissues and skin were found by analyzing results available in literature. Experimental load-displacement curves as well as stress relaxation characteristics allowed validating the heel pad model and to further investigate the visco-elastic nature of the heel pad. Computational simulations, indeed, permit to better understand the stress-strain relationship of the tissues, in order to evaluate phenomena that are not measurable with sufficient accuracy by means of experimental tests. The analyses described in this study were applied to one healthy subject, but can be extended to patients with a pathology. This procedure might be useful for patients, firstly evaluating the mechanical properties of the heel pad tissues using experimental tests and successfully implementing a numerical model capable of interpreting the mechanical response of the tissues by means of a damage model accounting for degenerative processes.

The heel pad thickness is a crucial parameter when assessing the elastic properties of the heel pad [9, 10], as it is used to calculate the change in shape of the heel pad due to the compression, and extract the stress-strain characteristics. For this reason it is necessary to investigate on the reliability of the ultrasound measurements of the heel pad thickness by comparing such technique with both MRI and true values (TV), as described in Chapter 5. A preliminary study conducted on two *in vivo* healthy heel pads pointed out a discrepancy between US and MRI with a difference between these two techniques up to 13.4%. Unfortunately, it was not possible to compare the results with a true value. Therefore, US and MRI measurements were performed on heel pad models. Statistical analyses demonstrated that there was a statistically significant difference between US calculated with the standard speed of sound (1540 m/s) and TV, whereas there was not statistically significant difference between MRI and TV as well as between US calculated at 1530 m/s and TV. These results confirmed, once minimized possible error measurements for all techniques, the necessity to investigate on the real speed of sound for the heel pad tissues, in order to have realistic measurements when dealing with human heel pad.

Bibliography

[1] Zimbabwe Human Rights NGO Forum. Only bruises on the soles of their feet! torture and falanga in zimbabwe. Technical report, 2009.

[2] J.G. Kuhns. Changes in elastic adipose tissue. *Bone Joint Surg Am.*, 31:541–547, 1949.

[3] A. Savnick, K. Amris, H Røgind, K. Prip, B. Danneskiold-Samsøe, F. Bojsen-Møller, E.M. Bartels, H. Bliddal, J. Boesen, and N. Egund. Mri of the plantar structures of the foot after falanga torture. *European Radiology*, 10:1655–1659, 2000.

[4] K. Amris, O.V. Rasmussen, T. Baykal, and V. Lök. The diagnostic value of clinical examination after falanga − a pilot validation study. *Journal on Rehabilitation of Torture Victims and Prevention of Torture*, 19(1):33–40, 2009.

[5] G. Altun and G. Durmus-Altun. Confirmation of alleged falanga torture by bone scintigraphy − case report. *International Journal of Legal Medicine*, 117:365–366, 2003.

[6] R. Sopher, J. Nixon, E. McGinnis, and A. Gefen. The influence of foot posture, support stiffness, heel pad loading and tissue mechanical properties on biomechanical factors associated with a risk of heel ulceration. *Journal of the Mechanical Behavior of Biomedical Materials*, 4(4):572–582, 2011.

[7] S.T. Torp-Pedersen, S. Matteoli, J.E Wiljhelm, K. Amris, R. Christensen, J.I. Bech, and B. Danneskiold-Samsøe. Diagnostic accuracy of heel pad palpation - a phantom study. *Forensic and Legal Medicine*, 15(7):437–442, 2008.

[8] K. Prip and A.L. Persson. Clinical findings in men with chronic pain after falanga torture. *The Clinical Journal of Pain*, 24(2):135–141, 2007.

[9] M. Uzel, E. Cetinus, E . Bilgic, H.C. Ekerbicer, and A. Karaoguz. Comparison of ultrasonography

and radiography in assessment of the heel pad compressibility index of patients with plantar heel pain syndrome. *Joint Bone Spine*, 73:196–199, 2006.

[10] Flint A. Haslock I Rome K., Campbell R. Ultrasonic heel pad thickness measurements: a preliminary study. *British Journal of Radiology*, 71:1149–1152, 1998.

[11] M. Backhaus, G.R. Burmester, T. Gerber, W. Grassi, K.P. Machold, W.A. Swen, and et al. Guidelines for musculoskeletal ultrasound in rheumatology. *Annals of the Rheumatic Diseases*, 60:641–649, 2001.

[12] H.L. Steinbach and W. Russell. Measurements of the heel-pas as an aid to diagnosis of acromegaly. *Radiology*, 82:418–423, 1964.

[13] M.H. Jahss, J.D. Michelson, P. Desai, R. Kaye, F. Kummer, W.R. Buschmann, F. Watkins, and S. Reich. Investigationsd into the fat pads of the sole of the foot: anatomy and histology. *Foot & Ankle*, 13:233–242, 1992.

[14] A. Cichowitz, W.R. Pan, and M. Ashton. The heel. anatomy, blood supply, and the pathophysiology of pressure ulcers. *Annals of Plastic Surgery*, 62(4):423–429, 2009.

[15] Mickael S., Lawrence M. R., Erik S., Edward D.L., and Udo S. *Atlas of Anatomy: general anatomy and musculoskeletal system.* 2006.

[16] J.K. Kimani. The structural organization of the connective tissue foot with reference to the histomorphology of the elastic fibre system. *Acta Morphol. Neerl.-Scand.*, 22:313–323, 1984.

[17] W.R. Buschmann, M.H. Jahss, F. Kummer, P. Desai, R.O. Gee, and J.L. Ricci. Histology and histomorphometric analysis of the normal and atrophic heel fat pad. *Foot & Ankle International*, 16:254–258, 1995.

[18] F. Bojsen-Moller. *Biomechanics of heel pad and plantar aponeurosis. In: disorders of the heel, rearfoot and ankle.* New York: Churchill Livingstone, 1999.

[19] C.C. Hsu, W.C. Tsai, C.L Wang, S.H. Pao, Y.W. Shau, and Y.S. Chuan. Microchambers and macrochambers in heel pads: Are they functionally different? *Journal of Applied Physiology*, 102:2227–2231, 2007.

[20] A.N. Natali, E.L. Carniel, and P.G. Pavan. Modelling of mandible bone properties in the numerical analysis of oral implant biomechanics. *Computer Methods Biomech Biomed Engoot & Ankle*, 100(2):158–165, 2010.

[21] E. Blechschmidt. The structure of the calcaneal padding. *Foot & Ankle*, 2:260–283, 1982.

[22] M.H. Jahss, F. Kummer, and J.D. Michelson. Investigationsd into the fat pads of the sole of the foot: heel pressure studies. *Foot & Ankle*, 13(5):227–232, 1992.

[23] A. Tietze. Concerning the architectural structure of the connective tissue in the human sole. *Foot & Ankle*, 2:252–259, 1982.

[24] W.E. Miller. The heel pad. *The American Journal of Sports Medicine*, 10:19–21, 1982.

[25] R.B. Resnick, L.C. Hudgins, W.R. Buschmann, F.J. Kummer, and M.H. Jahss. Analysis of the heel pad fat in rheumatoid arthritis. *Foot & Ankle International*, 20(8):481–484, 1999.

[26] P.F. Kao, B.L. Davis, and P.A. Hardy. Characterization of the calcaneal fat pad in diabetic and non-diabetic patients using magnetic resonance imaging. *Magnetic Resonance Imaging*, 17(6):851–857, 1999.

[27] J. Tong, C.S. Lim, and O.L. Goh. Technique to study the biomechanical properties of the human calcaneal heel pad. *The Foot*, 13:83–91.

[28] J.M. Olefsky and R.S. Sherwin. Diabetic mellitus management and complications. 1999.

[29] P.D. Brash, J. Foster, W. Vennart, P. Anthony, and J.E. Tooke. Magnetic resonance imaging techniques demonstrate soft tissue damage in the diabetic foot. *Diabetic Medicine*, 16:55–61, 1999.

[30] J. Bencardino, Z.S. Rosemberg, and E. Delfault. Mr imaging in sport injuries of foot and ankle. *Magnetic Resonance Imaging Clinic N American*, 7:131–149, 1999.

[31] J.A. Narvaez, J. Narvaez, R. Orthega, C. Aguilera, A. Sanchez, and E. Andia. Painful heel: Mr imaging findings. *Radiographics*, 20:333–352, 2000.

[32] K.M. Lazzarini, R.N. Troiano, and R.C. Smith. Can running cause the appareance of marrow edema on mr images of the foot and ankle? *Radiology*, 202:540–542, 1997.

[33] T.R. Yochum and M.S. Barry. Bone marrow edema caused by altered pedal biomechanics. *J. Man Phys. Ther.*, 20:56–59, 1997.

[34] M.F. Ker. The time-dependent mechanical properties of the human heel pad in the context of locomotion. *J. Exp. Biol.*, 199:1501–1508, 1996.

[35] K. Rome, R. Campbell, A. Flint, and I. Haslock. Heel pad thickness - a contributing factor associated with plantar heel pain. *Foot & Ankle International*, 23(2):142–147, 2002.

[36] K. Rome, P. Webb, A. Unsworth, and I. Haslock. Heel pad stiffness in runers with plantar heel pain. *Clinical Biomechanics*, 16:901–905, 2001.

[37] S.D. Karr. Subcalcaneal heel pain. *Orthop Clin North Am*, 25:161–173, 1994.

[38] A.B. Thomsen, J. Eriksen, and K. Smidt-Nielsen. Chronic pain in torture survivors. *Forensic Science International*, 108:155–163, 2000.

[39] Office of the high commissioner for human rights. *Istanbul Protocol. Manual on the effective investigation and documentation of torture and other cruel, inhuman or degrading treatment or punishment*. United Nations, Geneva, Switzerland, 1999.

[40] O.V. Rasmussen, S. Amris M. Blaauw, and L. Danielsen. Medical, physical examination in connection with torture: the musculoskeletal system. *Torture*, 15:37–45, 2005.

[41] K. Amris, S. Danneskiold-Samsøe, S.T. Torp-Pedersen, I. Genefke, and B. Danneskiold-Samsøe. Producing medico-legal evicence: Documentation of torture versus the saudi arabian state of denial. *Journal on Rehabilitation of Torture Victims and Prevention of Torture*, 17(3):181–195, 2007.

[42] K. Amris, H. Bliddal, S. Torp-Pedersen, and K. Prip. Changes in the plantar fascia after falanga torture diagnosed by ultrasound. preliminary results. In *Abstract*, Portland, Oregon, USA, 2001. 5th World Congress on Myofascial Pain and Fibromyalgia.

[43] K. Rome. Mechanical properties of the heel pad: current theory and review of the literature. *The Foot*, 8:179–185, 1998.

[44] T.C. Hsu, C.L. Wang, W.C. Tsai, J.K. Kuo, and F.T. Tang. Comparison of the mechanical properties of the heel pad between young and elderly adults. *Arch Phys Med Rehabil*, 79(9):1101–1104, 1998.

[45] M.W. Whittle. *The use of Viscoelastic Materials in Shoes and Insoles: A review*, 1996.

[46] H. Kinoshita, P.R. Francis, T. Murase, S. Kawai, and T. Ogawa. The mechanical properties of the heel pad in elderly adults. *European Journal of applied physiology and occupational physiology*, 73(5):404–409, 1996.

[47] M.B. Bennett and R.F. Ker. The mechanical properties of the human subcalcaneal fat pad in compression. *J. Anat.*, 171:131–138, 1990.

[48] T.C. Hsu, C.L. Wang, Y.W. Shau, F.T. Tang, K.L. Li, and C.Y. Chen. Altered heel-pad mechanical properties in patients with type 2 diabetes mellitus. *Diabetic Medicine*, 17(12):854–859, 2000.

[49] S. Prichasuk, P. Mulpruek, and P. Siriwongpairat. The heel-pad compressibility. *Clinical Orthopaedics and Related Research*, (300):197–200, 1994.

[50] S. Prichasuk. The heel pad in plantar heel pain. *Journal of Bone and Joint Surgery-British Volume*, 76B(1):140–142, 1994.

[51] U. Kanatli, H. Yetkin, A. Simsek, K. Besli, and A. Ozturk. The relationship of the heel pad compressibility and plantar pressure distribution. *Foot & Ankle International*, 22(8):662–665.

[52] M. Uzel, E. Cetinus, H.C. Ekerbicer, and A. Karaoguz. Heel pad thickness and athletic activity in healthy young adults: A sonographic study. *Journal of Clinical Ultrasound*, 34:231–236, 2006.

[53] A. Turgut, E. Gokturk, N. Kose, S. Seber, B. Hazer, and I. Gunal. The relationship of heel pad elasticity and plantar heel pain. *Clinical Orthopaedics and Related Research*, (360):191–196, 1999.

[54] I.R. Spears and J.E. Miller-Young. The effect of heel-pad thickness and loading protocol on measured heel-pad stiffness and a standardized protocol for inter-subject comparability. *Clinical Biomechanics*, 21(2):204–212, 2005.

[55] A. Gefen, M. Megido-Ravid, and Y. Itzchak. In vivo biomechanical behavior of the human heel pad during the stance of the gait. *Journal of Biomechanics*, 34:1661–1665, 2001.

[56] R. van Deursen. Mechanical loading and off-loading of the plantar surface of the diabetic foot. *Infectious Diseases Society of America*, 39(Suppl.2):87–91, 2005.

[57] W.C. Tsai, C.L. Wang, T.C. Hsu, F.J. Fsieh, and F.T. Tang. The mechanical properties of the heel pad in unilateral plantar heel pain syndrome. *Foot & Ankle International*, 20(10):663–668, 1999.

[58] D. De Clercq, P. Aerts, and M. Kunnen. The mechanical characteristics of the human heel pad during foot strike running: an *in vivo* cineradiography study. *Journal of Biomechanics*, 27(10):1213–1222, 1999.

[59] D.E. Thompson. Pathomechanics of soft tissue damage. *Diabetic foot*, 1983.

[60] W. Ledoux. The biomechanics of the diabetic foot.

[61] K.M. Kho, A.D. Wright, and F.H. Doyle. Heel pad thickness in acromegaly. *British Journal of Radiology*, 43(506):119–125, 1970.

[62] C.L. Wang, T.C. Hsu, Y.W. Shau, and M.K. Wong. Variations in heel pad mechanical properties variation between children and young adults. *J Formos Med Ass*, 97:850–854, 1998.

[63] R.L. Kwan, Y.F. Zheng, and G.L. Cheing. The effect of aging on the biomechanical properties of plantar soft tissue. *Clinical Biomechanics*, 25:601–605, 2010.

[64] S.E. Puckette. Fallibility of heel pad thickness in diagnosis of acromegaly. *Radiology*, 88(5):982–983, 1967.

[65] S.K. Gonticas. Evaluation of diagnostic value of heel pad thickness. *Radiology*, 92(2):304–307, 1969.

[66] S.P. Bohrer and A.C. Ude. Heel pad thickness in nigerians. *Skeletal Radiology*, pages 108–112, 1978.

[67] R. Raja. Heel pad thickness in kenyan africans. *The East African Medical Journal*, 57(3):208–211, 1980.

[68] H. Ozdemir, Y. Soyuncu, M. Ozgorgen, and K. Dabak. Effects of changes in heel fat pad thickness and elasticity on heel pain. *Journal of the American Podiatric Medical Association*, 94(1):47–52, 2004.

[69] K.J. Mickle, B.J. Munro, S.R. Lord, H.B. Menz, and J.R. Steele. Soft tissue thickness under the metatarsal heads is reduced in older people with toe deformities. *Journal of Orthopaedic Research*, pages 1042–1046, 1983.

[70] U. Jørgensen, E. Larsen, and J.E. Varmaken. The hpc-device - a method to quantify the heel pad shock absorbency. *Foot & Ankle*, 10(2):93–98, 1989.

[71] D.M. Jackson. Heel pad thickness in obese persons. *Radiology*, 90(1):129, 1968.

[72] R.K. Mittal. Heel pad thickness in normal nigerians and patients with acromegaly. *East African Medical Journal*, 60(3):156–159, 1983.

[73] J.H. Challis, C. Murdoch, and S.L Winter. Mechanical properties of the human heel pad: a comparison between populations. *Journal of Applied Biomechanics*, 24(4):377–381, 2008.

[74] A. Erdemir, M.L. Viveiros, J.S. Ulbrecht, and P.R. Cavanagh. An inverse finite-element model of heel-pad indentation. *Journal of Biomechanics*, 39(7):1279–1286, 2006.

[75] C.C Hsu, W.C. Tsai, T.Y. Hisao, F.Y. Tseng, Y.W. Shau, and C.L. Wang. Diabetic effect on micochambers amd macrochambers tissue properties in huma heel pads. *Clinical Biomechanics*, 24:682–686, 2009.

[76] G.A. Gooding, R.M. Stress, P.M. Graf, and C. Grunfeld. Heel pad thickness - determination by high-resolution ultrasonography. *Journal of Ultrasound in Medicine*, 4(4):173–174, 1985.

[77] C.Y. Chao, Y.P. Zheng, and G.L. Cheing. Epidermal thickness and biomechanical properties of plantar tissue in diabetic foot. *Ultrasound in Medicine and Biology*, 37(7):1029–1038, 2011.

[78] G.A. Gooding, R.M. Stress, P.M. Graf, K.M. Moss, K.S. Louie, and C. Grunfeld. Sonography of the sole of the foot evidence for loss of foot pad thickness in diabetes and its relationship to ulceration of the foot. *Investigative Radiology*, 21(1):45–48, 1986.

[79] Y.C. Zheng, Y.P. Zheng, Y.K. Choi, K. Wong, S. Chan, and A.F. Mak. Biomechanical assessment of plantar foot tissue in diabetic patients using an ultrasound indentation system. *Ultrasound in Medicine and Biology*, 26(3):451–456, 2000.

[80] O.N. Onwuanyi. Calcaneal spurs and plantar heel pad pain. *The Foot*, 10:182–185, 2000.

[81] W.C. Tsai, M.F. Chiu, C.L. Wang, F.T. Tang, and M.K. Wong. Ultrasound evaluation of plantar fascitiis. *Scandinavian Journal of Rheumatology*, 29:255–259, 2000.

[82] N. Karabay, T. Toros, and C. Hurel. Ultrasonography evaluation in plantar fascitiis. *The Journal of Foot & Ankle Surgery*, 46(6), 2007.

[83] S.C. Wearing, J.E. Smeathers, B. Yates, S.R. Urry, and P. Dubois. Bulk compressive properties of the fat pad during walking: A pilot investigation in plantar heel pain. *Journal of Clinical Biomechanics*, 24:397–402, 2009.

[84] S.C. Wearing, J.E. Smeathers, S.R. Urry, P.M. Sullivan, B. Yates, and P. Dubois. Thickening of the enthesis is correlated with energy dissipation of the plantar fat pad during walking. *Am. J. Sport Med.*, 38:2522–2527, 2010.

[85] M.L. Field, B.H. Greenber, and L.L. Burkett. Roentgenographic measurement of skin and heel-pad thickness in the diagnosis of acromegaly. *The American journal of the medical sciences*, 254(4):528–533, 1967.

[86] P. Falsetti, B. Frediani, C. Acciai, F. Balsi, G. Filippou, and R. Marcolongo. Heel fat pad involvement in rheumatoid arthritis and in spondyloarthropathies: an ultrasound study. *Scandinavian Journal of Rheumatology*, 33:327–331, 2004.

[87] P.S. Kerr, D.A. Silver, K. Telford, H.S Andrews, and R.M Atkins. Heel-pad compressibility after calcaneal fractures − ultrasound assessment. *Journal of Bone and Joint Surgery-British Volume*, 77B(3):504–505, 1995.

[88] A.S. Levy, R. Berkowitz, P. Franklin, M. Corbett, and G.P. Whitelaw. Magnetic resonance imaging evaluation of calcaneal fat pads in patients with os calcis fractures. *Foot & Ankle*, 13(2):57–62, 1992.

[89] D.A. Silver, P.S. Kerr, H.S Andrews, and R.M Atkins. Heel pad thickness following calcaneal fractures − ultrasound findings. *Injury-International Journal of the Care of the Injured*, 25(1):39–40, 1994.

[90] E. Alcantara, A. Forner, E. Ferrus, A.C. Garcia, and J. Ramiro. Influence of age, gender, and obesity on the mechanical properties of the heel pad under walking impact conditions. *Journal of Applied Biomechanics*, 18(4).

[91] R.L. Boros and J.H. Challis. Heel pad properties of males and females. *Medicine and Science in Sports & Exercises*, 35(5):360, 2003.

[92] J.W. Klaesner, M.K. Hastings, D.Q. Zou, C. Lewis, and M.J. Mueller. Plantar tissue stiffness in patients with diabetes mellitus and peripheral neuropathy. *Archives of Physical Medicine and Rehabilitation*, 83(12):1796–1801, 2002.

[93] J.T.M. Cheung and M. Zhang. Parametric design of pressure-relieving foot orthosis using statics-based finite element method. *Med. Eng. Phys.*, 30:269–277, 2006.

[94] T.C. Hsu, Y.S. Lee, and Y.W. Shau. Biomechanics of the heel pad for type 2 diabetic patients. *Clinical Biomechanics*, 17(4):291–296, 2002.

[95] A. Gefen. Plantar soft tissue loading under the medial metatarsals in the standing diabetic foot. *Medical Engineering & Physics*, 25:491–499, 2003.

[96] J. Amis, L. Graham, and C.E. Graham. Painful heel syndrome: radiographic and treatment assessment. *Foot & Ankle*, 9:91–95, 1988.

[97] K. Rome, R. Campbell, A. Flint, and I. Haslock. Reliability of weight-bearing heel pad thickness measurements by ultrasound. *Clinical Biomechanics*, 13:374–375, 1988.

[98] J.Q. Yao and B.B. Seedhom. Ultrasonic measurement of the thickness of human articular cartilage in situ. *Rheumatology*, 38:1269–1271, 1999.

[99] W.D. Middleton and G.L. Melson. Renal duplication artifact in us imaging. *Radiology*, 173:427–429, 1989.

[100] N. Sabir, S. Demirlenk, B. Yagci, N. Karabulut, and S. Cubukcu. Clinical utility of sonography in diagnosing plantar fasciitis. *Journal of Ultrasound in Medicine*, 24(8):1041–1048, 2005.

[101] Mri stands out among soft tissue imaging innovations. *Medical Imaging*, 42(7):1–2, 2006.

[102] V. Campanelli, M. Fantini, N. Faccioli, A. Cangemi, A. Pozzo, and A. Sbarbati. Three-dimensional morphology of heel fat pad: an *in vivo* computed tomography study. *Journal of Anatomy*, 219:622–631, 2011.

[103] K. Holst, H. Liebgott, J.E. Wilhjelm, S. Nikolov, S.T. Torp-Pedersen, P. Delachartre, and J.A. Jensen. Estimation of elasticity in human heel pad phantoms with ultrasound and force measurements. In *Proceeding of International Congresson of Ultrasonic, Santiago del Chile, Chile*, page 185, 2009.

[104] The r project for statistical computing.

[105] R.A. Johnson. *Probability and Statistics for Engineers*. 2005.

[106] N.H. Bingham and J.M. Fry. *Regression: Linear Models in Statistics*. 2010.

[107] Y. Gu, J. Li, X. Ren, M.J Lake, and Y. Zeng. Heel skin stiffness effect on the hind foot biomechanics during heel strike. *Skin Res. Tech.*, 16(3):291–296, 2010.

[108] S. Goske, A. Erdermir, M. Petre, S. Budhabhatti, and P.R Cavanagh. Reduction of plantar heel pressure: insole design using finite element analysis. *Journal of Biomechanics*, 39:2363–2370, 2006.

[109] N. Even-Tzur, E. Weisz, Y. Hirsch-Falk, and A. Gefen. Role of eva viscoelastic properties in the protective performance of a sport shoe: Computational studies. *Bio-Medical Materials Eng.*, 30:289–299, 2006.

[110] A.N. Natali, C.G. Fontanella, E.L. Carniel, and J. Miller-Young. Biomechanical behaviour of heel pad tissue. experimental testing, constitutive formulation, and numerical modelling. *Proc. IME H J. Eng. Med.*, 225:449–459, 2011.

[111] A.N. Natali, C.G. Fontanella, and E.L. Carniel. Constitutive formulation and analysis of heel pad tissues mechanics. *Med. Eng. Phys.*, 32:516–522, 2010.

[112] J. Miller-Young, N.A. Duncan, and G. Baroud. Material properties of the human calcaneal fat pad in compression: experiment and theory. *Journal of Biomechanics*, 35:1523–1531, 2002.

[113] J.E Miller-Young. *Factors affecting human heel pad mechanics: a finite element study.* Doctoral dissertation, Department of Mechanical Engineering, University of Calgary, 2003.

[114] A. Elkhyat, C. Courderot-Masuyer, T. Gharbi, and P. Humbert. Influence of the hydrophobic and hydrophilic characteristics of sliding and slider surfaces on friction coefficient: in vivo human skin friction comparison. *Skin Res. Tech.*, 10:215–221, 2004.

[115] M. Zhang and F.T. Mak. *In vivo* friction properties of human skin. *Prosthet. Orthot. Int.*, 23:135–141, 1999.

[116] W. Ledoux and J. Blevins. The compressive material properties of the plantar soft tissue. *Journal of Biomechanics*, 40:2975–2981, 2007.

[117] S. Pai and W.R. Ledoux. The quasi-linear viscoelastic properties of diabetic and non-diabetic plantar soft tissue. *Annals of Biomedical Engineering*, 39(5):1517–1527, 2011.

[118] K.J.M. Surry, H.J.B Austin, A. Fenster, and T.M. Peters. Poly(vinyl alcohol) cryogel phantoms for use in ultrasound and mr imaging. *Physics in Medicine and Biology*, 49:5529–5546, 2004.

[119] J.E. Wilhjelm. *Guide to the SIS toolbox*. DTU Elektro, Danmarks Tekniske Uiversitet, Ørsteds Plads, Bygning 348, DK-2800, Kgs. Lyngby, 2010.

APPENDIX

- Appendix A: LabView and MATLAB codes used in Study I and II
- Appendix B: Mechanical drawings for assembling compression device
- Appendix C: Volunteers data
- Appendix D: Statistical plots for HPCI, E and EDR
- Appendix E: Papers

APPENDIX A

- Appendix A1: LabView code for data acquisition
- Appendix A2: LabView code for data visualization
- Appendix A3: LabView code for data analysis
- Appendix A4: Matlab code for video-processing

APPENDIX A1

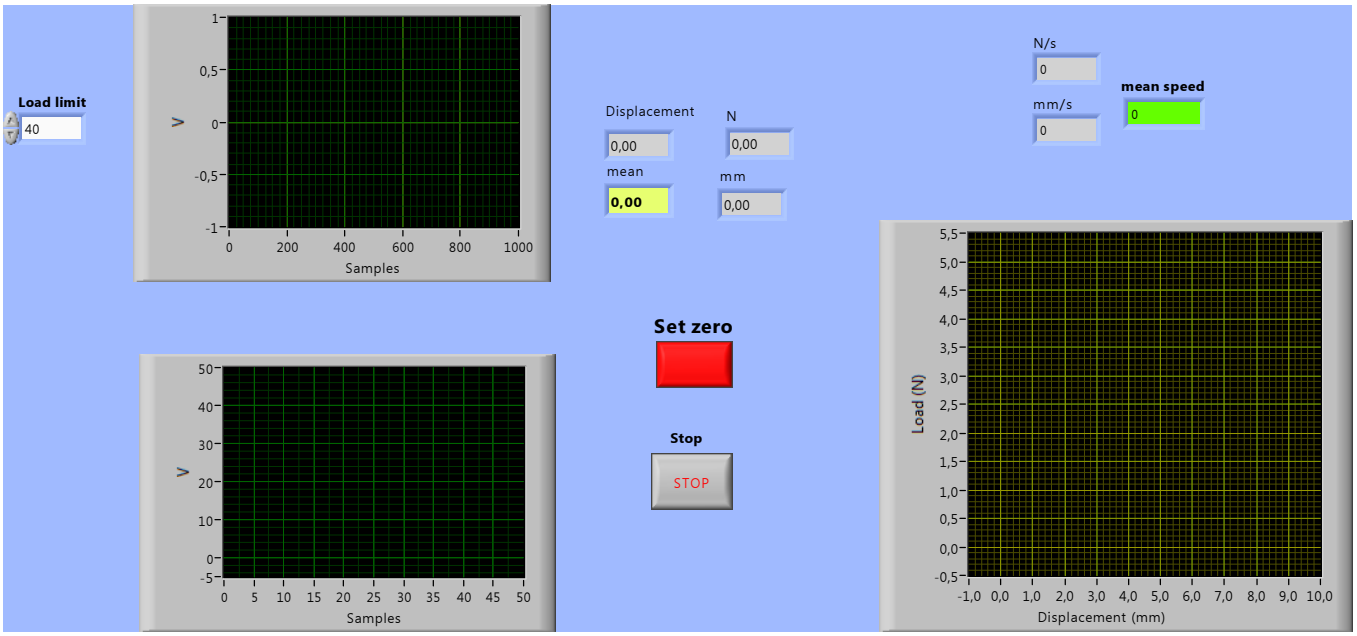
Load limit
40
V
Samples
Displacement
0,00
mean
0,00
N
0,00
mm
0,00
N/s
0
mm/s
0
mean speed
0
Set zero
Stop
STOP
Load (N)
Displacement (mm)

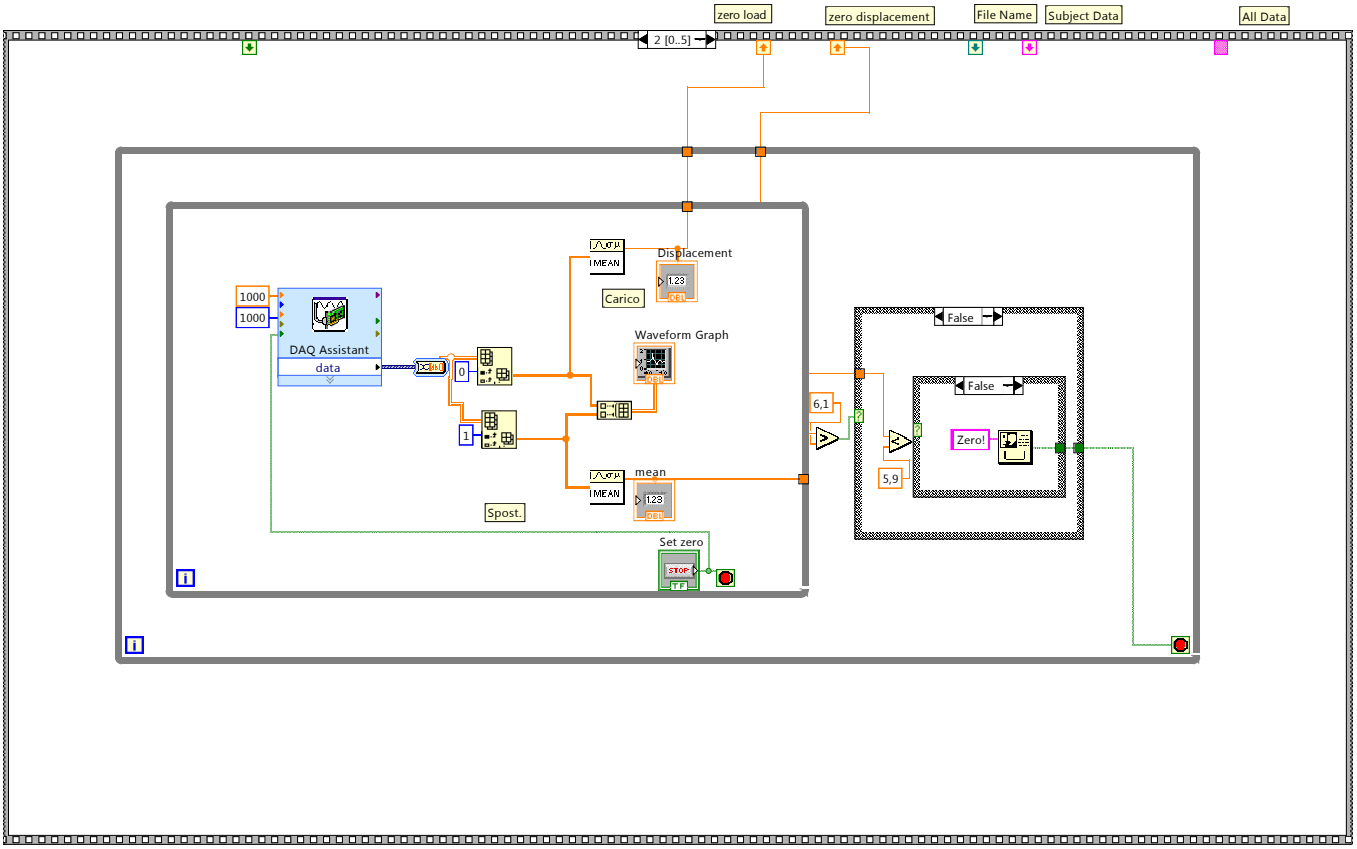
zero load
zero displacement
File Name
Subject Data
All Data
2 [0..5]
DAQ Assistant
data
1000
1000
Displacement
Carico
Waveform Graph
mean
Spost.
Set zero
False
False
Zero!
6,1
5,9

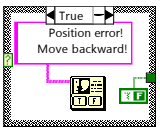
True
Position error!
Move backward!

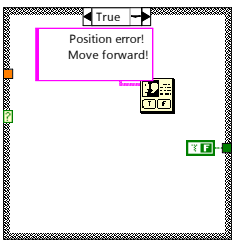
True
Position error!
Move forward!

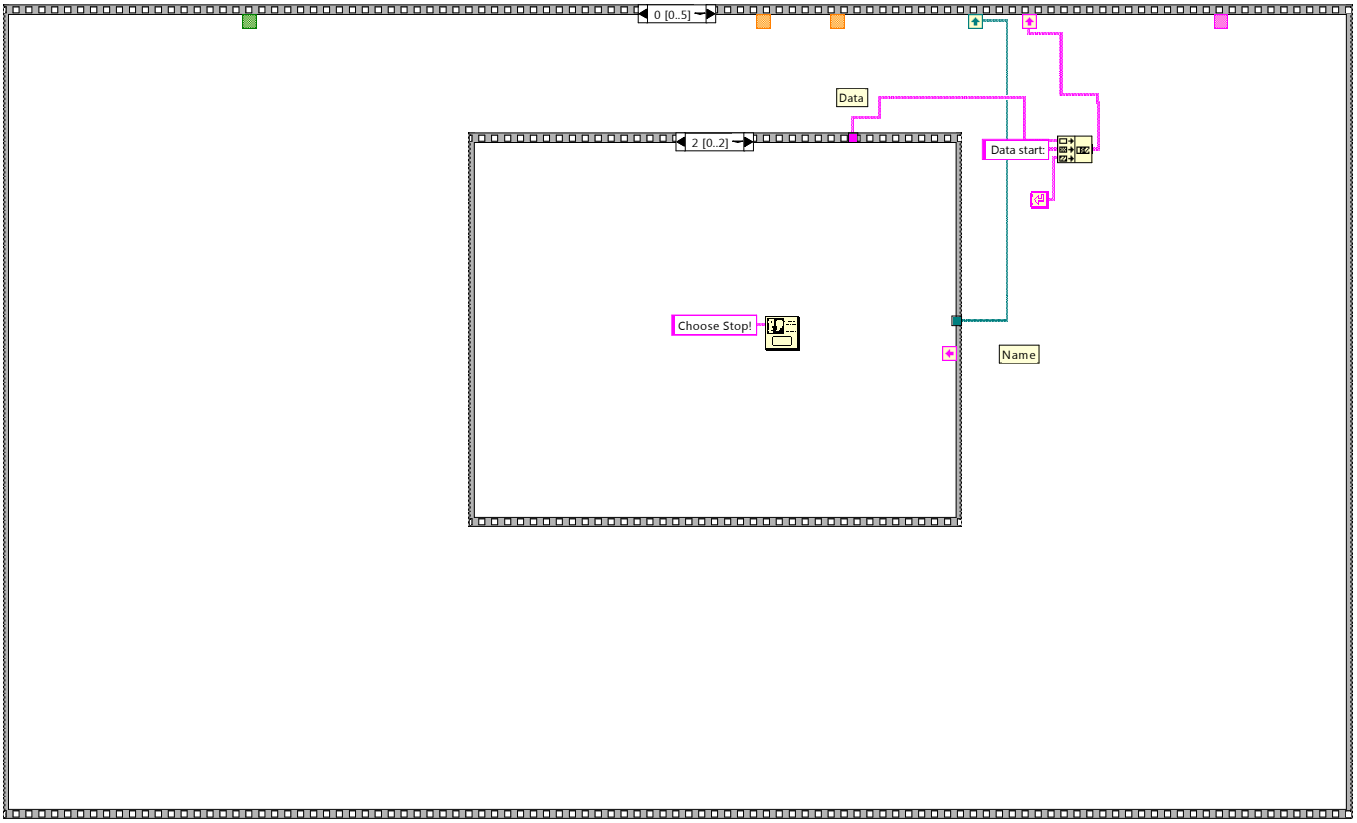
0 [0..5]
Data
2 [0..2]
Data start:
Choose Stop!
Name

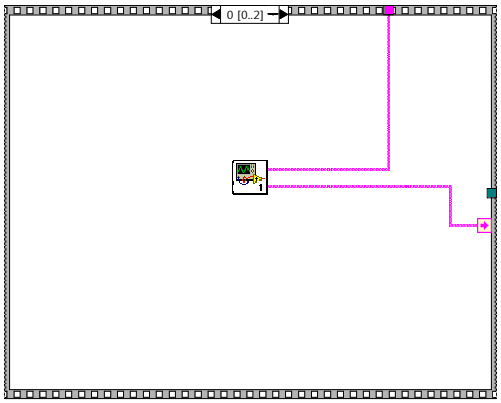
0 [0..2]

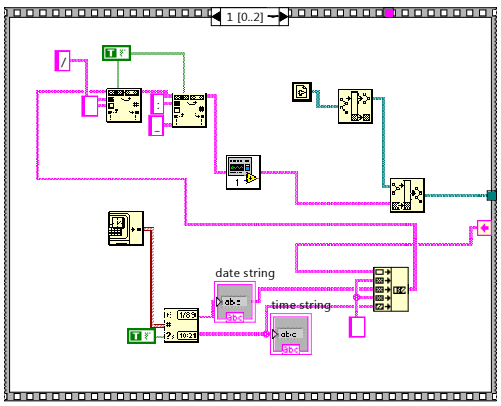
1 [0..2]
date string
time string

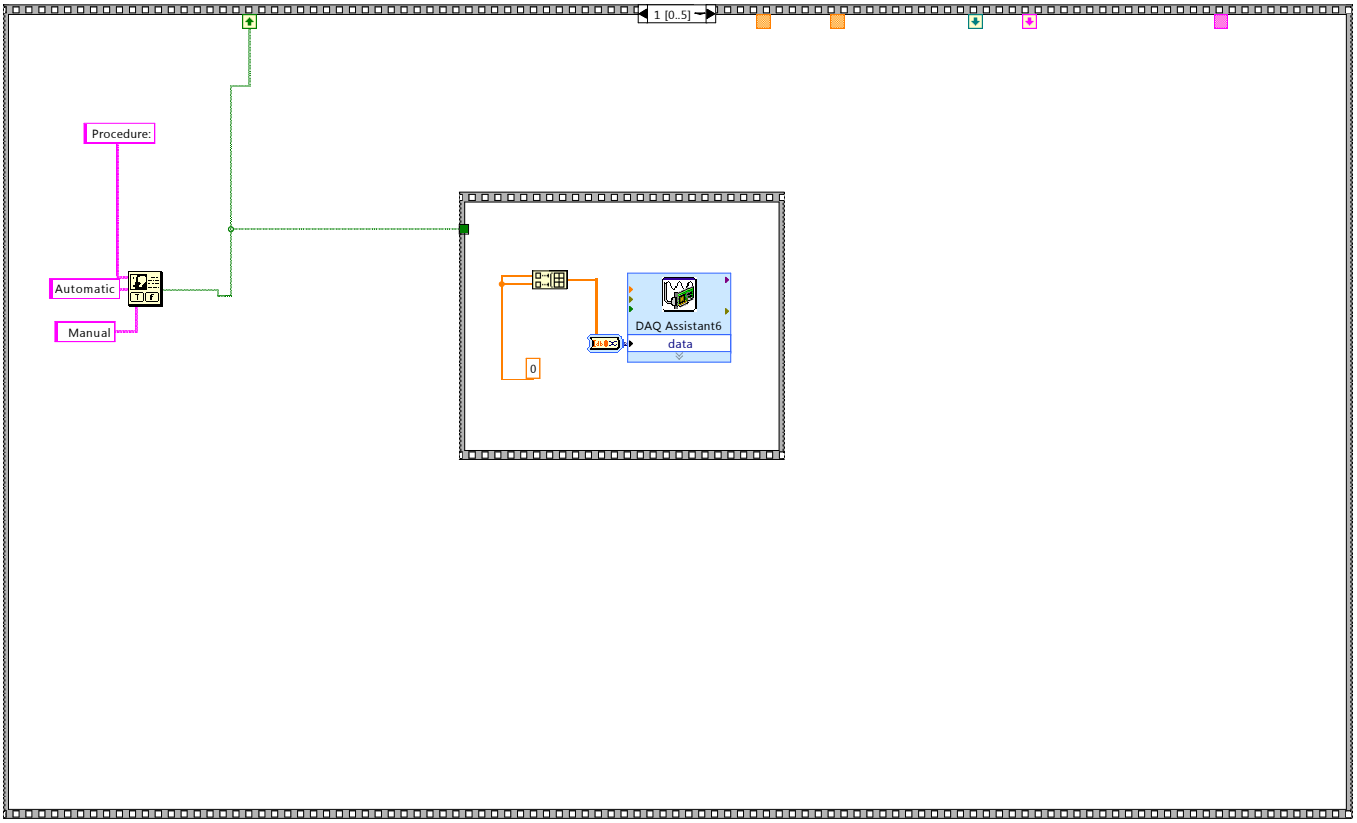
1 [0..5]
Procedure:
Automatic
Manual
DAQ Assistant6
data
0

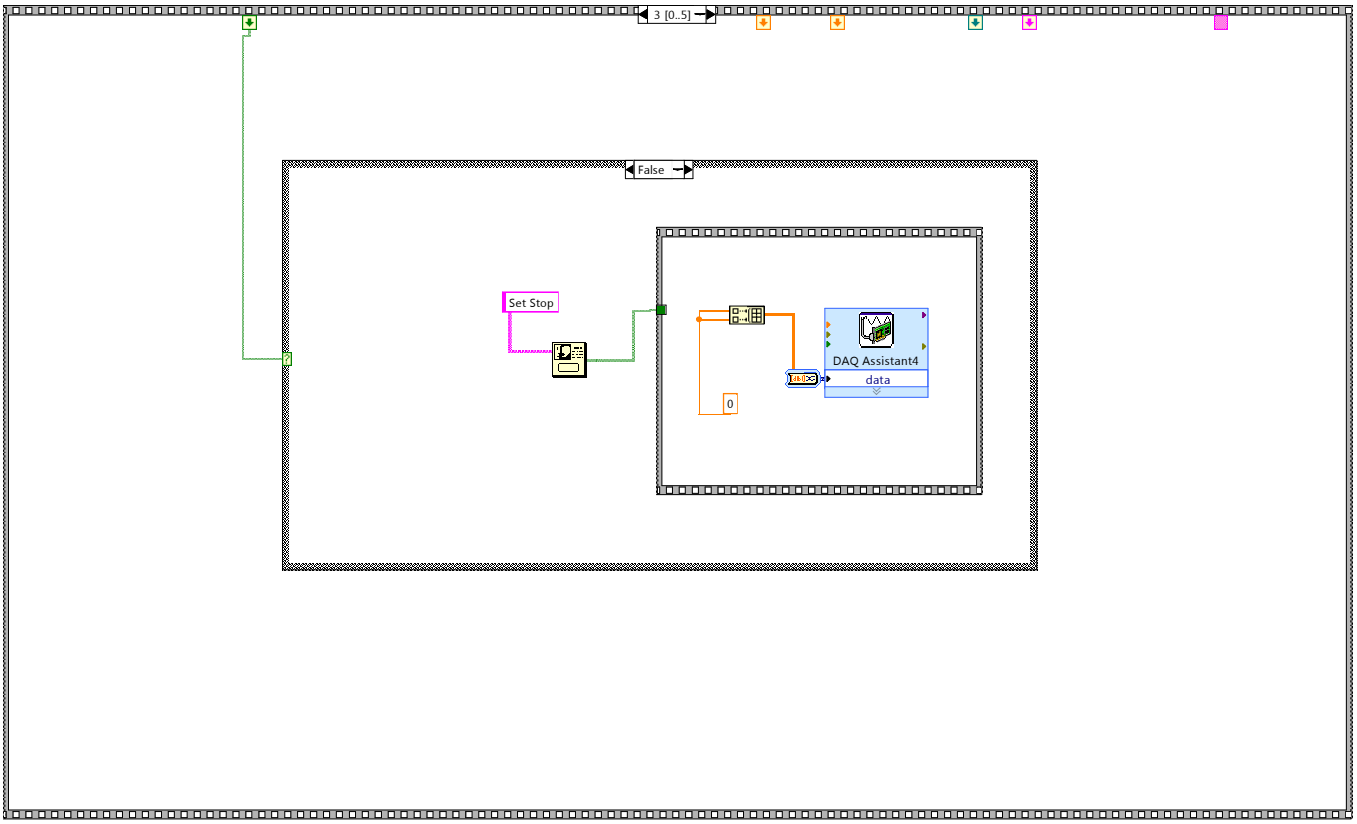
3 [0..5]
False
Set Stop
DAQ Assistant4
data
0

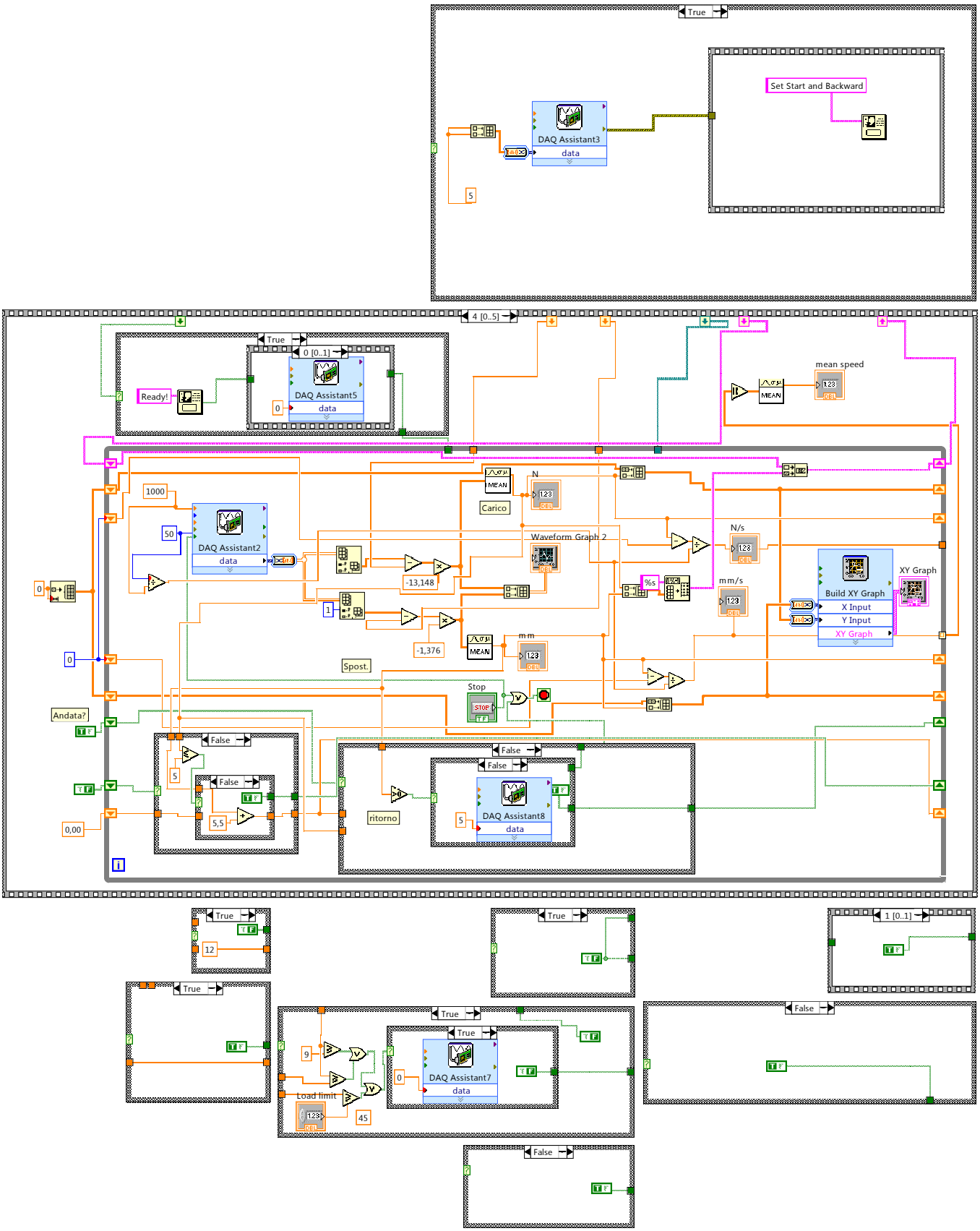
True
Set Start and Backward
DAQ Assistant3
data
5
4 [0..5]
True
0 [0..1]
Ready!
DAQ Assistant5
data
0
mean speed
MEAN
123
1000
50
DAQ Assistant2
data
Carico
N
Waveform Graph 2
-13,148
-1,376
Spost.
N/s
mm/s
%s
Build XY Graph
X Input
Y Input
XY Graph
Stop
STOP
Andata?
False
5
5,5
0,00
ritorno
DAQ Assistant8
data
12
1 [0..1]
9
Load limit
45
DAQ Assistant7
data

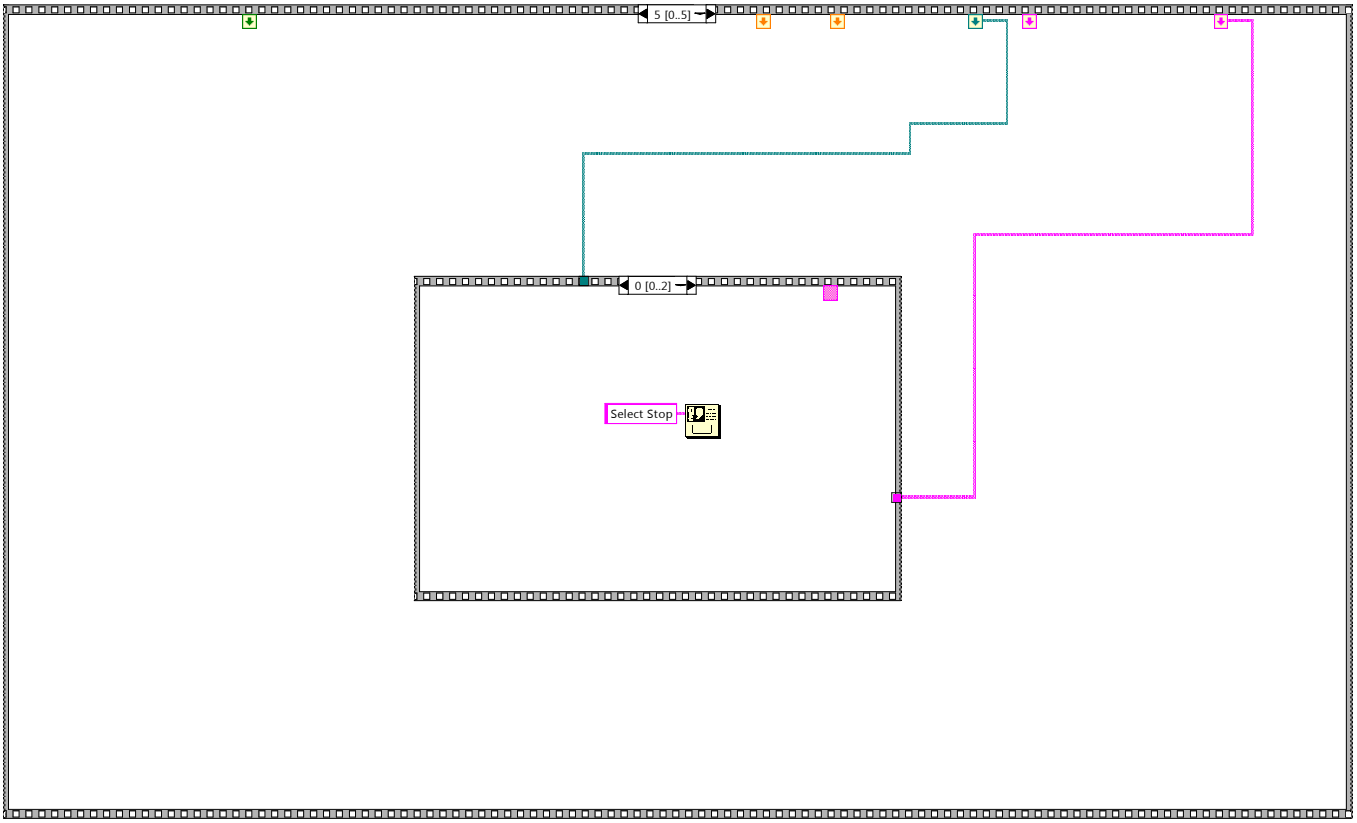
5 [0..5]
0 [0..2]
Select Stop

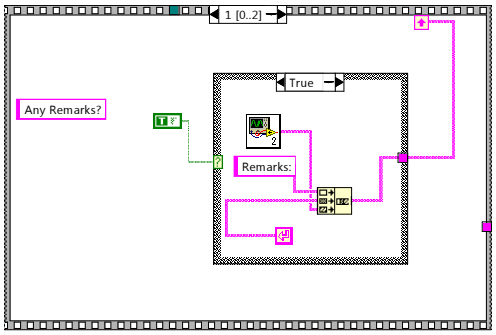
1 [0..2]
Any Remarks?
True
Remarks:

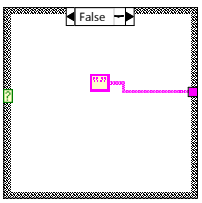
False

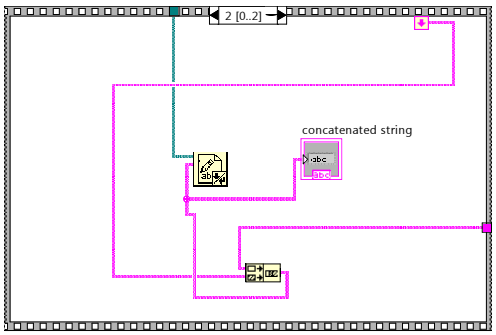
2 [0..2]
concatenated string

APPENDIX A2

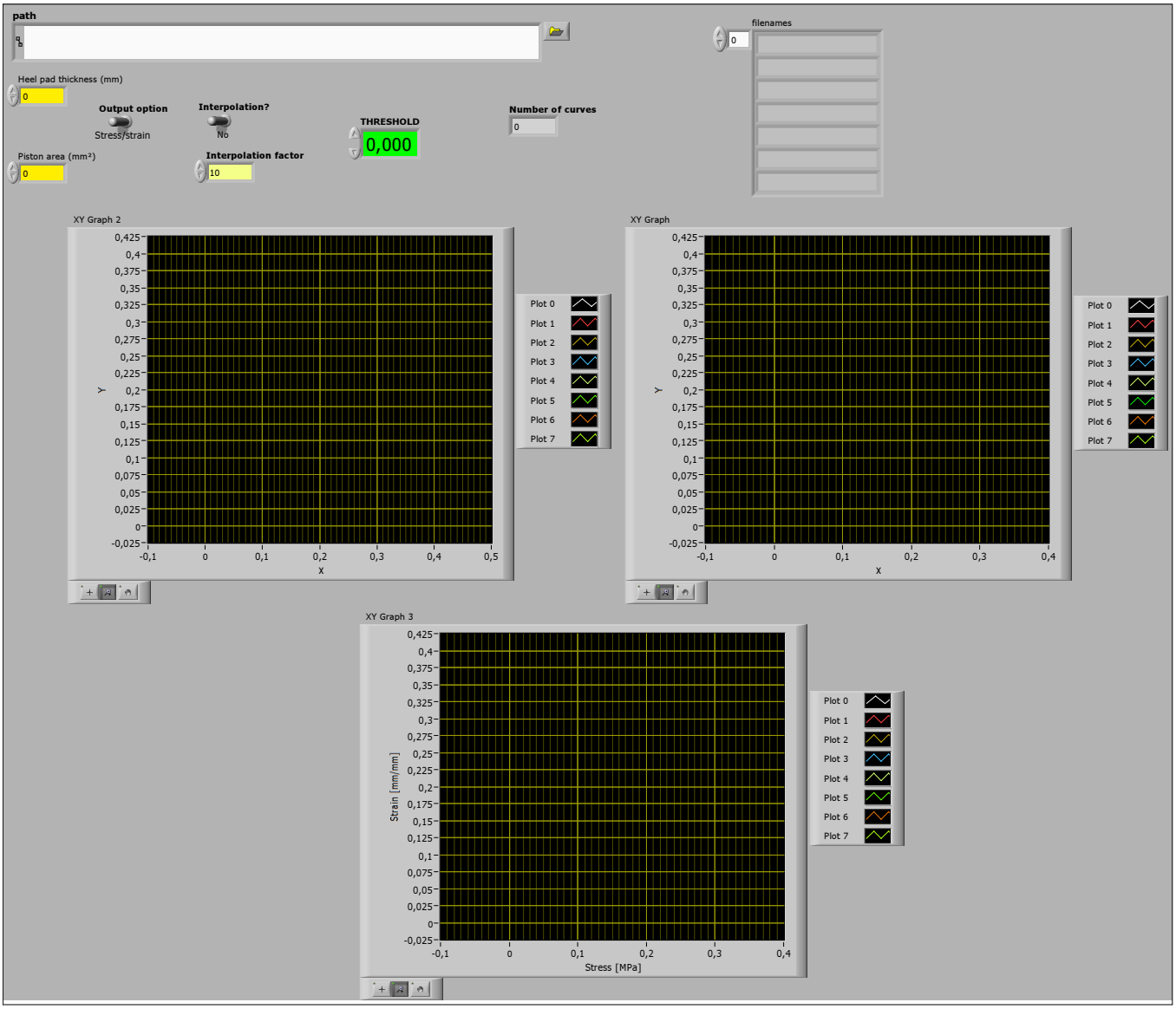
path
filenames
0
Heel pad thickness (mm)
0
Output option
Stress/strain
Interpolation?
No
THRESHOLD
0,000
Number of curves
0
Piston area (mm²)
0
Interpolation factor
10
XY Graph 2
XY Graph
XY Graph 3
Plot 0
Plot 1
Plot 2
Plot 3
Plot 4
Plot 5
Plot 6
Plot 7
X
Y
Strain [mm/mm]
Stress [MPa]

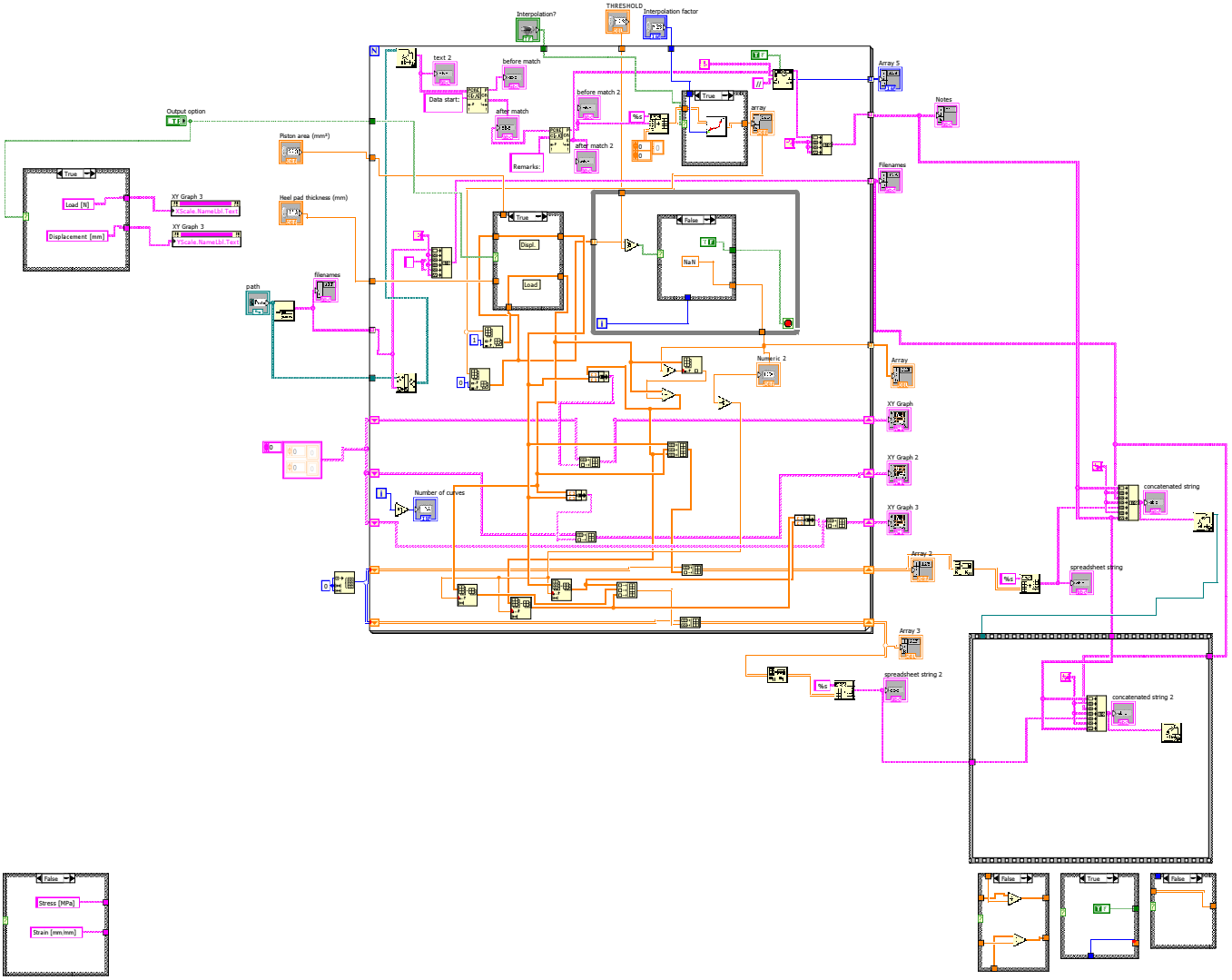
Interpolation?
THRESHOLD
Interpolation factor
Output option
Piston area (mm²)
Heel pad thickness (mm)
path
filenames
text 2
before match
Data start:
after match
before match 2
after match 2
Remarks:
Array 5
Notes
Filenames
Numeric 2
Array
XY Graph
XY Graph 2
XY Graph 3
Number of curves
Array 2
spreadsheet string
concatenated string
Array 3
spreadsheet string 2
concatenated string 2
Load [N]
Displacement [mm]
Stress [MPa]
Strain [mm/mm]
Displ.
Load
NaN

APPENDIX A3

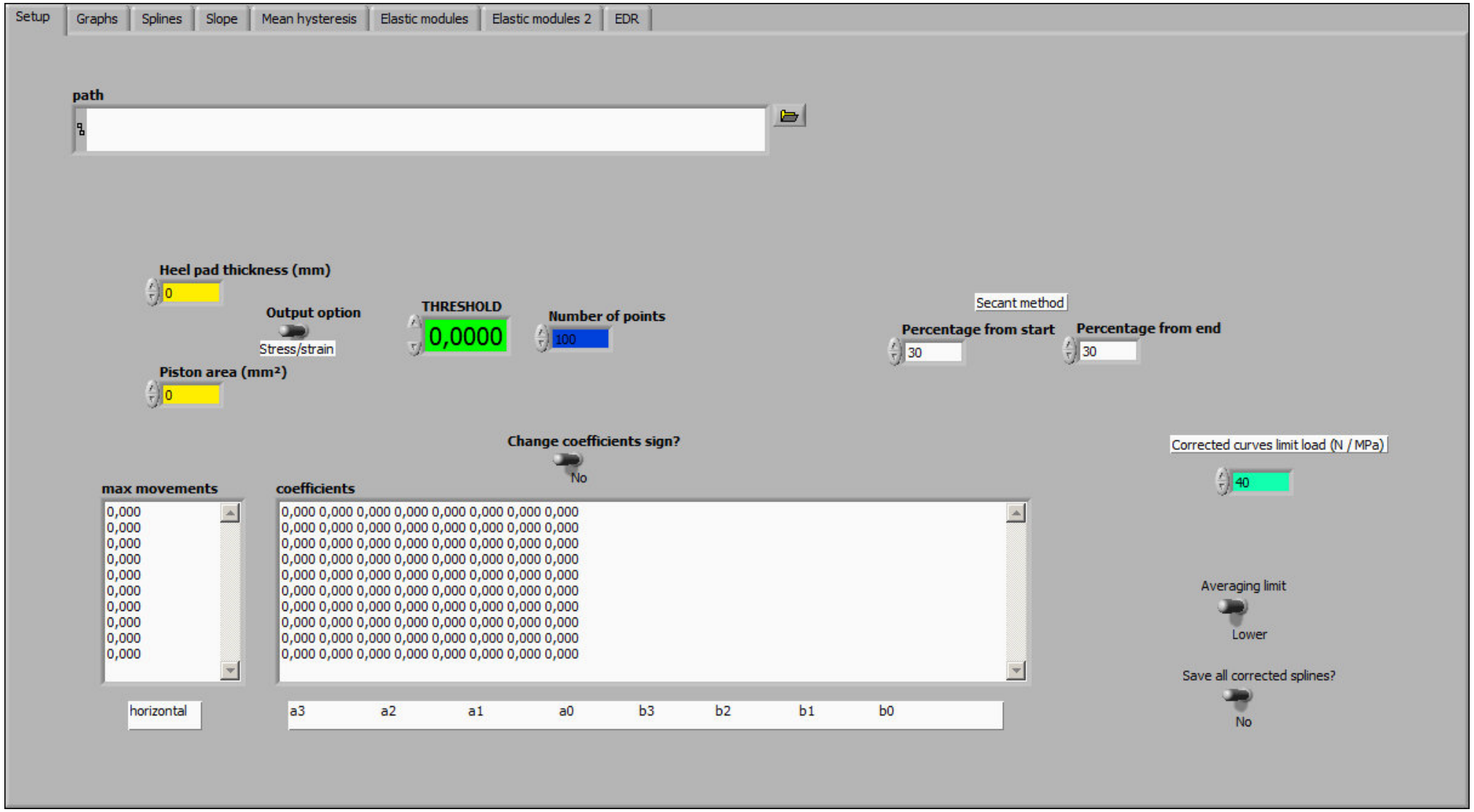
Setup
Graphs
Splines
Slope
Mean hysteresis
Elastic modules
Elastic modules 2
EDR
path
Heel pad thickness (mm)
0
Output option
Stress/strain
Piston area (mm²)
0
THRESHOLD
0,0000
Number of points
100
Secant method
Percentage from start
30
Percentage from end
30
Change coefficients sign?
No
Corrected curves limit load (N / MPa)
40
max movements
0,000
0,000
0,000
0,000
0,000
0,000
0,000
0,000
0,000
0,000
coefficients
0,000 0,000 0,000 0,000 0,000 0,000 0,000 0,000
horizontal
a3 a2 a1 a0 b3 b2 b1 b0
Averaging limit
Lower
Save all corrected splines?
No

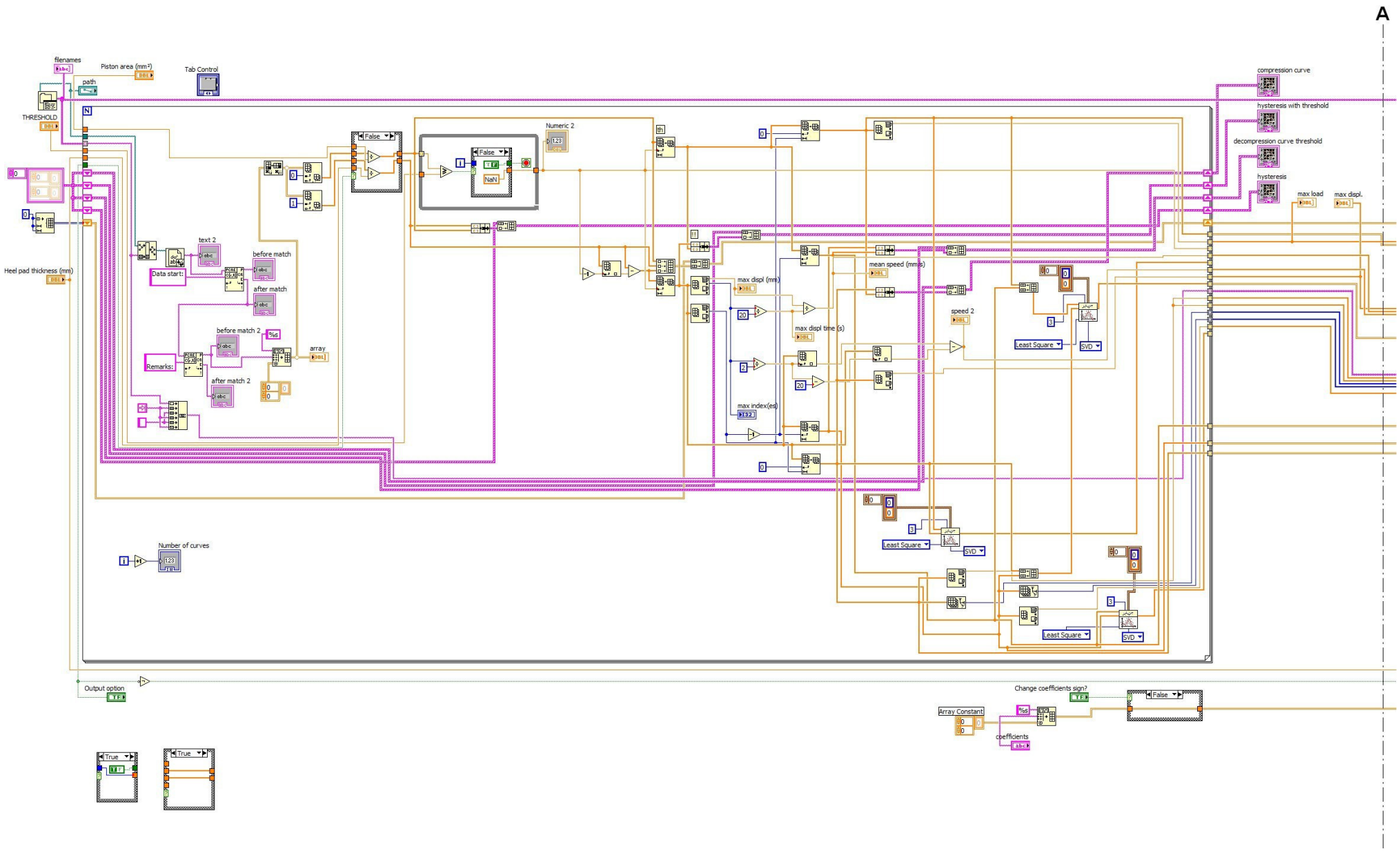
A
filenames
Piston area (mm²)
Tab Control
path
THRESHOLD
Heel pad thickness (mm)
text 2
Data start:
before match
after match
before match 2
Remarks:
after match 2
array
%s
False
Numeric 2
NaN
max displ (mm)
max displ time (s)
max index(es)
mean speed (mm/s)
speed 2
Least Square
SVD
compression curve
hysteresis with threshold
decompression curve threshold
hysteresis
max load
max displ.
Number of curves
Output option
Change coefficients sign?
Array Constant
coefficients
True

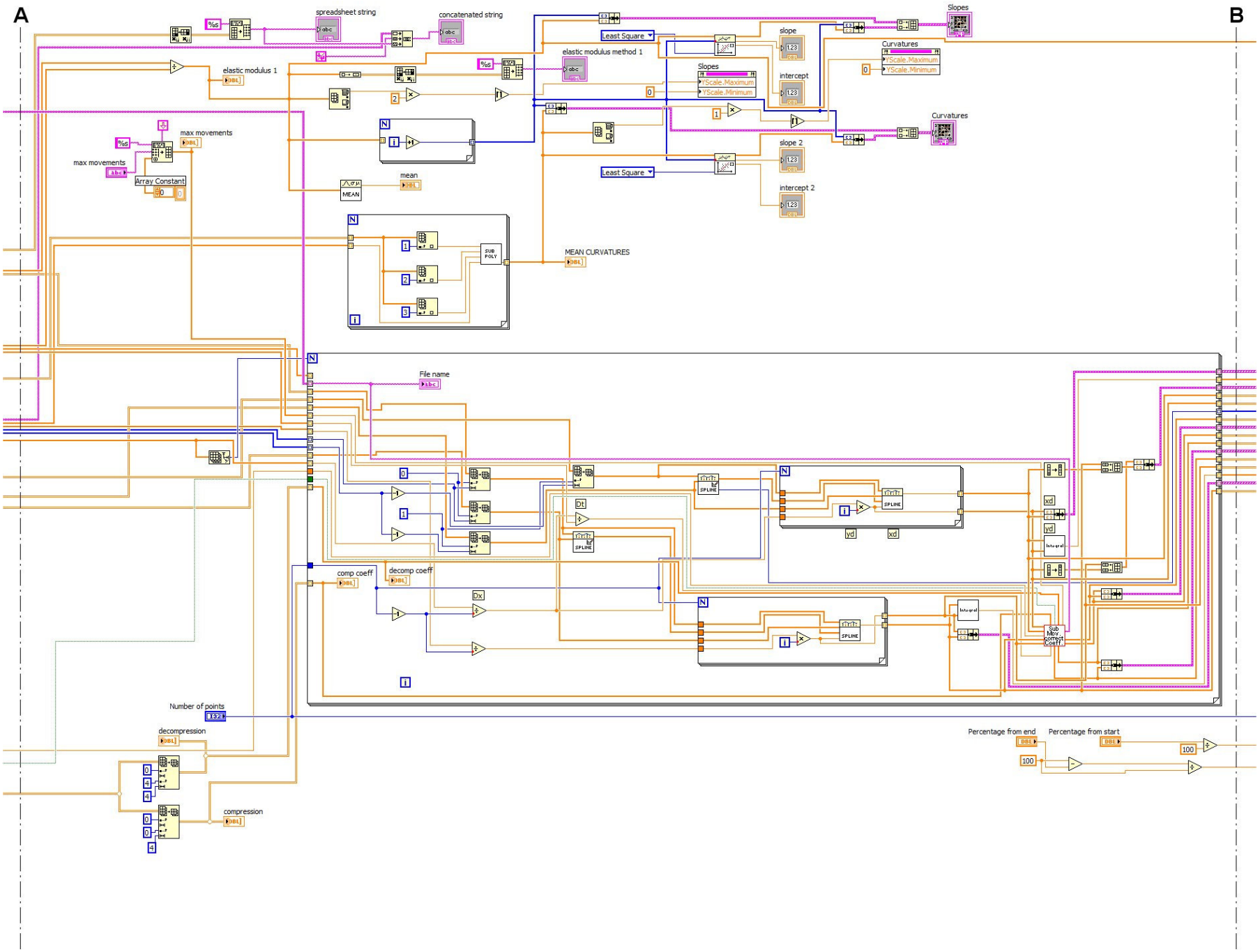
A
B
spreadsheet string
concatenated string
elastic modulus 1
elastic modulus method 1
Least Square
slope
intercept
Slopes
Curvatures
YScale.Maximum
YScale.Minimum
slope 2
intercept 2
max movements
Array Constant
mean
MEAN
SUB POLY
MEAN CURVATURES
File name
SPLINE
Dt
Dx
xd
yd
Integral
comp coeff
decomp coeff
Sub Mev correct Coeff
Number of points
decompression
compression
Percentage from end
Percentage from start
100

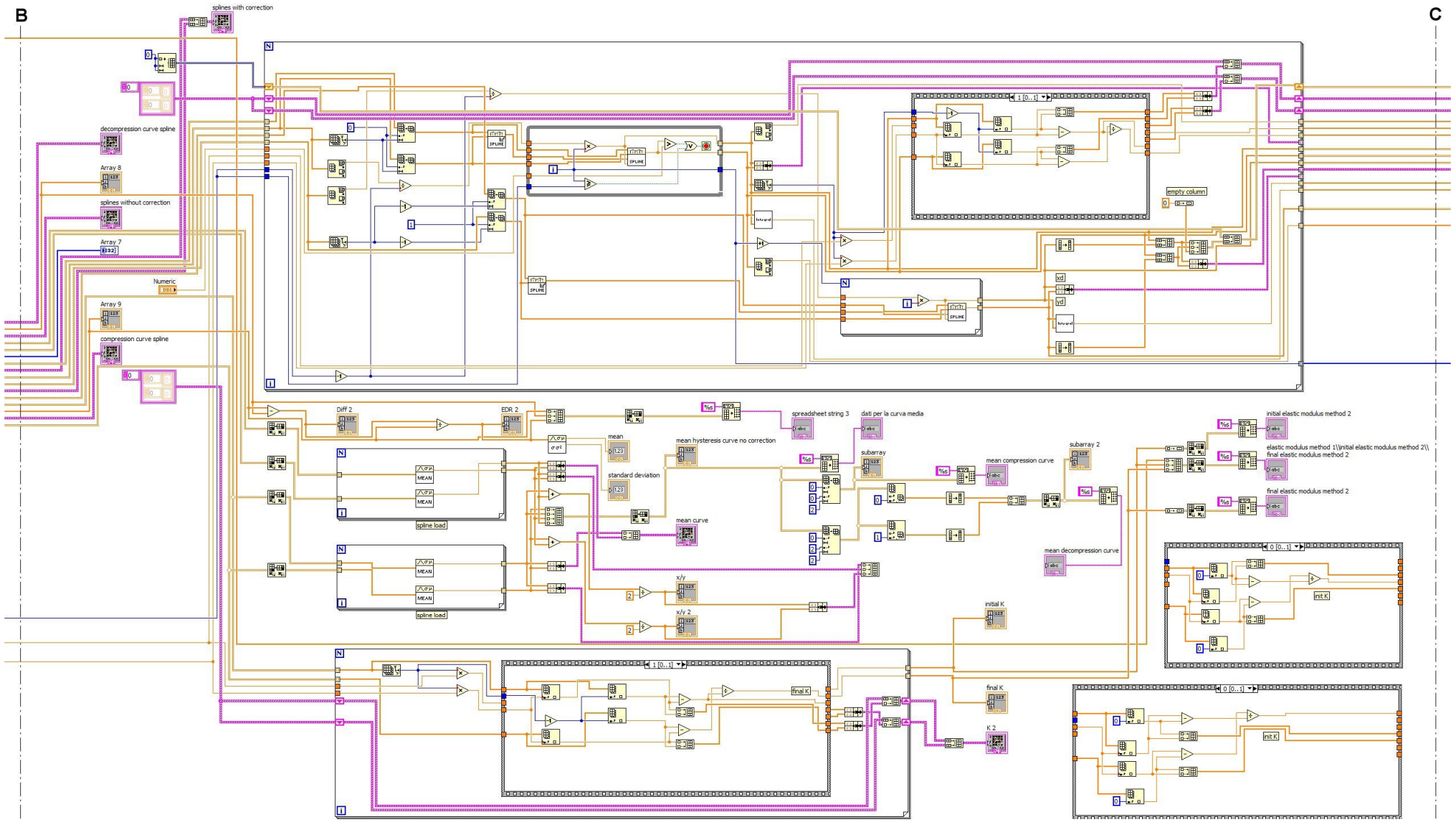
B
C
splines with correction
decompression curve spline
Array 8
splines without correction
Array 7
Numeric
Array 9
compression curve spline
empty column
Diff 2
EDR 2
mean
standard deviation
mean hysteresis curve no correction
mean curve
spline load
spline load
x/y
x/y 2
spreadsheet string 3
dati per la curva media
subarray
subarray 2
mean compression curve
mean decompression curve
initial elastic modulus method 2
elastic modulus method 1\\initial elastic modulus method 2\\final elastic modulus method 2
final elastic modulus method 2
initial K
final K
K 2
init K
init K
final K

C

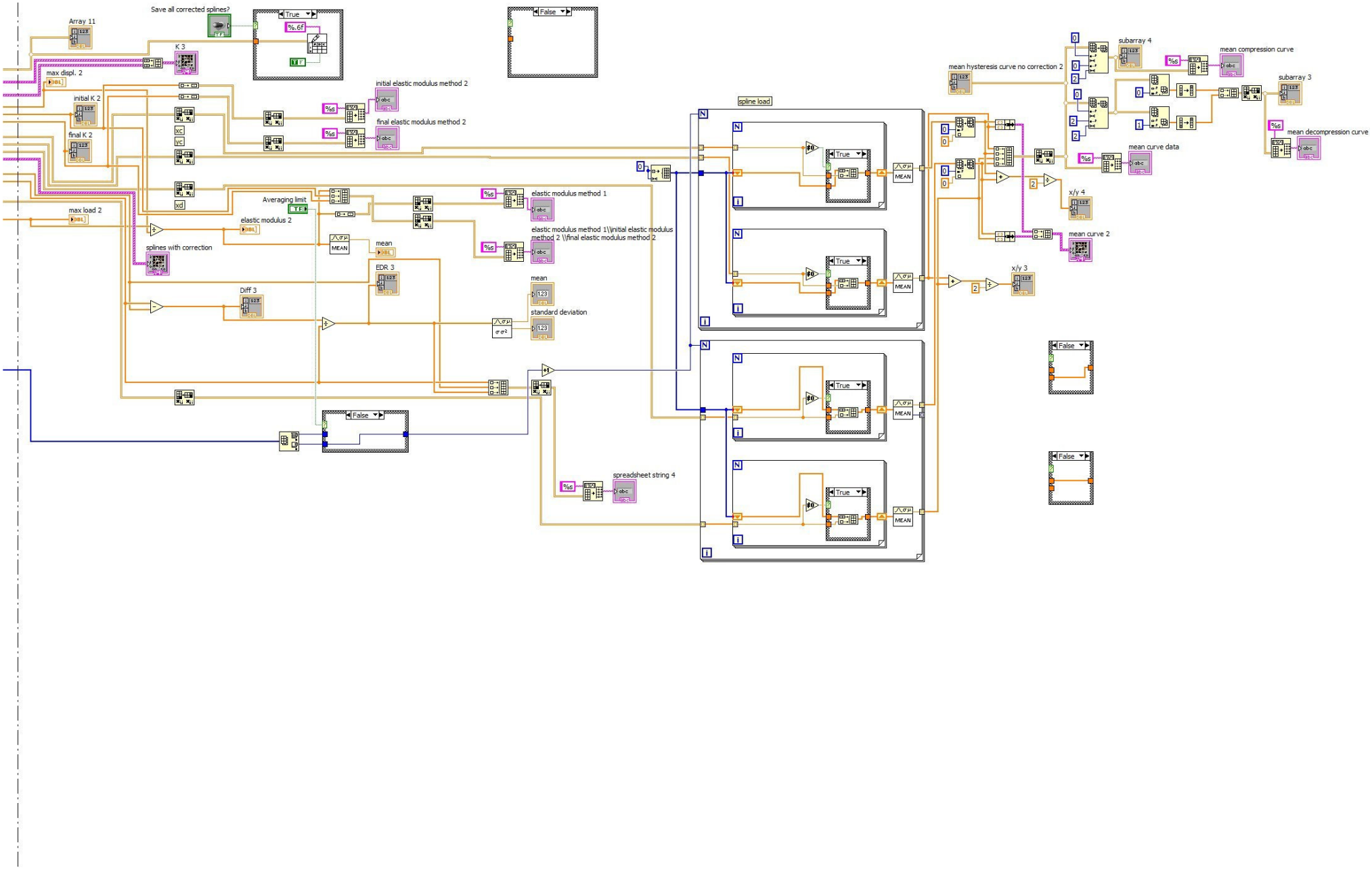
Save all corrected splines?
True
%.6f
False
Array 11
K 3
max displ. 2
initial K 2
final K 2
xc
yc
xd
initial elastic modulus method 2
final elastic modulus method 2
Averaging limit
elastic modulus method 1
elastic modulus method 1\\initial elastic modulus method 2 \\final elastic modulus method 2
max load 2
elastic modulus 2
splines with correction
mean
EDR 3
Diff 3
standard deviation
spline load
MEAN
spreadsheet string 4
mean hysteresis curve no correction 2
subarray 4
mean compression curve
subarray 3
mean decompression curve
mean curve data
x/y 4
mean curve 2
x/y 3

APPENDIX A4

MATLAB CODE: Videocode_interpolation.m

```
%% A path name directory
close all
name='Tom';
path_directory='Y:\=PHD_project2009_2011\+HeelPadResearch\HeelPadModelling\BiomedicalDevice\TestDTU-6straps-Summer2011\++Videos_volunteers_summer\Tom-281011';
cd (path_directory)
VideoList=get_dirc2('*i');
cd Y:\=PHD_project2009_2011\MATLAB\video_project_July2011

% %% B conversion and cross position
distance=29;
File1=VideoList(1,:);
conversion=conver(File1,path_directory,distance);

File2=VideoList(2,:);
[crossx crossy]=cross_position(File2,path_directory);
xlswrite('Y:\=PHD_project2009_2011\+HeelPadResearch\HeelPadModelling\BiomedicalDevice\TestDTU-6straps-Summer2011\++Videos_volunteers_summer\DataConvCross',[conversion crossx crossy],name)

%% C load the data
cd (path_directory)
conversion=xlsread('Y:\=PHD_project2009_2011\+HeelPadResearch\HeelPadModelling\BiomedicalDevice\TestDTU-6straps-Summer2011\++Videos_volunteers_summer\DataConvCross',name,'A1');
x_cross=xlsread('Y:\=PHD_project2009_2011\+HeelPadResearch\HeelPadModelling\BiomedicalDevice\TestDTU-6straps-Summer2011\++Videos_volunteers_summer\DataConvCross',name,'B1');
y_cross=xlsread('Y:\=PHD_project2009_2011\+HeelPadResearch\HeelPadModelling\BiomedicalDevice\TestDTU-6straps-Summer2011\++Videos_volunteers_summer\DataConvCross',name,'C1');

%% D displacement

close all
Mx=[];
My=[];
P1=[];
P2=[];

for v=2:size(VideoList,1)
    Filename=VideoList(v,:)
    video=mmreader(Filename);

    number_of_images=fix(video.NumberOfFrames/5);%%%% number of images to process

    p=fix(video.NumberOfFrames/number_of_images);
```

```
a=41;
b=71;
matrix=zeros(a,b,number_of_images);

for i=1:number_of_images
    Image=read(video,1+p*i-p);
    Image_zoom=Image(y_cross-((a-1)/2):y_cross+((a-1)/2),x_cross-((b-1)/2):x_cross+((b-1)/2),:);
    Image_zoom_ind=rgb2ind(Image_zoom,2);
    Image_zoom_ind=~Image_zoom_ind;
    matrix(:,:,i)=Image_zoom_ind;
end

big= padarray(matrix(:,:,1),[a b]);

conv=conv2(big, matrix(end:-1:1,end:-1:1,1),'valid');
matrix_conv=zeros(size(conv,1),size(conv,2),number_of_images);
matrix_c1=zeros(size(conv,1),size(conv,2),number_of_images-1);
matrix_c2=zeros(size(conv,1),size(conv,2),number_of_images-1);

matrix_conv(:,:,1)=conv;
line0=fix(size(matrix_conv,1)/2)+1;
column0=fix(size(matrix_conv,2)/2)+1;

for i=1:((number_of_images)-1)
    conv=conv2(big,matrix(end:-1:1,end:-1:1,i+1),'valid');%% convolution 1-1 1-2 1-3 1-4 1-5...
    matrix_conv(:,:,i+1)=conv;
end

xi_h = 1:0.01:size(matrix_conv,2);
matrix_interp_h=zeros(size(xi_h,2),size(matrix_conv,3));
x_h = 1:1:size(matrix_conv,2);
xi_v = 1:0.01:size(matrix_conv,1);
matrix_interp_v=zeros(size(xi_v,2),size(matrix_conv,3));
x_v = 1:1:size(matrix_conv,1);

for k=1:size(matrix_conv,3)
    y_h= matrix_conv(line0,:,k);
    pp_h = interp1(x_h,y_h,'spline','pp');
    yi_h = ppval(pp_h,xi_h);
    matrix_interp_h(:,k)= ppval(pp_h,xi_h);
    y_v= matrix_conv(:,column0,k);
    pp_v = interp1(x_v,y_v,'spline','pp');
    yi_v = ppval(pp_v,xi_v);
    matrix_interp_v(:,k)= ppval(pp_v,xi_v);
end
```

```
horiz_axis=([1:number_of_images]*p+1-p)/video.FrameRate;

Maxi_x =zeros(size(matrix_conv,3),1);
Abs_x =zeros(size(matrix_conv,3),1);
Maxi_y =zeros(size(matrix_conv,3),1);
Abs_y =zeros(size(matrix_conv,3),1);

for k=1:size(matrix_interp_h,2)
   [Maxi_x(k) Abs_x(k)]=max(matrix_interp_h(:,k));
   [Maxi_y(k) Abs_y(k)]=max(matrix_interp_v(:,k));
end

Abs_x=(Abs_x-Abs_x(1))*conversion/100;
Abs_y=(Abs_y-Abs_y(1))*conversion/100;

figure(1)
set(0,'DefaultAxesColorOrder',[1 0 1;0 1 0;0 0 0;0 1 1;1 0 0;1 0 0; 1 1 0],'DefaultAxesLineStyleOrder','-|-+')
hold all
plot(horiz_axis,Abs_x)
legend(VideoList(2:end,:),-1)
ylabel('movement[mm]')
xlabel('time[s]')
title('horizontal displacement of the ankle')
figure(2)
hold all
plot(horiz_axis,Abs_y)
ylabel('movement[mm]')
xlabel('time[s]')
legend(VideoList(2:end,:),-1)
title('vertical displacement of the ankle')

Mx=[Mx;max(abs(Abs_x))];
My=[My;max(abs(Abs_y))];

figure(1+v)
[M m]=max(abs(Abs_x));
p1=polyfit(horiz_axis(1:m)',Abs_x(1:m),3);
f1=polyval(p1,horiz_axis(1:m));
plot(horiz_axis(1:m),Abs_x(1:m),':black');
hold on
plot(horiz_axis(1:m),f1,'black')
p2=polyfit(horiz_axis(m:end)',Abs_x(m:end),3);
f2=polyval(p2,horiz_axis(m:end));
plot(horiz_axis(m:end),Abs_x(m:end),':red')
```

```
    plot(horiz_axis(m:end),f2,'red')
    legend ('displacement','interpolation','displacement','interpolation')
    xlabel('time[s]')
   ylabel('movement[mm]')

    title( VideoList(v,:))
    P1=[P1;p1];
    P2=[P2;p2];
end

printfig('Y:\=PHD_project2009_2011\+HeelPadResearch\HeelPadModelling\BiomedicalDevice\TestDTU-6straps-
Summer2011\++Videos_volunteers_summer\curve\',name);horiz={'horizontal'};
xlswrite('Y:\=PHD_project2009_2011\+HeelPadResearch\HeelPadModelling\BiomedicalDevice\TestDTU-6straps-
Summer2011\++Videos_volunteers_summer\Result',horiz,name,'A1');
xlswrite('Y:\=PHD_project2009_2011\+HeelPadResearch\HeelPadModelling\BiomedicalDevice\TestDTU-6straps-
Summer2011\++Videos_volunteers_summer\Result',Mx,name,'A2');
vert={'vertical'};
xlswrite('Y:\=PHD_project2009_2011\+HeelPadResearch\HeelPadModelling\BiomedicalDevice\TestDTU-6straps-
Summer2011\++Videos_volunteers_summer\Result',vert,name,'B1');
xlswrite('Y:\=PHD_project2009_2011\+HeelPadResearch\HeelPadModelling\BiomedicalDevice\TestDTU-6straps-
Summer2011\++Videos_volunteers_summer\Result',My,name,'B2');

coeff={'a3','a2','a1','a0'};
xlswrite('Y:\=PHD_project2009_2011\+HeelPadResearch\HeelPadModelling\BiomedicalDevice\TestDTU-6straps-
Summer2011\++Videos_volunteers_summer\Result',coeff,name,'C1')
xlswrite('Y:\=PHD_project2009_2011\+HeelPadResearch\HeelPadModelling\BiomedicalDevice\TestDTU-6straps-
Summer2011\++Videos_volunteers_summer\Result',P1,name,'C2')

coeff={'b3','b2','b1','b0'};
xlswrite('Y:\=PHD_project2009_2011\+HeelPadResearch\HeelPadModelling\BiomedicalDevice\TestDTU-6straps-
Summer2011\++Videos_volunteers_summer\Result',coeff,name,'G1')
xlswrite('Y:\=PHD_project2009_2011\+HeelPadResearch\HeelPadModelling\BiomedicalDevice\TestDTU-6straps-
Summer2011\++Videos_volunteers_summer\Result',P2,name,'G2')
```

APPENDIX B

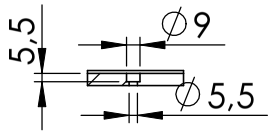

SECTION K-K

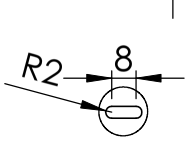

DETAIL I
SCALE 2 : 5

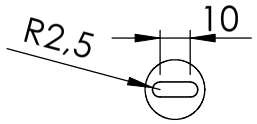

DETAIL H
SCALE 2 : 5

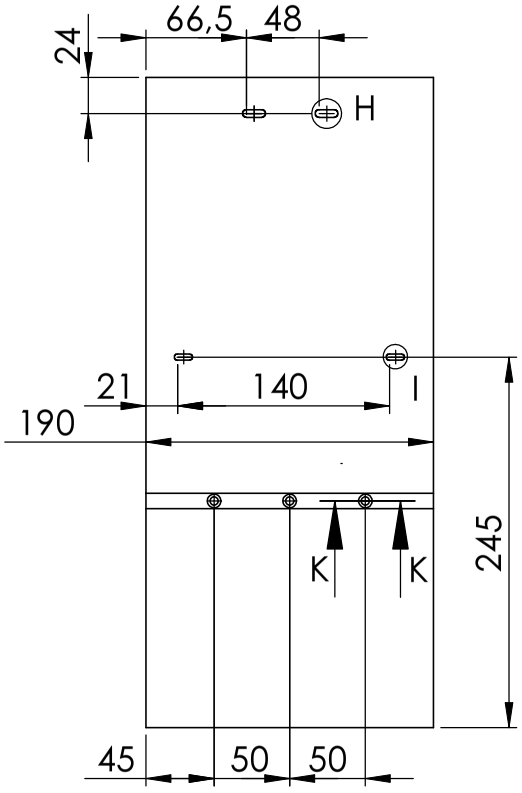

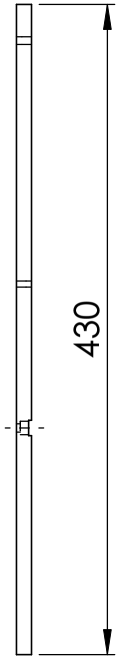

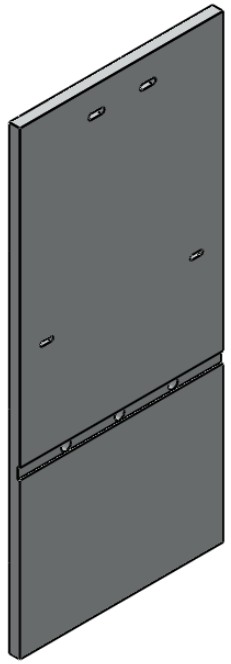

SE NON SPECIFICATO: QUOTE IN MILLIMETRI FINITURA SUPERFICIE: TOLLERANZE: LINEARE: ANGOLARE:		FINITURA:		SBAVATURA E INTERRUZIONE DEI BORDI NETTI	NON SCALARE IL DISEGNO	REVISIONE
	NOME	FIRMA	DATA		TITOLO: long base plate	
DISEGNATO						
VERIFICATO						
APPROVATO						
FATTO						
QUALITA'				MATERIALE: Aluminium	N. DISEGNO	A4
				PESO: $PRPSHEET:{Peso}	SCALA:1:5	FOGLIO 1 DI 1

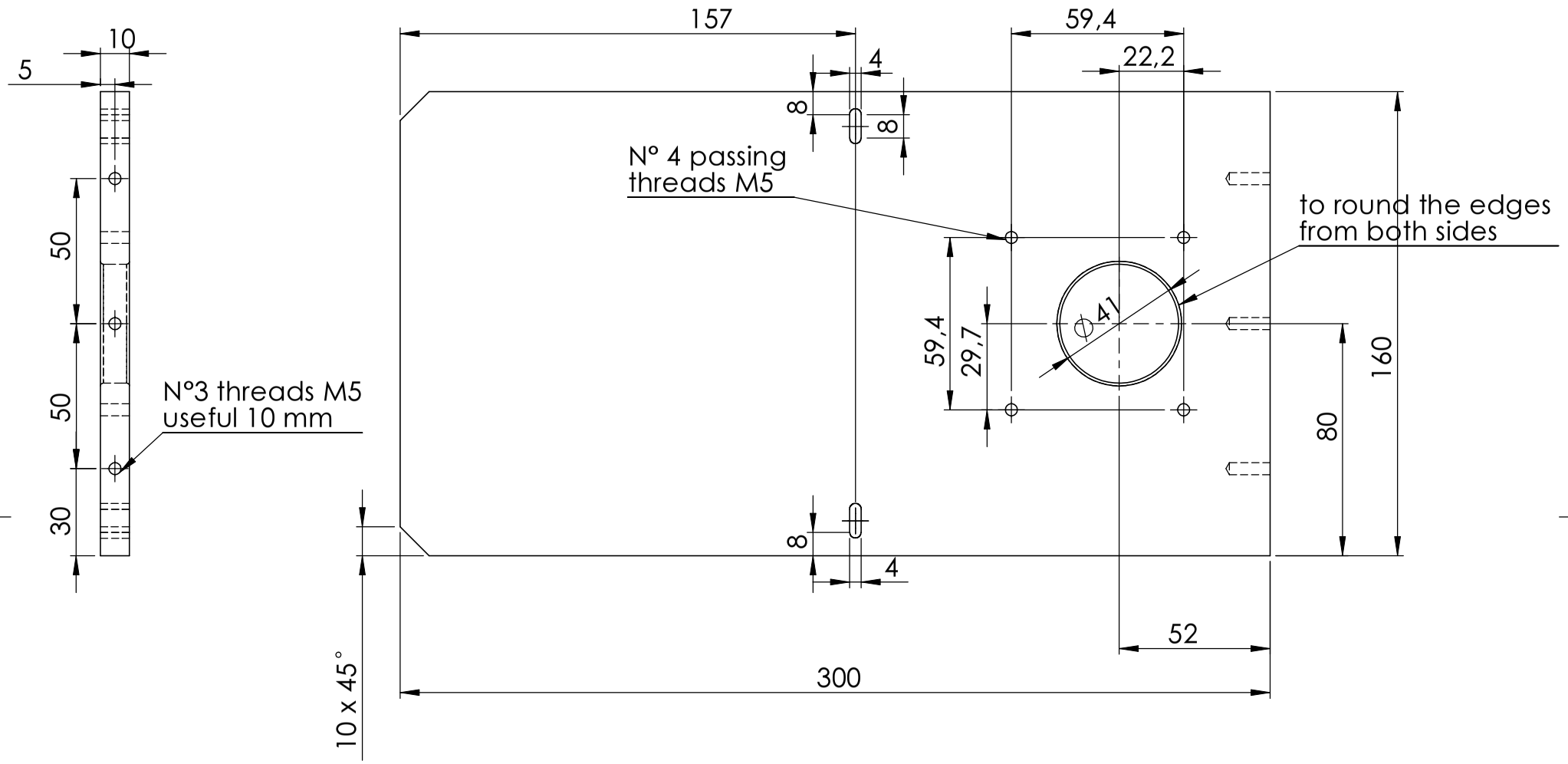

SE NON SPECIFICATO: QUOTE IN MILLIMETRI FINITURA SUPERFICIE: TOLLERANZE: LINEARE: ANGOLARE:		FINITURA:		SBAVATURA E INTERRUZIONE DEI BORDI NETTI		NON SCALARE IL DISEGNO	REVISIONE
	NOME	FIRMA	DATA			TITOLO:	
DISEGNATO						support plate	
VERIFICATO							
APPROVATO							
FATTO							
QUALITA'				MATERIALE: PMMA		N. DISEGNO	A4
				PESO: $PRPSHEET:{Peso}		SCALA:1:5	FOGLIO 1 DI 1

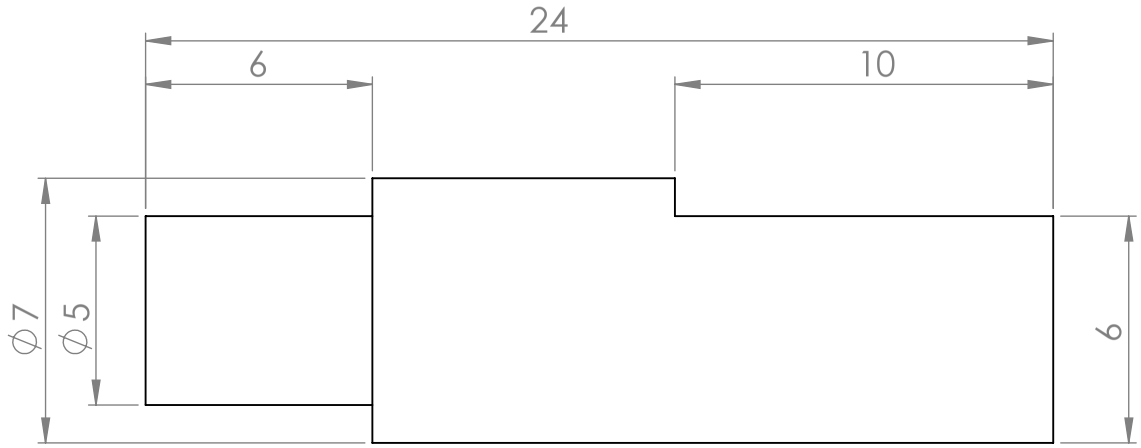

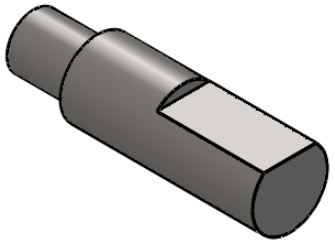

SE NON SPECIFICATO: QUOTE IN MILLIMETRI FINITURA SUPERFICIE: TOLLERANZE: LINEARE: ANGOLARE:		FINITURA:		SBAVATURA E INTERRUZIONE DEI BORDI NETTI	NON SCALARE IL DISEGNO	REVISIONE
	NOME	FIRMA	DATA		TITOLO:	
DISEGNATO					Shaft	
VERIFICATO						
APPROVATO						
FATTO						
QUALITA'				MATERIALE:	N. DISEGNO	A4
				AISI 303		
				PESO: $PRPSHEET:{Peso}	SCALA:2:1	FOGLIO 1 DI 1

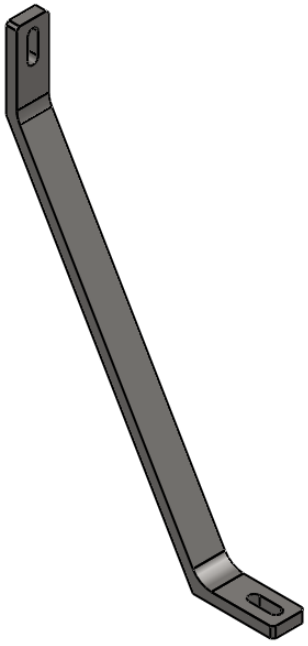

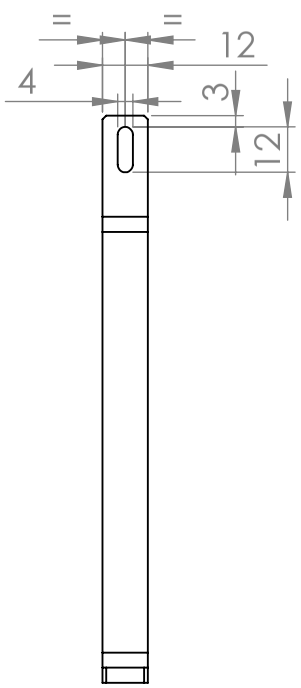

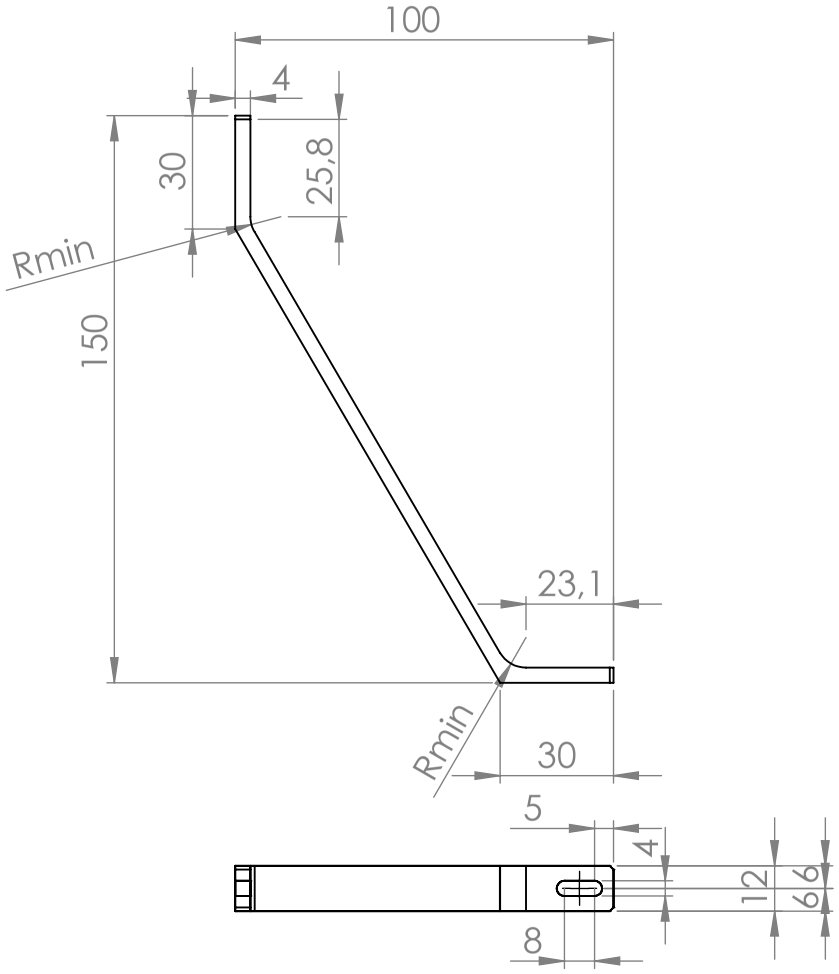

SE NON SPECIFICATO: QUOTE IN MILLIMETRI FINITURA SUPERFICIE: TOLLERANZE: LINEARE: ANGOLARE:	FINITURA:	SBAVATURA E INTERRUZIONE DEI BORDI NETTI	NON SCALARE IL DISEGNO / REVISIONE

	NOME	FIRMA	DATA
DISEGNATO			
VERIFICATO			
APPROVATO			
FATTO			
QUALITA'			

MATERIALE: AISI 304	TITOLO: bracket	
PESO: $PRPSHEET:{Peso}	N. DISEGNO	A4
	SCALA:1:2	FOGLIO 1 DI 1

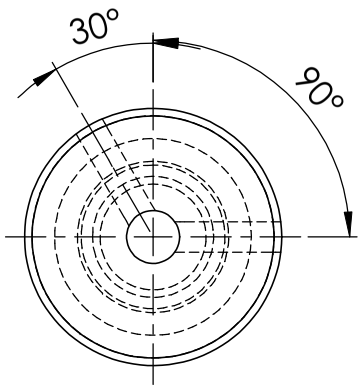

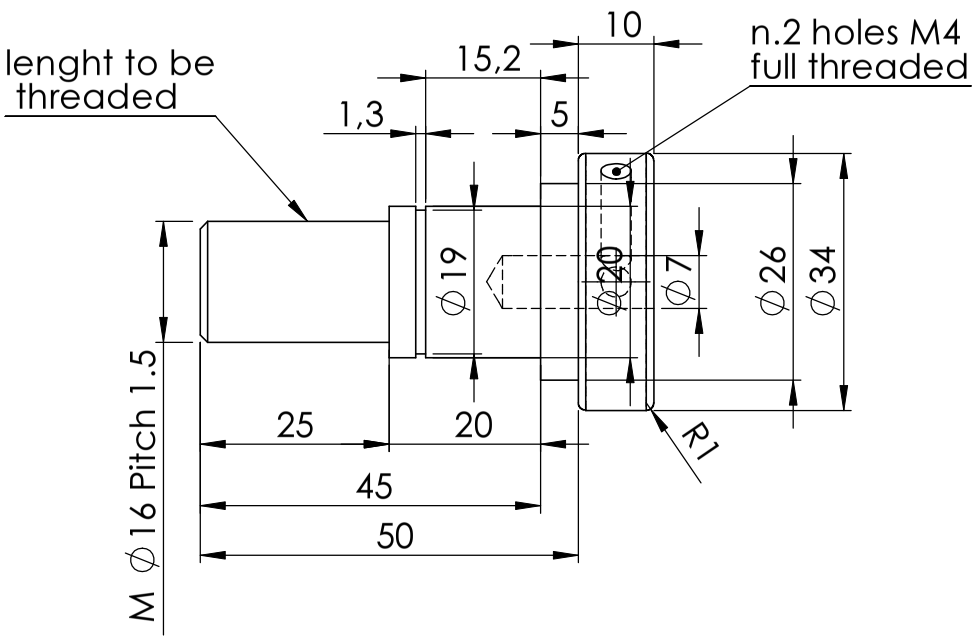

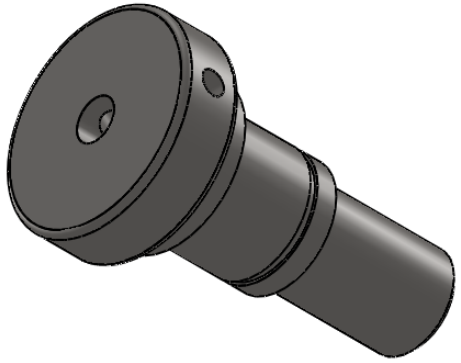

SE NON SPECIFICATO: QUOTE IN MILLIMETRI FINITURA SUPERFICIE: TOLLERANZE: LINEARE: ANGOLARE:		FINITURA: Aluminium		SBAVATURA E INTERRUZIONE DEI BORDI NETTI	NON SCALARE IL DISEGNO	REVISIONE
	NOME	FIRMA	DATA		TITOLO: Knob M16x1	
DISEGNATO						
VERIFICATO						
APPROVATO						
FATTO						
QUALITA'				MATERIALE:	N. DISEGNO	A4
				PESO: $PRPSHEET:{Peso}	SCALA:1:1	FOGLIO 1 DI 1

n.2 flaring holes M3

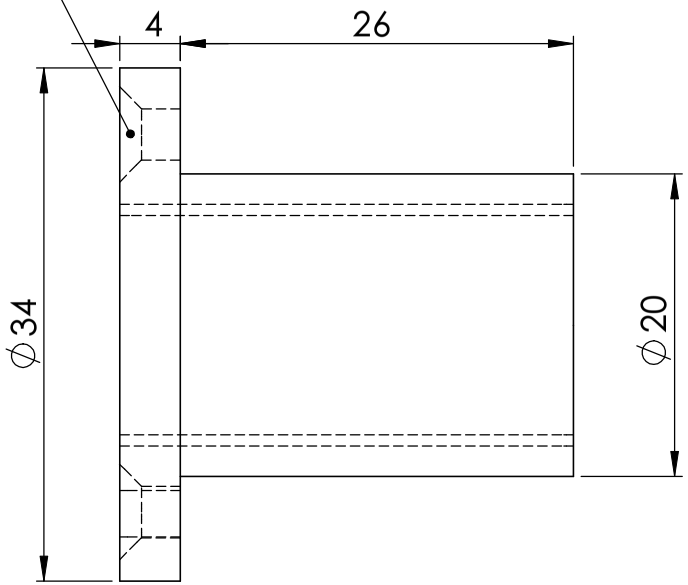

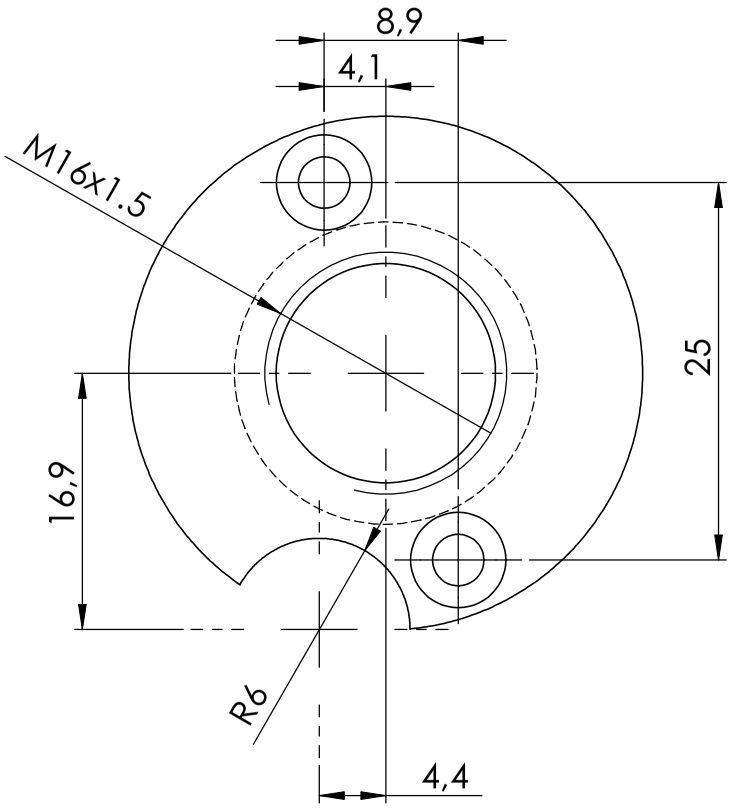

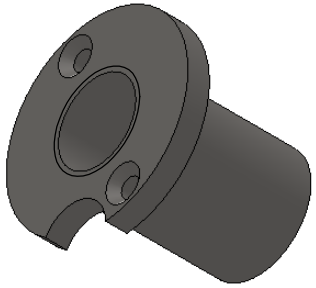

SE NON SPECIFICATO: QUOTE IN MILLIMETRI FINITURA SUPERFICIE: TOLLERANZE: LINEARE: ANGOLARE:		FINITURA:		SBAVATURA E INTERRUZIONE DEI BORDI NETTI	NON SCALARE IL DISEGNO	REVISIONE
	NOME	FIRMA	DATA		TITOLO:	
DISEGNATO					Drilled bushing M16x1.5	
VERIFICATO						
APPROVATO						
FATTO						
QUALITA'				MATERIALE: AISI 303	N. DISEGNO	A4
				PESO: $PRPSHEET:{Peso}	SCALA:1:1	FOGLIO 1 DI 1

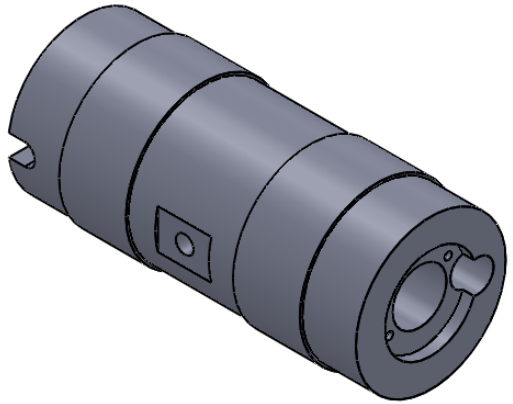

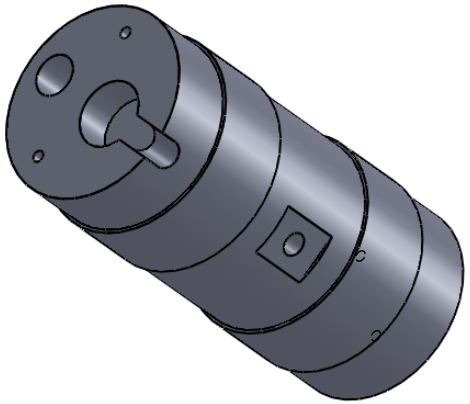

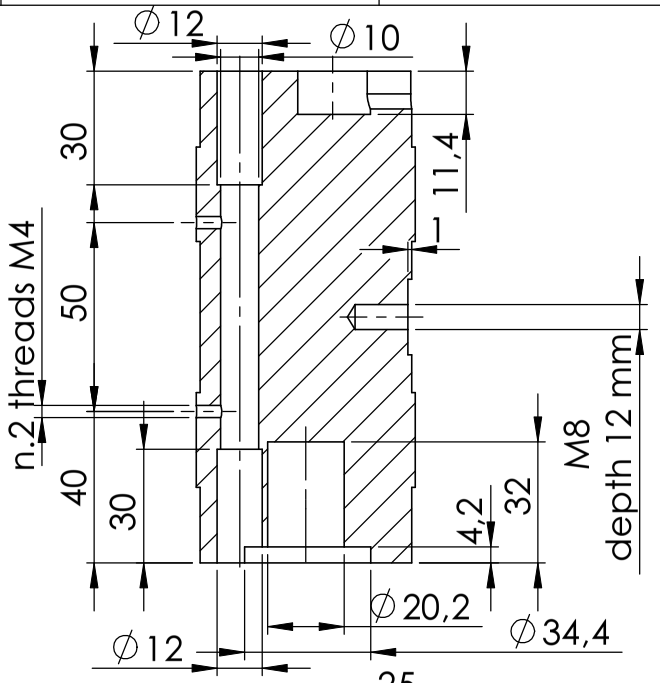

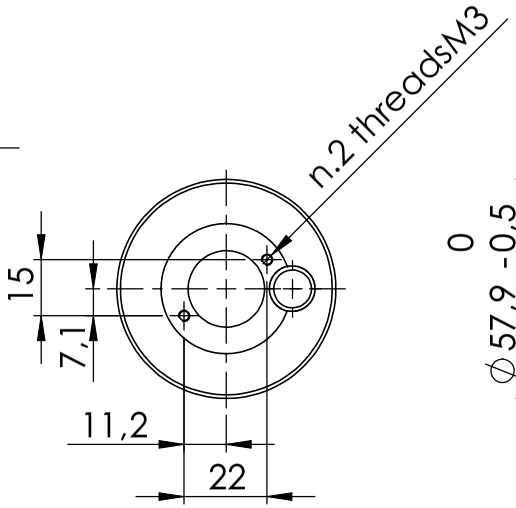

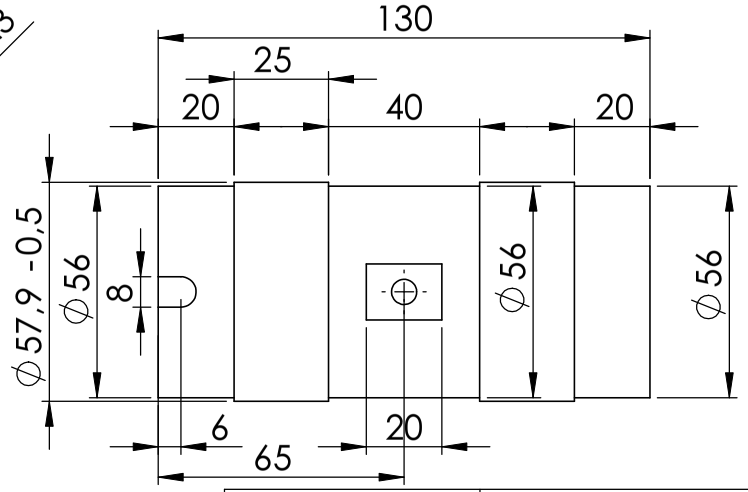

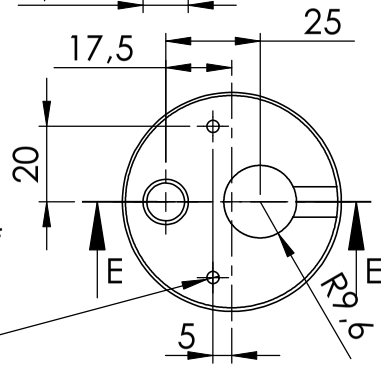

n.2 threads M4
useful depth
8 mm

SE NON SPECIFICATO: QUOTE IN MILLIMETRI FINITURA SUPERFICIE: TOLLERANZE: LINEARE: ANGOLARE:	FINITURA:	SBAVATURA E INTERRUZIONE DEI BORDI NETTI	NON SCALARE IL DISEGNO / REVISIONE

	NOME	FIRMA	DATA
DISEGNATO			
VERIFICATO			
APPROVATO			
FATTO			
QUALITA'			

TITOLO:

Cylindrical Body

MATERIALE: Aluminium

N. DISEGNO

A4

PESO: $PRPSHEET:{Peso}

SCALA:1:2

FOGLIO 1 DI 1

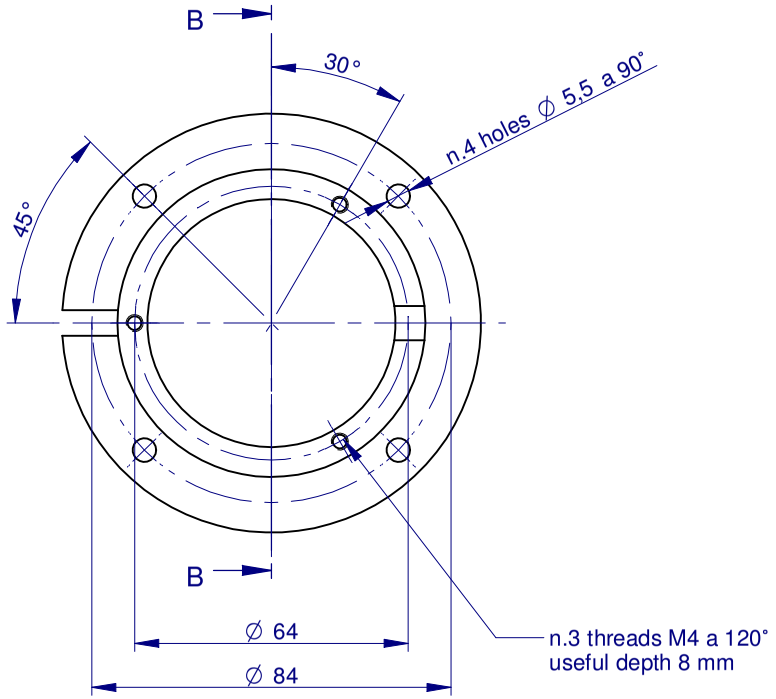

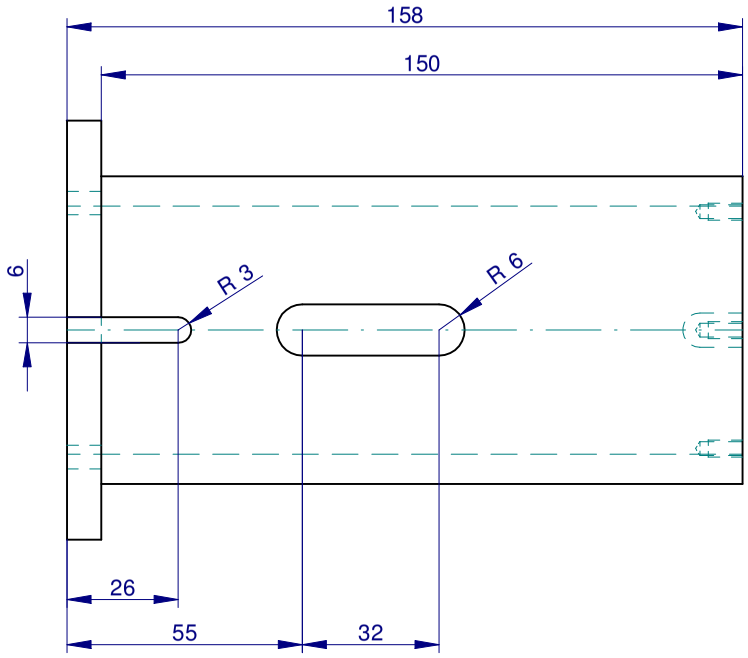

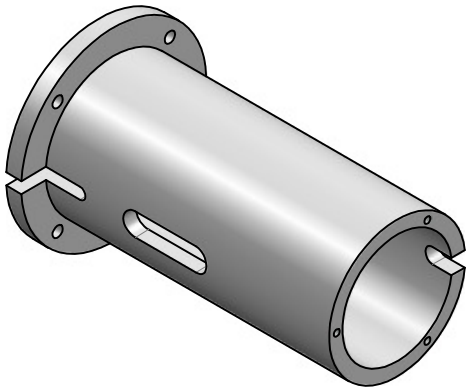

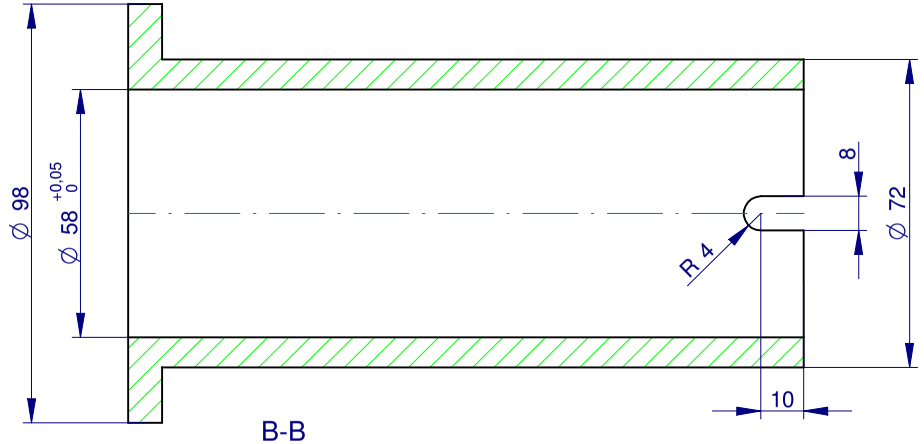

B-B

material	author	check	scale 1:1,25
Alluminium	Sara Matteoli		date 03.09.2005
OBJET: BUSHING			drawing n.: TSM 0503

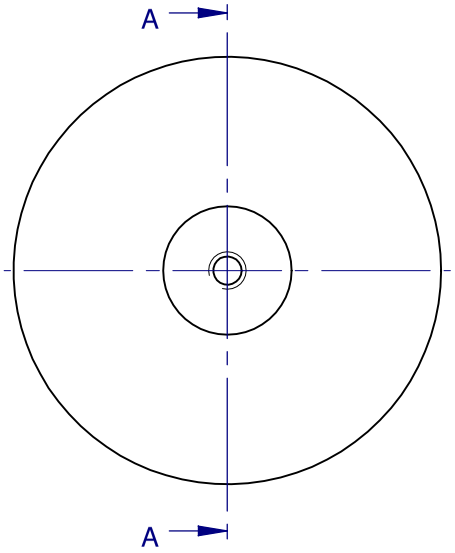

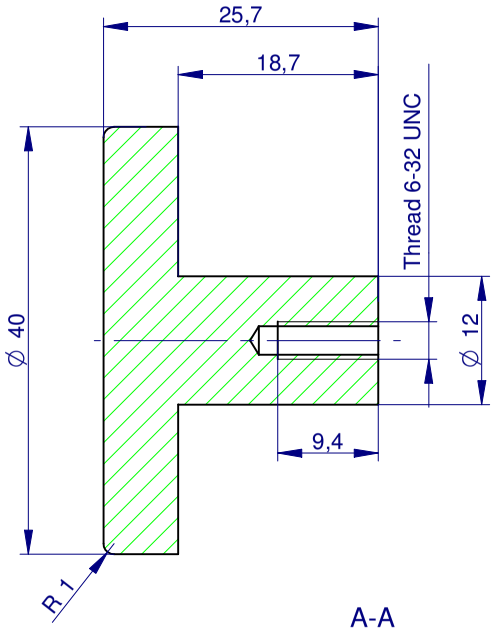

A-A

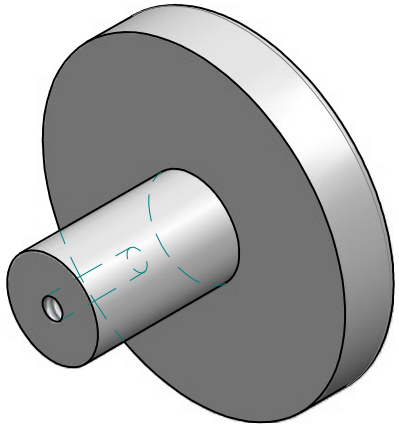

material	author	check	scale 2:1
Alluminium	Sara Matteoli		date 03.09.2005

OBJET	drawing n.
SENSOR	TSM 0504

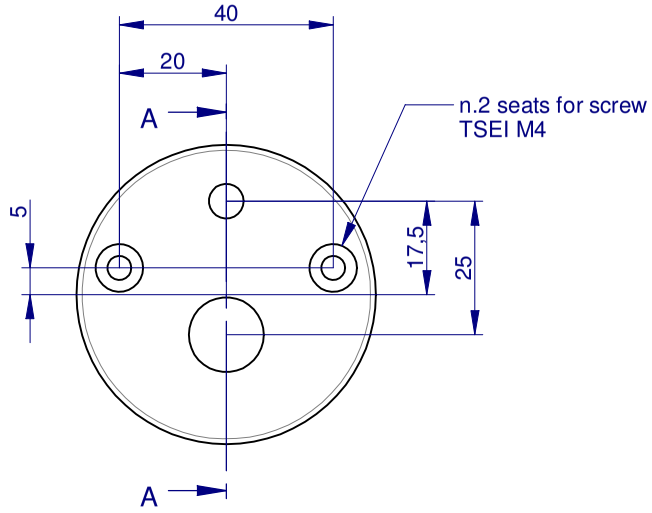

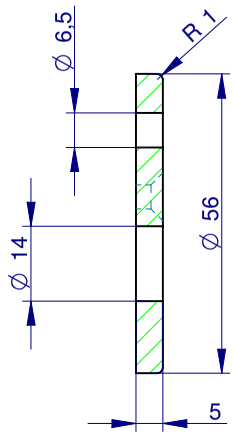

A-A

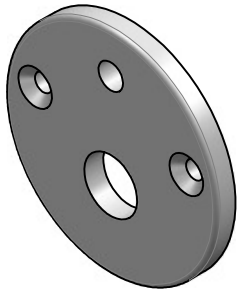

material	author	check	scale 1:1
Alluminium	Sara Matteoli		date 03.09.2005
OBJET: LID			drawing n.: TSM 0506

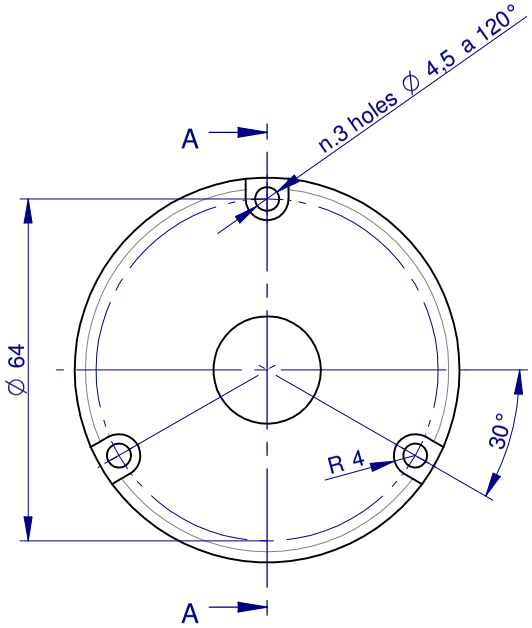

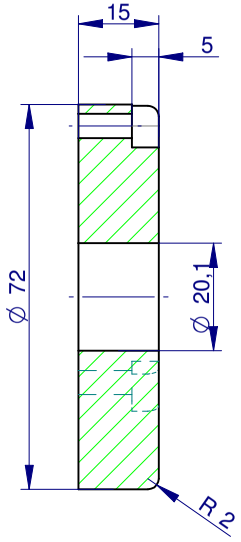

A-A

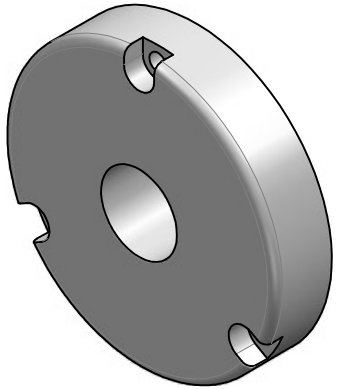

material	author	check	scale
Alluminium	Sara Matteoli		1:1
			date 03.09.2005

OBJET	drawing n.
THREADED LID	TSM 0507

APPENDIX C

- Appendix C1: Data for the 127 volunteers investigate to calculate Elastic modulus and Energy Dissipation Ratio
- Appendix C2: Data for the 134 volunteers investigate to calculate Unloaded and Loaded heel pad Thickness, and Heel Pad Compressibility Index

APPENDIX C1

		Subject characteristics											Load-displacement curve				Stress-strain curve			
													No correction		Correction 40 N		No correction		Correction 0,032 N/mm²	
N	Age group	Gender	Ethnicity	Age	Weight (kg)	Height (cm)	BMI (kg/m²)	Shoe size	Foot	Foot lenght (cm)	Foot width (cm)	Physical activity	Hours/week	Average EDR	SD	Average EDR	SD	Elastic modulus (Mpa)	SD	Elastic modulus (Mpa)	SD
1		M	E	20	69	168	24,45	42	Right	25,5	6	swimming	2	0,341	0,022	0,299	0,024	0,051	0,001	0,068	0,004
2		F	E	20	58,1	163	21,87	36	Right	24	6,2	football	4	0,361	0,051	0,307	0,053	0,044	0,001	0,061	0,005
3		M	E	21	73,2	178	23,10	43	Left	26,5	6	Running	1	0,309	0,041	0,305	0,048	0,067	0,003	0,071	0,004
4		M	E	21	70	173	23,39	41	Right	25,5	6,2	soccer	1	0,347	0,031	0,255	0,014	0,087	0,002	0,098	0,002
5		F	E	21	58,4	165,5	21,32	38	Right	24	6	cycle, gym	6	0,263	0,007	0,239	0,011	0,060	0,002	0,070	0,003
6		F	E	21	68,7	171,5	23,36	38	Right	24,2	5,5	run, swim, cycle	7	0,240	0,021	0,214	0,024	0,066	0,002	0,077	0,003
7		F	E	21	63,7	171,5	21,66	40	Right	26	6	football, run, gym	7	0,272	0,022	0,263	0,042	0,063	0,004	0,074	0,003
9		M	A	21	65,8	173	21,99	43	Right	25,8	6	cycle, walk	3	0,276	0,008	0,288	0,010	0,062	0,001	0,065	0,001
10		M	E	22	87,6	187	25,05	43	Right			gym, run, cycle	10	0,278	0,026	0,273	0,024	0,071	0,002	0,072	0,003
12		F	E	22	67,1	170	23,22	37	Left			boxing	4	0,267	0,019	0,279	0,021	0,073	0,002	0,086	0,002
13		F	E	22	51,5	166	18,69	37	Right	24,8	5,5	run, horseriding	9	0,267	0,018	0,272	0,023	0,063	0,004	0,065	0,004
14		F	E	22	65,7	166	23,84	36	Right	23,5		gym	1	0,316	0,029	0,327	0,030	0,079	0,001	0,095	0,003
15		M	E	22	79,7	187	22,79	44	Right	27,8	6,5	gym, bicycle	4	0,244	0,016	0,251	0,021	0,074	0,004	0,077	0,005
16		M	A	22	62,5	181	19,08	43	Right			tennis, run	1	0,298	0,024	0,296	0,034	0,058	0,002	0,059	0,003
17		M	E	22	68,9	178	21,75	41	Right			basket, cycle, kitesurfing	4	0,259	0,014	0,269	0,017	0,079	0,001	0,082	0,001
18		F	E	22	55,1	165	20,24	36	Right	22,3	5,2	swimming	2	0,294	0,004	0,287	0,007	0,061	0,001	0,065	0,001
19		M	E	23	70,9	196	18,46	45	Right			gym, run	3	0,269	0,015	0,276	0,023	0,084	0,002	0,086	0,003
20		M	E	23	89,9	186	25,99	42	Right	26,1	6,3	American football, gym	8	0,253	0,011	0,247	0,018	0,086	0,003	0,091	0,004
21		F	E	23	68,6	176	22,15	40	Right	26,2	5,9	Handball, gym, cycle	20	0,259	0,025	0,270	0,028	0,074	0,003	0,083	0,003
22		M	E	23	54	166	19,60	40	Right	23,9	6	Running	1	0,313	0,007	0,322	0,006	0,076	0,001	0,083	0,001
23		F	E	23	65,1	168	23,07	39	Right	24,9	5,5	cycling	7	0,328	0,012	0,343	0,012	0,070	0,002	0,083	0,002
24		F	A	23	53	156	21,78	36	Right	21,7	5,3	/	0	0,315	0,007	0,328	0,008	0,049	0,001	0,069	0,003
25		F	E	23	62,7	165	23,03	38	Right			cycle, gym	7	0,274	0,032	0,242	0,037	0,054	0,002	0,068	0,003
26		M	E	23	81,4	182	24,57	43	Right	26,5	6,3	run, cycle, swim, gym	20	0,266	0,009	0,273	0,012	0,086	0,002	0,090	0,002
27		F	E	23	60,1	168	21,29	40	Right			cycle, run	5	0,263	0,009	0,267	0,013	0,059	0,001	0,064	0,002
30		M	E	23	62,8	172	21,23	41	Right	24	5,58	running	2	0,291	0,029	0,300	0,034	0,062	0,002	0,071	0,001
31		M	E	23	78,5	194	20,86	42	Right	28,3	6,2	swimming	2	0,253	0,013	0,269	0,017	0,075	0,002	0,083	0,003
32		F	E	24	57,6	165	21,16	38	Right	23	5,3	badminton, cycling, gym	10	0,247	0,025	0,260	0,022	0,068	0,001	0,080	0,003
33		M	E	24	88,1	172,5	29,61	43	Right	26	6,3	cycle	1	0,232	0,013	0,232	0,013	0,100	0,004	0,105	0,004
34		M	E	24	82,3	189	23,04	44	Right	27	5	gym	5	0,240	0,012	0,249	0,022	0,092	0,002	0,095	0,003
35		F	E	24	59,2	167,5	21,10	39	Right	25,8	6,5	cycle, run	3	0,277	0,018	0,283	0,020	0,065	0,002	0,070	0,003
38	20-30	F	E	25	61,8	165	22,70	38,5	Right	25,9	6,8	running	2	0,278	0,017	0,247	0,024	0,055	0,001	0,073	0,002
39		M	E	25	72,1	183	21,53	42	Right	26,2	6,3	/	0	0,289	0,027	0,305	0,030	0,081	0,002	0,087	0,004
40		M	E	25	69,3	169,5	24,12	42	Right			/	0	0,277	0,005	0,243	0,008	0,076	0,003	0,087	0,004
41		F	E	25	74,6	177	23,81	41	Left	24,8	5,8	football	4	0,248	0,012	0,252	0,016	0,076	0,001	0,085	0,001
42		F	E	25	60,4	168	21,40	38	Right	22,2	5,3	spinning	4	0,261	0,021	0,271	0,021	0,079	0,001	0,085	0,001
43		M	E	25	88,7	178	28,00	45	Right	28,3	6,5	football, running, handball	10	0,272	0,007	0,282	0,008	0,076	0,007	0,083	0,008
44		M	A	25	74	169	25,91	42	Right	25,7	6,2	football, cycle	2	0,267	0,021	0,253	0,022	0,061	0,001	0,064	0,002
45		F	E	25	66	170	22,84	39	Right	24,6	6,4	/	0	0,347	0,042	0,369	0,052	0,071	0,003	0,087	0,004
46		F	E	25	64,4	160,5	25,00	38	Right	24,8	5,2	cycle, gym, run	6	0,315	0,017	0,317	0,021	0,066	0,001	0,071	0,001
47		F	E	26	61,7	175	20,15	40	Right	24,1	6	run, cycle	7,5	0,273	0,016	0,276	0,021	0,092	0,002	0,104	0,004
48		M	E	26	81,9	183,5	24,32	43	Right			run, gym, cycle	10	0,267	0,008	0,277	0,013	0,094	0,002	0,102	0,002
49		M	A	26	66,4	175	21,68	41	Right	24,2	6,4	basket ball	2	0,299	0,014	0,303	0,019	0,082	0,002	0,084	0,002
50		F	E	26	63,4	170	21,94	36	Right	22,8	5,3	/	0	0,253	0,012	0,241	0,013	0,055	0,001	0,061	0,005
51		F	E	26	51,1	168	18,11	38	Right	25,8	6,5	/	0	0,276	0,023	0,288	0,022	0,052	0,002	0,063	0,001
52		F	E	27	60,1	168	21,29	36	Right	23,5	5,8	running	2	0,319	0,010	0,325	0,014	0,049	0,001	0,053	0,001
53		M	E	27	72,1	172	24,37	41	Right	24,7	5,5	/	0	0,320	0,020	0,334	0,013	0,088	0,001	0,100	0,006
54		M	E	27	79,5	179	24,81	43	Right	27,5	5,5	football	4	0,257	0,008	0,273	0,017	0,067	0,001	0,077	0,002
55		F	E	27	63,7	167	22,84	37	Right	22,9	5,6	cycling, gym	7	0,309	0,016	0,319	0,030	0,073	0,002	0,084	0,005
56		M	A	28	62,7	168	22,22	42	Right	25,6	6,4	cycle	1	0,295	0,031	0,281	0,033	0,095	0,003	0,098	0,006
57		M	E	28	86,7	177,5	27,52	43	Right	24,2	6	Handball	5	0,252	0,006	0,267	0,010	0,092	0,002	0,097	0,001
58		F	E	28	74,9	175	24,46	41	Right	25,8	5,3	Badminton, spinning	7	0,277	0,010	0,287	0,021	0,071	0,002	0,078	0,002
59		M	E	28	87,4	194	23,22	44	Left	27,2	6,8	Cross fit	4	0,265	0,006	0,260	0,005	0,067	0,001	0,069	0,002
60		F	E	28	52	160	20,31	36	Right	23,9	5	run	2	0,246	0,013	0,246	0,024	0,077	0,001	0,080	0,001
61		M	E	28	68,7	167,5	24,49	42	Right	24,8	6,1	football, cycle	10	0,256	0,009	0,261	0,012	0,075	0,002	0,077	0,001
62		F	E	28	75,5	173	25,23	41	Right	25,8	6,6	handball, cycle	10	0,216	0,005	0,221	0,006	0,092	0,001	0,092	0,009
63		M	A	28	53,1	178	16,76	42	Right	26,2	6,4	/	0	0,254	0,004	0,255	0,005	0,060	0,001	0,066	0,001
64		M	E	28	82,5	182	24,91	42	Right	26	7	/	0	0,268	0,044	0,263	0,044	0,062	0,002	0,075	0,003
65		F	E	28	47,2	161	18,21	36	Right	21,9	6	running, cycling	1	0,290	0,011	0,297	0,008	0,060	0,001	0,073	0,001
66		M	E	29	86,6	188	24,50	45	Right	27,7	5,4	(run, cycle)	0	0,250	0,008	0,253	0,008	0,092	0,001	0,096	0,001
67		F	E	29	60,9	160	23,79	38	Right	24	5,5	cycling	2	0,266	0,014	0,273	0,015	0,077	0,001	0,084	0,001
68		F	E	30	55,5	157	22,52	36	Left	22,6	5,7	BodyBuilding. Thai Box	4	0,396	0,049	0,408	0,070	0,043	0,002	0,056	0,001
69		F	E	30	69,1	169	24,19	38	Right	23,8	6	thaiboxing, run	5	0,308	0,006	0,319	0,006	0,078	0,002	0,086	0,001
70		M	E	30	85,3	183	25,47	42	Right	25,1	6,6	Badminton	1	0,261	0,002	0,269	0,006	0,103	0,002	0,111	0,001
71		F	E	31	54,5	165	20,02	38	Right	24,7	6,3	swim, gym	7	0,240	0,021	0,246	0,018	0,071	0,002	0,078	0,002
72		M	E	32	73	183	21,80	43	Right			Badminton, cycle	6	0,286	0,010	0,289	0,015	0,099	0,002	0,103	0,002
74		M	E	34	80	174,5	26,27	42	Left	25,7	6,5	cyle, gym	7	0,271	0,007	0,275	0,006	0,080	0,001	0,089	0,002
75		M	E	34	76,2	178	24,05	45	Right	27,1	6,8	running, cycling	6	0,389	0,046	0,391	0,057	0,059	0,007	0,068	0,010
76		F	E	35	75,6	177	24,13	41	Right	25,5	5,7	gym,cycling	3	0,275	0,009	0,285	0,007	0,070	0,001	0,077	0,002
77		F	E	35	61,9	167	22,20	38,5	Right	24,2	5,5	running, cycling	5	0,310	0,039	0,320	0,045	0,059	0,002	0,066	0,003
78		F	E	35	66,5	168	23,56	39	Right	25,3	6,3	/	0	0,296	0,015	0,293	0,026	0,080	0,002	0,087	0,004
79		M	E	35	71,3	183,5	21,17	42	Right	25,9	6,8	fresbee	4	0,305	0,027	0,323	0,034	0,081	0,003	0,090	0,003
80		M	E	35	91,8	178	28,97	42	Right	26,5	6,8	walking	1	0,281	0,011	0,294	0,014	0,097	0,002	0,109	0,003
81		M	E	36	79,6	178	25,12	41	Right	27,6	6	Running	4	0,285	0,017	0,300	0,016	0,068	0,001	0,080	0,002
82		M	E	36	127,4	184	37,63	45	Right	26,7	6,6	karate	4,5	0,264	0,015	0,271	0,021	0,092	0,004	0,098	0,004
83	31-41	M	E	37	75,5	170	26,12	42	Right	27	8	/	0	0,296	0,013	0,304	0,024	0,097	0,001	0,116	0,002
84		M	E	37	88,5	176	28,57	42,5	Right	27,3	6,7	Running	5	0,298	0,015	0,311	0,017	0,075	0,001	0,083	0,0002
85		M	E	38	75,3	172	25,45	40	Right	25,2	5,9	football, running, bike	4	0,351	0,023	0,365	0,030	0,064	0,003	0,075	0,003
86		F	E	38	79,3	169	27,77	39	Right	23,6	6,1	running, cycling, gym	3	0,293	0,004	0,319	0,008	0,079	0,001	0,089	0,003
87		F	E	39	58,8	171	20,11	40	Right	25,7	6	swimming, walking, cycling	3	0,250	0,011	0,252	0,025	0,052	0,001	0,058	0,003
88		F	E	39	57,7	164,5	21,32	37	Right	23	5,3	/	0	0,282	0,018	0,292	0,022	0,080	0,002	0,089	0,003
89		F	E	39	62	171	21,20	39	Right	24,6	5,6	dancing, gym	1,5	0,279	0,012	0,273	0,028	0,052	0,001	0,059	0,004
90		F	E	40	66	169	23,11	39	Left	24,8	6,3	/	0	0,357	0,031	0,377	0,044	0,065	0,003	0,085	0,005
91		F	E	41	67,8	163	25,52	37	Left	23,2	6,4	fitness, cycling	2	0,285	0,016	0,297	0,013	0,080	0,001	0,088	0,001
92		M	E	40	71,1	169	24,89	41	Right	26,2	6,8	/	0	0,312	0,012	0,298	0,016	0,063	0,004	0,071	0,005
93		M	E	42	70,8	185	20,69	42	Left	27,5	6,7	/	0	0,326	0,011	0,348	0,012	0,067	0,001	0,081	0,001
94		F	E	42	87,2	175	28,47	40	Left	26,3	6,2	/	0	0,320	0,020	0,345	0,024	0,071	0,002	0,080	0,0004
95		M	E	42	78	196	20,30	46	Right	30	6,9	cycling	3	0,324	0,023	0,330	0,025	0,064	0,002	0,083	0,002
96		M	E	43	96,5	187	27,60	45	Right	27	6,9	Running	3	0,302	0,008	0,308	0,011	0,091	0,002	0,098	0,002
97		F	E	43	87,4	170	30,24	37	Right	22,7	5,8	Badminton, Horseriding	2	0,267	0,005	0,278	0,003	0,083	0,001	0,077	0,002
98		M	E	44	79,3	194	21,07	46	Right	29	6,5	Running	3	0,307	0,012	0,315	0,014	0,060	0,001	0,071	0,001
99		M	E	45	97,3	193	26,12	44	Right	27,6	6,6	badminton, cycling	5	0,289	0,012	0,291	0,018	0,084	0,001	0,089	0,001
100		F	E	46	63,2	161,5	24,23	36	Right	23,2	6	swimming, running	3	0,294	0,009	0,297	0,014	0,066	0,004	0,079	0,001
102	42-52	F	E	47	58,4	166	21,19	38	Right	23,7	6,3	yoga, running	3,5	0,290	0,020	0,299	0,025	0,062	0,003	0,071	0,002
103		M	E	47	101,7	185	29,72	44	Right	27,7	6,3	/	0	0,286	0,029	0,276	0,017	0,092	0,002	0,100	0,001
104		F	E	48	74,9	162	28,54	39	Right	24,2	6,4	cycling	8	0,322	0,008	0,291	0,002	0,054	0,004	0,064	0,005
105		F	E	48	69,4	169	24,30	37	Right	24,5	6,2	running	2,5	0,312	0,021	0,298	0,021	0,061	0,001	0,070	0,006
106		F	E	48	49,3	157	20,00	35,5	Right	22,3	5,2	running	3	0,312	0,008	0,320	0,013	0,057	0,001	0,072	0,001
107		M	E	49	67,4	182	20,35	42	Right	27	6,5	yoga, fitness	4	0,333	0,021	0,336	0,026	0,059	0,002	0,066	0,001
108		F	E	49	80,3	173	26,83	40	Right	25	6,9	Cycling	7	0,276	0,018	0,282	0,016	0,078	0,002	0,091	0,002

109		F	E	49	65,9	171	22,54	38	Right	24,1	6	karate, running, zumba	9	0,345	0,024	0,351	0,020	0,053	0,002	0,067	0,002
110		F	E	51	80,3	176	25,92	41	Right	25,5	6,3	race walking	3	0,282	0,020	0,300	0,022	0,084	0,001	0,093	0,002
111		M	E	51	79,4	184	23,45	43	Right	26,6	6,5	tennis, gym	3	0,355	0,011	0,361	0,012	0,082	0,001	0,089	0,001
112		F	E	52	61,6	166	22,35	38,5	Right	24,5	6,3	horseriding	20	0,303	0,008	0,313	0,006	0,061	0,002	0,066	0,002
113		M	E	53	85,4	188,5	24,03	45	Left	28,2	7,3	Running, golf, cycling	11	0,306	0,090	0,305	0,016	0,089	0,002	0,099	0,002
114		F	E	54	61,7	153	26,36	36,5	Right	23,1	5,3	fitness	1	0,314	0,017	0,369	0,019	0,059	0,001	0,072	0,002
115		F	E	55	66,4	174	21,93	39	Right	26	6	walking, gym	6	0,327	0,015	0,339	0,019	0,063	0,001	0,073	0,004
116		F	E	55	54,9	167	19,69	39	Left	26	5,6	running	7	0,328	0,022	0,335	0,024	0,051	0,002	0,053	0,002
117		M	E	56	118,5	200	29,63	47	Right	29	7	tabletennis	2	0,284	0,027	0,290	0,027	0,094	0,003	0,098	0,003
118		F	E	56	81	168,5	28,53	38	Left	25	7	fitness, running, cycling	8	0,310	0,013	0,311	0,013	0,060	0,003	0,071	0,002
119		M	E	57	86,6	180	26,73	43	Right	27	6,4	/	0	0,312	0,024	0,315	0,028	0,088	0,002	0,098	0,001
120	53-63	M	E	58	78,2	181	23,87	43	Right	26,8	6,9	/	0	0,338	0,010	0,361	0,015	0,080	0,004	0,093	0,006
121		M	E	58	83,5	177	26,65	44	Right	27,8	6,9	/	0	0,326	0,024	0,339	0,022	0,079	0,002	0,089	0,002
122		M	E	58	83,7	192	22,71	43	Right	26,6	6,4	running, cycling	5	0,341	0,027	0,364	0,031	0,098	0,003	0,115	0,002
123		F	E	59	48,4	153,5	20,54	36	Right	22,9	5,5	/	0	0,305	0,012	0,325	0,016	0,057	0,001	0,063	0,002
124		M	E	59	64,5	173	21,55	41	Right	24,7	5,6	Running	1	0,298	0,203	0,319	0,024	0,085	0,002	0,093	0,002
125		M	E	61	83,6	180	25,80	43,5	Right	27,5	7,2	Running	1	0,370	0,009	0,394	0,013	0,070	0,002	0,081	0,002
126		F	E	61	78,3	162	29,84	39	Right	24,5	6,2	golf	8	0,283	0,010	0,286	0,023	0,070	0,002	0,080	0,001
127		F	E	62	59,4	170	20,55	39	Right	25,5	6,3	cycling,walking	10	0,311	0,022	0,274	0,023	0,059	0,003	0,075	0,004
128		M	E	63	72	178	22,72	43	Right	27,1	6,1	Running, cycling	5	0,334	0,019	0,349	0,019	0,061	0,001	0,073	0,001
129		F	E	65	66,2	160	25,86	39	Right	24,1	6,2	walking	10	0,348	0,032	0,355	0,031	0,098	0,002	0,115	0,004
130		F	E	67	53	159	20,96	37	Right	24,3	5,8	gym	3	0,301	0,017	0,316	0,016	0,068	0,001	0,081	0,000
131		M	E	67	98,7	194	26,22	44	Right	28,5	7,2	Tennis	2	0,414	0,033	0,391	0,031	0,037	0,003	0,040	0,003
132	> 64	M	E	68	77	172	26,03	39,5	Right	24,2	6,2	/	0	0,344	0,022	0,363	0,020	0,083	0,002	0,094	0,002
133		M	E	68	74,7	170	25,85	42	Right	26,1	6,1	running	2	0,371	0,030	0,379	0,021	0,048	0,002	0,053	0,003
134		F	E	79	62,9	162,5	23,82	39	Left	25,5	6,6	Gym, watergym	2	0,353	0,029	0,328	0,019	0,052	0,002	0,057	0,004
135		M	E	71	81	176	26,15	44	Right	28	6,5	Gym	1,5	0,356	0,028	0,366	0,024	0,063	0,001	0,072	0,001

APPENDIX C2

		Subject characteristics												Heel pad thickness		
N	Age group	Gender	Ethnicity	Age	Weight (kg)	Height (cm)	BMI (kg/m^2)	Shoe size	Foot	Foot lenght (cm)	Foot width (cm)	Physical activity	Hours/week	UHPT (mm)	LHPT (mm)	HPCI (%)
1		M	E	20	69	168	24,45	42	Right	25,5	6	swimming	2	17,90	9,20	51,40
2		F	E	20	58,1	163	21,87	36	Right	24	6,2	football	4	15,15	8,90	58,75
3		M	E	21	73,2	178	23,10	43	Left	26,5	6	Running	1	15,10	9,45	62,58
4		M	E	21	70	173	23,39	41	Right	25,5	6,2	soccer	1	16,20	8,30	51,23
5		F	E	21	58,4	165,5	21,32	38	Right	24	6	cycle, gym	6	16,45	8,88	53,95
6		F	E	21	68,7	171,5	23,36	38	Right	24,2	5,5	run, swim, cycle	7	15,63	8,90	56,96
7		F	E	21	63,7	171,5	21,66	40	Right	26	6	football, run, gym	7	14,73	8,55	58,06
8		M	A	21	66,9	174	22,10	42	Right	26,5	6,5	football, cycle	2	12,15	5,98	49,18
9		M	A	21	65,8	173	21,99	43	Right	25,8	6	cycle, walk	3	12,25	5,98	48,82
10		M	E	22	87,6	187	25,05	43	Right			gym, run, cycle	10	16,08	10,05	62,50
11		F	A	22	54,7	166,5	19,73	38	Right	23,1	6	-	0	13,85	7,13	51,44
12		F	E	22	67,1	170	23,22	37	Left			boxing	4	14,00	8,90	63,57
13		F	E	22	51,5	166	18,69	37	Right	24,8	5,5	run, horseriding	9	13,78	8,30	60,23
14		F	E	22	65,7	166	23,84	36	Right	23,5		gym	1	18,15	11,55	63,64
15		M	E	22	79,7	187	22,79	44	Right	27,8	6,5	gym, bicycle	4	15,43	9,20	59,62
16		M	A	22	62,5	181	19,08	43	Right			tennis, run	1	14,38	6,15	42,77
17		M	E	22	68,9	178	21,75	41	Right			basket, cycle, kitesurfing	4	14,35	9,53	66,41
18		F	E	22	55,1	165	20,24	36	Right	22,3	5,2	swimming	2	14,65	7,93	54,10
19		M	E	23	70,9	196	18,46	45	Right			gym, run	3	15,60	7,58	48,56
20		M	E	23	89,9	186	25,99	42	Right	26,1	6,3	American football, gym	8	17,10	9,70	56,73
21		F	E	23	68,6	176	22,15	40	Right	26,2	5,9	Handball, gym, cycle	20	16,03	7,93	49,44
22		M	E	23	54	166	19,60	40	Right	23,9	6	Running	1	16,25	9,15	56,31
23		F	E	23	65,1	168	23,07	39	Right	24,9	5,5	cycling	7	14,90	9,95	66,78
24		F	A	23	53	156	21,78	36	Right	21,7	5,3	/	0	11,05	6,95	62,90
25		F	E	23	62,7	165	23,03	38	Right			cycle, gym	7	14,93	8,43	56,43
26		M	E	23	81,4	182	24,57	43	Right	26,5	6,3	run, cycle, swim, gym	20	16,75	10,58	63,13
27		F	E	23	60,1	168	21,29	40	Right			cycle, run	5	13,18	8,25	62,59
28		F	A	23	55,5	160	21,68	37	Right	23,1	5,4	/	0	14,85	8,88	59,76
29		M	M	23			Right		Right					13,70	8,20	59,85
30		M	E	23	62,8	172	21,23	41	Right	24	5,58	running	2	15,55	10,20	65,59
31		M	E	23	78,5	194	20,86	42	Right	28,3	6,2	swimming	2	14,35	8,45	58,89
32		F	E	24	57,6	165	21,16	38	Right	23	5,3	badminton, cycling, gym	10	12,55	8,45	67,33
33		M	E	24	88,1	172,5	29,61	43	Right	26	6,3	cycle	1	18,33	9,30	50,74
34		M	E	24	82,3	189	23,04	44	Right	27	5	gym	5	16,63	10,10	60,73
35	20-30	F	E	24	59,2	167,5	21,10	39	Right	25,8	6,5	cycle, run	3	13,73	6,65	48,43
36		M	E	24	66	175	21,55	42	Right	25,7	6,5	football	2	17,00	10,10	59,41
37		M	E	24	84,5	182	25,51	45	Right			run	1	18,10	9,50	52,49
38		F	E	25	61,8	165	22,70	38,5	Right	25,9	6,8	running	2	15,40	11,13	72,24
39		M	E	25	72,1	183	21,53	42	Right	26,2	6,3	/	0	16,75	9,25	55,22
40		M	E	25	69,3	169,5	24,12	42	Right			/	0	18,03	9,53	52,83
41		F	E	25	74,6	177	23,81	41	Left	24,8	5,8	football	4	13,18	7,15	54,25
42		F	E	25	60,4	168	21,40	38	Right	22,2	5,3	spinning	4	15,30	8,33	54,41
43		M	E	25	88,7	178	28,00	45	Right	28,3	6,5	football, running, handball	10	17,98	10,40	57,84
44		M	A	25	74	169	25,91	42	Right	25,7	6,2	football, cycle	2	17,38	7,68	44,16
45		F	E	25	66	170	22,84	39	Right	24,6	6,4	/	0	15,05	10,10	67,11
46		F	E	25	64,4	160,5	25,00	38	Right	24,8	5,2	cycle, gym, run	6	12,98	8,30	63,94
47		F	E	26	61,7	175	20,15	40	Right	24,1	6	run, cycle	7,5	15,53	8,95	57,63
48		M	E	26	81,9	183,5	24,32	43	Right			run, gym, cycle	10	17,00	11,00	64,71
49		M	A	26	66,4	175	21,68	41	Right	24,2	6,4	basket ball	2	14,80	8,75	59,12
50		F	E	26	63,4	170	21,94	36	Right	22,8	5,3	/	0	13,20	8,15	61,74
51		F	E	26	51,1	168	18,11	38	Right	25,8	6,5	/	0	11,95	6,40	53,56
52		F	E	27	60,1	168	21,29	36	Right	23,5	5,8	running	2	11,75	8,30	70,64
53		M	E	27	72,1	172	24,37	41	Right	24,7	5,5	/	0	18,50	11,55	62,43
54		M	E	27	79,5	179	24,81	43	Right	27,5	5,5	football	4	13,30	7,35	55,26
55		F	E	27	63,7	167	22,84	37	Right	22,9	5,6	cycling, gym	7	16,25	8,30	51,08
56		M	A	28	62,7	168	22,22	42	Right	25,6	6,4	cycle	1	17,93	12,25	68,32
57		M	E	28	86,7	177,5	27,52	43	Right	24,2	6	Handball	5	18,25	8,93	48,90
58		F	E	28	74,9	175	24,46	41	Right	25,8	5,3	Badminton, spinning	7	13,10	7,23	55,15
59		M	E	28	87,4	194	23,22	44	Left	27,2	6,8	Cross fit	4	13,93	6,48	46,48
60		F	E	28	52	160	20,31	36	Right	23,9	5	run	2	13,70	8,50	62,04
61		M	E	28	68,7	167,5	24,49	42	Right	24,8	6,1	football, cycle	10	15,33	7,88	51,37
62		F	E	28	75,5	173	25,23	41	Right	25,8	6,6	handball, cycle	10	17,83	10,33	57,91
63		M	A	28	53,1	178	16,76	42	Right	26,2	6,4	/	0	12,68	6,58	51,85
64		M	E	28	82,5	182	24,91	42	Right	26	7	/	0	16,65	9,05	54,35
65		F	E	28	47,2	161	18,21	36	Right	21,9	6	running, cycling	1	13,90	6,95	50,00
66		M	E	29	86,6	188	24,50	45	Right	27,7	5,4	(run, cycle)	0	14,45	8,75	60,55
67		F	E	29	60,9	160	23,79	38	Right	24	5,5	cycling	2	13,00	8,95	68,85
68		F	E	30	55,5	157	22,52	36	Left	22,6	5,7	BodyBuilding. Thai Box	4	12,10	6,05	50,00
69		F	E	30	69,1	169	24,19	38	Right	23,8	6	thaiboxing, run	5	15,58	9,13	58,57
70		M	E	30	85,3	183	25,47	42	Right	25,1	6,6	Badminton	1	17,60	10,20	57,95
71		F	E	31	54,5	165	20,02	38	Right	24,7	6,3	swim, gym	7	16,25	8,40	51,69
72		M	E	32	73	183	21,80	43	Right			Badminton, cycle	6	17,40	11,73	67,39
73		M	E	33	109	192	29,57	49	Right			run, handball, basl	7	17,25	8,25	47,83
74		M	E	34	80	174,5	26,27	42	Left	25,7	6,5	cyle, gym	7	16,33	10,98	67,21
75		M	E	34	76,2	178	24,05	45	Right	27,1	6,8	running, cycling	6	16,10	9,95	61,80
76		F	E	35	75,6	177	24,13	41	Right	25,5	5,7	gym,cycling	3	13,80	7,10	51,45
77		F	E	35	61,9	167	22,20	38,5	Right	24,2	5,5	running, cycling	5	11,20	8,60	76,79
78		F	E	35	66,5	168	23,56	39	Right	25,3	6,3	/	0	15,00	8,50	56,67
79		M	E	35	71,3	183,5	21,17	42	Right	25,9	6,8	fresbee	4	15,55	10,10	64,95
80		M	E	35	91,8	178	28,97	42	Right	26,5	6,8	walking	1	17,65	9,60	54,39
81		M	E	36	79,6	178	25,12	41	Right	27,6	6	Running	4	14,15	8,55	60,42
82	31-41	M	E	36	127,4	184	37,63	45	Right	26,7	6,6	karate	4,5	17,80	12,10	67,98
83		M	E	37	75,5	170	26,12	42	Right	27	8	/	0	17,50	10,95	62,57
84		M	E	37	88,5	176	28,57	42,5	Right	27,3	6,7	Running	5	16,95	8,35	49,26
85		M	E	38	75,3	172	25,45	40	Right	25,2	5,9	football, running, bike	4	14,15	9,70	68,55

86		F	E	38	79,3	169	27,77	39	Right	23,6	6,1	running, cycling, gym	3	18,00	11,90	66,11
87		F	E	39	58,8	171	20,11	40	Right	25,7	6	swimming, walking, cycling	3	10,20	5,40	52,94
88		F	E	39	57,7	164,5	21,32	37	Right	23	5,3	/	0	15,40	9,65	62,66
89		F	E	39	62	171	21,20	39	Right	24,6	5,6	dancing, gym	1,5	10,95	6,05	55,25
90		F	E	40	66	169	23,11	39	Left	24,8	6,3	/	0	15,35	8,30	54,07
91		F	E	41	67,8	163	25,52	37	Left	23,2	6,4	fitness, cycling	2	17,35	6,45	37,18
92		M	E	40	71,1	169	24,89	41	Right	26,2	6,8	/	0	16,70	8,75	52,40
93		M	E	42	70,8	185	20,69	42	Left	27,5	6,7	/	0	14,35	8,70	60,63
94		F	E	42	87,2	175	28,47	40	Left	26,3	6,2	/	0	16,50	10,00	60,61
95		M	E	42	78	196	20,30	46	Right	30	6,9	cycling	3	12,00	7,50	62,50
96		M	E	43	96,5	187	27,60	45	Right	27	6,9	Running	3	17,80	10,45	58,71
97		F	E	43	87,4	170	30,24	37	Right	22,7	5,8	Badminton, Horseriding	2	14,70	8,50	57,82
98		M	E	44	79,3	194	21,07	46	Right	29	6,5	Running	3	13,20	7,90	59,85
99		M	E	45	97,3	193	26,12	44	Right	27,6	6,6	badminton, cycling	5	15,85	9,13	57,57
100		F	E	46	63,2	161,5	24,23	36	Right	23,2	6	swimming, running	3	16,70	9,10	54,49
101		F	E	46	64,8	175	21,16	39,5	Right	26,7	6	yoga, running	5	14,55	9,25	63,57
102	42-52	F	E	47	58,4	166	21,19	38	Right	23,7	6,3	yoga, running	3,5	13,50	8,30	61,48
103		M	E	47	101,7	185	29,72	44	Right	27,7	6,3	/	0	17,70	11,75	66,38
104		F	E	48	74,9	162	28,54	39	Right	24,2	6,4	cycling	8	15,15	8,50	56,11
105		F	E	48	69,4	169	24,30	37	Right	24,5	6,2	running	2,5	15,00	8,45	56,33
106		F	E	48	49,3	157	20,00	35,5	Right	22,3	5,2	running	3	12,05	5,85	48,55
107		M	E	49	67,4	182	20,35	42	Right	27	6,5	yoga, fitness	4	14,60	7,80	53,42
108		F	E	49	80,3	173	26,83	40	Right	25	6,9	Cycling	7	18,05	12,40	68,70
109		F	E	49	65,9	171	22,54	38	Right	24,1	6	karate, running, zumba	9	14,75	8,70	58,98
110		F	E	51	80,3	176	25,92	41	Right	25,5	6,3	race walking	3	16,25	10,75	66,15
111		M	E	51	79,4	184	23,45	43	Right	26,6	6,5	tennis, gym	3	15,25	9,55	62,62
112		F	E	52	61,6	166	22,35	38,5	Right	24,5	6,3	horseriding	20	14,30	8,00	55,94
113		M	E	53	85,4	188,5	24,03	45	Left	28,2	7,3	Running, golf, cycling	11	17,95	10,50	58,50
114		F	E	54	61,7	153	26,36	36,5	Right	23,1	5,3	fitness	1	12,30	7,50	60,98
115		F	E	55	66,4	174	21,93	39	Right	26	6	walking, gym	6	12,20	6,40	52,46
116		F	E	55	54,9	167	19,69	39	Left	26	5,6	running	7	12,20	8,65	70,90
117		M	E	56	118,5	200	29,63	47	Right	29	7	tabletennis	2	18,15	10,25	56,47
118		F	E	56	81	168,5	28,53	38	Left	25	7	fitness, running, cycling	8	15,85	10,65	67,19
119		M	E	57	86,6	180	26,73	43	Right	27	6,4	/	0	18,45	12,85	69,65
120	53-63	M	E	58	78,2	181	23,87	43	Right	26,8	6,9	/	0	15,20	9,35	61,51
121		M	E	58	83,5	177	26,65	44	Right	27,8	6,9	/	0	18,15	10,55	58,13
122		M	E	58	83,7	192	22,71	43	Right	26,6	6,4	running, cycling	5	16,85	10,20	60,53
123		F	E	59	48,4	153,5	20,54	36	Right	22,9	5,5	/	0	13,70	7,90	57,66
124		M	E	59	64,5	173	21,55	41	Right	24,7	5,6	Running	1	14,55	8,50	58,42
125		M	E	61	83,6	180	25,80	43,5	Right	27,5	7,2	Running	1	13,45	9,85	73,23
126		F	E	61	78,3	162	29,84	39	Right	24,5	6,2	golf	8	16,75	10,95	65,37
127		F	E	62	59,4	170	20,55	39	Right	25,5	6,3	cycling,walking	10	15,10	8,50	56,29
128		M	E	63	72	178	22,72	43	Right	27,1	6,1	Running, cycling	5	13,45	8,50	63,20
129		F	E	65	66,2	160	25,86	39	Right	24,1	6,2	walking	10	19,85	12,60	63,48
130		F	E	67	53	159	20,96	37	Right	24,3	5,8	gym	3	14,05	9,75	69,40
131		M	E	67	98,7	194	26,22	44	Right	28,5	7,2	Tennis	2	13,05	7,60	58,24
132	> 64	M	E	68	77	172	26,03	39,5	Right	24,2	6,2	/	0	14,70	10,65	72,45
133		M	E	68	74,7	170	25,85	42	Right	26,1	6,1	running	2	11,70	7,70	65,81
134		F	E	79	62,9	162,5	23,82	39	Left	25,5	6,6	Gym, watergym	2	17,45	10,25	58,74
135		M	E	71	81	176	26,15	44	Right	28	6,5	Gym	1,5	11,95	9,95	83,26

APPENDIX D

- Appendix D1: Statistical plots for Heel Pad Compressibility Index
- Appendix D2: Statistical plots for Elastic modulus
- Appendix D3: Statistical plots for Energy Dissipation Ratio

APPENDIX D1

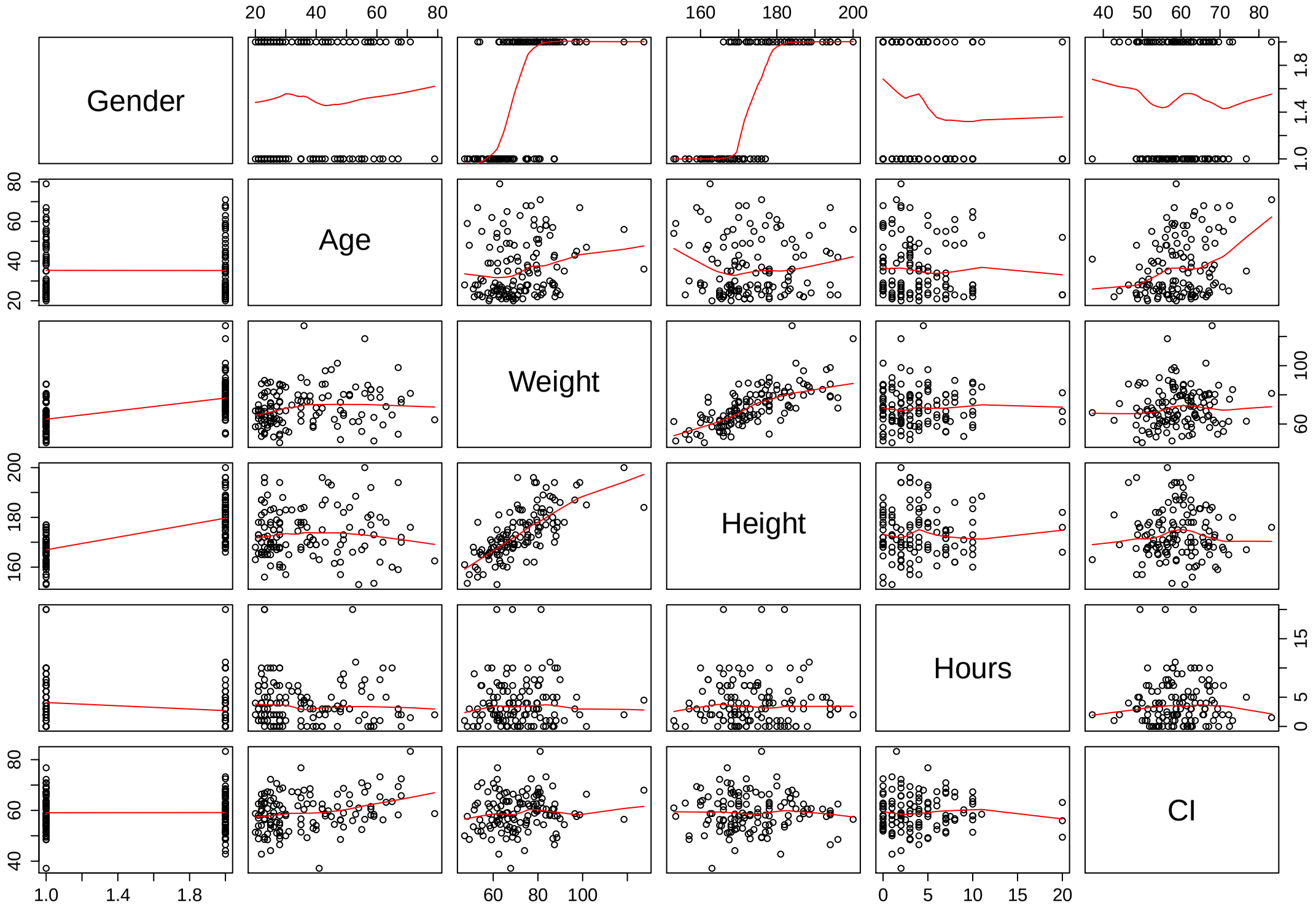
Gender
Age
Weight
Height
Hours
CI
20 40 60 80
160 180 200
40 50 60 70 80
1.0 1.4 1.8
20 40 60 80
60 100
160 180 200
0 5 15
40 60 80
1.0 1.4 1.8
60 80 100
0 5 10 15 20

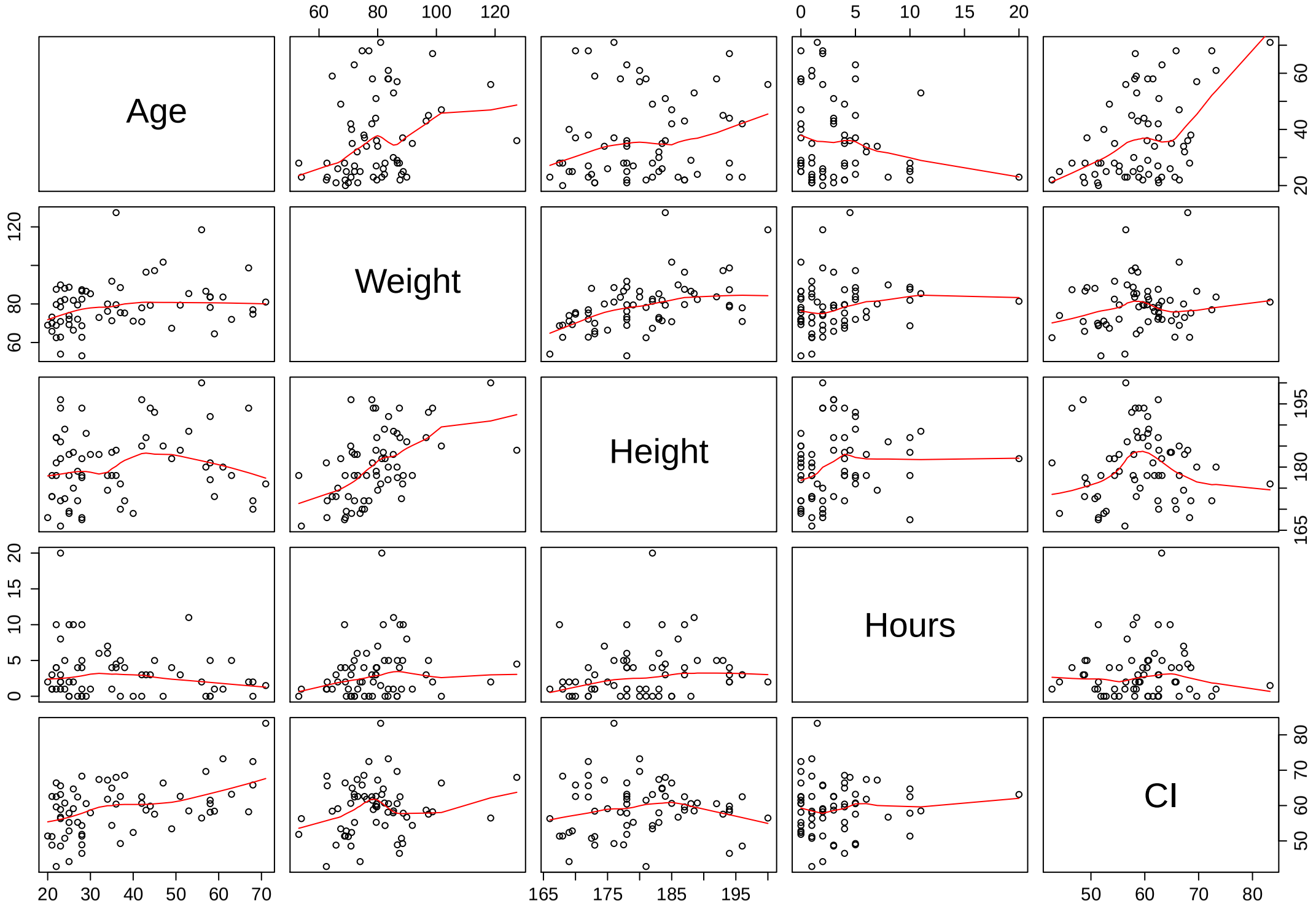
Age
Weight
Height
Hours
CI
60 80 100 120
0 5 10 15 20
20 30 40 50 60 70
165 175 185 195
50 60 70 80

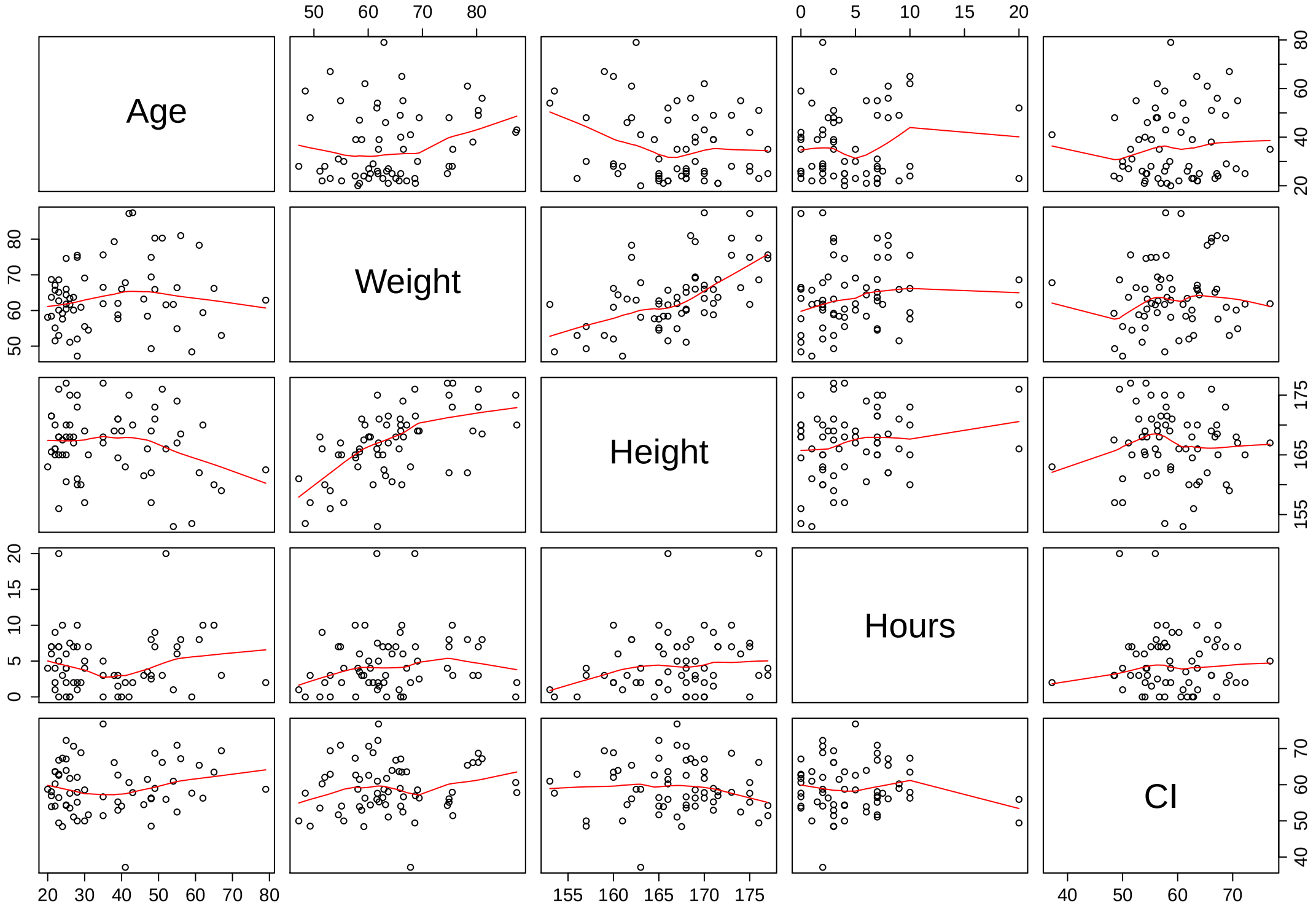
Age
Weight
Height
Hours
CI
50 60 70 80
0 5 10 15 20
20 30 40 50 60 70 80
50 60 70 80
155 160 165 170 175
155 165 175
0 5 10 15 20
40 50 60 70

APPENDIX D2

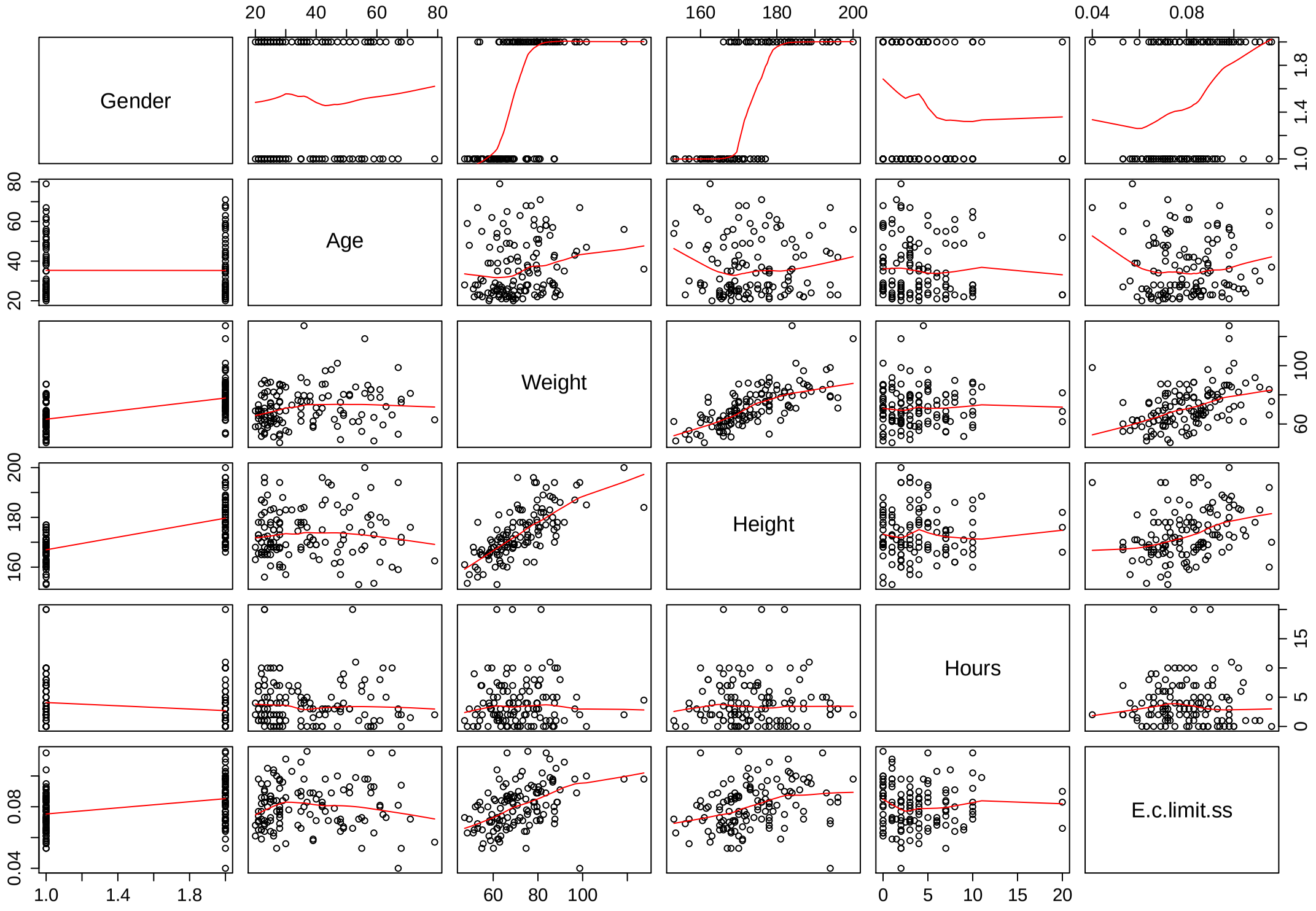
Gender
Age
Weight
Height
Hours
E.c.limit.ss
20 40 60 80
160 180 200
0.04 0.08
1.0 1.4 1.8
20 40 60 80
60 80 100
160 180 200
0.04 0.08
1.0 1.4 1.8
60 80 100
0 5 10 15 20
0 5 15

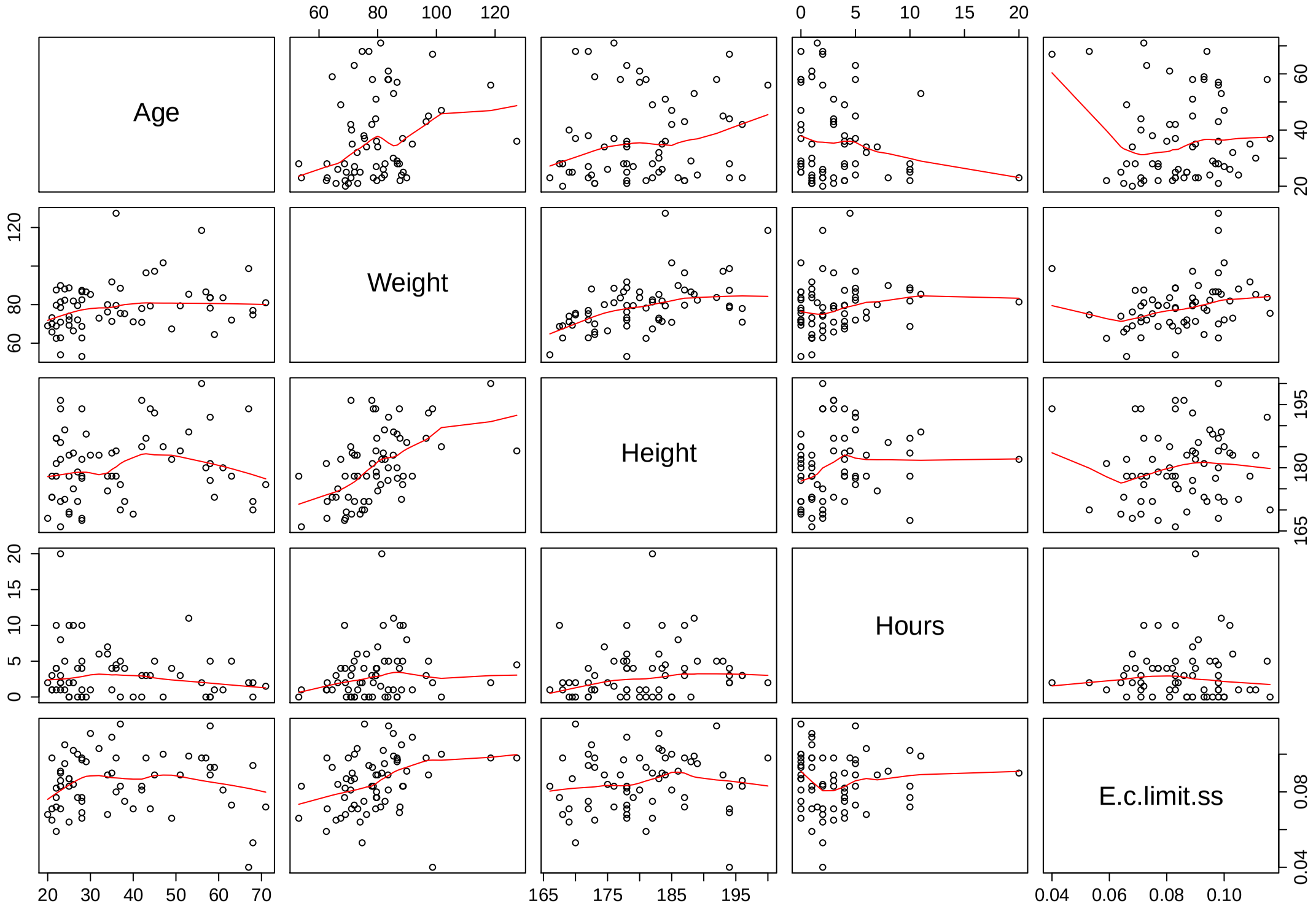
Age
Weight
Height
Hours
E.c.limit.ss
60 80 100 120
0 5 10 15 20
20 30 40 50 60 70
165 175 185 195
0.04 0.06 0.08 0.10

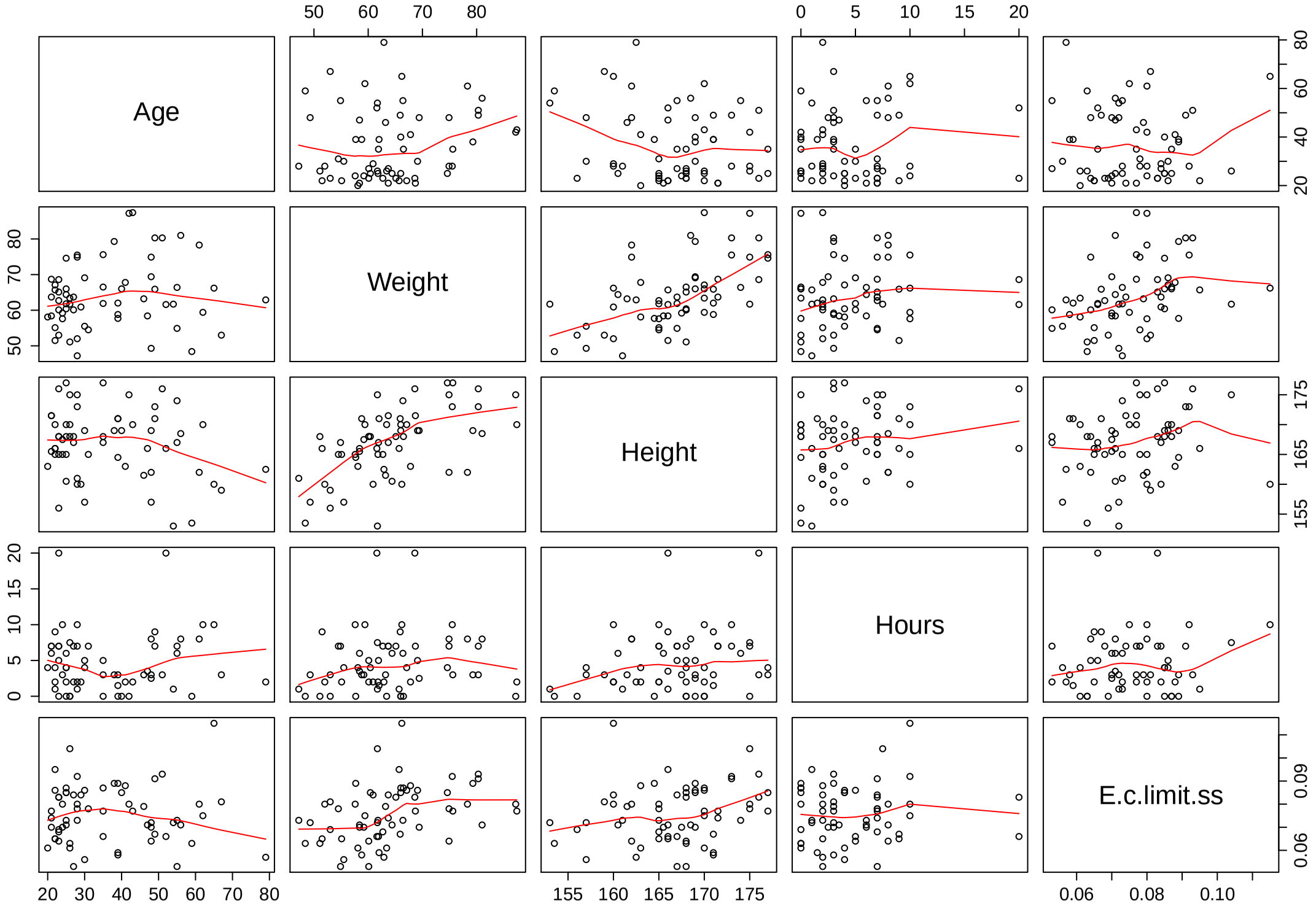
Age
Weight
Height
Hours
E.c.limit.ss
20 30 40 50 60 70 80
155 160 165 170 175
0.06 0.08 0.10

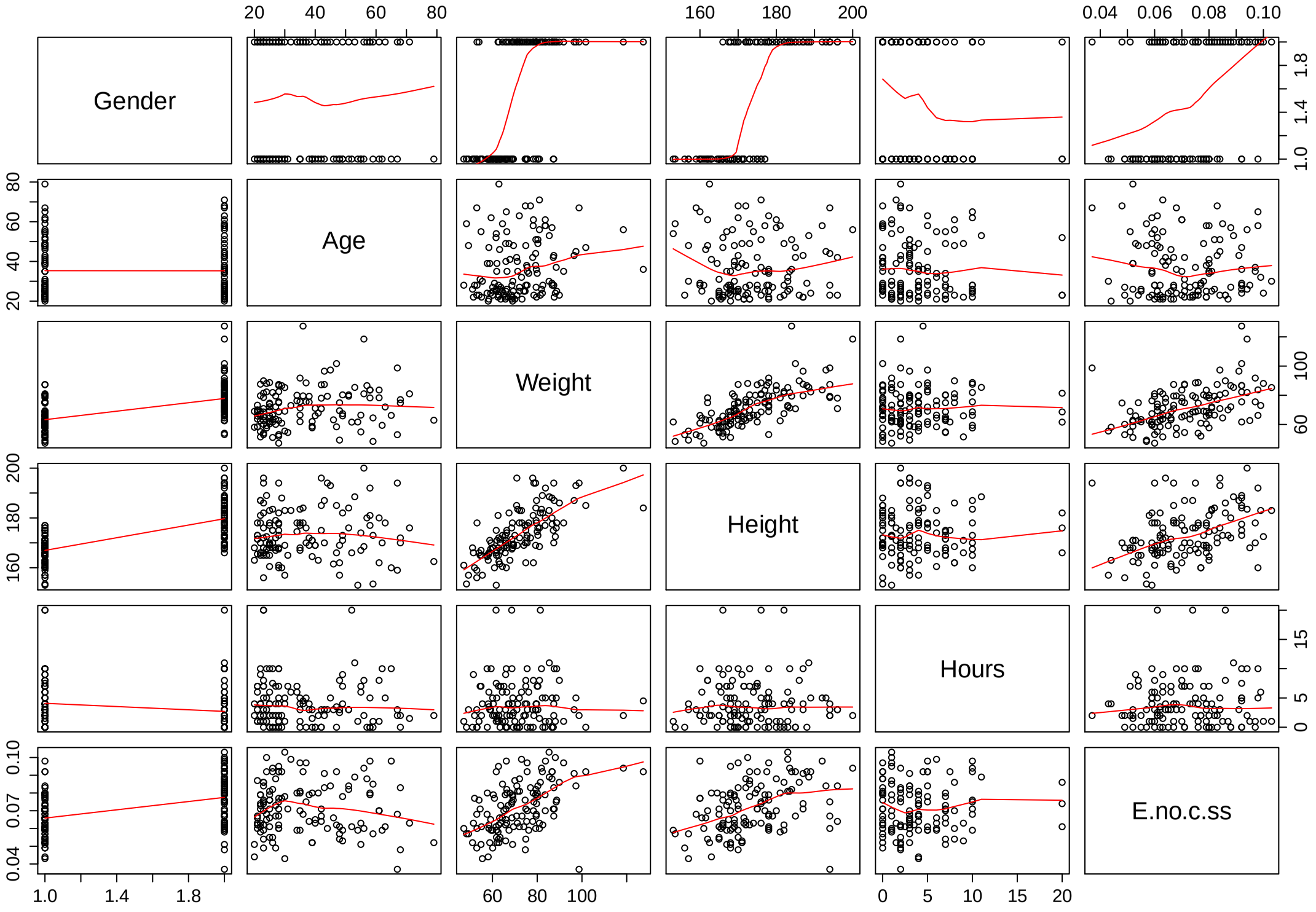
Gender
Age
Weight
Height
Hours
E.no.c.ss
20 40 60 80
160 180 200
0.04 0.06 0.08 0.10
1.0 1.4 1.8
20 40 60 80
60 80 100 120
160 180 200
60 80 100
0 5 10 15
0 5 10 15 20
0.04 0.07 0.10
1.0 1.4 1.8
60 80 100

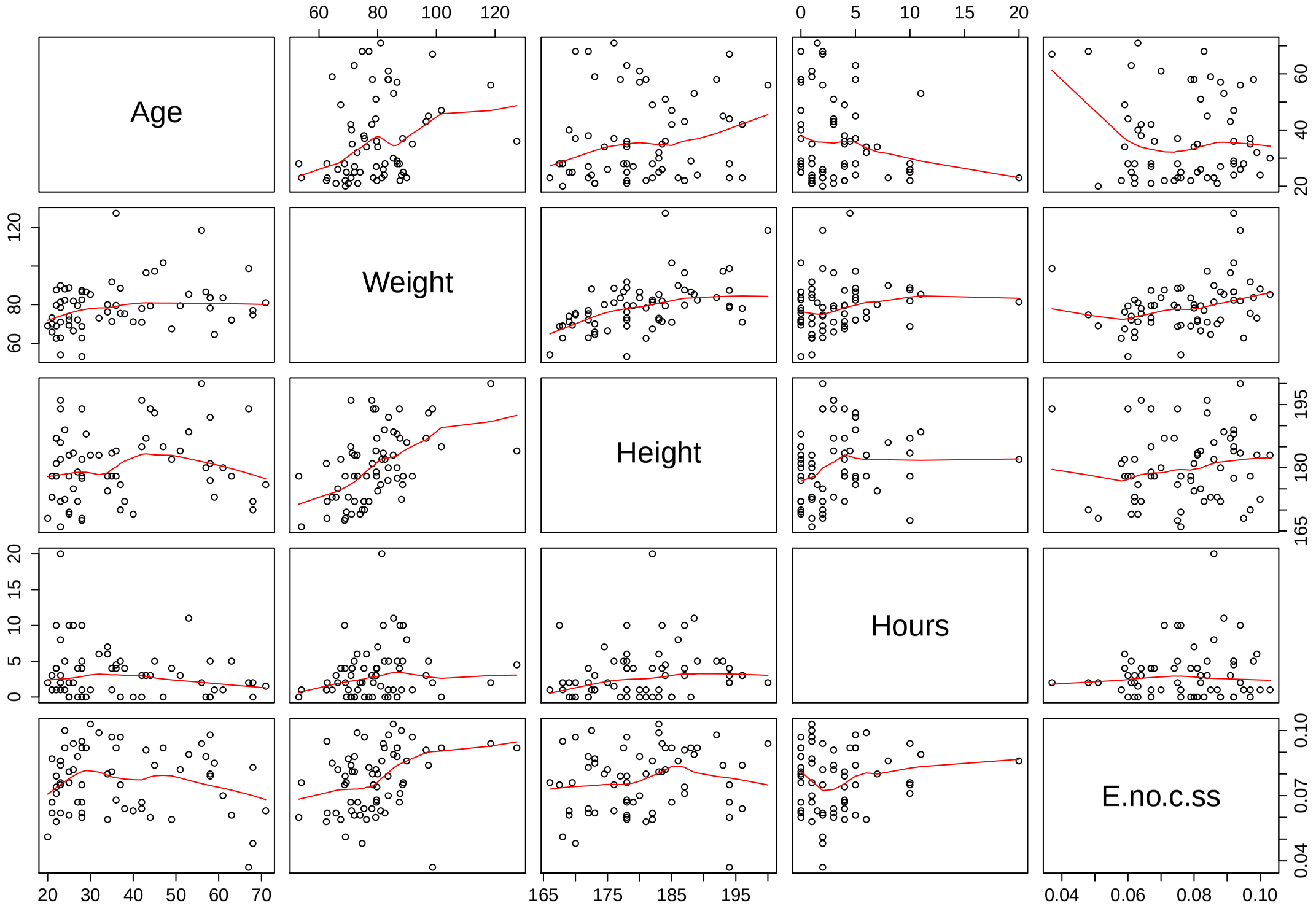
Age
Weight
Height
Hours
E.no.c.ss
60 80 100 120
0 5 10 15 20
20 40 60
120 80 60
195 180 165
20 15 10 5 0
0.10 0.07 0.04
20 30 40 50 60 70
165 175 185 195
0.04 0.06 0.08 0.10

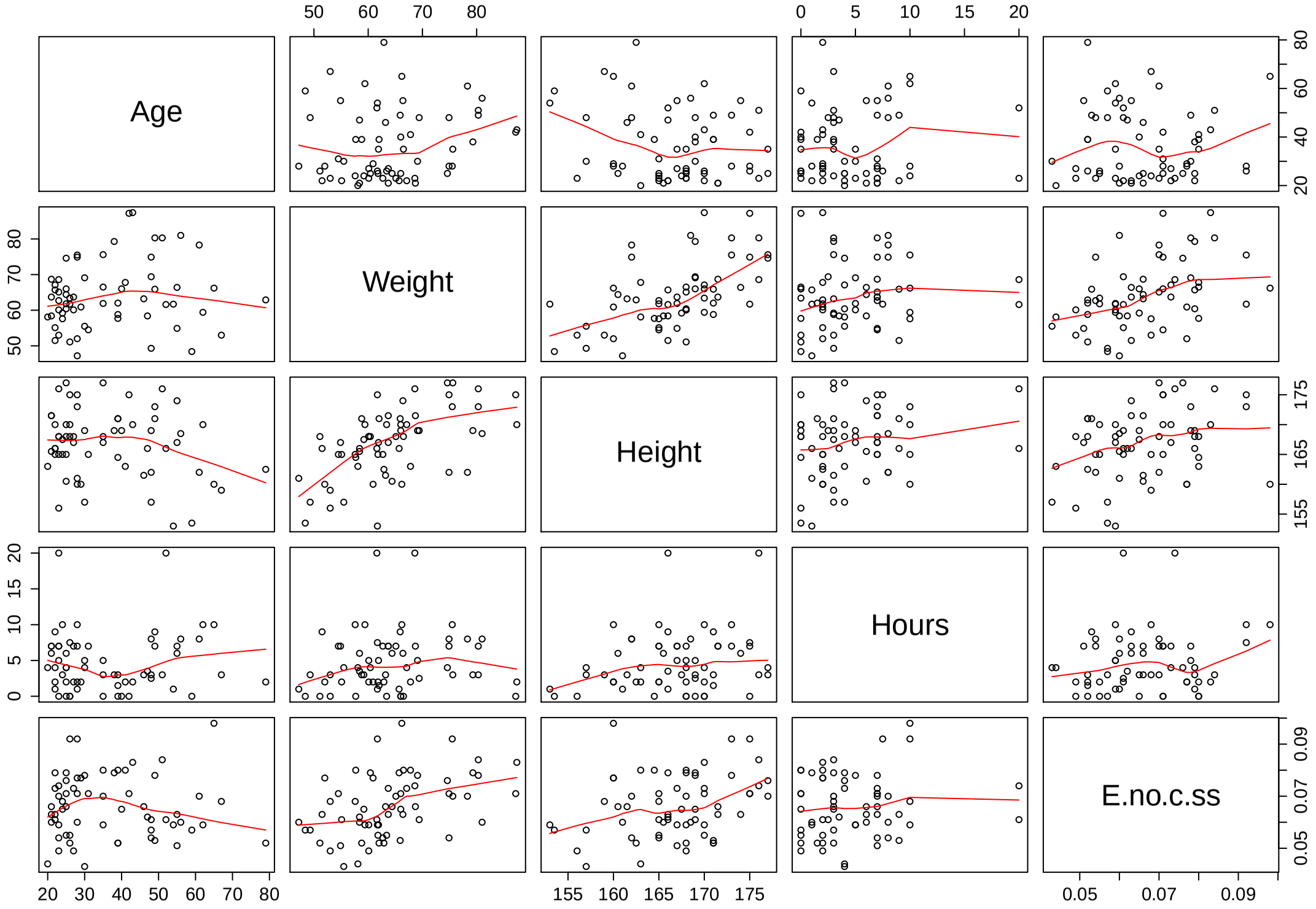
Age
Weight
Height
Hours
E.no.c.ss
50 60 70 80
0 5 10 15 20
20 40 60 80
50 60 70 80
155 165 175
0 5 10 15 20
0.05 0.07 0.09
20 30 40 50 60 70 80
155 160 165 170 175
0.05 0.07 0.09

APPENDIX D3

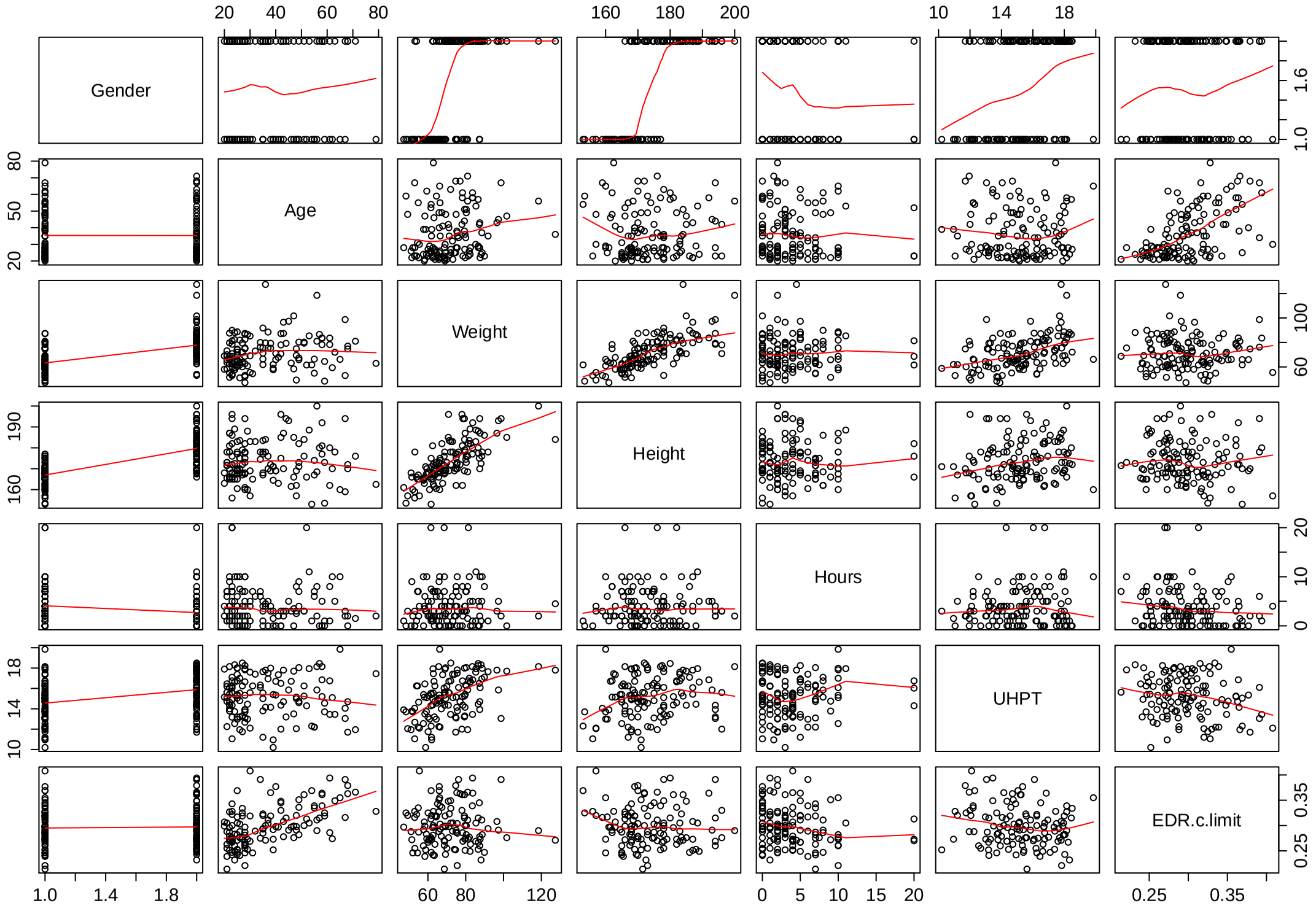
Gender
Age
Weight
Height
Hours
UHPT
EDR.c.limit

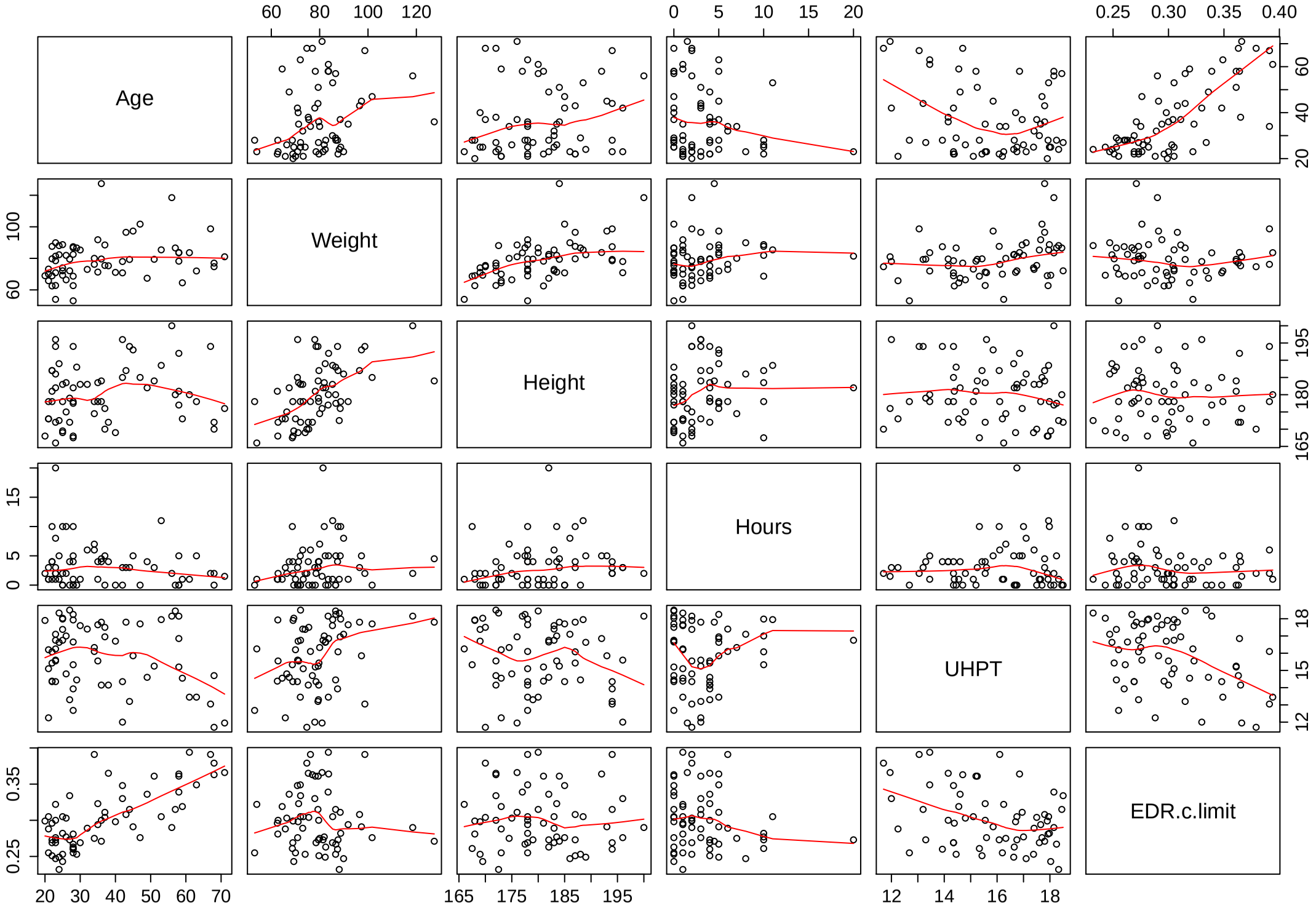
Age
Weight
Height
Hours
UHPT
EDR.c.limit
60 80 100 120
0 5 10 15 20
0.25 0.30 0.35 0.40
20 40 60
60 100
165 180 195
0 5 15
12 15 18
0.25 0.35
20 30 40 50 60 70
165 175 185 195
12 14 16 18

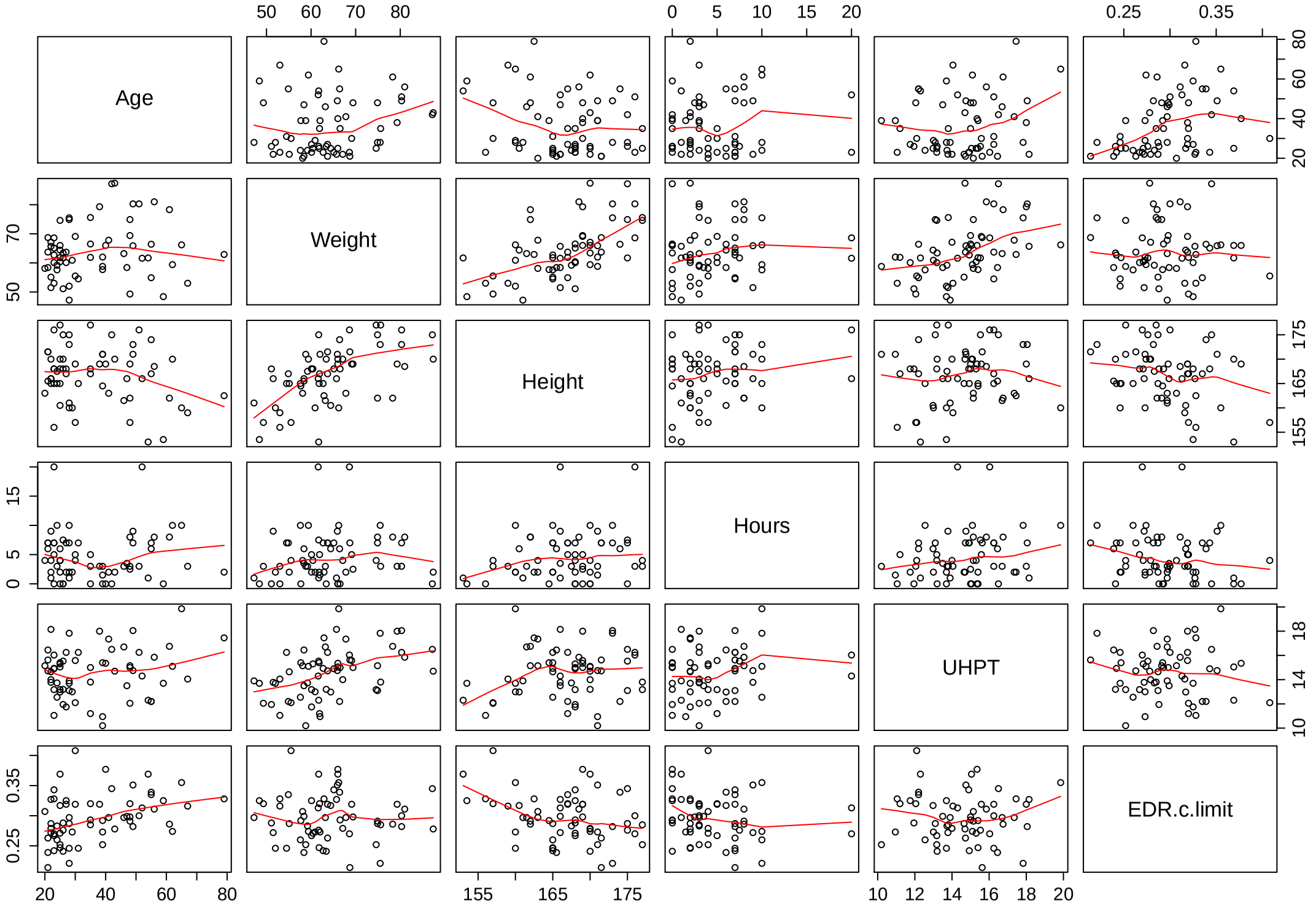
Age
Weight
Height
Hours
UHPT
EDR.c.limit
50 60 70 80
0 5 10 15 20
0.25 0.35
20 40 60 80
50 70
155 165 175
0 5 15
10 12 14 16 18 20
0.25 0.35

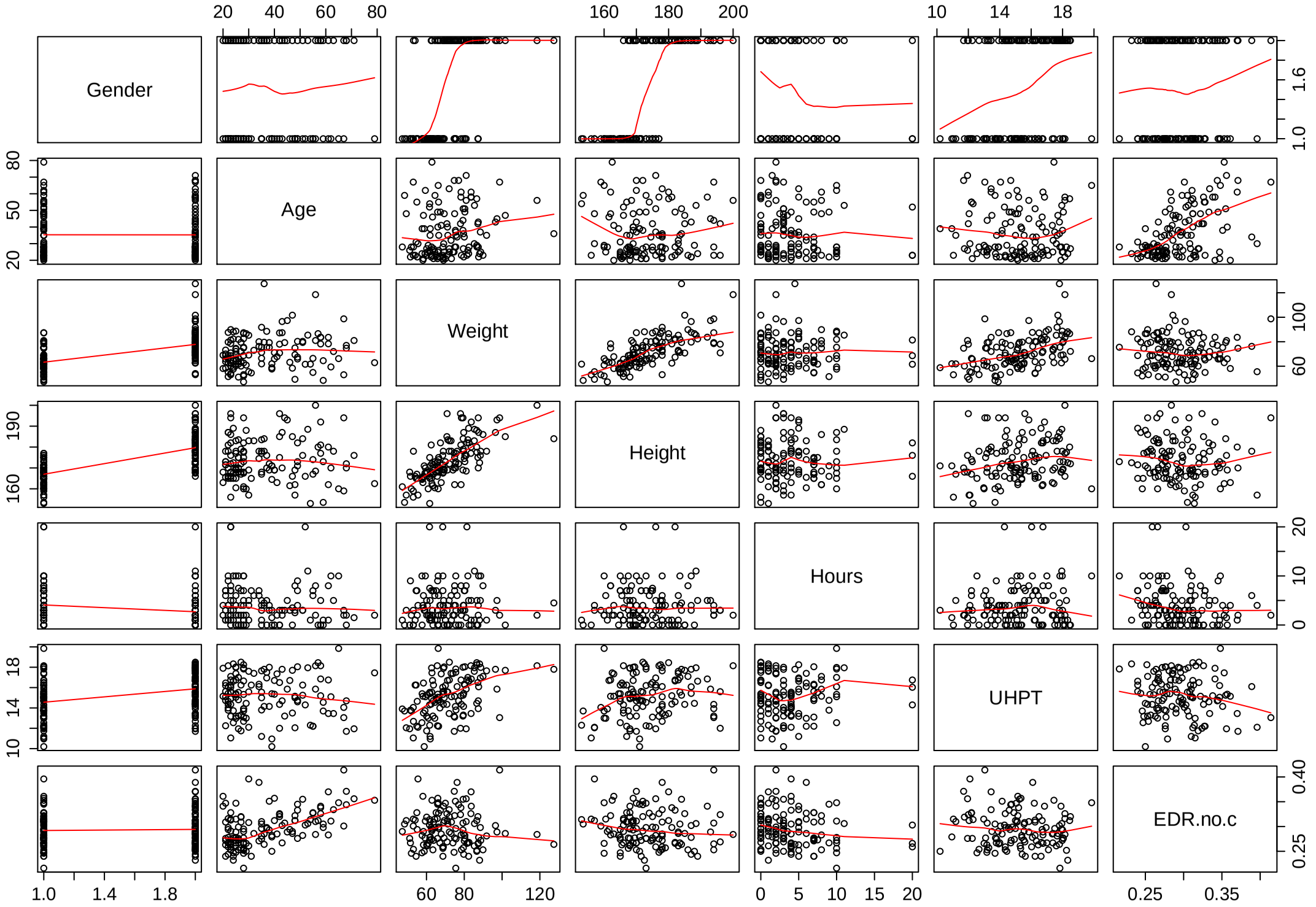
Gender
Age
Weight
Height
Hours
UHPT
EDR.no.c

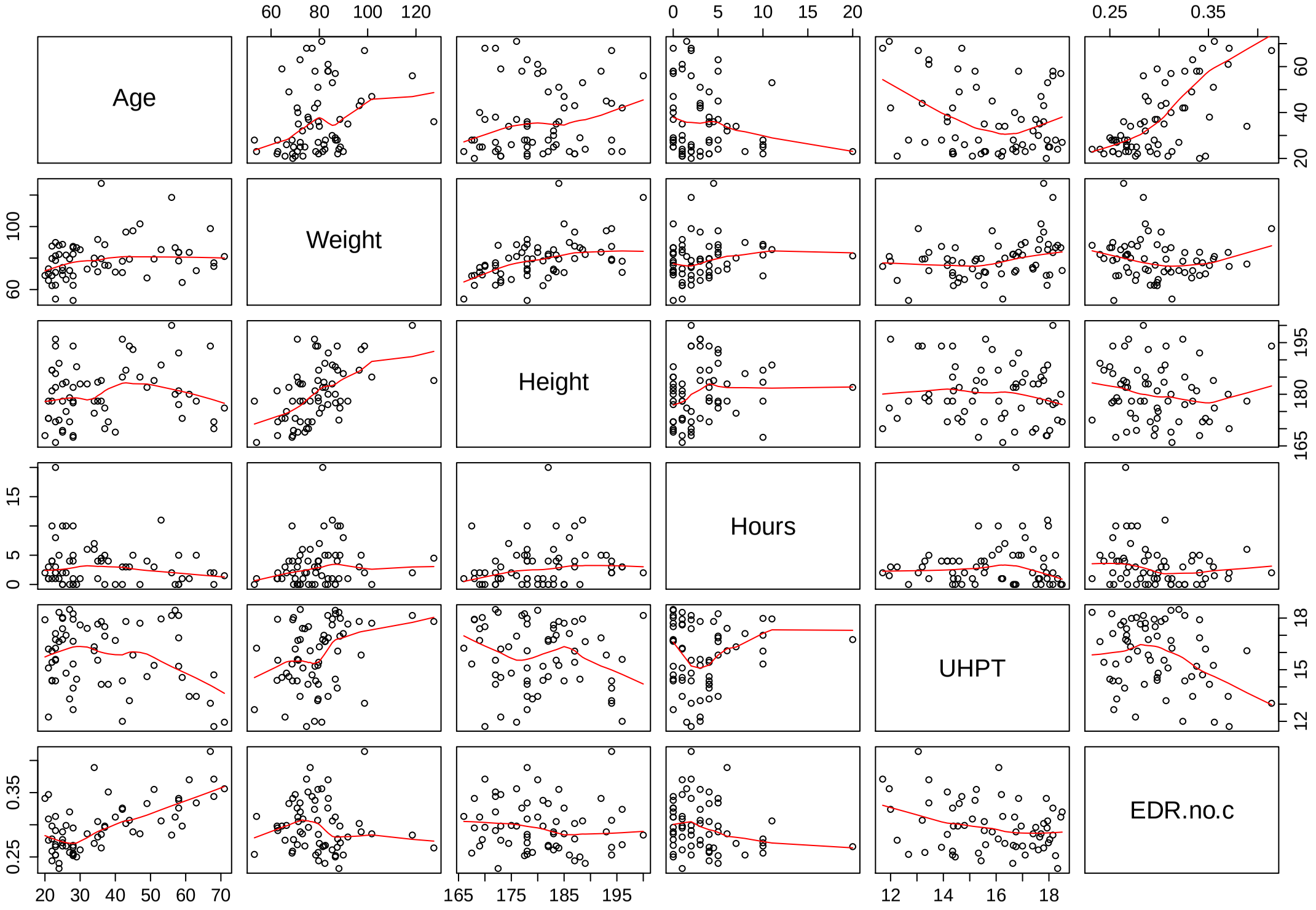
Age
Weight
Height
Hours
UHPT
EDR.no.c
60 80 100 120
0 5 10 15 20
0.25 0.35
60 100
165 175 185 195
0 5 15
12 14 16 18
0.25 0.35
20 30 40 50 60 70

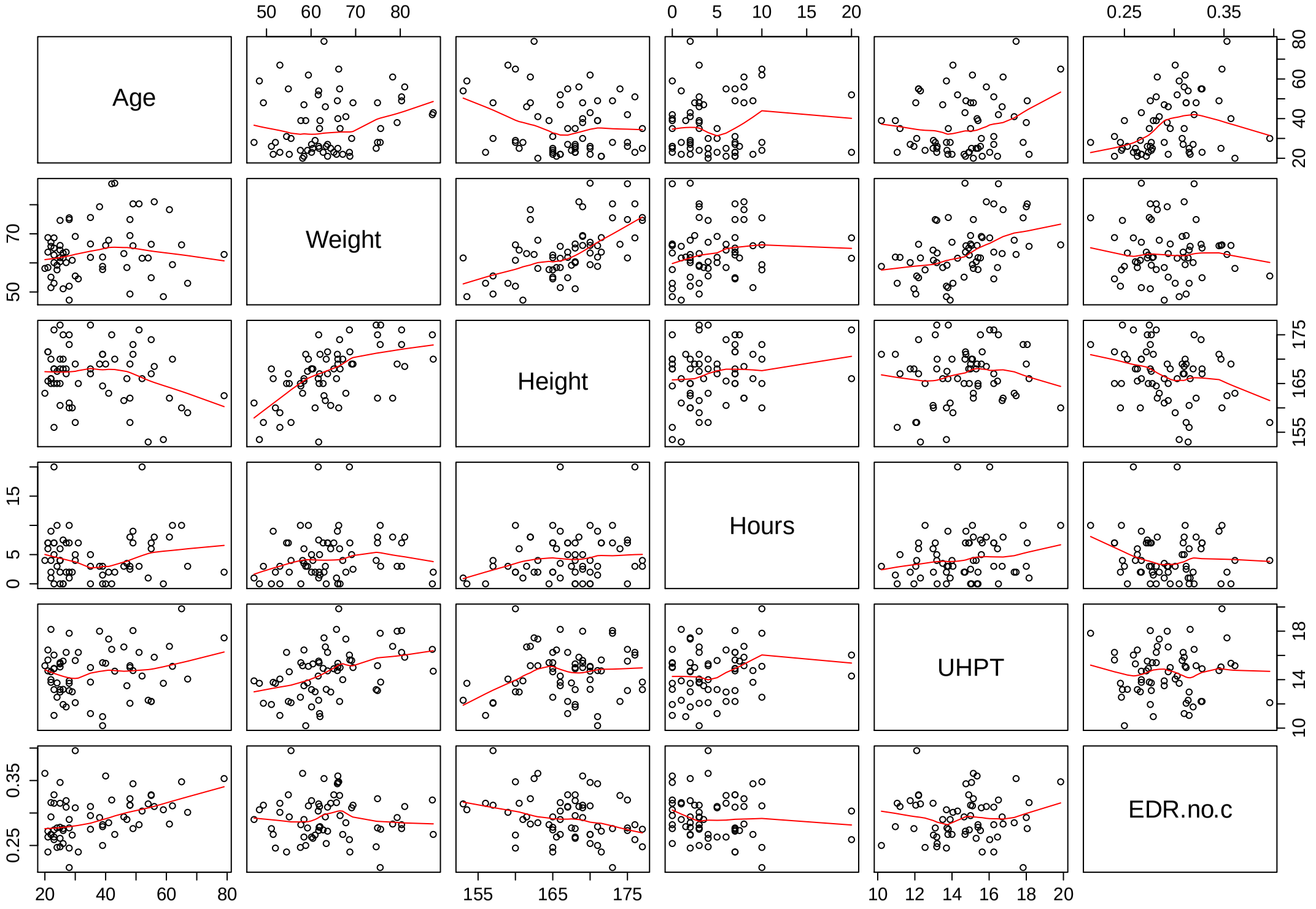
Age
Weight
Height
Hours
UHPT
EDR.no.c
50 60 70 80
0 5 10 15 20
0.25 0.35
20 40 60 80
50 70
155 165 175
0 5 15
10 12 14 16 18 20
0.25 0.35

APPENDIX E

I PAPER

Title: Intrinsic factors influencing biomechanical measures of *in vivo* human heel pad: A systematic review.

Authors: Sara Matteoli, Jens E. Wilhjelm, Else M. Bartels, Robin Christensen, Søren T. Torp-Pedersen.

Journal: Journal of Applied Biomechanics

Submission: Sent to the editor on November 28, 2011.

Intrinsic factors influencing biomechanical measures of *in vivo* human heel pad: A systematic review

Sara Matteoli[a], Jens E. Wilhjelm[a], Else M. Bartels[b], Robin Christensen[b], Søren T. Torp-Pedersen[b]

[a]Technical University of Denmark, Department of Electrical Engineering, Ørsteds Plads, DK-2800, Kgs. Lyngby, DK

[b]The Parker Institute, Frederiksberg Hospital, Nordre Fasanvej 57, DK-2000 Frederiksberg, DK

Key words: Heel pad biomechanics, heel pad compressibility, intrinsic factor

Words count: 3767

Corresponding author:

Sara Matteoli

Technical University of Denmark,

Department of Electrical Engineering,

Ørsteds Plads, Building 349

DK-2800 Kgs. Lyngby, DK

Phone: +45 4525 3705

Fax: +45 4588 0117

Email: sma@elektro.dtu.dk

Abstract

Background: Investigations of the biomechanics of the heel pad are challenged by intrinsic factors such as age, weight, height, gender, ethnicity, and physical activity. For proper diagnosis, the normal range of the biomechanical measure must be known, together with the variation with the intrinsic factors. The influence of a single intrinsic factor may only be revealed if all other factors are controlled.

Objectives: 1) to identify studies dealing with heel pad biomechanics in order to identify the methods used; 2) to disclose the effect of intrinsic factors; and 3) to recommend which intrinsic factors need to be controlled in future trials.

Methods: Structured literature search in bibliographic databases. Only studies involving *in vivo* measurements on at least six subjects, aged >17 years, and in the English language were included.

Results: One hundred and forty six studies were identified. 50 studies fulfilled the criteria. Forty of these considered Unloaded Heel Pad Thickness, 12 considered Loaded Heel Pad Thickness and Compressibility Index, 13 considered Stiffness, and 10 considered Energy Dissipation Ratio. Type of methods and subject number varied and yielded a large variation and discrepancy within the results.

Conclusions: In future investigations all intrinsic factors must be considered and included in the analysis.

Introduction

The human heel pad is a complex structure which features non-linear visco-elastic characteristics as is seen for the majority of human soft tissue. It acts as an efficient shock absorber, reducing the impact forces and trauma to the heel pad. Extensive stress or diseases may cause damage to its intricate septation, resulting in permanent damage of its shock absorbency capability (Blechschmidt, 1982; Altun & Durmus-Altun, 2003).

There is an increasing awareness of the effect of anatomical and physiological changes on the heel pad structure and its biomechanical properties (Spears & Miller-Young, 2005). This could be an important factor in the development of heel pain in athletes (like runners) and heel pad problems in the increasing diabetic population (Spears & Miller-Young, 2005). Understanding heel pad biomechanics is necessary to understand stress-related injuries (*e.g.* plantar fasciitis and diabetic ulceration), and also important to improve orthotics and footwear design, especially by considering stress induced in the plantar region, (*e.g.* distribution of the plantar pressure).

The biomechanical aspects of the heel pad have been investigated for more than 25 years. These investigations are rather challenging since they may be influenced by intrinsic factors such as age, weight, height, gender, ethnicity, and physical activity (Alcantara et al., 2002; Hsu et al., 1998; Kinoshita et al., 1996; Prichasuk et al., 1994). When measuring a biomechanical variable of the heel pad for the purpose of diagnosis, the normal range of this variable must be known, as well as the variation with the common intrinsic factors like age, weight, height, gender, physical activity and disease. The influence of any intrinsic factor may, however, only be revealed if all other factors are controlled. As a consequence, it is possible that an effect of a given factor may be overlooked or falsely detected, if the whole range of factors is not taken into account. Uncontrolled factors become confounding factors, where confounding gives a wrong assessment of the potential "causal" association (Vandenbroucke et al., 2007).

The aims of this study are 1) to identify studies dealing with heel pad biomechanics in order to identify the methods used for assessing heel pad properties; 2) to disclose the effect of intrinsic factors such as age, weight, height, gender, ethnicity, and physical activity; and 3) to recommend which intrinsic factors need to be controlled in future trials.

Material and Methods

Literature search

Structured literature searches were carried out in the bibliographic databases Inspec (Incl. Archive) from 1898, Biosis Previews via Ovid from 1969, EMBASE via Ovid from 1980, Medline via Pubmed from 1966, and Web of Science from 1900, all until ultimo April 2011

Search strategy

The following search strategy was applied, where words were searched both as free text and, where applicable, also as keywords: heel pad thickness OR (heel pain AND (compressibility OR elderly OR diabetes OR diabetic OR stiffness)).

Selection criteria

Only studies dealing with *in vivo* measurements carried out on a group with a least six subjects, and subjects/patients of age 17 years or older, were included. The included studies were limited to English language. Conference papers were not included.

Reference lists of found reviews and selected references were searched for further studies fulfilling the selection criteria.

Data handling

The heel pad

The human heel pad is located between the calcaneus and the skin on the posterior part of the foot, as shown in Figure 1. It consists of a complex structure with neuronal, vascular, fibrous and elastic components that are intertwined with fat cells (Rome, 1998). Due to the visco-elastic nature of the heel pad tissue, and its capability of deforming under a load, when a loading/unloading cycle is applied, a characteristic load-displacement curve (hysteresis) is obtained (Fung, 1993).

A simple representation of the heel pad and the calcaneus, with or without the application of a load, is shown in Figure 2. The **Unloaded Heel Pad Thickness** (UHPT) is defined as the shortest distance between the lowest part of the plantar tuberosity of the calcaneus and the skin (unloaded condition, Figure 2a). The **Loaded Heel Pad Thickness** (LHPT) is defined the same way, but with a load *F* applied (loaded condition, Figure 2b).

The **Heel Pad Compressibility Index** (HPCI), in percentage, is defined as the ratio of the heel pad thickness in loaded conditions to unloaded conditions. It is expressed as (Hsu et al., 2000; Hsu et al., 1998; Prichasuk et al., 1994; Prichasuk, 1994)

$$HPCI = \frac{LHPT}{UHPT} * 100 \quad (1)$$

HPCI shows the ability of the heel pad to be compressed. If HPCI is close to 100%, then the elasticity of the heel pad approaches zero (Prichasuk, 1994). When loads are applied sequentially, as seen in some studies (Hsu et al.,2000; Hsu et al., 1998; Kerr et al., 1995; Tsai et al.,1999), the value of LHPT is the one corresponding to maximum load (F_{max}).

The **Displacement (**δ) indicates, in this work, the difference between the initial position and the final position of the heel pad when a load (F_{max}) is applied. Using the notation illustrated in Figure 1, the displacement can be expressed as:

$$\delta = UHPT - LHPT \quad (2)$$

Strain is an expression of the normalized deformation, and it is expressed as:

$$\varepsilon = \frac{LHPT - UHPT}{UHPT} \quad (3)$$

The **Stiffness** (S) in units N/m, is a measure of the resistance of an elastic body to a deformation. It is defined as the force applied to the heel pad (*F*) divided by the magnitude of the resulting deformation (*d*) (Alcantara et al., 2002; Erdemir et al., 2006; Klaesner et al., 2002; Rome, 1998):

$$S = \frac{F}{\mathrm{d}} \quad (4)$$

Stiffness (in unit N/m^2) may be also calculated from stress and strain, so that:

$$S = \frac{\sigma}{\varepsilon} = \frac{F/A}{\varepsilon} \quad (5)$$

where σ is the stress, and ε is the strain as before defined.

Stiffness thus can be calculated from either the force-deformation or stress-strain curve by calculating the slope of the tangent to the loading curve. Stiffness on a loading curve describes the function of the heel pad as a cushion during heel strike (Rome, 1998). The heel pad, as most of the other human soft tissues, shows a non-linear visco-elastic behavior when loaded. It is sensitive to the speed at which a load is applied. At a given level of strain the behavior is the faster the loading, the higher the displacement (Rome, 1998). Due to this, a more complicated equation would be necessary to calculate the tissue stiffness considering the non- linear relationship between force and displacement. However, (4) and (5) are the equations often used when calculating stiffness (Alcantara et al., 2002; Erdemir et al., 2006; Hsu et al., 1998; Rome et al., 2001; Rome, 1998). Specifically, equations (4) and (5) are usually applied along the linear parts of the loading curve. When loads are applied sequentially on the heel pad, the maximum load (*Fmax*) is used in the calculation of stiffness.

The **Energy Dissipation Ratio (EDR)**: For a visco-elastic substance a characteristic loop, showing hysteresis, is observed when a force is applied and then removed, as shown in Figure 3. The area under the loading curve, A_L, represents the energy used to compress the heel pad, while the area under the unloading curve, A_U, shows the energy returned during the elastic restitution of the heel pad (Kinoshita et al., 1996). The area inside the loop represents the energy absorbed by the heel pad (converted to heat) during the impact.

The Energy Dissipation Ratio in percentage can be expressed as (Bennett & Ker, 1990):

$$EDR = \frac{A_L - A_U}{A_L} * 100 \quad (5)$$

For the heel pad, the shock absorbency is related to the energy dissipation during the loading-unloading cycle, and it can be seen as the area enclosed by the loop (Zheng, 2000).

Data handling

Due to different methodologies used, it is not possible to compare the numerical results between studies. The results are reported as a tendency, and in order to indicate whether there was a correlation between a particular intrinsic factor and the biomechanical parameter, the following symbols are used:

- 1: indicates that there is a correlation between the intrinsic factor (age, weight, height, gender. etc), and the biomechanical measure taken into consideration. Specifically, the tendency is increasing (P-value < 0.05)
- 0: indicates that there was no evidence supporting a correlation between the intrinsic factor (age, weight, height, gender. etc), and the biomechanical measure taken into consideration. Specifically, there was no statistically significant change (P-value > 0.05)

- -1: indicates that there is a correlation between the intrinsic factor (age, weight, height, gender. etc) and the biomechanical measure taken into consideration. Specifically, the tendency is decreasing (P-value < 0.05)

When the intrinsic factor is binary (*i.e.*, gender, physical activity), the symbols above indicate that the first element (*e.g.*, male) has higher/lower values for the biomechanical parameter than the second element (*e.g.*, female).

Results

A flow diagram of the selection procedure is shown Figure 4. One hundred and forty six papers were identified. Out of these, 95 did not fulfill the selection criteria and one was a review, leaving us with 50 studies for further data mining (Table 1). Scanning reference lists did not identify additional studies. In the studies considered, both UHPT and LHPT were measured by lateral radiography, ultrasonic imaging, or MRI of the region from skin to the tuberosity of the calcaneus. Table 1 shows an overview of the selected studies. For each study, the number of subjects investigated is reported, as well as the methods applied for measurement of the biomechanical parameters of the heel pad (UHPT, LHPT, HPCI, Stiffness and EDR). Type of methods and number of subjects varied a great deal, Table 1. There was a large variation and discrepancy within the results.

Forty studies investigated the effect of intrinsic factors on **UHPT**, as shown in Appendix 1. When considering the effect of age on UHPT, seven studies out of 15 demonstrated a positive correlation (Kho et al., 1970; Prichasuk, 1994; Prichasuk et al., 1994; Wang et al., 1998; Hsu et al., 1998; Turgut et al., 1999; Kwan et al., 2010), while the remaining eight studies demonstrated no statistical significant effect (Steinbach, 1964; Puckette, 1967; Gonticas, 1969; Kho et al., 1970; Bohrer & Ude, 1978; Raja, 1980; Ozdemir et al., 2004-, Mickle et al., 2011). One of these studies

considered only acromegalic patients (Kho et al., 1970), while two studies considered only subjects of African origin Bohrer & Ude, 1978; Raja, 1980). The effect of weight on UHPT was considered positive in five studies out of seven (Gonticas, 1969; Kho et al., 1970; Bohrer & Ude, 1978; Jørgensen et al., 1989; Turgut et al., 1999), whereas the other two studies (Jackson, 1968; Ozdemir et al., 2004) demonstrated no statistically significant effect. One of the studies showing a positive correlation (Jackson, 1968) considered only obese subjects. The effect of height on UHPT is considered to be positive even though only one study (Gonticas, 1969) invetigated this intrinsic factor. When considering the effect of gender on UHPT, seven studies out of 12 indicated a positive correlation (Kho et al., 1970; Bohrer & Ude, 1978; Jørgensen et al., 1989; Prichasuk et al., 1994; Prichasuk, 1994; Turgut et al., 1999; Ozdemir et al., 2004). It has to be said that one study considered only people of African origin (Bohrer & Ude, 1978), and another one investigated only acromegalic patients (Kho et al., 1970). The remaining five studies demonstrated no difference between males and females (Steinbach, 1964; Puckette, 1967; Kho et al., 1970; Raja, 1980; Mittal, 1983). Within the latter studies, two considered only subjects of African origin (Raja, 1980; Mittal, 1983). The effect of race on UHPT is also considered to be positive even though only one study (Puckette, 1967) investigated this intrinsic factor. When considering the effect of physical activity on UHPT two studies out of three (Rome et al., 2002; Uzel et al., 2006) demonstrated no statistically significant effect, while the remaining study (Challis et al., 2008) demonstrated a positive correlation. It has to be said that one of the studies (Rome et al., 2002) considered only runners, while another study (Challis et al., 2008) indicated that cyclist had a higher UHPT than runners. When taking the effect of diabetes on UHPT into consideration, four out of eight studies demonstrated no statistical significant change (Hsu et al., 2000; Tong et al., 2003, Erdemir et al., 2006; Hsu et al., 2009), two studies demonstrated a positive correlation (Gooding et al., 1995, Chao et al., 2011), while the remaining two studies indicated a negative correlation (Gooding et al., 1986, Zheng et al., 2000). Eight studies out of 11 demonstrated that there is no correlation between heel

pain and UHPT (Tsai et al., 1999; Turgut et al., 1999; Onwuanyi, 2000; Tsai et al., 2000; Tong et al., 2003; Karabay et al., 2007; Wearing et al., 2009; Wearing et al., 2010), while the remaining two studies reported a positive correlation (Prichasuk, 1994; Rome et al., 2002). It has to be said that one of the studies included only runners (Rome et al., 2002). Three studies out of five (Steinbach, 1964; Raja, 1980; Mittal, 1983) demonstrated that acromegaly has a positive effect on UHPT, while the remaining two studies (Field et al., 1967; Gonticas, 1969) demonstrated no statistical significant change. It has to be said that for acromegaly two studies out of the three demonstrating a positive correlation considered only subjects of African origin (Raja, 1980; Mittal, 1983). The effect of Rheumatoid Arthritis (RA) and SpondyloArthropathies (SpA) on UHPT was shown to be positive, even though only one study investigated these two intrinsic factor (Falsetti et al., 2004). Two studies out of three reported no statistical significant effect on UHPT after fractures (Kerr et al., 1995; Levy et al., 1992), while a study demonstrated a positive correlation (Silver et al., 1994)\

Twelve studies investigated the effect of intrinsic factors on **LHPT**, as shown in Appendix 2. Then considering the effect of age on LHPT, three studies out of four demonstrated that there is a positive correlation (Prichasuk et al., 1994; Wang et al., 1998; Turgut et al., 1999), while the remaining study (Ozdemir et al., 2004) demonstrated no statistically significant change. When considering the effect of weight on LHPT, one study out of two demonstrated a positive correlation (Turgut et al., 1999), while the remaining study demonstrated no statistically significant change (Ozdemir et al., 2004). The effect of gender on LHPT is considered positive, as three studies out of three demonstrated a positive correlation (Prichasuk et al., 1994; Turgut et al., 1999; Ozdemir et al., 2004). The effect of physical activity on LHPT is considered to be of no statistical significance, although only one study demonstrated such tendency (Uzel et al., 2006). The effect of diabetes and heel fractures on LHPT is reported to be positive, even though only one study investigated each intrinsic factor (Tong et al., 2003; Kerr et al., 1995). When looking at the effect of heel pain on

LHPT, five studies out of seven demonstrated no statistically significant effect (Turgut et al., 1999; Onwuanyi, 2000; Kanatli et al., 2001; Wearing et al., 2009; Wearing et al., 2010), while the remaining two studies demonstrated a positive correlation (Prichasuk, 1994; Tong et al., 2003).

Twelve studies investigated the effect of intrinsic factors on **HPCI**, as shown in Appendix 3. When considering the effect of age on HPCI, five studies out of six demonstrated a positive correlation (Prichasuk, 1994; Prichasuk et al., 1994; Hsu et al., 1998; Turgut et al., 1999; Ozdemir et al., 2004), while the remaining study indicated no statistically significant effect (Wang et al., 1998). The effect of weight on HPCI is considered positive as all three studies reported a positive correlation (Prichasuk et al., 1994; Turgut et al., 1999; Ozdemir et al., 2004). When considering the effect of gender on HPCI, three studies out of four demonstrated no statistically significant difference (Prichasuk, 1994; Prichasuk et al., 1994; Turgut et al., 1999), while the remaining study demonstrated a positive correlation (Ozdemir et al., 2004). The effect of physical activity on HPCI is shown to be of no statistical significance, although only one study showed such tendency (Uzel et al., 2006). The effect of diabetes on HPCI is not clear since one study demonstrated a positive correlation (Tong et al., 2003), while the other reported no statistically significant difference (Hsu et al., 2000). The effect of heel pain on HPCI is also not clear, as three studies out of six reported no statistically significant difference (Turgut et al., 1999; Tsai et al., 1999; Kanatli et al., 2001), while the remaining three studies demonstrated a positive correlation (Prichasuk, 1994; Onwuanyi, 2000; Tong et al., 2003).

Fourteen studies investigated the effect of intrinsic factors on **Stiffness**, as shown in Appendix 4. Two studies out of three demonstrated no significant correlation between age and Stiffness (Wang et al., 1998; Alcantara et al., 2002), while the other study demonstrated a positive correlation (Kwan et al., 2010). Only one study investigated the effect of weight on heel pad Stiffness, and it demonstrated a negative correlation (Alcantara et al., 2002). When looking at the effect of gender

findings are contrasting as one study reported that males had lower heel pad stiffness than females, (Boros & Challis, 2003), while another study reported the opposite result (Alcantara et al., 2002). Only one study investigated the effect of physical activity on heel pad Stiffness, and it demonstrated a positive correlation (Challis et al., 2008). This study compared runners vs. cyclist, and the positive correlation indicates that cyclists have higher Stiffness than runners. Four studies out of six investigating the effect of diabetes on Stiffness demonstrated no statistically significant effect (Hsu et al., 2000; Klaesner et al., 2002; Cheung et al., 2006; Hsu, et al., 2009), while the remaining two studies reported a positive correlation (Zheng et al., 2000; Chao et al., 2011). When looking at the effect of heel pain on Stiffness, two studies out of three demonstrated no statistically significant effect (Wearing et al., 2009; Wearing et al., 2010), while the other study indicated a negative correlation (Rome et al., 2001). It has to be said that this study the subjects were only runners with heel pain.

Eleven studies investigated the effect of intrinsic factors on **EDR**, as shown in Appendix 5. When considering the effect of age on EDR, two studies out of five demonstrated a negative correlation (Kinoshita et al., 1996; Jørgensen et al., 1989), one study reported a positive correlation (Hsu et al., 1998), and the remaining two studies demonstrated no statistically significant effect (Wang et al., 1998, Alcantara et al., 2002). The effect of weight on EDR was considered positive even though only a study investigated on that parameter (Alcantara et al., 2002).When looking at the effect of gender on EDR, two studies out of three reported that men have lower EDR than women (Jørgensen et al., 1989; Boros & Challis, 2003), while the remaining study reported the opposite result (Alcantara et al., 2002). The effect of physical activity is investigated, but only in one study which demonstrated no statistically significant difference (Challi et al., 2008). In particular, this study reported that there was no difference between runners and cyclists when comparing EDR values. Diabetes is considered to have a positive effect on EDR, but only one study looked at this intrinsic

factor (Hsu et al., 2002). Two studies out of three looking at effect of heel pain demonstrated a negative correlation(Wearing et al., 2009; Wearing et al., 2010), while the remaining study reported no statistically significant effect (Tsai et al., 1999).

Discussion and Conclusions

Our study identified 50 studies dealing with measurements assessing heel pad biomechanical properties. Forty (80%) out of the 50 selected studies looked at Unloaded Heel Pad Thickness, 12 (24%) looked at Loaded Heel Pad Thickness and Compressibility Index, 13 (26%) looked at Stiffness, and 10 (20%) looked at Energy Dissipation Ratio. Our results are therefore in some cases based on one study only, and the quality of these single studies may not all be high.

Studies investigating the same biomechanical measure of the heel pad differed both in terms of method applied and population studied, as shown in Table 1. Therefore, it was not feasible to compare the numerical results. Furthermore, our results cannot, based on the obtained results, be considered reliable enough to conclude on degree of effect of the confounding factors.

One of our aims was to disclose the effect of intrinsic factors such as age, weight, height, gender, ethnicity and physical activity on heel pad biomechanics. Due to varying analyses of these confounding factors in the different studies, as shown in Table 1, it became clear that it was not possible to carry out an overall quantitative analysis (*e.g.* meta-analysis) on the available data. We could therefore not obtain a measure for the effect of each of these factors on heel pad biomechanics. However, we can conclude that age and weight do have an effect on the heel pad biomechanics, based on the found data. The other intrinsic factors may have an important role in the heel pad biomechanics as well, but it is not possible to assess such effects based on available data.

We recommend that the intrinsic factors age and weight are controlled in future trials. The effect of age, causing changes in mechanical properties in the heel pad of elderly are most likely due to age-

related changes in anatomical, morphological and histological characteristic of the heel pad (Kinoshita et al., 1996). Kuhns (1949), findings on anatomical and histological changes of the heel with age, support this, since he reported that degenerative changes with increasing age are the most constant findings in elastic adipose tissue. He also stated that aging leads to a gradual loss of collagen, a decrease in the elastic fibrous tissue, and a decrease in water content. Looking at the effect of the weight, an increase in body fat and/or weight may be the cause of the increased thickness of the heel pad (Kwan et al., 2010) which plays a fundamental role when determining the stiffness of the tissue.

We speculate that diabetes and physical activity play an important role in the heel pad biomechanics. Diabetes is known for excessive glycation of proteins (Furth, 1997). This changes the mechanical properties of the proteins, and will especially affect elasticity in soft tissue. Sports involving running and jumping apply repetitive stress to the heel pad (Uzel et al., 2006). This may lead to overuse and damage of soft tissue (Uzel et al., 2006).

In Table 2 we have listed a ranking for all the confounding factors considered in this review, which should be taken into account in future investigations.

In future studies, all variables should be defined and considered for inclusion in analyses, like outcomes, exposures, predictors, potential confounders, and potential effect modifiers. These can be handled – and adjusted for - using statistical software that allows the estimation to adjust for a multitude of confounding covariates, which are measured in the participating cohort. A simple way is to apply a general linear model (GLM) framework which adjusts for many covariates at the same time.

Future investigations must therefore control for all possible intrinsic factors and a set of standard procedures when measuring heel pad biomechanics is asked for to give reliable and comparable

results between subjects and between studies. This will finally make it possible to give guide lines for which confounding factors are the ones affecting measurements and results in different scenarios.

Acknowledgments

This study was supported by The Oak Foundation.

Conflict of Interest Statement

All the authors (S. Matteoli, J.E. Wilhjelm, E.M. Bartels, R. Christensens, S.T. Torp-Pedersen) have no proprietary, financial, professional or other personal interest of any nature or kind in any product, service and/or company that could be construed as influencing the position presented in, or the review of, the present manuscript entitled ”Intrinsic factors influencing biomechanical measures of *in vivo* human heel pad: A systematic review”.

References

Alcantara, E., Forner, A., Ferrus, E., Garcia, A.-C., & Ramiro, J. (2002). Influence of age, gender, and obesity on the mechanical properties of the heel pad under walking impact conditions. *Journal of Applied Biomechanics , 18* (4), 345-356.

Altun, G., & Durmus-Altun, G. (2003). Confirmation of alleged falanga torture by bone scintigraphy -case report. *Internation Journal Of Legal Medicine , 117* (6), 365-366.

Bennett, M. B., & Ker, R. F. (1990). The mechanical properties of the human subcalcaneal fat pad in compression. *J. Anat. , 171*, 131-138.

Blechschmidt, E. (1982). The structure of the calcaneal padding. *Foot Ankle , 2* (5), 260-283.

Bohrer, S. P., & Ude, A. C. (1978). Heel pad thickness in Nigerians. *Skeletal Radiology* , 108-112.

Boros, R. L., & Challis, J. H. (2003). Heel pad properties of males and females. *Medicine and Science in Sports & Exercises , 35* (5), 360.

Challis, J. H., Murdoch, C., & Winter, S. L. (2008). Mechanical properties of the human heel pad: a comparison between populations. *Journal of Applied Biomechanics , 24* (4), 377-381.

Chao, C. Y., Zheng, Y. P., & Cheing, G. L. (2011). Epidermal thickness and biomechanical properties of plantar tissue in diabetic foot. *Ultrasound in Medicine and Biology , 37* (7), 1029-1038.

Cheung, Y. Y., Doyley, M., Miller, T. B., Kennedy, F., Lynch, F., Wrobel, J. S., et al. (2006). Magnetic resonance elastography of the plantar fat pads - Preliminary study in diabetic patients and asymptomatic volunteers. *Journal of computer assisted tom , 30* (2), 321-326.

Erdemir, A., Viveiros, M. L., Ulbrecht, J. S., & Cavanagh, P. R. (2006). An inverse finite-element model of heel-pad indentation. *Journal of Biomechanics , 39* (7), 1279-1286.

Falsetti, P., Frediani, B., Acciai, C., Balsi, F., Filippou, G., & Marcolongo, R. (2004). Heel fat pad involvement in rheumatoid arthritis and in spondyloarthropathies: an ultrasound study. *Scandinavian Journal of Rheumatology , 33*, 327-331.

Field, M. L., Greenber, B. H., & Burkett, L. L. (1967). Roentgenographic measurement of skin and heel-pad thickness in the diagnosis of acromegaly. *The American journal of the medical sciences. , 254* (4), 528-533.

Fung, Y. C. (1993). Viscoelasticity. In Y. Fung, *Biomechanics mechanical properties of living tissue* (p. 41-48).

Furth, A. J. (1997). Glycated proteins in diabetes. British Journal of Biomedical Science. 54 (3) (pp 192-200). *British Journal of Biomedical Science. , 54* (3), 192-200.

Gonticas, S. K. (1969). Evaluation of diagnostic value of heel pad thickness. *Radiology , 92* (2), 304-307.

Gooding, G. A., Stress, R. M., Graf, P. M., & Grunfeld, C. (1985). Heel pad thickness - determination by high-resolution ultrasonography. *Journal of Ultrasound in Medicine , 4* (4), 173-174.

Gooding, G. A., Stress, R. M., Graf, P. M., Moss, K. M., Louie, K. S., & Grunfeld, C. (1986). Sonography of the sole of the foot evidence for loss of foot pad thickness in diabetes and its relationship to ulceration of the foot. *Investigative Radiology , 21* (1), 45-48.

Hsu, C. C., Tsai, W. C., Hisao, T. Y., Tseng, F. Y., Shau, Y. W., Wang, C. L., et al. (2009). Diabetic effect on micochambers amd macrochambers tissue properties in huma heel pads. *Clinical Biomechanics , 24*, 682-686.

Hsu, C. C., Tsai, W. C., Wang, C. L., Pao, S. H., Shau, Y. W., & Chuan, Y. S. (2007). Microchambers and macrochambers in heel pads: are they functionally different? *Journal of Applied Physiology , 102*, 2227-2231.

Hsu, T. C., Lee, Y. S., & Shau, Y. W. (2002). Biomechanics of the heel pad for type 2 diabetic patients. *Clinical Biomechanics , 17* (4), 291-296.

Hsu, T. C., Wang, C. L., Shau, Y. W., Tang, F. T., Li, K. L., & Chen, C. Y. (2000). Altered heel-pad mechanical properties in patients with Type 2 diabetes mellitus. *Diabetic Medicine , 17* (12), 854-859.

Hsu, T. C., Wang, C. L., Tsai, W. C., Kuo, J. K., & Tang, F. T. (1998). Comparison of the mechanical properties of the heel pad between young and elderly adults. *Archives of Physical Medicine and Rehabilitation , 79* (9), 1101-1104.

Jackson, D. M. (1968). Heel pad thickness in obese persons. *Radiology , 90* (1), 129.

Jørgensen, U., Larsen, E., & Varmaken, J. E. (1989). The HPC-device - a method to quantify the heel pad shock absorbency. *Foot & Ankle , 10* (2), 93-98.

Kanatli, U., Yetkin, H., Simsek, A., Besli, K., & Ozturk, A. (2001). The relationship of the heel pad compressibility and plantar pressure distribution. *Foot & Ankle International , 22* (8), 662-665.

Karabay, N., Toros, T., & Hurel, C. (2007). Ultrasonography evaluation in plantar fascitiis. *The Journal of Foot & Ankle Surgery , 46* (6).

Kerr, P. S., Silver, D. A., Telford, K., Andrews, H. S., & Atkins, R. M. (1995). Heel-pad compressibility after calcaneal fractures - ultrasound assessment. *Journal of Bone and Joint Surgery-British Volume , 77B* (3), 504-505.

Kho, K. M., Wright, A. D., & Doyle, F. H. (1970). Heel pad thickness in acromegaly. *British Journal of Radiology , 43* (506), 119-125.

Kinoshita, H., Francis, P. R., Murase, T., Kawai, S., & Ogawa, T. (1996). The mechanical properties of the heel pad in elderly adults. *European Journal of applied physiology and occupational physiology , 73* (5), 404-409.

Klaesner, J. W., Hastings, M. K., Zou, D. Q., Lewis, C., & Mueller, M. J. (2002). Plantar tissue stiffness in patients with diabetes mellitus and peripheral neuropathy. *Archives of Physical Medicine and Rehabilitation , 83* (12), 1796-1801.

Kuhns, J. G. (1949). Changes in elastic adipose tissue. *Journal of Bone and Joint Surgery , 31*, 541-547.

Kwan, R. L., Zheng, Y. P., & Cheing, G. L. (2010). The effect of aging on the biomechanical properties of plantar soft tissue. *Clinical Biomechanics , 25*, 601-605.

Levy, A. S., Berkowitz, R., Franklin, P., Corbett, M., & Whitelaw, G. P. (1992). Magnetic Resonance Imaging evaluation of calcaneal fat pads in patients with os calcis fractures. *Foot&Ankle , 13* (2), 57-62.

Mickle, K. J., Munro, B. J., Lord, S. R., Menz, H. B., & Steele, J. R. (2011). Soft tissue thickness under the metatarsal heads is reduced in older people with toe deformities. *Journal of Orthopaedic Research* , 1042-1046.

Mittal, R. K. (1983). Heel pad thickness in normal Nigerians and patients with acromegaly. *East African Medical Journal , 60* (3), 156-159.

Onwuanyi, O. N. (2000). Calcaneal spurs and plantar heel pad pain. *The Foot , 10*, 182-185.

Ozdemir, H., Soyuncu, Y., Ozgorgen, M., & Dabak, K. (2004). Effects of changes in heel fat pad thickness and elasticity on heel pain. *Journal of the American Podiatric Medical Association , 94* (1), 47-52.

Prichasuk, S. (1994). The Heel Pad in Plantar Heel Pain. *Journal of Bone and Joint Surgery-British Volume , 76B* (1), 140-142.

Prichasuk, S., Mulpruek, P., & Siriwongpairat, P. (1994). The Heel-Pad Compressibility. *Clinical Orthopaedics & Related Research , 300*, 197-200.

Puckette, S. E. (1967). Fallibility of heel pad thickness in diagnosis of acromegaly. *Radiology , 88* (5), 982-983.

Raja, R. (1980). Heel pad thickness in Kenyan Africans. *The East African Medical Journal , 57* (3), 208-211.

Rome, K. (1998). Mechanical properties of the heel pad: current theory and review of literature. *The Foot , 8*, 179-185.

Rome, K., Campbell, R., Flint, A., & Haslock, I. (2002). Heel pad thickness - A contributing factor associated with plantar heel pain in young adults. *Foot & Ankle International , 23* (2), 142-147.

Rome, K., Webb, P., Unsworth, A., & Haslock, I. (2001). Heel pad stiffness in runners with plantar heel pain. *Clinical Biomechanics , 16* (10), 901-905.

Sabir, N., Demirlenk, S., Yagci, B., Karabulut, N., & Cubukcu, S. (2005). Clinical utility of sonography in diagnosing plantar fascitiis. *Journal of Ultrasound in Medicine , 24*, 1041–1048.

Silver, D. A., Kerr, P. S., Andrews, H. S., & Atkins, R. M. (1994). Heel Pad Thickness Following Calcaneal Fractures - Ultrasound Findings. *Injury-International Journal of the Care of the Injured , 25* (1), 39-40.

Spears, I. R., & Miller-Young, J. E. (2005). The effect of heel-pad thickness and loading protocol on measured heel-pad stiffness and a standardized protocol for inter-subject comparability. *Clinical Biomechanics , 21* (2), 204-212.

Steinbach, H. (1964). Measurement of the heel pas as an aid to diagnosis of acromegaly. *Radiology , 82* (3), 418-423.

Tong, J., Lim, C. S., & Goh, O. H. (2003). Technique to study the biomechanical properties of the human calcaneal heel pad. *The Foot , 13* (2), 83-91.

Tsai, W. C., Chiu, M. F., Wang, C. L., Tang, F. T., & Wong, M. K. (2000). Ultrasound evaluation of plantar fascitiis. *Scandinavian Journal of Rheumatology , 29*, 255-259.

Tsai, W. C., Wang, C. L., Hsu, T. C., Hsieh, F. J., & Tang, F. T. (1999). The mechanical properties of the heel pad in unilateral plantar heel pain syndrome. *Foot & Ankle International , 20* (10), 663-668.

Turgut, A., Gokturk, E., Kose, N., Seber, S., Hazer, B., & Gunal, I. (1999). The relationship of heel pad elasticity and plantar heel pain. *Clinical Orthopaedics And Related Research* , 191-196.

Uzel, M., Cetinus, E., Bilgic, E., Ekerbicer, H., & Karaoguz, A. (2006). Comparison of ultrasonography and radiography in assessment of the hel pad compressibility index of patients with

plantar heel pain syndrome. Measurement of the fat pad in plantar heel pad syndrome. *Joint Bone Spine , 73*, 196-199.

Uzel, M., Cetinus, E., Ekebircer, H. C., & Karaoguz, A. (2006). Heel pad thickness and athletic activity in healthy young adults: a sonographic study. *Journal of Clinical Ultrasound , 34* (5), 231-236.

Vandenbroucke, J. P., von Elm, E., Altman, D. G., Gøtzsche, P. C., & Mulrow, C. D. (2007). Strengthening the Reporting of Observational Studies in Epidemiology (STROBE): Explanation and Elaboration. *Annals of Internal Medicine* , 163-194.

Wang, C. L., Hsu, T. C., Shau, Y. W., & Wong, M. K. (1998). Variations in heel pad mechanical properties variation between children and young adults. *J Formos Med Ass , 97*, 850-854.

Wearing, S. C., Smeathers, J. E., Urry, S. R., Sullivan, P. M., Yates, B., & Dubois, P. (2010). thicknening of the enthisis is correlated with energy dissipation ratio of the plantar fat pad during walking. *the American Journal of Sports Medicine , 38* (12), 2522-2527.

Wearing, S. C., Smeathers, J. E., Yates, B., Urry, S., & Dubois, P. (2009). Bulk compressive properties of the fat pad during walking: A pilot investigation in plantar heel pain. *Journal of Clinical Biomechanic , 24*, 397-402.

Zheng, Y. C., Zheng, Y. p., Choi, Y. K., Wong, K., Chan, S., & Mak, A. F. (2000). Biomechanical assessment of plantar foot tissue in diabetic patients using an ultrasound indentation system. *Ultrasound in Med. & Biol , 26* (3), 451-456.

Figure captions

Figure 1 MR imaging of the posterior region of the foot. Lateral view. C= calcaneus, HP= heel pad, S= skin

Figure 2 Schematic illustration of unloaded (a) and loaded (b) heel pad.

Figure 3 A typical load-displacement curve (hysteresis) of an *in vivo* human heel pad subjected to an external compression.

Figure 4 Flow diagram illustrating the selection procedure of studies to be included.

Table 1: Selected studies with their methodologies used to investigate the heel pad biomechanics

Paper	Title	N	UHPT	LHPT	Compressibility Index Stiffness Energy Dissipation Ratio
(Steinbach, 1964)	Measurement of the heel-pad as an aid to diagnosis of acromegaly.	131	X-ray		
(Puckette, 1967)	Fallibility of heel-pad thickness in diagnosis of acromegaly.	200	X-ray		
(Field et a., 1967)	Roentgenographic measurements of skin and heel-pad thickness in the diagnosis of acromegaly	101	X-ray		
(Jackson, 1968)	Heel pad thickness in obese persons	20	X-ray		
(Gonticas, 1969)	Evaluation of diagnostic value of heel pad thickness	265	X-ray		
(Kho et al., 1970)	Heel pad thickness in acromegaly.	131	X-ray		
(Bohrer & Ude, 1978)	Heel pad thickness in Nigerians.	343	X-ray		
(Raja, 1980)	Heel pad thickness in Kenyan Africans.	114	X-ray		
(Mittal, 1983)	Heel pad thickness in normal Nigerians and patients with acromegaly.	147	X-ray		
(Gooding et al., 1985)	Heel pad thickness - determination by high-resolution ultrasonography.	48	US		
(Gooding et al., 1986)	Sonography of the sole of the foot evidence for loss of foot pad thickness in diabetes and its relationship to ulceration of the foot.	73	US		
(Jørgensen et al., 1989)	The HPC-device - a method to quantify the heel pad shock absorbency.	100	X-ray	X-ray weight-bearing + Device CA=9cm^2 V=1,1mm/s	
(Levy et al., 1992)	Magnetic resonance imaging evaluation of calcaneal fat pads in patients with os calcis fractures	15	MRI		
(Prichasuk et al., 1994)	The heel pad compressibility	400	X-ray	X-ray	X-ray
(Silver et al., 1994)	Heel Pad Thickness Following Calcaneal Fractures - Ultrasound Findings.	21	US		
(Prichasuk, 1994)	The heel pad in plantar heel pain.	270	X-ray	X-ray	X-ray
(Kerr et al.,1995)	Heel-pad compressibility after calcaneal fractures - ultrasound assessment.	10	US	5MHz US CA=2cm^2 Fmax=3Kg	5MHz US CA=2cm^2 Fmax=3Kg

(Kinoshita et al., 1996)	The mechanical properties of the heel pad in elderly adults.	30		free fall impact mass 5kg v=0,56m/s & v=0,94m/s	free fall impact mass 5kg v=0,56m/s & v=0,94m/s
(Wang et al.,1998)	Variation in the heel pad mechanical properties variation between children and young adults.	30	US		US, CA=6cm^2 Fmax=30N, V=6mm/s manual, S=L_{max}/$displ_{max}$
(Hsu et al., 1998)	Comparison of the mechanical properties of the heel pad between young and elderly adults.	33	US		US, CA=6cm^2, Fmax=30N,V=6mm/s manual, S=L_{max}/$displ_{max}$
(Tsai et al., 1999)	The mechanical properties of the heel pad in unilateral plantar heel pain syndrome.	20	US	US, CA=5,04cm^2 Fmax=3Kg, V=6mm/s	US, CA=5,04cm^2 , Fmax=3Kg, V=6mm/s
(Turgut et al., 1999)	The relationship of heel pad elasticity and plantar heel pain.	193	X-ray	X-ray	X-ray
(Zheng et al., 2000)	Biomechanical assessment of plantar foot tissue in diabetic patients using an ultrasound indentation system.	8	US		US indentation device V=1-2mm/s manual
(Onwuanyi, 2000)	Calcaneal spurs and plantar heel pain.	264	X-rays	X-ray	X-ray
(Hsu et al., 2000)	Altered heel-pad mechanical properties in patients with Type 2 diabetes mellitus.	53	US		US 10MHz CA=3,96cm^2 Fmax=74KPa V=6mm/s manual
(Tsai et al., 2000)	Ultrasound evaluation of plantar fasciitis.	135	US		
(Rome et al., 2001)	Heel pad stiffness in runners with plantar heel pain.	166			portable device φ=6mm Fmax=20N V=manual S=L_{max}/$displ_{max}$
(Kanatli et al., 2001)	The relationship of the heel pad compressibility and plantar pressure distribution.	106	X-ray	X-ray weightbearing	X-ray weightbearing
(Rome et al., 2002)	Heel pad thickness - A contributing factor associated with plantar heel pain in young adults.	204		US	
(Klaesner et al., 2002)	Plantar tissue stiffness in patients with diabetes mellitus and peripheral neuropathy.	40			indentation device ϕ =7,9mm Fmax=9N K1 e K2 in diff part of Load-displ. curve
(Hsu et al., 2002)	Biomechanics of the heel pad for type 2 diabetic patients.	41			US, CA=3,96cm^2 Fmax=74KPa V=6mm/s manual
(Alcantara et al., 2002)	Influence of age, gender, and obesity on the mechanical properties of the heel pad under walking impact conditions	54			ballistic pendulum V=0,64m/s CA=38,48 cm^2
(Boros & Challis, 2003)	Heel pad properties of males and females	10			heel pad indenter
(Tong et al., 2003)	Technique to study the biomechanical properties of the human calcaneal heel pad.	35	US	US with test rig Fmax=30N	US + test rig Fmax=30N
(Ozdemir et al., 2004)	Effects of changes in heel fat pad thickness and elasticity on heel pain.	50	X-ray	X-ray	

(Falsetti et al., 2004)	Heel fat pad involvement in rheumatoid arthritis and in SpondyloArthropathies: an ultrasonographic study	401	US		
(Sabir et al., 2005)	Clinical utility of sonography in diagnosing plantar fascitiis	105	MRI & US		
(Uzel et al., 2006)	Heel pad thickness and athletic activity in healthy young adults: A sonographic study.	110	US	US weight.-bearing	US weight.-bearing
(Uzel et al., 2006)	Comparison of ultrasonography and radiography in assessment of the heel pad compressibility index of patients with plantar heel pain syndrome. Measurement of the fat pad in plantar heel pain syndrome	42	X-ray vs. US	X-ray vs. US	X-ray vs. US
(Erdemir et al., 2006)	An inverse finite-element model of heel-pad indentation.	40	US		
(Cheung, et al., 2006)	Magnetic resonance elastography of the plantar fat pads - Preliminary study in diabetic patients and asymptomatic volunteers.	16			MR Elastography
(Karabay et al., 2007)	Ultrasonography evaluation of plantar fascitiis	46	US		
(Hsu et al., 2007)	Microchambers and macrochambers in heel pads: are they functionally different?	6	US		US, ϕ =39,7mm CA=0,00125m^2 Fmax=196N V=0,052 mm/s E=$\sigma_{max}/\varepsilon_{hp}$
(Challis et al., 2008)	Mechanical properties of the human heel pad: a comparison between populations.	20	US		US + Indentation Dev. ϕ =6mm Fmax=50N V=1mm/s
(Wearing et al., 2009)	Bulk compressive properties of the fat pad during walking: A pilot investigation in plantar heel pain.	18	X-ray	X-ray + fluoroscopy (dynamic measurements)	X-ray + fluoroscopy (dynamic measurements)
(Hsu, et al., 2009)	Diabetic effects on microchambers and macrochambers tissue properties in human heel pads	34	US		US CA=0,00125m^2, Fmax=98N V=6 mm/s E=$\sigma_{max}/\varepsilon_{hp}$
(Kwan et al., 2010)	The effect of aging on the biomechanical properties of plantar soft tissues	60	US		US palpation system Fmax=10 N Manual
(Wearing et al., 2010)	Plantar Enthesopathy Thickening of the Enthesis Is Correlated With Energy Dissipation of the Plantar Fat Pad During Walking	18	US		US + fluoroscopy (dynamic measurements
(Chao et al., 2011)	Epidermal thickness and biomechanical properties of plantar tissues in diabetic foot	112	US		US ϕ =5mm, Fmax=10N V=manual
(Mickle et al., 2011)	Soft Tissue Thickness under the Metatarsal Heads is Reduced in Older People with Toe Deformities	216	US		

US=Ultrasound; MRI=Magnetic Resonance Imaging; CA=Contact Area; V=Velocity; F= Force; L= Load; E= Elastic modulus; S= Stiffness; displ= displacement.

Table 2: Ranking the confounding factors

Confounding factor	Rank
Age	5
Weight	5
Height	1
Gender	2
Race	1
Physical activity	4
Diabetes	4
Heel pain	3
Acromegaly	2
Heel fracture	3

0=not influence; 5=high influence

Appendix 1: Influence of subject factors on Unloaded Heel Pad Thickness

Paper	Title	A	W	H	G	Race	Physical activity	Diabetes	Heel pain	RA	SpA	Acromegaly	Heel fractures
(Steinbach, 1964)	Measurement of the heel-pad as an aid to diagnosis of acromegaly.	0			0							1	
(Puckette, 1967)	Fallibility of heel-pad thickness in diagnosis of acromegaly.	0			0	1							
(Field et al.,1967)	Roentgenographic measurements of skin and heel-pad thickness in the diagnosis of acromegaly											0	
(Jackson, 1968)**	Heel pad thickness in obese persons		0**										
(Gonticas, 1969)	Evaluation of diagnostic value of heel pad Thickness	0	1	1								0	
(Kho et al., 1970)*	Heel pad thickness in acromegaly.	1 - 0*	1		0 - 1*								
(Bohrer & Ude, 1978)	Heel pad thickness in Nigerians.	0°	1°		1°								
(Raja, 1980)°	Heel pad thickness in Kenyan Africans.	0°			0°							1°	
(Mittal, 1983)○	Heel pad thickness in normal Nigerians and patients with acromegaly.				0°							1°	
(Gooding et al., 1985)	Heel pad thickness - determination by high-resolution ultrasonography.							1					
(Gooding et al., 1986)	Sonography of the sole of the foot evidence for loss of foot pad thickness in diabetes and its relationship to ulceration of the foot.							-1					
(Jørgensen et al., 1989)	The HPC-device - a method to quantify the heel pad shock absorbency.		1		1								
(Levy et al., 1992)	Magnetic resonance imaging evaluation of calcaneal fat pads in patients with os calcis fractures												0
(Prichasuk, et al., 1994)	The heel pad compressibility	1			1								
(Silver et al., 1994)	Heel Pad Thickness Following Calcaneal Fractures - Ultrasound Findings.												1
(Prichasuk, 1994)	The heel pad in plantar heel pain	1			1				1				

(Kerr et al., 1995)	Heel-pad compressibility after calcaneal fractures - ultrasound assessment.												0
(Wang et al., 1998)	Variation in the heel pad mechanical properties variation between children and young adults	1											
(Hsu et al., 1998)	Comparison of the mechanical properties of the heel pad between young and elderly adults.	1											
(Tsai et al., 1999)	The mechanical properties of the heel pad in unilateral plantar heel pain syndrome.								0				
(Turgut et al., 1999)	The relationship of heel pad elasticity and plantar heel pain	1	1		1				0				
(Zheng et al., 2000)	Biomechanical assessment of plantar foot tissue in diabetic patients using an ultrasound indentation system.							-1					
(Onwuanyi, 2000)	Calcaneal spurs and plantar heel pain								0				
(Tsai et al., 2000)	Ultrasound evaluation of plantar fasciitis								0				
(Hsu et al., 2000)	Altered heel-pad mechanical properties in patients with Type 2 diabetes mellitus.							0					
(Rome et al., 2002)□	Heel pad thickness - A contributing factor associated with plantar heel pain in young adults.						0□		1□				
(Tong, et al., 2003)	Technique to study the biomechanical properties of the human calcaneal heel pad.							0	0				
(Ozdemir et al., 2004)	Effects of changes in heel fat pad thickness and elasticity on heel pain.	0	0		1								
(Falsetti et al., 2004)	Heel fat pad involvement in rheumatoid arthritis and in SpondyloArthropathies: an ultrasonographic study									0	0		
(Uzel et al., 2006)	Heel pad thickness and athletic activity in healthy young adults: A sonographic study.						0						
(Erdemir et al., 2006)	An inverse finite-element model of heel-pad indentation.							0					
(Karabay et al., 2007)	Ultrasonographic evaluation in plantar fasciitis								0				
(Challis et al., 2008)***	Mechanical properties of the human heel pad: a comparison between populations.						1***						

(Wearing et al., 2009)	Bulk compressive properties of the fat pad during walking: A pilot investigation in plantar heel pain.								0				
(Hsu, et al., 2009)	Diabetic effects on microchambers and macrochambers tissue properties in human heel pads							0					
(Wearing et al., 2010)	Plantar Enthesopathy Thickening of the Enthesis Is Correlated With Energy Dissipation of the Plantar Fat Pad During Walking								0				
(Kwan et al., 2010)	The effect of aging on the biomechanical properties of plantar soft tissues	1											
(Chao et al., 2011)	Epidermal thickness and biomechanical properties of plantar tissues in diabetic foot							1					
(Mickle et al., 2011)	Soft Tissue Thickness under the Metatarsal Heads is Reduced in Older People with Toe Deformities	0											

A= age; W= weight; H = height; G= gender; RA = Rheumatoid Arthritis; SpA = SpondyloArthropathies.

Notes:

* The second value refers to all acromegalic patients

** Only overweight person

***Cyclists have higher than runners

° Only people with African origin

□ Runners

Appendix 2: Influence of subject factors on Loaded Heel Pad Thickness

Paper	Title	Age	Weight	Gender	Physical activity	Diabetes	Heel pain	Heel fractures
(Prichasuk et al., 1994)	The heel pad compressibility	1		1				
(Prichasuk, 1994)	The heel pad in plantar heel pain						1	
(Kerr et al., 1995)	Heel-pad compressibility after calcaneal fractures - ultrasound assessment.							1
(Wang et al., 1998)	Variation in the heel pad mechanical properties variation between children and young adults	1						
(Turgut et al., 1999)	The relationship of heel pad elasticity and plantar heel pain	1	1	1			0	
(Onwuanyi, 2000)	Calcaneal spurs and plantar heel pain						0	
(Kanatli et al., 2001)	The relationship of the heel pad compressibility and plantar pressure distribution.						0	
(Tong et al., 2003)	Technique to study the biomechanical properties of the human calcaneal heel pad.					1	1	
(Ozdemir et al., 2004)	Effects of changes in heel fat pad thickness and elasticity on heel pain.	0	0	1				
(Uzel et al., 2006)	Heel pad thickness and athletic activity in healthy young adults: A sonographic study.				0			
(Wearing et al., 2009)	Bulk compressive properties of the fat pad during walking: A pilot investigation in plantar heel pain.						0	
(Wearing et al., 2010)	Plantar Enthesopathy Thickening of the Enthesis Is Correlated With Energy Dissipation of the Plantar Fat Pad During Walking						0	

Appendix 3: Influence of subject factors on Heel Pad Compressibility Index

Paper	Title	Age	Weight	Gender	Physical activity	Diabetes	Heel pain
(Prichasuk et al., 1994)	The heel pad compressibility	1	1	0			
(Prichasuk, 1994)	The heel pad in plantar heel pain	1		0			1
(Hsu et al., 1998)	Comparison of the mechanical properties of the heel pad between young and elderly adults.	1					
(Wang et al., 1998)	Variation in the heel pad mechanical properties variation between children and young adults	0					
(Tsai et al., 1999)	The mechanical properties of the heel pad in unilateral plantar heel pain syndrome.						0
(Turgut et al., 1999)	The relationship of heel pad elasticity and plantar heel pain	1	1	0			0
(Hsu et al., 2000)	Altered heel-pad mechanical properties in patients with Type 2 diabetes mellitus.					0	
(Onwuanyi, 2000)	Calcaneal spurs and plantar heel pain						1
(Kanatli et al., 2001)	The relationship of the heel pad compressibility and plantar pressure distribution.						0
(Tong et al., 2003)	Technique to study the biomechanical properties of the human calcaneal heel pad.					1	1
(Ozdemir et al., 2004)	Effects of changes in heel fat pad thickness and elasticity on heel pain.	1	1	1			
(Uzel et al., 2006)	Heel pad thickness and athletic activity in healthy young adults: A sonographic study.				0		

Appendix 4: Influence of subject factors on Stiffness

Paper	Title	Age	Weight	Gender	Physical activity	Diabetes	Heel pain
(Wang et al., 1998)	Variation in the heel pad mechanical properties variation between children and young adults	0					
(Zheng et al., 2000)	Biomechanical assessment of plantar foot tissue in diabetic patients using an ultrasound indentation system.					1	
(Hsu et al., 2000)	Altered heel-pad mechanical properties in patients with Type 2 diabetes mellitus.					0	
(Rome et al., 2001)**	Heel pad stiffness in runners with plantar heel pain.						-1**
(Alcantara et al., 2002)	Influence of age, gender, and obesity on the mechanical properties of the heel pad under walking impact conditions.	0	-1	1			
(Klaesner et al., 2002)	Plantar tissue stiffness in patients with diabetes mellitus and peripheral neuropathy.					0	
(Boros & Challis, 2003)	Heel pad properties of males and females			-1			
(Cheung, et al., 2006)	Magnetic resonance elastography of the plantar fat pads - Preliminary study in diabetic patients and asymptomatic volunteers.					0	
(Challis et al., 2008)*	Mechanical properties of the human heel pad: a comparison between populations.				1*		
(Wearing et al., 2009)	Bulk compressive properties of the fat pad during walking: A pilot investigation in plantar heel pain.						0
(Hsu, et al., 2009)	Diabetic effects on microchambers and macrochambers tissue properties in human heel pads					0	
(Wearing et al., 2010)	Plantar Enthesopathy Thickening of the Enthesis Is Correlated With Energy Dissipation of the Plantar Fat Pad During Walking						0
(Kwan et al., 2010)	The effect of aging on the biomechanical properties of plantar soft tissues	1					
(Chao et al., 2011)	Epidermal thickness and biomechanical properties of plantar tissues in diabetic foot					1	

Notes:

* Runners have lower than cyclists ; ** All subjects are runners

Appendix 5: Influence of subject factors on Energy Dissipation Ratio

Paper	Title	Age	Weight	Gender	Physical activity	Diabetes	Heel pain
(Jørgensen et al., 1989)	The HPC-device - a method to quantify the heel pad shock absorbency.	**-1**		**-1**			
(Kinoshita et al., 1996)	The mechanical properties of the heel pad in elderly adults.	**-1**					
		-1					
(Hsu et al., 1998)	Comparison of the mechanical properties of the heel pad between young and elderly adults.	**1**					
(Wang et al., 1998)	Variation in the heel pad mechanical properties variation between children and young adults	**0**					
(Tsai et al., 1999)	The mechanical properties of the heel pad in unilateral plantar heel pain syndrome.						**0**
(Alcantara et al., 2002)	Influence of age, gender, and obesity on the mechanical properties of the heel pad under walking impact conditions.	**0**	**1**	**1**			
(Hsu et al., 2002)	Biomechanics of the heel pad for type 2 diabetic patients.					**1**	
(Boros & Challis, 2003)	Heel pad properties of males and females			**-1**			
(Challis et al., 2008)*****	Mechanical properties of the human heel pad: a comparison between populations.				**0***		
(Wearing et al., 2009)	Bulk compressive properties of the fat pad during walking: A pilot investigation in plantar heel pain.						**-1**
(Wearing et al., 2010)	Plantar Enthesopathy Thickening of the Enthesis Is Correlated With Energy Dissipation of the Plantar Fat Pad During Walking						**-1**

Notes:

* No difference between cyclists and runners

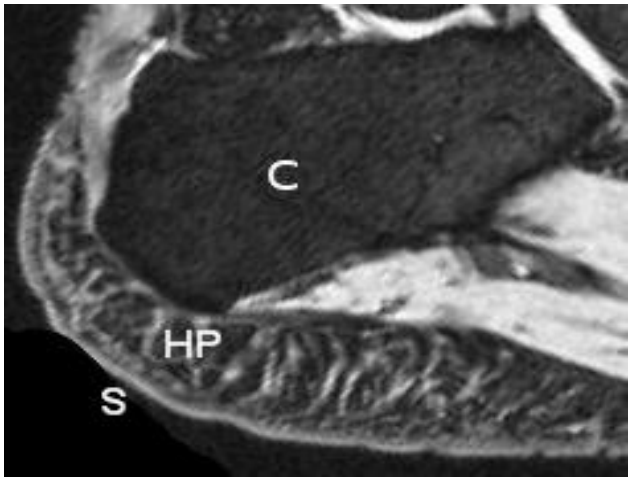

Figure 1 MR imaging of the posterior region of the foot. Lateral view. C= calcaneus, HP= heel pad, S= skin

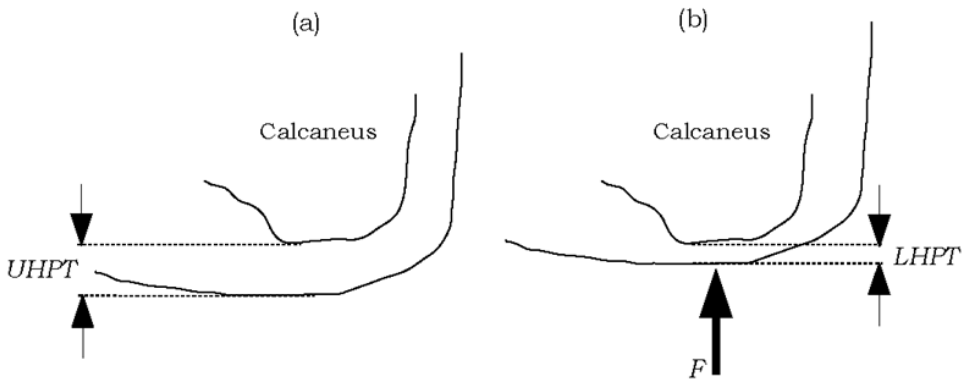

Figure 2 Schematic illustration of unloaded (a) and loaded (b) heel pad.

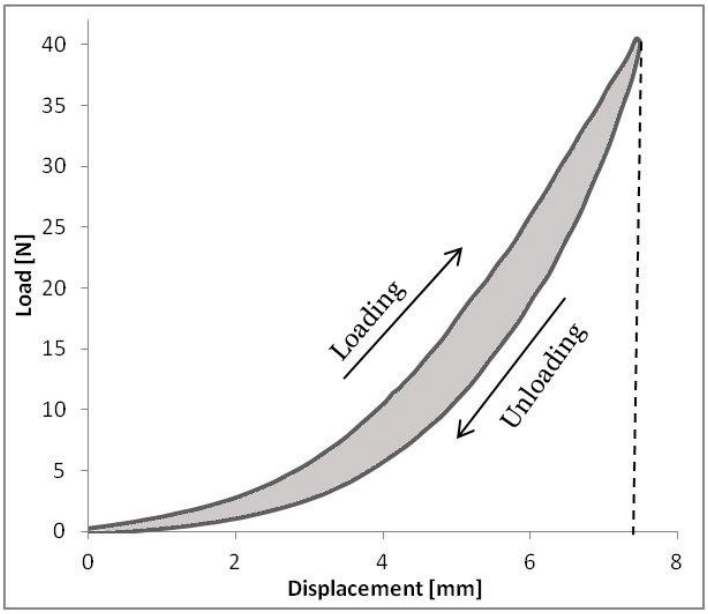

Figure 3 A typical load-displacement curve (hysteresis) of an *in vivo* human heel pad subjected to an external compression.

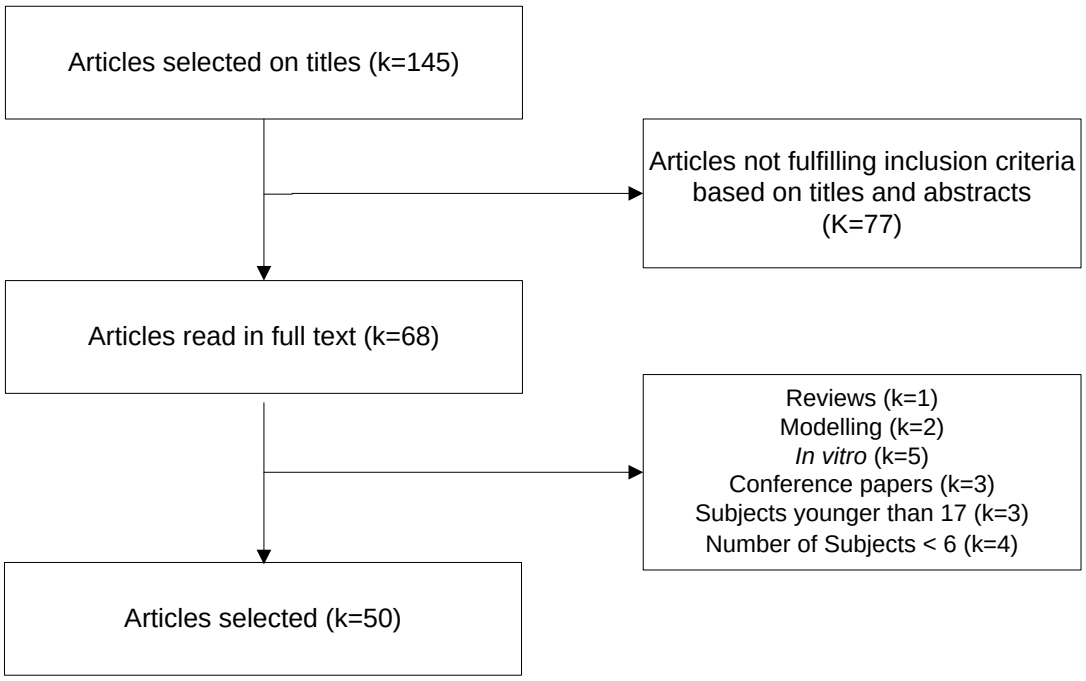

Figure 4 Flow diagram illustrating the selection procedure of studies to be included.

II PAPER

Title: Some of the factors influencing the Heel Pad Compressibility Index (HPCI)

Authors: Sara Matteoli, Jens E. Wilhjelm, Søren T. Torp-Pedersen.

Contribution: Poster contribution at the International Conference on the Ultrasonic Measurement and Imaging of Tissue Elasticity **Submission:** Submitted for publication in proceeding on September 17, 2009.

035 SOME OF THE FACTORS INFLUENCING THE HEEL PAD COMPRESSIBILITY INDEX (HPCI)

Sara Matteoli[1], Jens E. Wilhjelm[1], Søren Torp-Pedersen[2].*

[1]DTU Elektro, Biomedical Engineering, Technical University of Denmark, Ørsteds Plads, Bldg.348, DK-2800 Kgs. Lyngby, DENMARK;

[2]The Parker Institute, Frederiksberg Hospital, University of Copenhagen, Nordre Fasanvej 57, DK-2000 Frederiksberg, DENMARK.

Submitted for publication in final form: September 17, 2009.

Abstract: The human heel pad is a complex structure that features non-linear visco-elastic characteristics as the majority of the human soft tissues. The biomechanical aspects of the heel pad are still under investigation and the influence of subject factors such as age, weight, gender, height, race, and body activity have been reported. The aim of this paper is to study the literature in order to identify the influence of subject factors and diseases on the heel pad compressibility index.

I. Introduction

The human heel pad is a complex structure that features non-linear visco-elastic characteristics as the majority of the human soft tissues. It acts as an efficient shock absorber reducing the impact forces during gait. Trauma to the heel pad and/or diseases may cause the "destruction" of its intricate septation with resulting permanent damage of its shock absorbency capability.

The biomechanical aspects of the heel pad are still under investigation especially when a disorder is present. When measuring a biomechanical parameter of the heel pad for the purpose of diagnosis, the normal range of this parameter must be known as well as the variation with factors such as age, weight, gender, height, etc [1], [2], [3]. The influence of any single subject factor may, however, only be revealed if all other factors are controlled. As a consequence, it is possible that an effect of a given factor may be overlooked or falsely detected if the whole range of factors is not taken into account. Uncontrolled factors thus become confounding factors. We therefore found it important to review the literature in order to define factors with influence on heel pad compressibility index. The present study concentrates on the variation of the heel pad compressibility index (HPCI).

The aims of this literature review are to identify subject factors influencing on heel pad compressibility index and investigate whether consistent conclusions may be drawn in order to recommend which subject factors need to be controlled in future trials.

II. Method

Literature searches have been carried out in the bibliographic databases Inspec, EMBASE via Ovid, Medline via Pubmed, and Web of Science ultimo April 2009.

The following keywords were used: heel pad thickness, heel pad compressibility, heel pad-elderly/diabetes/heel pain, heel pad elasticity

Thirty nine papers were identified. Concentrating on studies only dealing with *in vivo* measurements of the heel pad compressibility index, and subjects/patients at least 18 years of age resulted in 10 papers. Each identified paper was scanned for missing papers in the list of reference. Within the 10 selected papers, 16 studies were performed.

In order to establish whether or not the subject factors are controlled within each study, a difference of ±5 years for the age, ±5 kg for the weight, and ±5 cm for the height between the groups under investigation is considered acceptable.

The studies were divided into two main groups depending on whether a control group was present or not. Subsequently both groups were divided into subgroups, as illustrated in Table 1.

Table 2: Increase of HPCI as a function of the subject factors

Studies <u>without</u> control group	<u>A) Normal conditions</u>: normal healthy subjects are investigated for the influence of age, weight, (height), and physical activity.
	<u>B) Heel pain</u>: subjects suffering of heel pain are investigated on the influence of age and weight
Studies <u>with</u> control group	<u>C) Diseased conditions</u>: subjects with diseases/trauma such as diabetes and heel pain are investigated

III. Definition

A simple representation of the heel pad and the calcaneum bone, with or without the application of a load, is shown in Figure 1. Specifically, F is the load applied on the skin of the heel pad; Y_0 is the starting point located on the lowest part of the plantar tuberosity of the calcaneum; Y_L is the value of thickness when a load F is applied (loaded condition); Y_U is the value of the heel pad thickness when a load F is not applied (unloaded condition).

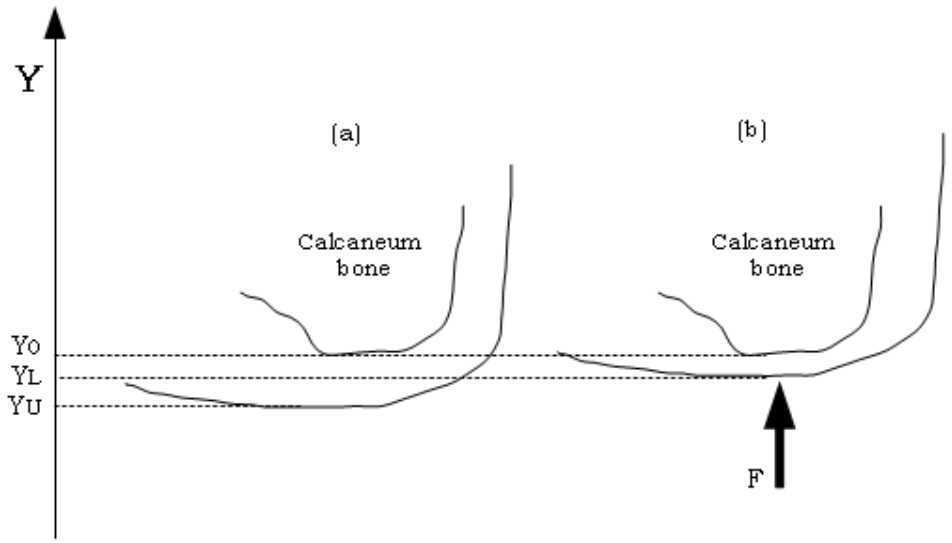

Figure 1: Schematic illustration of unloaded (a) and loaded (b) heel pad

The ***<u>Unloaded Heel Pad Thickness (UHPT)</u>*** is defined as:

$$UHPT = YU - Y0 \quad (1)$$

The ***<u>Loaded Heel Pad Thickness (LHPT)</u>*** is defined as:

$$LHPT = YL - Y0 \quad (2)$$

Both UHPT and LHPT were measured by using either lateral radiography or ultrasonic imaging of the region from skin to bone.

The ***<u>Heel Pad Compressibility Index (HPCI)</u>*** is defined as the ratio of the heel pad thickness in loaded conditions to unloaded positions. It is expressed as:

$$HPCI = (LHPT/UHPT)*100 \quad [\%] \quad (3)$$

The HPCI expresses the ability of the heel pad to be compressed. If *HPCI* is close to 100%, then the elasticity of the heel pad approaches 0 [2], [3]. When loads are applied sequentially, the maximum load (F_{max}) is used in the calculation of the loaded heel pad thickness [1], [4], [5].

IV. Results

Each of the papers that met the inclusion criteria were considered with respect to the HPCI (described in the Method section), and to a possible control of the subject factors.

The results are shown in Table 2 and Table 3. The body of Table 2 shows the tendency of HPCI for each study considered. The tendency is represented by a symbol that shows a statistical significant (p-value ≤ 0.05) increase or decrease of HPCI (↑, ↓), or a not-statistically-significant change (≈) when the subject factor in the leftmost column is increasing.

The symbol is followed by square brackets containing information about the study size. The first number identifies the paper in the list of reference, while the remaining numbers indicate the amount of heels under investigation. E.g. in [8, 2*120 + 102#], 8 indicates the reference number of the paper. A total of 342 heel pads were investigated: 2*120 from subjects having both heel pads analyzed, plus 120 heel pads from a number of subjects were one or two heel pads were analyzed. Especially when either unilateral and bilateral heel pain or fractured heels are investigated within the same study, the number of the analyzed heel pads could not be the same as the number of patients.

The following tables reveal tendencies instead of absolute values; since the methodologies used in the selected papers vary, absolute values cannot be compared.

Table 2: Increase of HPCI as a function of the subject factors

	Mechanical Parameter / **Subject Factors**	**Heel Pad Compressibility Index (HPCI) [%]**
A) Normal conditions	**Age**	↑[1,65#] ↑[2,2*200] ↑[3,2*400] ↑[8, 2*120]
	Weight	↑[3,2*400] ↑[8, 2*120]
	Physical activity (low vs. high activity)	≈[6, 2*110]
B) Heel Pain	**Age**	↑[10,67#]
	Weight	↑[10,67#]
C) Diseases vs. Normal	**Diabetes**	↑[7,38#] ≈[4,2*21+14#+2*20]
	Heel pain	↑[2,2*200+70#] ↑[7,38#] ≈[8, 2*120+102#] ≈[9, 2*47+94#] ≈[5,2*20]

≈ No statistical significant difference (p>0.05), ↑ or ↓ statistical significant difference (p≤0.05).

Arrow [Ref, N] = tendency [reference number, number of heel pad under investigation]

Table 3 shows results for the heel pad compressibility index pointing out which studies have been controlling the subject factors. Specifically, the table is made of two parts each one divided into three columns (where tendencies are shown). The first part of the table contains all the studies considered (joining together group A and B), while the second part contains only the studies controlling subject factors.

Table 3: Overview of tendencies found from the selected studies.

Subject factors	All studies			Studies controlling subject factors		
	↑	≈	↓	↑	≈	↓
Age (normal and heel pain)	[1] [2] [3] [8] [10]			[3] [8]		
Weight (normal and heel pain)	[3] [8]	[10]		[8]		
Physical activity (normal)		[6]				
Diabetes (disease vs. normal)	[7]	[4]			[4]	
Heel pain (disease vs. normal)	[2] [7]	[8][9][5]		[7]	[8][5]	

≈ No statistical significant difference ($p>0.05$); ↑ or ↓ statistical significant difference ($p\leq0.05$); [Ref] = [reference number]

V. Discussion and Conclusions

As seen from Table 3, no study found a decrease in HPCI.

- 6 studies investigating age and weight in normal subjects showed that HPCI increases with increasing age and weight. Of these 6 studies, 3 were controlling the subject factors.

- 2 uncontrolled studies investigated age and weight in subjects with heel pain. HPCI still increases with age and weight.

- 1 uncontrolled study investigating physical activity in normal subjects showed that HPCI does not change.

We conclude that studies on HPCI must control for age and weight when investigating possible effects on other factors such as e.g. various diseases, race, gender, nationality. No studies investigated the effect of height on HPCI. It is not surprising that it might have an effect. Therefore we propose further studies here.

-When presence of diabetes was investigated, an uncontrolled study showed an increase in HPCI whereas one controlled study showed no effect. Based on that data, we conclude that there is no evidence to support an influence of diabetes.

- When presence of heel pain was investigated, 2 studies (1 controlled) showed an increase in HPCI and 3 studies (2 controlled) showed no effect. Based on that data, we cannot rule out an effect of heel pain and future studies need to control for this entity.

Because the literature showed an effect of age, weight and a possible effect of the presence of heel pain, future studies on HPCI need to control for these factors. If these factors are not controlled for, they may become confounding factors that may hide a true effect or provoke a false effect on the behavior of the HCPI.

References:

[1] Hsu, T. C., Wang, C. L., Tsai, W. C., Kuo, J. K., & Tang, F. T., 1998. Comparison of the mechanical properties of the heel pad between young and elderly adults. *Archives of Physical Medicine and Rehabilitation*, 79 (9), pp.1101-1104.

[2] Prichasuk, S., 1994. The heel pad in plantar heel pain. *J. Bone Joint Surg.-British Volume*, 76B (1), pp.140-142.

[3] Prichasuk, S., et al., 1994. The heel-pad compressibility. *Clin. Orthop. and Rel. Res.*, 300, pp.197-200.

[4] Hsu, T. C., Wang, C. L., Shau, Y. W., Tang, F. T., Li, K. L., & Chen, C. Y., 2000. Altered heel-pad mechanical properties in patients with type 2 diabetes mellitus. *Diabetic Medicine*, 17 (12), pp. 854-859.

[5] Tsai, W. C., Wang, C. L., Hsu, T. C., Hsieh, F. J., & Tang, F. T., 2001. The mechanical properties of the heel pad in unilateral compressibility and plantar pressure distribution. *Foot & Ankle International*, 22 (8), pp. 662-665.

[6] Uzel, M., Cetinus, E., Ekerbicer, H. C., & Karaoguz, A., 2006. Heel pad thickness and athletic activity in healthy young adults: A sonographic study. *Journal of Clinical Ultrasound*, 34 (5), pp. 231-236.

[7] Tong, J., Lim, C. S., Goh, O. L., 2003. Technique to study the biomechanical properties of the human calcaneal heel pad. *The Foot*, 13, pp.83-91.

[8] Turgut, A., Gokturk, E., Kose, N., Seber, S., Hazer, B., & Gunal, I., 1999. The relationship of heel pad elasticity and plantar heel pain. *Clin. Orthop. and Rel. Res.*, 360, 191-196.

[9] Kanatli, U., Yetkin, H., Simsek, A., Besli, K., & Ozturk, A., 1999. The relationship of the heel pad plantar heel pain syndrome. *Foot & Ankle International*, 20 (10), pp. 663-668.

[10] Ozdemir, H., Soyuncu, Y., Ozgorgen, M., & Dabak, K., 2004. Effects of changes in heel fat pad thickness and elasticity on heel pain. *Journal of the American Podiatric Medical Association*, 94 (1), pp.47-52.

III PAPER

Title: Initial studies on the variations of load-displacement curves of *in vivo* human healthy heel pads.
Authors: Sara Matteoli, Jens E. Wilhjelm, Antonio Virga, Andrea Corvi, and Søren T. Torp-Perdersen.
Contribution: Oral presentation at the 15^{th} Nordic-Baltic Conference on Biomedical Engineering & Medical Physics, Aalborg, Denmark.
Submission: Submitted for publication in proceeding: April 6, 2011.

Initial Studies on the Variations of Load-Displacement Curves of *in vivo* Human Healthy Heel Pads

Sara Matteoli[1], Jens E. Wilhjelm[1], Antonio Virga[2], Andrea Corvi[2], and Søren T. Torp-Perdersen[3]

[1] Department of Electrical Engineering, Technical University of Denmark, Ørsteds Plads, Building 349, DK-2800 Kgs. Lyngby, Denmark
[2] Department of Mechanics and Industrial Technologies, University of Florence, via S. Marta 3, 50139 Florence, Italy
[3] The Parker Institute, Frederiksberg Hospital, DK-2000, Frederiksberg, Denmark

Abstract— **The aim of this study was to quantify on the measurement variation of *in vivo* load-displacement curves by using a group of human healthy heel pads. The recordings were done with a compression device measuring force and displacement. Twenty three heel pads, one from each of 23 subjects aged 20-35 years, were tested. The load-displacement curves showed the hysteresis, typical for a visco-elastic tissue. Seven load-displacement curves were measured for each subject. Each hysteresis was approximated by a 3rd degree polynomial, which in turn was described by two parameters: the slope and the average curvature. No statistically significant tendency (increasing or decreasing) were found for the seven polynomials (χ^2 test, P-values of 0.81 and 0.17 for the two parameters, respectively). The study revealed no systematic error in the recorded load-displacement curves. The mean slope and the average curvature for the 23 subjects were found to be 6.02±1.54 N/mm and 0.02±0.01, respectively. The new apparatus shows its reliability for further clinical investigations.**

Keywords— **Compressibility, hysteresis, reproducibility.**

I. Introduction

Quantitative measurements of the biomechanical properties of heel pad tissue are an important component in development of methods for diagnosis of heel pad diseases.

The human heel pad tissue is located between the calcaneus and the skin on the posterior part of the foot. It is a highly specialized visco-elastic structure that provides shock absorption during gait. Due to the nature of the heel pad tissue and its capability to deform under a load, when a loading/unloading cycle is applied, a characteristic load-displacement curve (hysteresis) is obtained. An obvious way to perform a loading/unloading cycle [1]-[3] is to use a compression device. Use of these hysteresis curves requires, however, knowledge of their variation from measurement to measurement. The literature shows a few studies dealing with the behavior of the load-deformation of *in vivo* heel pads [4]-[8]. Unfortunately, these studies are not comparable as the methodologies used are different (equipment, applied load, impact velocity, etc.) and none of the papers describes the variation in the data recorded.

This study proposes a new compression device which is not meant to reproduce the physiological condition of walking, but to be a possible clinical device capable to characterize the biomechanics of injured heel pads. The study attempts to investigate the measurement variation in load-displacement curves of *in vivo* human healthy heel pads. Each curve was described by two parameters: the slope and the average curvature. These were investigated for systematic errors and variation in order to assess the reliability of the apparatus and the consistency of the results.

II. Material and methods

B. Subjects

Twenty-three healthy subjects (11 males, 12 females) were enrolled. Table 1 shows the anthropometric characteristics. Only one foot was tested, the foot normally used to hit the ball during football. All subjects declared to be in healthy conditions, and have ever had injuries/trauma to any of the feet. The enrolled subjects had different lifestyles, including some being sporty and some following a more sedentary routine. Subjects engaged in professional sport were not included in this study. All participants were volunteers and were informed about the conditions of the test that involved no harmful procedures or physical pain. The weight and height of the subject were measured. Before starting the compression test the subject was asked to give information about age, nature of physical activity and hours per week, as well as size of shoe.

Table 1 Anthropometric characteristics of subjects under investigation grouped according to the gender given as mean plus/minus one standard deviation

	Females	Males
Subjects	12	11
Age (years)	24.7±2.7	24.9±3.9
Body Mass (kg)	61.9±6.1	70.5±9.0
Height (cm)	167.1±5.7	173.5±7.3

K. Dremstrup, S. Rees, M.Ø. Jensen (Eds.): 15th NBC on Biomedical Engineering & Medical Physics, IFMBE Proceedings 34, pp. 152–155, 2011.
www.springerlink.com

A. Equipment

The measurement part of the device consisted of a load cell (model 31, RDP Electronics Ltd, UK) and a linear transducer (LVDT, RDP Electronics Ltd, UK), both connected to an amplifier (E725, RDP Electronics Ltd, UK). The load cell and the linear transducer were both assembled in a cylindrical aluminium body. One end was fixed to a vertical aluminium plate, as shown in Fig. 1. The other end of the cylinder consisted of a threaded shaft which was connected to a stepper motor (PK245-03A, Oriental motor, Japan) by a shaft and a flexible joint, also visible in Fig.1. The more the threaded shaft was tightened by the stepper motor, the more compression was applied to the heel pad by a flat cylinder (diameter of 40 mm) guided by the threaded shaft. The sole of the foot under investigation was in contact with the aluminium vertical plate covered by an electrically insulating layer of rubber, while the heel pad touched the cylinder during the compression and decompression. A hole in the vertical plate allowed the cylinder to be in contact with the heel pad. The stepper motor, the load cell and the linear transducer were connected to PC through a digital acquisition board (NI USB-6009, National Instruments). The sampling frequency used was 10 Hz.

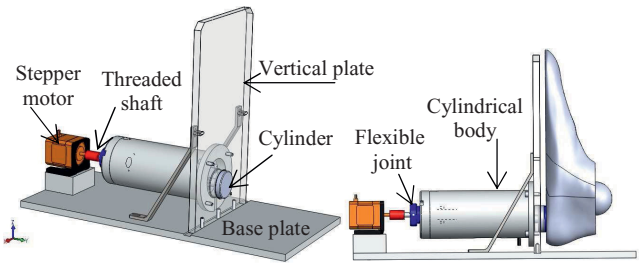

Fig. 1 The compression device. The stepper motor is connected to the threaded shaft with a shaft and flexible joint.

C. Procedure for compression test

The same procedure was applied to each volunteer. The subject removed the shoe and the sock from the foot to be investigated, and then laid down on an adjustable hospital bed with both legs completely straight and relaxed. The compression device was fixed on an appropriate table in front of the hospital bed.

The selected foot was positioned in such a way that the anterior part touched the vertical aluminium plate, with the heel pad in front of the cylinder. Specifically, the heel pad was placed with the center almost coincident with the center of the cylinder, as shown in Fig. 2, on the right.

Once the foot was well positioned, it is blocked with four Velcro fasteners (two to strap down the anterior part of the foot, one to keep the heel in front of the cylinder, and one to stabilize the ankle), as shown in Fig 2, on the left. When necessary, a cushion was positioned under the calf in order to better position the heel pad in front of the cylinder.

The subject was asked to remain as relaxed as possible and to maintain the foot in the same position for the duration of the test.

Fig. 2 Position of the foot on the vertical plate, on the left. Position of the cylinder on the heel pad, on the right. The print of the cylinder is made by placing some talcum powder on its surface

A program made with LabView (version 2009, National Instruments) was used to control the entire measurement (on/off of system, start/stop of stepper motor, direction of rotation of the stepper motor). The velocity used for applying the compression was 1.7 mm/s. Before starting the compression test on the heel pad, an idling test was done in order to verify the system functionality.

As soon as the subject was completely relaxed and ready to be tested, the examiner ran the LabView program controlling each step of the measurement procedure. For each subject, the compression test was repeated M=7 times with a one-minute break between each trial, to allow the heel pad tissue to return to its initial shape.

The value of the displacement determining the point of inversion of rotation of the stepper motor was fixed at 9 mm (to avoid arriving at the end of the thread of the shaft that guides the cylinder), while the superior limit of the force was fixed at 40 N.

The entire approach was designed to minimize any discomfort and any sensation of being strapped in order to be applicable to victims of torture.

D. Parameterization of hysteresis curves

In order to analyze the variation in the data of each subject, the best fit to a 3rd degree polynomial curve, y, was calculated for each load-displacement curve, $F(x)$, of each subject

$$y = a \cdot x^3 + b \cdot x^2 + c \cdot x + d \quad (1)$$

where x is the displacement, y is the force, a, b, c are coefficients, and d is a constant. The polynomial is exemplified in Fig. 3. In this study, the curves start at very near (0 mm, 0 N). Any distance interval where the load was not increasing, was subtracted from all measurement points, so that $F(x)$ starts at x=0 (d = 0 in (1)).

For each 3rd degree polynomial curve two parameters were chosen to describe the load-displacement curves. The slope, $\alpha_{n,m}$, representing the inclination of the straight line connecting the two extremes of the polynomial curve

$$\alpha_{n,m} = \frac{y(x_{\max})}{x_{\max}} \quad (2)$$

where n is the subject number, m is the measurements number for subject n and x_{max} is the value of x corresponding to the maximum of the polynomial curve.

The other parameter is the average curvature, $\bar{k}_{m,n}$, obtained by averaging the local curvatures ($k_{m,n,q}$). The latter was calculated by dividing the polynomial curve into Q equidistant intervals. At each interval, an expression for the curvature was found by

$$k_{m,n,q} = \frac{1}{R_q} = \frac{\left|\frac{d^2y}{dx^2}\right|}{\left[1+\left(\frac{dy}{dx}\right)^2\right]^{\frac{3}{2}}} \quad (3)$$

where R_q is the radius of the local curvature. Q ≈ 80 - 90.

III. Results

Considering the seven polynomial curves for a typical subject, Fig. 4 shows the trend of $\alpha_{n,m}$ and $\bar{k}_{m,n}$. For each parameter the tendency line is drawn as well.

The tendency lines for the 23 subjects were next analyzed to see if there was a prevailing slope. The slope of the tendency line of $\alpha_{n,m}$ is denoted β_α while the one of $\bar{k}_{m,n}$ is denoted β_k. These are shown in Fig. 5. By assuming that the variability can be approximated with a Gaussian distribution characterized by a mean of zero and a given standard deviation (SD = 0.213 for $\alpha_{n,m,}$ and SD = 0.00043 for $\bar{k}_{m,n}$), the χ^2 test was applied. A P-value < 0.1 was chosen to indicate a statistically significant tendency [9]. As seen from Table 2, no statistically significant tendency was identified.

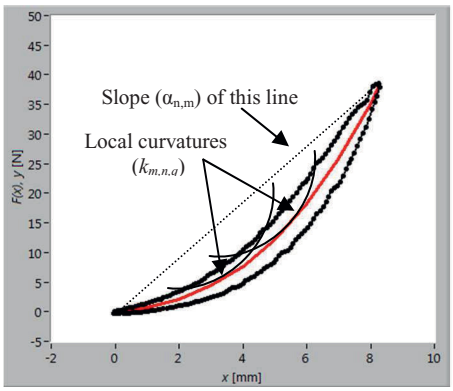

Fig. 3 Typical load-displacement curve with inside its best fitting 3rd degree polynomial curve.

Table 3 shows the typical variation of the hysteresis curves over the seven measurements. Calculating the final hysteresis curve for a subject by averaging the parameters for the seven measurements, Table 4 shows the variation over the 23 subjects.

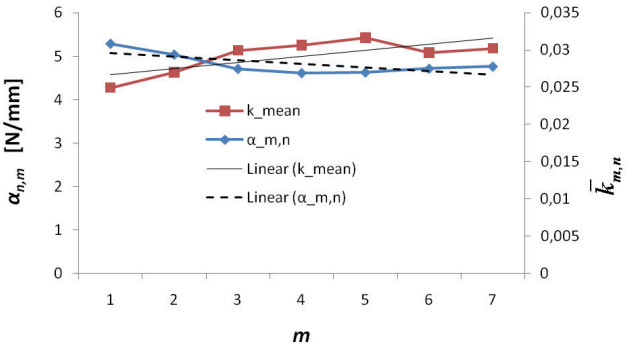

Fig. 4 Trend of $\alpha_{n,m}$ and $\bar{k}_{m,n}$ of all 7 polynomial curves for a typical subject. The correlation lines are drawn.

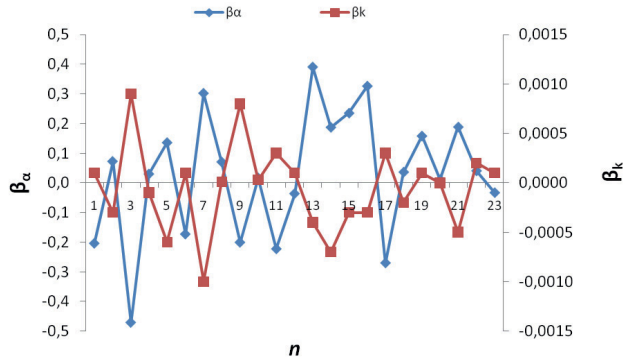

Fig. 5 Trend of β_α and β_k for all subjects

Table 2: Results obtained from the χ^2 test on $\alpha_{n,n}$ and $\bar{k}_{m,n}$

Parameter	χ^2	P-value
$\alpha_{n,n}$	0.81	0.85
$\bar{k}_{m,n}$	5.07	0.17

Table 3 Typical variation of hysteresis over the seven measurements of a subject. Specifically, for each subject the *SD* of a parameter was calculated over the seven measurements. Then the mean value of all these *SD* was calculated.

$\underset{n}{mean}\{\underset{m}{SD}\{\alpha_{n,m}\}\}$	0.78	[N/mm]
$\underset{n}{mean}\{\underset{m}{SD}\{\bar{k}_{n,m}\}\}$	0.0015	

Table 4 Typical variation of hysteresis over the 23 subjects. Specifically, for each subject the mean value of a parameter was calculated over the seven measurements, and then the mean value ± *SD* was calculated over the 23 subject.

$\underset{n}{mean}\{\underset{m}{mean}\{\alpha_{n,m}\}\}$	6.02±1.54 [N/mm]
$\underset{n}{mean}\{\underset{m}{mean}\{\bar{k}_{n,m}\}\}$	0.02±0.01

IV. Discussion

The load-displacement curves exhibited the hysteresis behavior, typical for a visco-elastic tissue. The hysteresis curves obtained for each subject were not completely overlapping, which is reflected by the deviations in Fig. 4. Such spread in data might be due to:

- Rotation and translation of the structure consisting of the heel pad tissue and its support apparatus (the calcaneus and the soft tissue surrounding the heel pad tissue). The support apparatus cannot be completely fixed relative to the measurement device, thus both rotation and translation of the heel pad tissue can occur.
- Muscles in the leg might not be completely relaxed during all measurements. An unconscious pressure against *e.g.* the approaching piston cannot be completely ruled out.

The two points above could theoretically be further reduced by *e.g.* a vacuum cushion, but the effect on the tissue by a more tight support is unknown. On a more speculative basis, it is not known if the individual components of the heel pad tissue returns to exactly the same position after every trial and neither are the influence of possible variations in liquid content (*e.g.* blood perfusion) known.

Nevertheless, the result of Fig. 5 and the P-values in Table 2 indicates that no systematic error is taking place during the seven individual recordings. Likewise, the variation among the seven hysteresis curves found in Table 3 is smaller than among the twenty-three subjects.

V. Conclusions

The study reveals no systematic error in the recorded load-displacement curves of a group of twenty-three healthy humans. The mean slope and the average curvature for a polynomial fit to these curves were found to be 6.02±1.54 N/mm and 0.02±0.01, respectively. The new apparatus shows its reliability for further clinical investigations.

Acknowledgments

We would like to thank the anonymous reviewers. We really appreciated the helpful comments.

References

[1] Hsu T.C., Wang C.L., Tsai W.C., et al. (1998). Comparison of the mechanical properties of the heel pad between young and elderly adults. Arch Phys Med Rehab 79(9):1101-1104.
[2] Jørgensen, U., Larsen, E., & Varmarken, J. E. (1989). The HPC-device: a method to quantify the heel pad shock absorbency, Foot Ankle,10(2):93-98.
[3] Aerts P, Ker RF, De Clercq D, Ilsley DW, Alexander RM. (1995). The mechanical properties of the human heel pad: a paradox resolved. J Biomech. 28(11):1299-308.
[4] Challis J.H., Murdoch C., Winter S.L. (2008). Mechanical properties of the human heel pad: a comparison between populations. J Appl Biomech 24(4):377-381.
[5] Tsai W.C., Wang C.L., Hsu T.C., et al. (1999). The mechanical properties of the heel pad in unilateral plantar heel pain syndrome. Foot Ankle Int 20(10):663-668.
[6] Erdemir A., Viveiros M.L., Ulbrecht J.S., Cavanagh P.R. (2006). An inverse finite-element model of heel-pad indentation. J Biomech, 39(7): 1279-1286.
[7] Rome K., Webb P., Unsworth A., et al. (2001). Heel pad stiffness in runners with plantar heel pain. Clin Biomech, 16(10):901-905.
[8] Tong J., Lim C.S., Goh O.L. (2003). Technique to study the biomechanical properties of the human calcaneal heel pad. The Foot, 13:83-91.
[9] Navidi W., Statistics for Engineers and Scientists, McGraw-Hill 2006

IV PAPER

Title: Investigations on *in vivo* human heel pad thickness.
Authors: Sara Matteoli, Maja M. Madsen, Antonio Virga, Jens E. Wilhjelm, Søren T. Torp-Pedersen.
Contribution: European Society of Biomechanics (ESB), Lisbon, Portugal.
Submission: Abstract submission on December 1, 2011

INVESTIGATIONS ON *IN VIVO* HUMAN HEEL PAD THICKNESS

Sara Matteoli(1), Maja M. Madsen(1), Antonio Virga(2), Jens E. Wilhjelm(1), Søren T. Torp-Pedersen(3)

1. Department of Electrical Engineering, Technical University of Denmark, DK;
2. Department of Mechanics and Industrial Technologies, University of Florence, IT;
3. The Parker Institute, Frederiksberg Hospital, DK

Introduction

The human heel pad thickness is one of the intrinsic factors which must be taken into account when investigating the biomechanics of the heel pad [Rome, 1998; Uzel, 2006]. In fact, heel pad thickness has been reported to be an important factor in determining stresses observed in healthy as well as pathological feet [Rome, 1998; Uzel, 2006]. Furthermore, the heel pad compressibility index (HPCI), indicating the ability of the heel pad to be compressed, is also an important parameter.

Methods

134 healthy subjects (66F, 68M) were enrolled in the present study. All participants were volunteers. The subject characteristics are shown in Table 1. For each subject the dominant foot was scanned, in both loaded and unloaded conditions with a 14 MHz 3D US (LogicE9, GE Healthcare). In unloaded condition the subject was lying down. In loaded condition the subject was standing on a Plexiglas platform with all the body weight on the dominant foot. The scan was made through the Plexiglas plate. The heel pad thickness was measured from 3D-block in the acquisition plane. The HPCI was then found as [Kanatli, 2001, Prichasuk, 1994; Prichasuk et al., 1994]:

$$HPCI = LHPT/UHPT \quad (1)$$

The statistical analysis was performed with the program R. A linear regression model was fitted to the data to investigate whether there was a correlation between HPCI and the intrinsic factors: age, gender, weight, height and duration of physical activity. The model included HPCI as a response variable and the intrinsic factors as explanatory variables. In the linear regression model the significance of each factor was evaluated by using the sum of squares. A P-value <0.05 was chosen as significant.

	All	Females	Males
Age (years)	36.0±14.4	36.7±14.4	36.6±14.4
Weight (kg)	71.7±13.7	64.2±9.2	79.2±12.8
Height (m)	173.7±9.8	166.8±5.7	180.4±8.3
BMI (kg/m^2)	23.6±3.1	23.0±2.7	24.3±3.3
Sport (h/week)	3.9±3.9	4.7±4.1	3.3±3.6

Table 1: Characteristics grouped according to the gender given as mean ± SD.

Results

The linear regression model showed that gender (P-value=0.048) and interaction between gender and age (P-value=0.029) were statistically significant, while age was not a significant variable (P-value= 0.444). Table 2 shows results for UHPT, LHPT and HPCI. A statistically significant difference between males and females was found in weight, height and hours of physical activity (P-value<0.05), while no statistically significant difference in age and BMI was found (P-value>0.05). A statistically significant difference between males and females was found in UHPT and LHPT (P-value=0.0006 and 0.007, respectively), while no statistically significant difference was found in HPCI (P-value= 0.889).

	Females	Males
UHPT (mm)	14.59±2.02	15.80±1.88
LHPT (mm)	8.65±1.55	9.35±1.47
HPCI (%)	59.29±6.94	59.30±7.38

Table 2: Results grouped according to the gender given as mean ± SD.

Discussion

Literature shows discordant results when dealing with heel pad biomechanics. The main reasons are the different methodologies applied and the different number of subjects investigated. Our study confirms that the interaction between gender and age plays a significant role on HPCI, as indicated by [Ozdemir, 2004]. [Prichasuk, 1994; Prichasuk et al., 1994; Hsu, 1998; Turgut, 1999] reported that age has a significant effect on HPCI, while [Prichasuk et al., 1994; Turgut, 1999; Ozdemir, 2004] indicated the weight as a significant factor.

References

Kanatli U *et al*, Foot Ankle Int, 22(8):662-5, 2001.
Prichasuk S, J Bone Joint Surg Br, 76B(1):140-142, 1994.
Prichasuk S *et al*, Clin Orthop Relat Res, 300:197-200, 1994.
Rome K *et al*, Br J Rad, 71:1149-1152, 1998.
Ozdemir H *et al*, J Am Podiatr Med Assoc, 94(1):47-52, 2004.
Turgut A *et al*, Clin Orthop Relat Res, 360:191-196, 1999.
Uzel M *et al*, Joint Bone Spine, 73:196-199, 2006.

V PAPER

Title: Modeling the human heel pad.
Authors: Sara Matteoli, Andrea Corvi, Jens E. Wilhjelm.
Contribution: Oral presentation at the Simpleware Users Workshop, Solihull, UK
Submission: Abstract submission on April 15, 2010.

Modeling the human heel pad

S. Matteoli[a,b], A. Corvi[b], J. E. Wilhjelm[a],
[a] Department of Electrical Engineering, Technical University of Denmark, Kgs. Lyngby, Denmark
[b] Dipartimento di Meccanica e Tecnologie Industriali, Università degli Studi di Firenze, Firenze, Italy

INTRODUCTION

The human heel pad acts as an efficient shock absorber reducing the impact forces during gait. It presents anisotropic, non-linear, visco-elastic characteristics as with the majority of the human soft tissues. It constitutes a complex structure with neuronal, vascular, fibrous and elastic components intertwined with fat cells [1]. Trauma to the heel pad and/or diseases of the heel may cause the "destruction" of its intricate septation which results in permanent damage of its shock absorbency capability. Palpation is still widely used as an important diagnostic tool. The standard medical practice of soft tissue palpation is based on qualitative assessment of the low-frequency stiffness of the tissue. Unfortunately, this qualitative technique is not powerful enough for a medico-legal assessment. In order to obtain a quantitative evaluation, and to gather information on the complete deformation of the tissues it is necessary to develop and use a device based on an indentation experiment. However, this alone does not provide sufficient information allowing a description of the tissue damage at a microscopic level. A computational simulation of the heel pad seems necessary, in order to obtain such description. The aim of the present work is to develop the model of a healthy heel pad in order to simulate the biomechanical behavior when subjected to a known external compression. Once validated by experimental tests, such simulation may pave the way for quantitative classification of healthy and diseased heel pad tissue.

MATERIALS AND METHODS

In the present work the 3D model of a 30 year-old Caucasian female's heel pad was built on the basis of MRI scan data [Siemens Magnetom Trio (3T), Fat-suppressed 3D dual echo steady state (DESS) sequence with (0.7 mm)^3 isotropic resolution, matrix 320x576x104. TE/TR=5.5/13ms, flip angle 25 degrees, 5 min. acq. time)]. All MR images (DICOM format) were imported in SIMPLEWARE®-ScanIP 3.2. The segmentation of the images was done in order to characterize the different tissues forming the heel pad. By applying proper thresholds, region growing and the function pain has been possible to distinguish the calcaneum bone, muscles, fat tissue, septa and skin. Two filters - morphological close filter and recursive Gaussian smoothing filter - were then applied to merge each identical structure and to improve the consistency of the final model. The 3D heel pad model was then exported in SIMPLEWARE®-+ScanFE 3.1.4. Mesh parameters were assigned, nodes and contact surface were defined in order to export the mesh in Ansys.

RESULTS

Fig.1 shows the segmentation of the heel pad images and creation of the model in ScanIP. Specifically, the bone is shown in red, the muscle in green, the skin in violet, the septa in pink and the fat tissue in light blue. Fig. 2 shows the mesh of the heel pad created in +ScanFE, ready to be exported in Ansys.

.

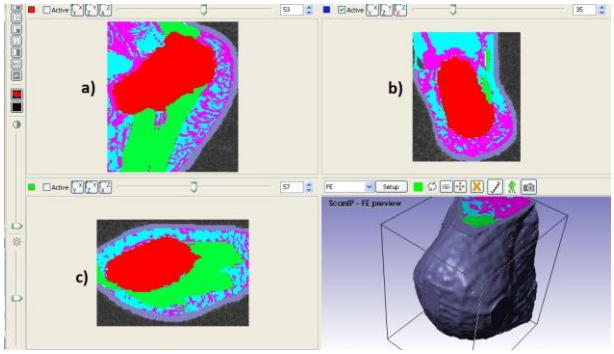

Fig. 1: Segmentation in ScanIP. a) sagittal view, b) axial view, c) coronal view.

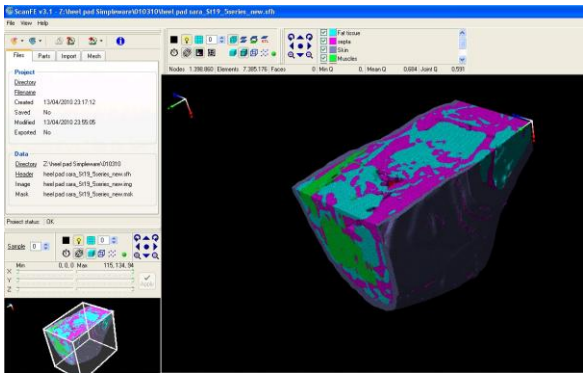

Fig. 2: Mesh creation in ScanFE

DISCUSSION

So far, the challenging part of the heel pad modeling is the identification of the intricate internal structure of the heel fat pad, made of fat tissue and septa. The reconstruction of this honeycomb microstructure [1] may help in differentiating diseased tissues from healthy ones. Indeed, the mechanical integrity and functioning of the heel pad as a whole is dependent on the integrity of the septa that enclose each independent chamber [1].

REFERENCES

[1] Jahss, M.H., et al., Investigations into the fat pads of the sole of the foot: anatomy and histology. Foot&Ankle, 1992, 5: 233-242.

VI PAPER

Title: On the heel pad elasticity modeling.
Authors: Sara Matteoli, Andrea Corvi, Jens E. Wilhjelm, Søren T. Torp Pedersen.
Contribution: Poster contribution at the Second National Congress of Bioengineering, Turin, Italy
Submission: Submitted for publication in proceeding on May 7, 2010.

ON HEEL PAD ELASTICITY MODELING

S. Matteoli[a,b], A. Corvi[b], J. E. Wilhjelm[a], S.T. Torp-Pedersen[c]
[a] *Department of Electrical Engineering, Technical University of Denmark, Kgs. Lyngby, Denmark*
[b] *Dipartimento di Meccanica e Tecnologie Industriali, Università degli Studi di Firenze, Firenze, Italy*
[c] *The Parker Institute, Frederiksberg Hospital, University of Copenhagen, Frederiksberg, Denmark*

INTRODUCTION

The human heel pad anatomically consists of a complex structure with neuronal, vascular, fibrous and elastic components that are intertwined with fat cells [1]. It presents anisotropic non-linear visco-elastic characteristics as with the majority of the human soft tissues, and it acts as an efficient shock absorber reducing the impact forces during gait. The biomechanical aspects of the heel pad are still under investigation particularly when there is a disorder.

Trauma to the heel pad and/or diseases of the heel may cause the "destruction" of its intricate septation which results in permanent damage of its shock absorbency capability. Specifically, falanga torture, a widespread corporal punishment in many countries, represents prolonged repetitive high-energy injury to the heel [2]. The effects related to this kind of torture are very difficult to identify medically, even though there is permanent damage that leads to impaired gait and chronic pain [3].

Palpation is still widely used as an important diagnostic tool. The standard medical practice of soft tissue palpation is based on qualitative assessment of the low-frequency stiffness of the tissue. Unfortunately, this qualitative technique, as well as MRI, is not powerful enough for a medico-legal assessment of falanga torture. In order to obtain a quantitative evaluation, and to gather information on the complete deformation of the tissues it is necessary to develop and use a device based on an indentation experiment. However, this alone does not provide information which allows a description of the tissue damage at a microscopic level. A computational simulation of the heel pad has also to be done, in order to have such description.

The aim of the present work is to develop heel pads model in order to simulate the biomechanical behavior (both in healthy and damaged cases) when subjected to a known external compression.

METHODS

The 3D finite element model of the heel pad, based on real MRI data, is created by assuming the constitutive law of the tissue and imposing the behavior found through indentation tests. The 3D model is then optimized by applying an iterative process comparing the results with those from the indentation test, and therefore adapting the tissues constitutive law. Once the 3D model is set up, the simulation of the heel pad can be first used to define test conditions (proper load and velocity at which the load must be applied) for real investigations, and then to relate the tissue damage to the stiffness measured with the indentation test.

In the present work the 3D finite element mesh of the heel pad was built on the basis of MRI scan data [Siemens Magnetom Trio (3T), Fat-suppressed 3D dual echo steady state (DESS) sequence with (0.7 mm)^3 isotropic resolution, matrix 320x576x104. The echo and repetition time was 5.4ms and 16ms respectively and the excitation angle was 25 degrees. The acquisition time was 5 minutes.].
All MR images (DICOM format) were imported in SIMPLEWARE® (ScanIP 3.2, +ScanFE 3.1.4) to create a solid model, as shown in Figure 1. The segmentation of the images was done by using proper thresholds and region growing, while filters as morphological close filter and recursive Gaussian smoothing filter were applied to merge the structures and to improve the quality of the final model. Segmented images were then exported to LS-DYNA Finite Element Software. In order to take into account all the non-linearities and visco-elasticities of the tissues, the hyperlastic parameters were chosen for the computational model [4]. All the values characterizing the modeled skin-muscle-soft tissue-bone complex were based on literature [5].

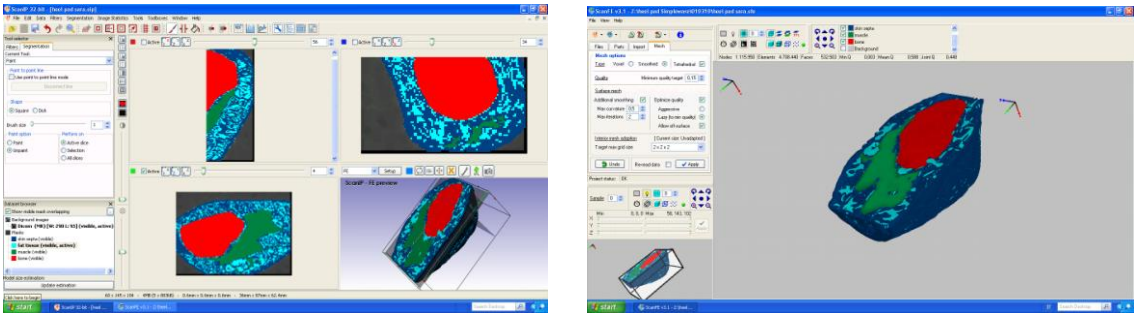

Fig. 1: 3D mesh of the heel pad created with Simpleware.

The indentation device is made of a load cell (RDP Electronics model 31) and a linear transducer (RDP Electronics LVDT Displacement Transducer), both connected to amplifiers (RDP Electronics E725) and assembled inside an aluminium cylindrical body. An additional large screw is needed for the indentation test. This is placed at the bottom of the cylindrical body. A circular shaped sensor (Φ=40 mm) is attached to the load cell at the other extremity (see Figure 2). The more the screw is tightened in, the more compression is applied to the heel pad by the sensor. The real displacement of the heel pad tissue starts from when the sensor touches the skin of the heel and the load cell shows an increasing load. Until the load is zero, the recorded displacement is only the feed of the sensor. For the present experiment five compressions are applied with an interval of 10 minutes between each trial, allowing the tissue to relax. Data are then acquired and processed by using LabVIEW and Excel**.**

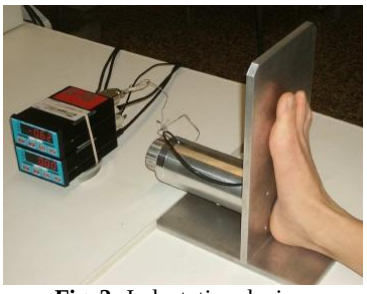

Fig. 2: Indentation device.

DISCUSSION

So far the crucial point of the heel pad modeling is the design of the intricate internal structure of the heel fat pad. Specifically, the septal walls and the fat cell chambers should be simulated with their characteristic honeycomb microstructure [1]. Such microstructure could be built by doing a computational sub-modeling that would allow to define the constitutive laws describing the behavior of the heel pad tissues at the microstructural level. By applying this procedure it will be possible to differentiate diseased tissues from healthy ones. Indeed, the mechanical integrity and functioning of the heel pad as a whole is dependent on the integrity of the septa that enclose each independent chamber [1].

REFERENCES

[1] Jahss, M.H., et al., Investigations into the fat pads of the sole of the foot: anatomy and histology. Foot&Ankle, 1992, 5: 233-242.

[2] Savnick, A., et al., MRI of the plantar structures of the foot after Falanga torture. European Radiology, 2000, 10: 1655-1659.

[3] Torp-Pedersen, S.T., et al., Diagnostic accuracy of heel pad palpation - a phantom study. J. Forensic Leg. Med., 2008, 15(7): 437-442.

[4] Natali, A.N., Carniel, E.L., Pavan, P.G., Dario, P., Izzo, I., Hyperelastic models for the analysis of soft tissue mechanics: definition of constitutive parameters, BioRob, Pisa, 2006.

[5] Fung, Y. C., Biomechanics: Mechanical Properties of Living Tissues, Springer, 1993.

VII PAPER

Title: Investigation on the load-deformation curves of a human healthy heel pad: *in vivo* compression data compared to numerical results.

Authors: Chiara G. Fontanella, Sara Matteoli, Emanuele L. Carniel, Jens E. Wilhjelm, Antonio Virga, Andrea Corvi, Arturo N. Natali

Journal: Medical Engineering & Physics

Submission: Accepted on December 14, 2011. Available online from January 19, 2012

Medical Engineering & Physics xxx (2012) xxx–xxx

Contents lists available at SciVerse ScienceDirect

Medical Engineering & Physics

journal homepage: www.elsevier.com/locate/medengphy

Investigation on the load-displacement curves of a human healthy heel pad: *In vivo* compression data compared to numerical results

C.G. Fontanella[a,*], S. Matteoli[b], E.L. Carniel[a], J.E. Wilhjelm[b], A. Virga[c], A. Corvi[c], A.N. Natali[a]

[a] Centre of Mechanics of Biological Materials, University of Padova, Via F. Marzolo 9, 35131 Padova, Italy
[b] Department of Electrical Engineering, Technical University of Denmark, Ørsteds Plads, DK-2800, Kgs. Lyngby, Denmark
[c] Department of Mechanics and Industrial Technologies, University of Florence, via S. Marta 3, 50139 Florence, Italy

ARTICLE INFO

Article history:
Received 29 June 2011
Received in revised form
12 December 2011
Accepted 14 December 2011

Keywords:
Heel pad analysis
Experimental tests
Visco-elasticity
Numerical model

ABSTRACT

The aims of the present work were to build a 3D subject-specific heel pad model based on the anatomy revealed by MR imaging of a subject's heel pad, and to compare the load–displacement responses obtained from this model with those obtained from a compression device used on the subject's heel pad. A 30 year-old European healthy female (mass = 54 kg, height = 165 cm) was enrolled in this study. Her left foot underwent both MRI and compression tests. A numerical model of the heel region was developed based on a 3D CAD solid model obtained by MR images. The calcaneal fat pad tissue was described with a visco-hyperelastic model, while a fiber-reinforced hyperelastic model was formulated for the skin. Numerical analyses were performed to interpret the mechanical response of heel tissues. Different loading conditions were assumed according to experimental tests. The heel tissues showed a non-linear visco-elastic behavior and the load–displacement curves followed a characteristic hysteresis form. The energy dissipation ratios measured by experimental tests (0.25 ± 0.02 at low strain rate and 0.26 ± 0.03 at high strain rate) were comparable with those evaluated by finite element analyses (0.23 ± 0.01 at low strain rate and 0.25 ± 0.01 at high strain rate). The validity and efficacy of the investigation performed was confirmed by the interpretation of the mechanical response of the heel tissues under different strain rates. The mean absolute percentage error between experimental data and model results was 0.39% at low strain rate and 0.28% at high strain rate.

1. Introduction

The human heel pad is a complex structure consisting of a fat pad with micro- and macro-chambers separated by an intricate fibro-elastic septation. Individual fat cells and fat globules are sealed off by delicate membranes [1], creating a so-called honeycomb configuration [2]. The structure of the septation is capable of bonding fat tissue from single compartments and hence such compartments are resistive to compressive loads [3,4]. The heel pad acts as an efficient shock absorber, smoothing the effects of impact forces during gait.

The heel pad exhibits non-linear visco-elastic behavior [5,6], like most soft biological tissue does. Due to the visco-elastic nature of the heel pad and its capability to deform under loading, when a loading/unloading cycle is applied a load–displacement curve is obtained [7] showing a characteristic hysteresis [8,9]. The mechanical behavior of the heel pad is determined by the mechanical responses of the adipose tissues and skin and by the interaction phenomena between these two tissues. Under compression loading, the heel pad initially has low stiffness, then the collagen fibers of the fat pad and skin come under tension, limiting the deformation of the tissue and resulting in an increase of the stiffness [10–12]. A way to perform a loading/unloading cycle and determine the mechanical behavior of heel pad is to use a mechanical compression device [13–15,16–21].

The analysis of hysteresis curves obtained from experimental tests on human heel pad allows for quantitative and qualitative investigation of the mechanical response of the tissue. Knowledge of the biomechanical properties of healthy and diseased heel pads may be used for screening patients (*e.g.* diabetic subjects, heel pain subjects, *etc.*) and for the prevention of pathologies. The experimental approach can be investigated and integrated with a computational model of the heel pad. Such a model would allow a better understanding of the stress–strain relationship of the tissues, in order to evaluate phenomena that are not measurable with sufficient accuracy by means of experimental tests. Finite element modeling of the soft tissues of the foot would pave the way for understanding stress-related injuries (*e.g.* plantar fasciitis and

* Corresponding author at: University of Padova, Centre of Mechanics of Biological Materials, Via F. Marzolo 9, I-35131 Padova, Italy. Tel.: +39 049 827 5605; fax: +39 049 827 5604.
E-mail address: chiaragiulia.fontanella@unipd.it (C.G. Fontanella).

1350-4533/$ – see front matter © 2011 IPEM. Published by Elsevier Ltd. All rights reserved.
doi:10.1016/j.medengphy.2011.12.013

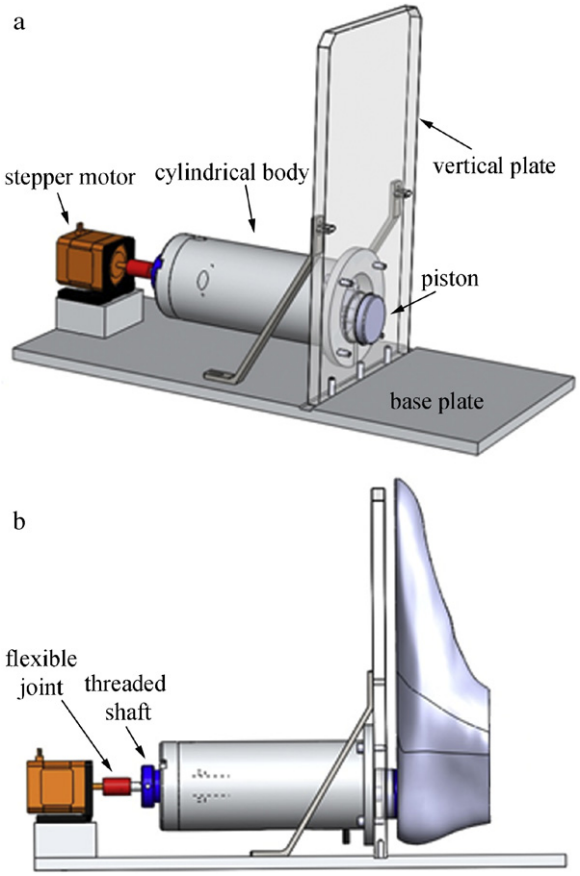

Fig. 1. (a) The compression device. (b) The stepper motor is connected to the threaded shaft with a shaft and flexible rotational joint.

diabetic ulceration [22,23]), as well as improve orthotics and footwear design, considering the stress induced in the plantar region (*e.g.* distribution of the plantar pressure [15,24–26]).

The aim of the present study was to build a three-dimensional quantitative subject-specific heel pad model, composed of fat pad and skin, on the basis of MRI data. The mechanical properties of the tissues were determined by experimental data previously collected [10–12]. These data were checked for accuracy and completeness and represent a reliable basis for the analysis. The load–displacement curves obtained from the finite element analysis representing the mechanical behavior of the model when subjected to an external compression are compared with those obtained by experiments using a compression device on an *in vivo* healthy heel pad. The device used here is not intended to reproduce the physiological condition of walking or running, but to be a possible clinical device capable to characterizing the biomechanics of injured heel pads. The procedure described in the present study, applied to a healthy foot, allows defining a numerical model which can interpret the mechanical response of heel tissues under specific configuration.

2. Methods

2.1. Subject characteristics

A 30 year-old European female (mass = 54 kg, height = 165 cm) was enrolled in this study. Her left foot underwent both MRI and compression tests. She declared to be in healthy condition, to have an active lifestyle, and to have never had injuries/trauma to any of the feet. She was informed that the test did not involve harmful procedures or physical pain.

2.2. MRI and 3D subject-specific heel pad model

A 3D model of the left heel was built on the basis of MRI data [3T Siemens Magnetom Trio, Fat-suppressed 3D dual echo steady state (DESS) sequence with (0.7 mm) [3] isotropic resolution, size matrix $320 \times 576 \times 104$. TE/TR = 5.5/13 ms, flip angle 25 degrees, TA = 5 min]. The DICOM images were processed using Simpleware, imaging density segmentation software that allows obtaining 3D CAD solid model by applying density segmentation techniques. The 3D CAD solid model of the heel region, composed of calcaneus, muscles and plantar fascia, fat pad and skin, was meshed by four hundred thousand tetrahedral elements [12], using the software MSC-Patran (MSC.Software Corporation, Santa Ana, CA).

2.3. Compression device and test procedure

The measurement part of the compression device consisted of a load cell (model 31, RDP Electronics Ltd., UK), a linear transducer (LVDT, RDP Electronics Ltd., UK) and an amplifier (E725, RDP Electronics Ltd., UK). The load cell and the linear transducer were both assembled in a cylindrical aluminium body. One end was fixed to a Plexiglas vertical plate, as shown in Fig. 1(a). The other end of the cylinder consisted of a threaded shaft which was connected to a stepper motor (PK245-03A, Oriental motor, Japan) by a shaft and a flexible joint (Fig. 1(b)). The more the threaded shaft was

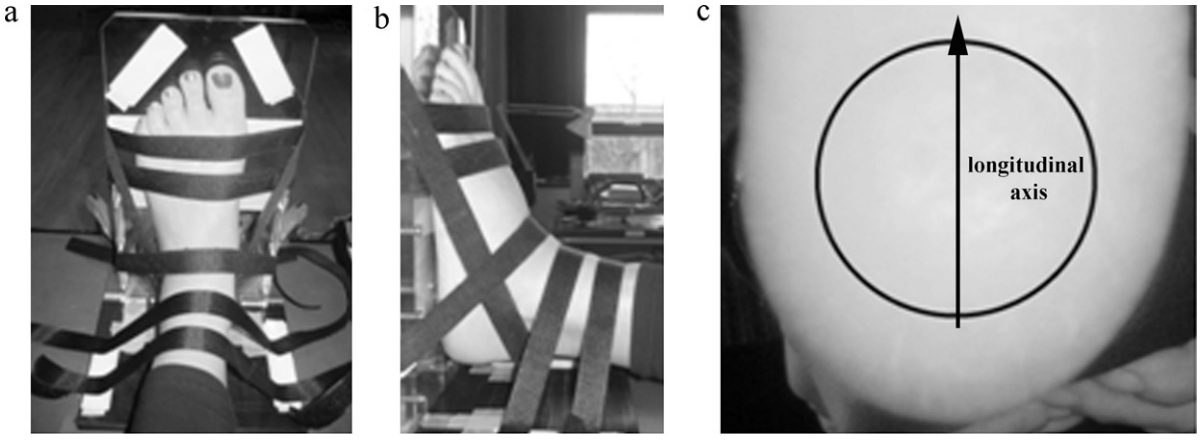

Fig. 2. (a and b) Position of the foot on the vertical Plexiglas plate and (c) position of the piston on the heel pad during the compression tests.

Please cite this article in press as: Fontanella CG, et al. Investigation on the load-displacement curves of a human healthy heel pad: *In vivo* compression data compared to numerical results. Med Eng Phys (2012), doi:10.1016/j.medengphy.2011.12.013

Table 1
Hyperelastic constitutive parameters adopted for fat pad tissues mechanical characterization.

K_ν (MPa)	r	C_1 (MPa)	α_1
7.50×10^{-2}	1.05×10^{1}	7.00×10^{-3}	1.19×10^{0}

tightened by the stepper motor, the more compression was applied to the heel pad by a piston (diameter of 40 mm). A hole in the vertical plate allowed the piston to be in contact with the heel pad. The stepper motor, the load cell and the linear transducer were connected to PC through a digital acquisition board (NI USB-6009, National Instruments). The sampling frequency was 10 Hz.

The subject, once barefoot, laid down on a table with both legs completely straight and relaxed. The compression device was fixed at one extremity of the same table. The foot was positioned in such a way that the anterior part touched the vertical plate, with the heel pad in front of the indenter. The placement of the foot was such that the longitudinal axis of the foot was coincident with the vertical axis of the piston, as shown in Fig. 2(c). Once the foot was well positioned, it was fixed with six Velcro fasteners (two to strap down the anterior part of the foot, one to keep the heel in front of the piston, one to stabilize the ankle and other two to stabilize the lower part of leg), as shown in Fig. 2(a) and (b). The subject was asked to maintain the foot in the same position for the duration of the test and remain as relaxed as possible in order to not influence the measurements with voluntary muscular tension.

A program made with LabView (version 2009, National Instruments) was used to control the entire set of measurements (on/off of system, start/stop of stepper motor, direction of rotation of the stepper motor). Two strain rates were used: 0.80 and 1.96 mm/s. Before starting the compression test on the heel pad, an idling test was performed in order to verify system functionality. As soon as the subject was completely relaxed and ready, the examiner ran the LabView program controlling each step of the measurement procedure. The compression test was repeated five times with one-minute break between each trial. The upper limit of the displacement was fixed at 9 mm, to avoid arriving at the end of the thread of the shaft that guides the piston, while the maximum value of the load was set to 40 N. The entire approach was designed for subsequent applications to clinical evaluation of injured heel pads.

2.4. Constitutive formulation of the model

A linear elastic model was adopted to describe the mechanical properties of the bone [27], while the muscles and plantar fascia were described using a hyperelastic formulation [28]. Detailed information on the constitutive formulations adopted for the calcaneal fat pad and skin tissues are reported in Appendix A. A specific visco-hyperelastic constitutive model accounting for the typical stress–strain behavior of the fat pad tissues was formulated. The constitutive model describes the material and geometric non-linearity typical for soft tissues, as well as the almost

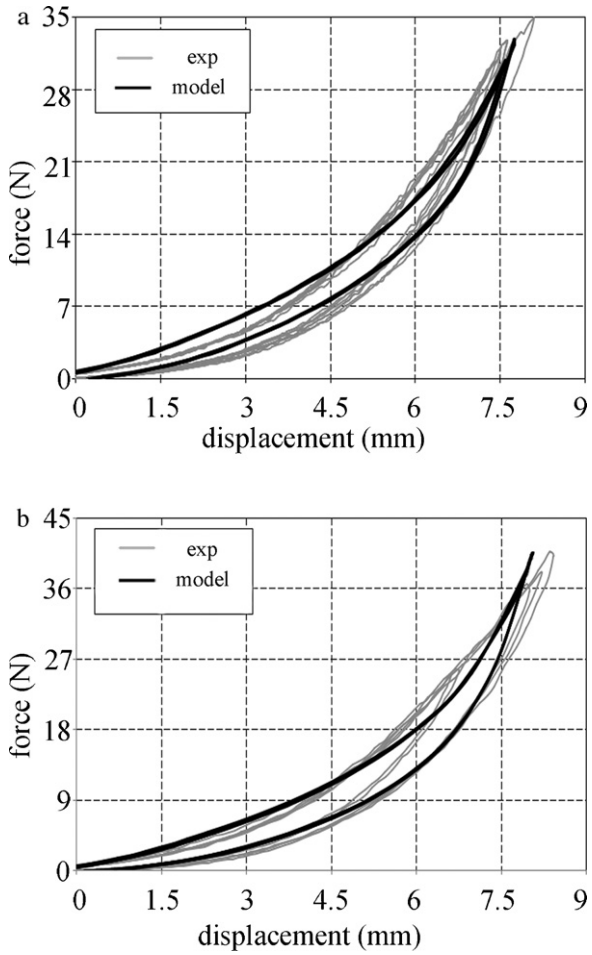

Fig. 3. Compression tests with a 1-min break between each cycle. Comparison of experimental (grey lines) and model (black lines) hysteresis for five cycles of loading and unloading compression tests with cylindrical piston: (a) 0.80 mm/s strain rate tests and (b) 1.96 mm/s strain rate tests.

incompressible behavior and time dependent response of the fat pad tissues [10,11]. The formulation is based on the definition of the Helmholtz free energy, ψ, as a function of strain and evaluated by the Right Cauchy–Green tensor $\mathbf{C}$ and viscous variables $\mathbf{q}^i$:

$$\psi(\mathbf{C}, \mathbf{q}^i) = W^0(\mathbf{C}) - \sum_{i-1}^{n} \int_0^t \frac{1}{2}\mathbf{q}^i(s) : \dot{\mathbf{C}} ds \quad (1)$$

where W^0 is the hyperelastic potential associated with the instantaneous response of the material and the second term specifies the viscous contribution. Viscous variables were associated with the assumed set of n viscous processes that developed within the material under loading and represented the structural rearrangement phenomena, such as movement of liquid components in the

Table 2
Viscous constitutive parameters adopted for fat pad tissues mechanical characterization.

γ_1	τ_1 (s)	γ_2	τ_2 (s)	γ_3	τ_3 (s)	γ_4	τ_4 (s)
7.17×10^{-1}	6.23×10^{-4}	1.55×10^{-1}	1.55×10^{-2}	6.52×10^{-2}	9.88×10^{4}	6.26×10^{-2}	9.82×10^{5}

Table 3
Hyperelastic constitutive parameters adopted for skin mechanical characterization.

K_ν (MPa)	r	C_1 (MPa)	α_1	C_4 (MPa)	α_4
3.9×10^{1}	1.40×10^{0}	9.55×10^{-1}	2.31×10^{0}	6.47×10^{0}	5.48×10^{0}

Please cite this article in press as: Fontanella CG, et al. Investigation on the load-displacement curves of a human healthy heel pad: *In vivo* compression data compared to numerical results. Med Eng Phys (2012), doi:10.1016/j.medengphy.2011.12.013

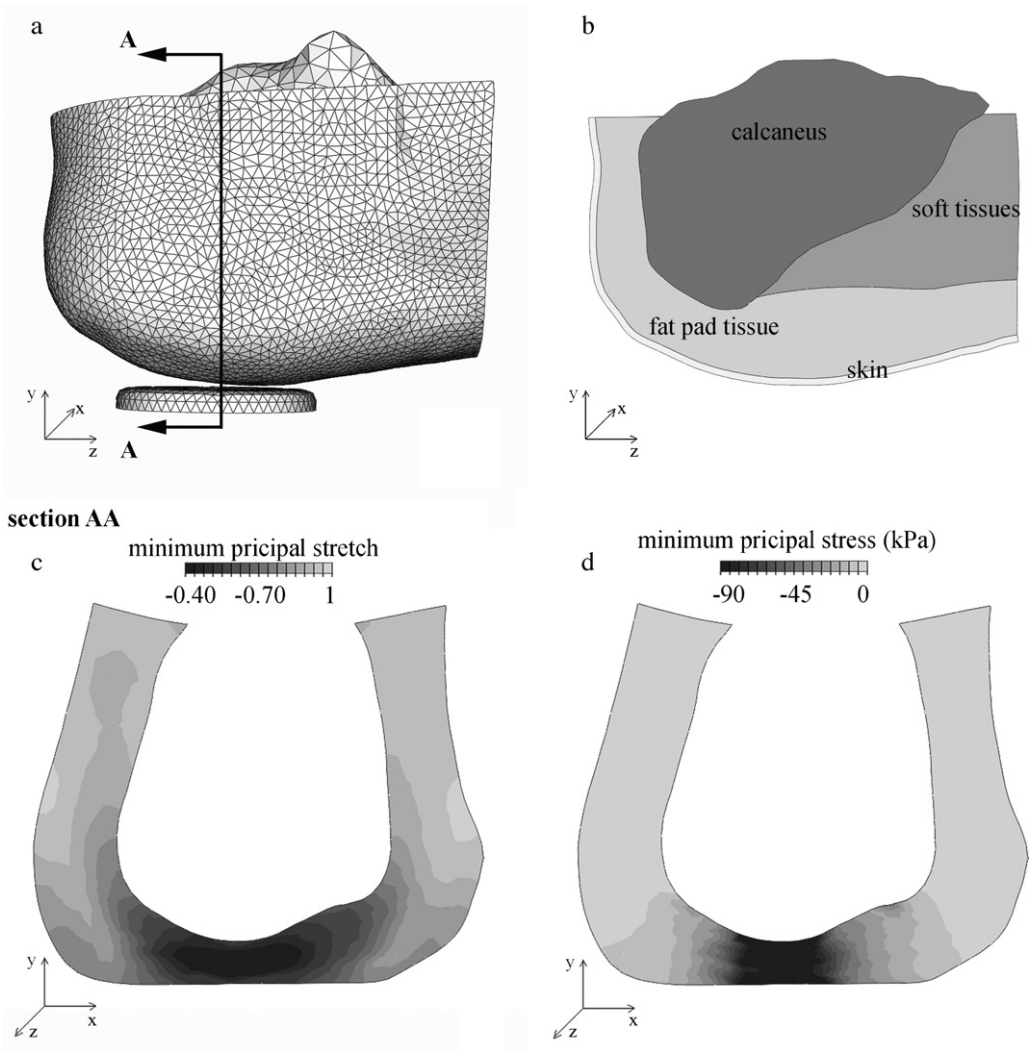

Fig. 4. (a) Numerical model of heel region with indication of sagittal section AA and (b) longitudinal section to show calcaneus, soft tissues, fat pad tissue and skin. Results from the numerical analysis of compression test on section AA after the first loading: contours of minimum principal stretch field at 1.96 mm/s strain rate (c) and of minimum principal stress fields at 1.96 mm/s strain rate (d).

adipose chambers and fiber rearrangement of connective septa. The constitutive parameters of the fat pad tissues were found by analyzing *in vitro* and *in vivo* tests developed by [5] and [29] such as described in Natali et al. [10,11].

The heel skin tissue mechanical response was characterized by a strong non-linearity, almost incompressible behavior and anisotropic characteristics induced by the organization of the collagen fibers. A fiber-reinforced hyperelastic model was considered to describe the heel skin tissue [12]. The following general formulation of strain energy was assumed:

$$W(\mathbf{C}, I_4) = W_m(\mathbf{C}) + W_f(I_4) \quad (2)$$

where W_m refers to the isotropic ground matrix contribution, W_f refers to the fibers and I_4 is a structural invariant that represents the stretch of the fibers during loading. The procedure adopted for the evaluation of the constitutive parameters followed the procedure already provided for soft tissue characterization and reported in detail in [10–12].

The set of constitutive parameters used for the calcaneal fat pad are reported in Tables 1 and 2 for hyperelastic and viscous parameters, respectively. Table 3 shows the hyperelastic constitutive parameters for describing the mechanical behavior of heel skin.

The finite element analyses were developed in order to interpret the experimental tests previously described. A numerical model of the piston (40 mm in diameter) was positioned under the heel skin in the same position of the experimental tests. The superior surface of the calcaneus was fully fixed and the piston was moved upward to the plantar skin in order to mimic the configuration of the experimental tests. The contact between heel skin and indenter was modeled with a friction coefficient of 0.42 [30,31]. Five loading–unloading cycles with one-minute break between each were computed, in order to match the conditions of the experimental tests.

3. Results

Fig. 3 shows the experimental load–displacement curves compared with the curves obtained from the finite element analyses. Specifically, hysteresis curves obtained by applying five loading–unloading cycles on the heel pad with a velocity of 0.80 mm/s (Fig. 3(a), grey lines) and 1.96 mm/s (Fig. 3(b), grey lines), were compared to those of the computational model (Fig. 3(a) and (b), black lines). The discrepancy between the experimental data and model results is reported as the mean absolute percentage error in terms of loads. The value of the discrepancy at 0.80 mm/s

Please cite this article in press as: Fontanella CG, et al. Investigation on the load-displacement curves of a human healthy heel pad: *In vivo* compression data compared to numerical results. Med Eng Phys (2012), doi:10.1016/j.medengphy.2011.12.013

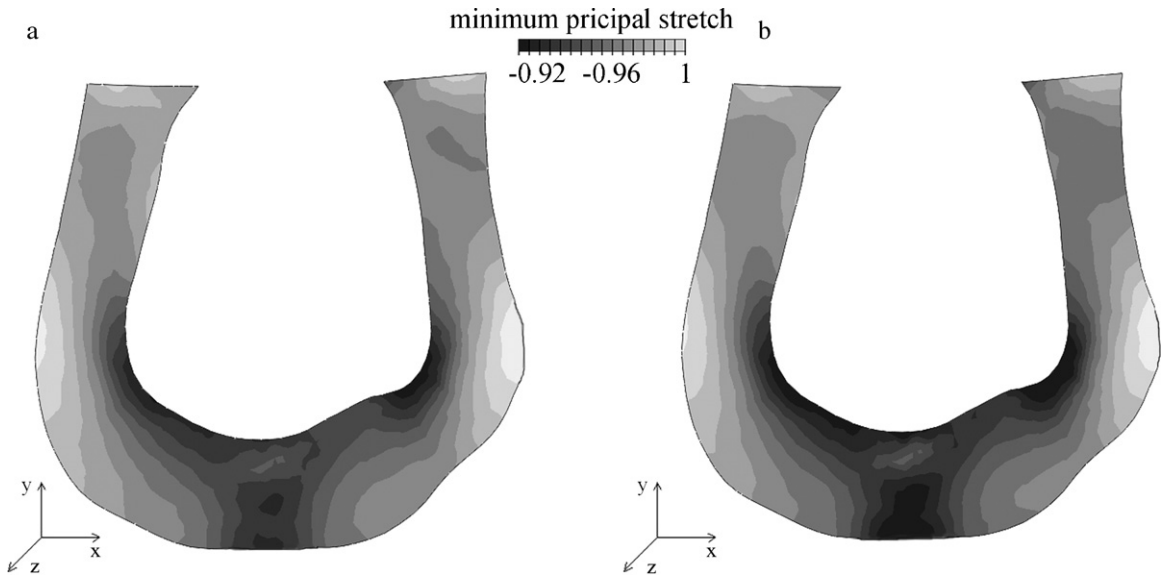

Fig. 5. Results from the numerical analysis of compression test at (a) 0.80 mm/s and (b) 1.96 mm/s strain rate. Contours of minimum principal stretch in the deformed configuration of heel pad structure after the first cycle of loading–unloading. Contours are reported over a sagittal section AA of heel pad structure.

was 0.39%, while at 1.96 mm/s was 0.28%. The energy dissipation ratio (EDR) is defined as the ratio between the area of the hysteretic cycle and the area under the loading curve. For the experimental tests, the EDR for the loading rate of 0.80 mm/s and 1.96 mm/s were 0.25 ± 0.02 and 0.26 ± 0.03, respectively. For the finite element analyses, the EDR for the loading rate of 0.80 mm/s and 1.96 mm/s were 0.23 ± 0.01 and 0.25 ± 0.01, respectively. The values were calculated considering the mean of the EDR for each of the five trials.

Fig. 4(a) and (b) shows the numerical models of heel region and piston. This figure illustrates the details of the proposed numerical model and the initial position of the piston, matching the experimental condition. Deformed configurations of the heel region after compression are reported with regard to minimum principal stretch (Fig. 4(c)) and stress fields (Fig. 4(d)) for the strain rates of 1.96 mm/s. All contours are reported over a transverse section of the fat pad, reported in Fig. 4(a), and pertain to the configuration achieved when a compression of 8.2 mm is imposed.

Fig. 5 shows the deformed configuration of fat pad after the first loading–unloading cycle. The minimum principal stretch fields for the analysis with a velocity of 0.80 mm/s (Fig. 5(a)) and 1.96 mm/s (Fig. 5(b)) are compared. These figures allow evaluation of residual deformation after the loading condition.

4. Discussion and conclusions

The present study describes the development of a subject-specific computational model of the heel pad. The procedure adopted for the definition of constitutive formulation and the evaluation of the constitutive parameters followed the procedure adopted in previous works [10–12]. The anisotropic characteristics of skin tissues induced by collagen fibers were considered with a fiber-reinforced constitutive model. The visco-hyperelastic model was used for representing calcaneal fat pad tissues with regard to the material and geometric non-linearity, the almost incompressible behavior and time dependent response. These formulations make the model capable of interpreting the typical hysteretic curve of the heel pad under loading/unloading condition. Experimental compression tests and computational simulations follow the same trend, highlighting the reliability of the computational model developed.

Some observations must be made with regard to the experimental procedure. The developed compression device uses low force at a low speed compared with the condition of walking. This limitation is due to the fact that this device is designed for use in a clinical setting involving diseased heel pads which cannot necessarily tolerate high loads.

The experimental load–displacement curves exhibited the hysteresis behavior, typical for a visco-elastic tissue. The five curves recorded were not completely overlapping which might be due to different reasons: the tissue fixing the heel pad (skin, calcaneus, connective tissue, *etc.*) cannot be completely fixed relative to the measurement device, thus both rotation and translation of the heel pad tissue can occur. Moreover, muscles in the leg might not be completely relaxed during all measurements. An unconscious pressure against *exempli gratia* the approaching piston cannot be completely ruled out. The two points above could theoretically be further reduced by *exempli gratia* a vacuum cushion, but the effect on the tissue by a more tight support is unknown. On a more speculative basis, it is not known if the individual components of the heel pad tissue returns to exactly the same position after every trial and neither are the influence of possible variations in liquid content known (*e.g.* blood perfusion). On the contrary, the finite element analysis is not influenced by these external conditions and the five curves overlap. Some small differences between the five numerical/experimental curves must be associated to the not complete recovery of the stretches.

The numerical model developed in this study can be used for evaluating loading conditions which are not possible with experimental tests. For example, a small recovery time between each trial or different displacements and forces imposed, allowing for a more detailed evaluation of the mechanical behavior of heel pad tissues under loading. Moreover, the numerical results allow for the investigation of the mechanical response of the calcaneal fat pad after a cycle of loading/unloading. The results show a distribution of residual stretches and stresses, pointing out the visco-elastic response. Further developments are underway in order to evaluate the stress relaxation and the creep phenomena of the heel pad.

Please cite this article in press as: Fontanella CG, et al. Investigation on the load-displacement curves of a human healthy heel pad: *In vivo* compression data compared to numerical results. Med Eng Phys (2012), doi:10.1016/j.medengphy.2011.12.013

This study represents a preliminary analysis applied to a healthy subject, which can be extended to patients with a pathology and, in the present form, can be interpreted as validation of the overall procedure. This analysis may be useful for patients, firstly evaluating the mechanical properties of the heel pad tissues using experimental tests and successfully implementing a numerical model capable of interpreting the mechanical response of the tissues by means of a damage model accounting for degenerative processes.

Acknowledgment

The authors would like to thank Associate Prof. Lars G. Hanson for the help with the MR measurements.

Appendix A

With regard to the visco-hyperelastic formulation adopted for calcaneal fat pad tissue, the stress–strain relationship was defined to be consistent from a thermo-mechanical point of view, as:

$$\mathbf{S}(\mathbf{C}, \mathbf{q}^i) = \frac{2\partial\psi(\mathbf{C}, \mathbf{q}^i)}{\partial\mathbf{C}} = \mathbf{S}^0(\mathbf{C}) - \sum_{i-1}^{n}\mathbf{q}^i \tag{A.1}$$

where $\mathbf{S}$ was the second Piola–Kirchhoff stress tensor, while $\mathbf{S}^0 = 2\partial\mathbf{W}^0/\partial\mathbf{C}$ was the instantaneous stress. Viscous variables $\mathbf{q}^i$ specified relaxed stresses because of the development of structural rearrangement phenomena over time. The evolution of viscous variables $\mathbf{q}^i$ was defined as by integral formulations:

$$\mathbf{q}^i(t) = \frac{\gamma^i}{\tau^i}\int_0^t \exp\left(-\frac{t-s}{\tau^i}\right)\mathbf{S}^0(s)ds \tag{A.2}$$

where τ^i were relaxation times, as measures of time for the viscous processes development, γ^i were relative stiffnesses defining the stiffness contribution of viscous processes, related to the equilibrium relative stiffness, as $\gamma^\infty = 1 - \sum_{i-1}^{n}\gamma^i$.

Assuming the almost incompressible behavior, the hyperelastic potential W^0 can be split into volumetric U^0 and iso-volumetric $\tilde{W}^0$ terms:

$$U^0(I_3) = \frac{K_v}{2 + r(r+1)}[(I_3^{1/2} - 1)^2 + I_3^{-r/2} + rI_3^{1/2} - (r+1)] \tag{A.3}$$

$$\tilde{W}^0(\tilde{I}_1) = \frac{C_1}{\alpha_1}\{\exp[\alpha_1(\tilde{I}_1 - 3)] - 1\} \tag{A.4}$$

where $\tilde{I}_1$ was the first iso-volumetric invariant of the right Cauchy–Green strain tensor, as $\tilde{I}_1 = \mathrm{tr}(I_3^{-1/3}\mathbf{C})$, and I_3 was the third invariant, as $I_3 = \det(\mathbf{C})$. The constitutive parameters K_v and C_1 were related with the equilibrium initial volumetric and shear stiffness, respectively, as volumetric and shear response when both strain rate and strain approach zero. The parameters r and α_1 characterize the evolution of material stiffness with strain due to the non-linearity of the mechanical response.

Additional notes are reported with regard to the constitutive formulation adopted for the skin. The formulation of strain energy was determined by a contribution from ground matrix W_m and a contribution from fibers W_f. The hyperelastic contribution W_m was defined according to previously reported hyperelastic formulations (Eqs. (A.3) and (A.4)). The definition of fibers contribution had to account for strong non-linearity because of fibers uncrimping phenomena. A specific exponential formulation was provided:

$$W_f(I_4) = \frac{C_4}{(\alpha_4)^2}\{\exp[\alpha_4(I_4 - 1)] - \alpha_4(I_4 - 1) - 1\} \tag{A.5}$$

where C_4 was a constant that defines the fibers initial stiffness, as $E_f = 4C_4$, while α_4 depended on the initial wavy conformation of fibers.

Conflict of interest

All the authors (C.G. Fontanella, S. Matteoli, E.L. Carniel, J.E. Wilhjelm, A. Virga, A. Corvi, A.N. Natali) have no proprietary, financial, professional or other personal interest of any nature or kind in any product, service and/or company that could be construed as influencing the position presented in, or the review of, the present manuscript entitled "Investigation on the load–displacement curves of a human healthy heel pad: *in vivo* compression tests and numerical analysis".

References

[1] Tietze A. Concerning the architectural structure of the connective tissue of the human sole. Foot Ankle 1982:252–9.
[2] Jahss MH, Michelson JD, Kummer F. Investigations into the fat pads of the sole of the foot: heel pressure studies. Foot Ankle Int 1992;13:233–42.
[3] Aert P, Ker RF, De CD, Ilsley DW, Alexander RM. The mechanical properties of the human heel pad: a paradox resolved. J Biomech 1995;28(11): 1299–308.
[4] Ahmadian MT. Modeling and prediction of soft tissue directional stiffness using in vitro force displacement data. Int J Sci Res 2005;15:1–4.
[5] Miller-Young JE, Duncan NA, Baroud G. Material properties of the human calcaneal fat pad in compression: experiment and theory. J Biomech 2002;35:1523–31.
[6] Ledoux W, Blevins J. The compressive material properties of the plantar soft tissue. J Biomech 2007;40:2975–81.
[7] Ker R. The time-dependent mechanical properties of the human heel pad in the context of locomotion. J Exp Biol 1996;199:1501–8.
[8] Wearing SC, Smeathers JE, Yates B, Urry SR, Dubois P. Bulk compressive properties of the heel fat pad during walking: a pilot investigation in plantar heel pain. Clin Biomech 2009;24(4). pp. 397-102.
[9] Wearing SC, Smeathers JE, Urry SR, Sullivan PM, Yates B, Dubois P. Thickening of the enthesis is correlated with energy dissipation of the plantar fat pad during walking. Am J Sports Med 2010;38:2522–7.
[10] Natali AN, Fontanella CG, Carniel EL. Constitutive formulation and analysis of heel pad tissues mechanics. Med Eng Phys 2010;32:516–22.
[11] Natali AN, Fontanella CG, Carniel EL, Miller-Young J. Biomechanical behaviour of heel pad tissue. Experimental testing, constitutive formulation, and numerical modelling. Proc IME H: J Eng Med 2011;225:449–59.
[12] Natali AN, Fontanella CG, Carniel EL. Constitutive formulation and numerical analysis of the heel pad region. Comput Methods Biomech Biomed Eng, in press.
[13] Hsu TC, Wang CL, Tsai WC, Kuo JK, Tang FT. Comparison of the mechanical properties of the heel pad between young and elderly adults. Arch Phys Med Rehabil 1998;79(8):1101–4.
[14] Jørgensen U, Larsen E, Varmarken JE. The HPC-device: a method to quantify the heel pad shock absorbency. Foot Ankle 1989;10(2):93–8.
[15] Challis JH, Murdoch C, Winter SL. Mechanical properties of the human heel pad: a comparison between populations. J Appl Biomech 2008;24(4): 377–81.
[16] Tsai WC, Wang CL, Hsu TC, Hsieh FJ, Tang FT. The mechanical properties of the heel pad in unilateral plantar heel pain syndrome. Foot Ankle Int 1999;20(10):663–8.
[17] Erdemir A, Viveiros ML, Ulbrecht JS, Cavanagh PR. An inverse finite-element model of heel-pad indentation. J Biomech 2006;39(7):1279–86.
[18] Tong J, Lim CS, Goh OL. Technique to study the biomechanical properties of the human calcaneal heel pad. The Foot 2003;13:83–91.
[19] Robbins SE, Gouw GJ, Hanna AM. Running-related injury prevention through innate impact-moderating behavior. Med Sci Sports Exerc 1989;21(2):130–9.
[20] Zheng YP, Choi YKC, Wong K, Chan S, Mak AFT. Biomechanical assessment of plantar foot tissue in diabetic patients using an ultrasound indentation system. Ultrasound Med Biol 2000;26(3):451–6.
[21] Klaesner JW, Hastings MK, Zou DQ, Lewis C, Mueller MJ. Plantar tissue stiffness in patients with diabetes mellitus and peripheral neuropathy. Arch Phys Med Rehabil 2002;83(12):1796–2180.
[22] Sopher R, Nixon J, McGinnis E, Gefen A. The influence of foot posture, support stiffness, heel pad loading and tissue mechanical properties on biomechanical factors associated with a risk of heel ulceration. J Mech Behav Biomed 2011;4(4):572–82.
[23] Gu Y, Li J, Ren X, Lake MJ, Zeng Y. Heel skin stiffness effect on the hind foot biomechanics during heel strike. Skin Res Tech 2010;16(3):291–6.
[24] Goske S, Erdermir A, Petre M, Budhabhatti S, Cavanagh PR. Reduction of plantar heel pressures: insole design using finite element analysis. J Biomech 2006;39:2363–70.
[25] Cheung JTM, Zhang M. Parametric design of pressure-relieving foot orthosis using statics-based finite element method. Med Eng Phys 2008;30:269–77.
[26] Even-Tzur N, Weisz E, Hirsch-Falk Y, Gefen A. Role of EVA viscoelastic properties in the protective performance of a sport shoe: computational studies. Bio-Med Mater Eng 2006;16:289–99.
[27] Natali AN, Carniel EL, Pavan PG. Modelling of mandible bone properties in the numerical analysis of oral implant biomechanics. Comput Methods Biomech Biomed Eng 2010;100(2):158–65.

Please cite this article in press as: Fontanella CG, et al. Investigation on the load-displacement curves of a human healthy heel pad: *In vivo* compression data compared to numerical results. Med Eng Phys (2012), doi:10.1016/j.medengphy.2011.12.013

[28] Goske S, Erdermir A, Petre M, Budhabhatti S, Cavanagh PR. Reduction of plantar heel pressure: insole design using finite element analysis. J Biomech 2006;39:2363–70.
[29] Miller-Young JE. Factors affecting human heel pad mechanics: a finite element study. Doctoral Dissertation. Department of Mechanical Engineering, University of Calgary, Canada; 2003.
[30] Zhang M, Mak FT. In vivo friction properties of human skin. Prosthet Orthot Int 1999;23:135–41.
[31] Elkhyat A, Courderot-Masuyer C, Gharbi T, Humbert P. Influence of the hydrophobic and hydrophilic characteristics of sliding and slider surfaces on friction coefficient: in vivo human skin friction comparison. Skin Res Tech 2004;10:215–21.

Please cite this article in press as: Fontanella CG, et al. Investigation on the load-displacement curves of a human healthy heel pad: *In vivo* compression data compared to numerical results. Med Eng Phys (2012), doi:10.1016/j.medengphy.2011.12.013

VIII PAPER

Title: Investigation on the visco-elastic behavior of a human healthy heel pad: *in vivo* compression data compared to numerical results.
Authors: Sara Matteoli, Chiara G. Fontanella, Emanuele L. Carniel, Jens E. Wilhjelm, Antonio Virga, Nadège Corbin, Andrea Corvi, Arturo N. Natali
Journal: Computer Methods in Biomechanics and Biomedical Engineering
Submission: Submitted on January.., 2012.

Investigation on the visco-elastic behaviour of a human healthy heel pad: in vivo compression tests and numerical analysis

S. Matteoli[1]*, C.G. Fontanella[2], E.L. Carniel[2], J.E. Wilhjelm[1], A. Virga[3], N. Corbin[1], A. Corvi[3], A.N. Natali[2]

1 Department of Electrical Engineering, Technical University of Denmark, Ørsteds Plads, DK-2800, Kgs. Lyngby, DK

2 Centre of Mechanics of Biological Materials, University of Padova, Via F. Marzolo 9, 35131 Padova, IT

3 Department of Mechanics and Industrial Technologies, University of Florence, via S. Marta 3, 50139 Florence, IT

* Corresponding author

Sara Matteoli

Department of Electrical Engineering, Technical University of Denmark,

Ørsteds Plads, Building 349

DK-2800, Kgs. Lyngby, DK

Tel. +45 4525 3705 – Fax +45 4588 0117

E-mail: sma@elektro.dtu.dk

Investigation on the visco-elastic behaviour of a human healthy heel pad: in vivo compression tests and numerical analysis

The aim of the present work was to investigate the visco-elasticity of the human heel pad by comparing the stress-relaxation curves obtained from a compression device used on an *in vivo* heel pad with those obtained from a computer based 3D subject-specific heel pad model subjected to external compressions. Specifically, the 3D heel pad model was based on the anatomy revealed by MR imaging of a 31-year-old European healthy female (mass=54 kg, height=165 cm). The calcaneal fat pad tissue was described with a visco-hyperelastic model, while a fibre-reinforced hyperelastic model was formulated for the skin. All numerical analyses were performed to interpret the mechanical response of heel tissues, with both loading conditions and strain rate in agreement with experimental tests. The heel tissues showed a non linear visco-elastic behaviour exhibiting a characteristic hysteresis curve, and stress relaxation phenomena. Results allowed evaluating viscous recovery phenomena, which can be useful for understanding the mechanical response during daily activities.

The validity and efficacy of the investigations performed was confirmed by the interpretation of the mechanical response of the heel tissues under the application of different pistons at the same strain rate, with mean absolute percentage error between experimental data and model results of 0.74% by using the biggest piston, and of 0.50% by using the smallest.

Keywords: stress relaxation, hysteresis, numerical model

Introduction

The heel pad is the most distal part of the human locomotion system. The main function of the heel pad is to sustain strain and pressure during walking and standing. Biomechanically the heel pad acts as an efficient shock absorber to attenuate the peak of dynamic forces and to dampen the vibrations during the gait (Hsu et al. 1998). This cushioning effect is achieved by its highly specialized and unique anatomic configuration, made of neuronal, vascular, fibrous and elastic components which are intertwined with fat cells (Jahss et al. 1992).

The heel pad exhibits non-linear visco-elastic behaviour, like most of the soft biological tissues do. Due to the visco-elastic nature of the heel pad and its capability to deform under loading, when a loading/unloading cycle is applied, a load-deformation curve is obtained (Ker 1996) showing a characteristic hysteresis (Miller-Young et al. 2002; Ledoux and Blevins 2007). The compressibility of the heel pad depends on how the load is applied, *i.e.* depends on the strain rate and time (Spears et al. 2005). Such non-linear, visco-elastic behaviour is described by the stress relaxation characteristic showing the decrease in load when a constant deformation is applied (Humphrey 2004; Ledoux et al. 2004; Pai and Ledoux 2011)

The biomechanical behaviour of the heel pad when subjected to an external compression can be evaluated by direct (*e.g.* experimental tests on *in vivo*/*in vitro* heel pads) and indirect (*e.g.* numerical simulations on models) methods.

A common experimental way to determine the mechanical properties of heel pad is to use a compression device (Hsu et al. 1998; Jørgensen et al. 1989; Challis et al. 2008; Tsai et al. 1999; Erdemir et al. 2006; Tong et al. 2003; Robbins et al. 1989, Zheng et al. 2000, Klaesner et al. 2002).

The analysis of experimental data allows for quantitative and qualitative investigation of the mechanical response of the tissue. This information can be used for

clinical and diagnostic purposes (*e.g.* diabetic subjects, heel pain subjects, etc.) and for prevention of pathologies.

The experimental tests are often integrated with numerical models that lead to a more complete and accurate information in terms of deformational and stress data. A numerical modelling approach based on the finite element method is a robust tool to deepen our knowledge of heel pad biomechanics for the integration and reciprocal validation of the experimental data. In this way, finite element analyses allow for evaluating the local interaction phenomena between the heel pad and orthotics/footwear design (*e.g.* distribution of the plantar pressure (Challis et al. 2008; Goske et al. 2006; Cheung and Zhang 2008; Even-Tzur et al. 2006)) and, more in detail, the mechanical behaviour of these tissues also in consideration of pathological and diseased conditions (*e.g.* plantar fasciitis and diabetic ulceration (Sopher et al. 2011; Gu et al. 2010)).

The aim of the present study was to compare the stress relaxation curves obtained by using a compression device on an *in vivo* healthy heel pad with those obtained from a numerical model representing the heel pad structure when subjected to an external compression. The numerical heel pad model - composed of fat pad and skin, and built on the basis of MRI data - demonstrated its accuracy and reliability in a previous study (Fontanella et al. 2012). The compression device used here, and described in details in (Fontanella et al. 2012) did not intend to reproduce the physiological conditions of walking or running. It was built in order to be a possible clinical device able to characterize the biomechanics of injured heel pads in future investigations.

Material and Methods

Subject characteristics

A 31-year-old European healthy female (mass=54 kg, height=165 cm) was enrolled in this study. Her left foot underwent both MRI scan and compression tests. She declared to have an active lifestyle, and to have never had injuries/trauma to any of the feet. She was informed that the test did not involve any harmful procedures or physical pain.

Compression device and test procedure

A detailed description of the compression device (Figure 1, (a)) and test procedure used for experimental tests can be found in (Fontanella et al. 2012). In the present study the loading/unloading cycle was applied on the heel pad by using three different pistons with diameter of 15, 20 and 40 mm (Figure 1, (b)). For each piston, the compression test was repeated seven times by using a strain rate of around 1.73 mm/s. with 1-minute-break between each trial and In order to investigate the stress relaxation characteristic of the heel pad the compression test was repeated with all pistons adding a pause of 40 s once the displacement reached its maximum limit. During this pause the piston remained in contact with the heel pad, so that it was possible to see the decrease in load with time at a constant deformation. Then, after 40 s the decompression started.

The relative low strain rate applied and the fixation of the foot with six straps are requirements that make the compression device be a possible future clinical application on injured heel pads.

In order to compensate for possible movements of the foot, a video was recorded during each trial. Specifically, a fiducial marker was attached on the skin of the ankle, as shown in Figure 2, and each video allowed following the movement of such marker during the compression/decompression of the heel pad. A program made with

MATLAB (MathWorks, R2007) based on 2D cross-correlation, was used to calculate the maximum horizontal and vertical movements of the marker. In the present study, the vertical movement appeared to be negligible, so only the horizontal was used for the correction procedure. Further, a program made with LabView (National Instrument, 2009) allowed correcting the hysteresis by taking into account the movement of the ankle. The procedure for such correction was defined after observing that the ankle movement occurred only during the stroke of the piston (either during loading and unloading), while was negligible during the pause. The maximum horizontal displacement calculated with MATLAB, was assumed to be coincident with the maximum displacement of the piston. Such assumption allowed synchronizing the time of the video-camera and compression device, as the two devices were not driven by the same control box. From the video processing, a 3rd degree polynomial correlation for the movement as a function of time was obtained, both for loading and unloading phase. The coefficients of such polynomials were used to correct the hysteresis. Specifically, the correction of the loading curve was done by using, as best estimate, the load-displacement characteristic recorded during unloading, since such movement implied a decrease in load. The same procedure was applied to correct movements during unloading by using the load-displacement characteristic recorded during loading. No correction was necessary during the pause of 40 s, due to the negligible movement of the foot revealed by the recorded videos.

MRI and 3D subject-specific heel pad model

A 3D model of the subject's left heel was built on the basis of the MRI data [3T Siemens Magnetom Trio, Fat-suppressed 3D dual echo steady state (DESS) sequence with 0.7 mm^3 isotropic resolutions, size matrix 320x576x104. TE/TR=5.5/13 ms, flip angle 25°, TA=5 min]. The DICOM images were processed by using Simpleware,

imaging density segmentation software and the 3D CAD solid model was created as described in (Fontanella et al. 2012). The numerical model of the heel region was composed of calcaneus, muscles and plantar fascia, fat pad and skin.

Constitutive formulation and numerical analysis

Detailed information about the constitutive analysis of different tissues can be found in (Fontanella et al. 2012). A linear elastic model was adopted to describe the mechanical properties of the bone (Natali et al. 2010), while the muscles and plantar fascia were described using a hyperelastic formulation (Goske et al. 2006). Specific constitutive models were adopted for calcaneal fat pad and skin. Taking into account the typical features of fat pad tissue mechanical response, such as the material and geometric non-linearity, as well as the almost incompressible behaviour and time dependent response (Natali et al. 2010, 2011), a specific visco-hyperelastic constitutive model was developed. According to both experimental and histological evidence, a fibre-reinforced hyperelastic model was adopted to interpret the mechanical behaviour of heel skin tissues, which accounts for different contributions from isotropic ground matrix and fibres. A transversally isotropic configuration was assumed. The constitutive parameters of the fat pad tissues and skin were found by analyzing *in vitro* and *in vivo* tests developed by (Miller-Young et al. 2002) and (Miller-Young 2003) such as described in (Natali et al. 2010, 2011; Fontanella et al. 2012).

Preliminarily, numerical analyses were developed in order to investigate stress relaxation phenomena within the heel tissues, according to the performed experimental conditions. Three numerical models of the pistons (40, 20 and 15 mm in diameter) were developed and positioned under the heel skin as done during each experimental test. The superior surface of the calcaneus was fully fixed and the piston was moved upward to the plantar skin. The contact between the heel skin and piston was modelled by a

standard Coulomb formulation, according to a friction coefficient of 0.42 (Zhang and Mak 1999; Elkhyat et al. 2004). In order to match the experimental conditions, all numerical analyses were computed considering a strain rate of 1.73 mm/s. Once the piston reached the displacement of 9 mm, it remained in contact with the heel pad for 40 s, and then the decompression started.

Further numerical analyses were computed to measure the viscous recovery phenomena of the heel pad after a simple loading-unloading cycle. The numerical analyses were developed considering the three pistons (40, 20 and 15 mm in diameter). After the loading-unloading cycle, strain recovery phenomena were investigated for one minute.

Results

Figure 3 shows the load-displacement curves obtained from the experimental tests with (in black) and without correction (in grey).

Figures 4, 5, and 6 show the results obtained from experimental tests and numerical analyses. Specifically, the experimental load-displacement (Figure 4(a), 5(a) and 6(a)) and load-time curves (Figure 4(b), 5(b) and 6(b)), obtained by applying five loading-stress relaxation-unloading cycles on the heel pad with a velocity of 1.73 mm/s (grey lines) are compared with the curves obtained from the numerical analyses (black lines).

Figure 7(a) shows the numerical models of heel region and piston, illustrating the details of the proposed numerical model and the initial position of the piston (the same for all diameters). Deformed configurations of the heel region when interacting with the piston of 40 mm diameter are reported with regard to minimum principal stress (Figure 7(b)) after compression and after the relaxation period (Figure 7(c)). All contours are reported over a transverse section of the fat pad, as reported in Figure 7(a).

Figure 8 shows the experimental load-displacement curves compared with those obtained from the numerical analyses. Specifically, experimental curves obtained by applying five loading-unloading cycles on the heel pad with a velocity of 1.73 mm/s by using pistons with diameter of 40 mm (Figure 8(a), grey lines), 20 mm (Figure 8(b), grey lines) and 15 mm (Figure 8(c), grey lines), were compared to those obtained by computational analyses (Figure 8(a), 8(b) and 8(c), black lines). The discrepancy between experimental data and computational results is reported as the mean absolute percentage error in terms of loads. The value of the discrepancy by using piston with diameter of 40 mm, 20 mm and 15 mm was 0.72%, 0.50% and 0.74%, respectively. In order to evaluate the hysteretic response, the energy dissipation ratio (EDR) - defined as the ratio between the area of the hysteretic cycle and the area under the loading curve (Bennett and Ker 1990) - was calculated for both the experimental and numerical method. Tables 1 and 2 show the EDR values, expressed as the average of the five trials plus/minus one standard deviation, calculated for all pistons from the load-displacement curves and stress relaxation characteristics, respectively.

Figure 9 shows the deformed configurations of the heel region when the piston of 40mm in diameter is used. These contours illustrate the viscous recovery phenomena with regard to the minimum principal stretch after a cycle of loading-unloading. The calcaneal fat pad tissues are able to recover the residual deformation in 60 s, with a sharp decrease of the stretch in the initial phase.

Discussion and Conclusions

The present study describes a comparison between experimental and numerical methods used for investigating the visco-elastic nature of the *in vivo* human heel pad. The experimental load-displacement curves exhibited the hysteretic behavior, typical for a visco-elastic tissue. Experimental compression tests and computational

simulations done on a subject-specific model follow the same trend, highlighting the reliability of the computational model developed, as shown in Figures 4, 5, and 6.

Some observations must be made with regard to the experimental procedure. The compression device produced strain rate and loads lower than those present in locomotion (the peak load is 2-3 times the bodyweight), but the 5 seconds of loading are far longer than the duration of the heel pad compression in the gait cycle (0.6 seconds). Furthermore, the foot was stabilized only by using six Velcro straps which did not guarantee the immobility of the foot. These features are requirements necessary to make the device usable in clinical setting involving diseased heel pads which cannot necessarily tolerate high loads nor fix the foot. In order to investigate the involuntary movements of the foot, videos were recorded during each compression test and a marker-video-procedure was applied to calculate the ankle movements. Such procedure allowed correcting both load-displacement curves and stress relaxation characteristics in order to have a more precise and realistic comparison with the curves obtained from the finite element analysis which are not influenced by these external conditions.

In literature, few experimental tests investigate on the stress relaxation response of heel pad tissues. Some notes are reported with regard to experimental tests developed on *in vitro* calcaneal fat pad specimen (Ledoux and Blevins 2007, Pai and Ledoux 2011; Miller-Young et al. 2002) in order to quantify the visco-elastic tissue properties. These results show the capability of the tissue to recover the stress quickly. However, these results are specific of the fat pad tissue and do not involve the whole structure of heel region. Furthermore, it is well known that there is a big variation among results obtained from *in vivo* and *in vitro* investigations (Miller-Young, 2003).

Numerical analyses allow quantification of viscous recovery after a specific loading condition. Indeed, in the present study the results show the capability of the heel

region to recover completely the residual deformation in one minute. This confirms that the one-minute-break applied between each trial of the experimental tests is a reasonable choice.

The Energy Dissipation Ratio (EDR) is a measure of the energy lost by viscous friction within the tissue (Wearing et al. 2010). The higher the EDR, the more energy is absorbed by the heel pad. Few studies (Jorgensen et al. 1989; Kinoshita et al. 1996; Hsu et al. 1998; Wang et al. 1998; Tsai et al. 1999; Hsu et al. 2002; Boros and Challis 2003; Challis et al. 2008; Wearing et al. 2009; Wearing et al. 2010) investigated on the EDR of the in vivo heel pad in both healthy and diseased conditions, but unfortunately the numerical results are not comparable due to the different number of subjects investigated and methods used. Within these studies percentage energy dissipation ranged between 23.7±6.9 (Hsu et al. 1998; Wang et al. 1998) and 84.6±6.2 (Alcantara et al. 2002). In the present study, percentage energy dissipation ranged between 22.5± 1.8 (diameter piston of 20 mm) and 27.1±2.1 (diameter piston of 40 mm) for load-displacement curves, while between 40.4± 4.2 (diameter piston of 20 mm) and 46.3 ±3.1 (diameter piston of 40 mm) for the stress relaxation characteristics. The percentage energy dissipations for the numerical simulations ranged between 21.6 ±1.0 (diameter piston of 15 mm) and 26.0 ±1.0 (diameter piston of 40 mm) for the load-displacement curves, while between 45.6 ±1.0 (diameter piston of 15 mm) and 61.0 ±1.0 (diameter piston of 20 mm) for the stress relaxation characteristics. Due to the complexity of the structure under investigation, it would not be accurate to correlate the dimension of the diameter with the EDR, even though the results obtained from the finite element analyses would suggest that the larger the diameter, the higher the EDR. The lack of correlation in case of in vivo investigations might be due to the inhomogeneous structure of the heel pad, made of neuronal, vascular, fibrous and elastic components

which are intertwined with fat cells (Jahss et al. 1992). Consequently, large piston may be used to analyse the mechanical properties of whole structure of heel pad and the results are determined predominantly by the least stiff material within the structure, i.e. calcaneal fat pad. On the contrary, small piston allows the identification of the mechanical properties of limited region and the affected tissues, i.e. calcaneal fat pad and skin. A study (Spears and Miller-Young 2006) reports similar considerations, saying that the large probe loading process may be likened to uniaxial bulk compression, while the small probe loading process may cause localized deformation of the superficial region of the heel and could be likened to indentation.

This study represents a preliminary analysis applied to a healthy subject, which might be extended to subjects with pathology and, in the present form, can be interpreted as validation of the overall procedure. This analysis may be useful for patients, firstly for evaluating the mechanical properties of the heel pad tissues using experimental tests and successfully implementing a numerical model capable of interpreting the mechanical response of the tissues by means of a damage model accounting for degenerative processes.

Acknowledgments

The authors would like to thank Prof. Lars G. Hanson for the help offered regarding the MR investigations.

Conflict of Interest Statement

All the authors (S. Matteoli, C.G. Fontanella, E.L. Carniel, J.E. Wilhjelm, A. Virga, N. Corbin, A. Corvi, A.N. Natali) have no proprietary, financial, professional or other

personal interest of any nature or kind in any product, service and/or company that could be construed as influencing the position presented in, or the review of, the present manuscript entitled ” Investigation on the visco-elastic behaviour of a human healthy heel pad: *in vivo* compression tests and numerical analysis”.

References

Alcantara E, Forner A, Ferrus E, Garcia AC, Ramiro J. 2002. Influence of age, gender, and obesity on the mechanical properties of the heel pad under walking impact conditions. J. Appl. Biomech.. 18(4):345-356.

Bennett MB, Ker RF. 1990. The mechanical properties of the human subcalcaneal fat padin compression. J. Anat. 171:131-138

Boros RL, Challis JH. 2003. Heel pad properties of males and females. Med Sci Sports Exerc. 35(5):360.

Challis JH, Murdoch C, Winter SL. 2008. Mechanical properties of the human heel pad: a comparison between populations. J. Appl. Biomech. 24(4):377-381.

Cheung JTM, Zhang M. 2008. Parametric design of pressure-relieving foot orthosis using statics-based finite element method. Med. Eng. Phys. 30:269-277.

Elkhyat A, Courderot-Masuyer C, Gharbi T, Humbert P. 2004. Influence of the hydrophobic and hydrophilic characteristics of sliding and slider surfaces on friction coefficient: in vivo human skin friction comparison. Skin Res. Tech. 10:215-221.

Erdemir A, Viveiros ML, Ulbrecht JS., Cavanagh PR. 2006. An inverse finite-element model of heel-pad indentation. J. Biomech. 39(7):1279-1286.

Even-Tzur N, Weisz E, Hirsch-Falk Y, Gefen A. 2006. Role of EVA viscoelastic properties in the protective performance of a sport shoe: Computational studies. Bio-Med. Mater. Eng. 16:289-299

Fontanella CG, Matteoli S, Carniel EL, Wilhjelm JE, Virga A, Corvi A, Natali AN. 2012. Investigation on the load-displacement curves of a human healthy heel pad: *In vivo* compression data compared to numerical results. Med Eng Phys, doi:10.1016/j.medengphy.2011.12.013

Goske S, Erdermir A, Petre M, Budhabhatti S, Cavanagh PR. 2006. Reduction of plantar heel pressures: Insole design using finite element analysis. J. Biomech. 39:2363-2370.

Gu Y, Li J, Ren X, Lake MJ, Zeng Y. 2010. Heel skin stiffness effect on the hind foot biomechanics during heel strike. Skin Res Tech. 16(3):291-296.

Hsu TC, Lee Y.S, Shau YW. 2002. Biomechanics of the heel pad for type 2 diabetic patients. Clin. Biomech. 17(4), 291-296.

Hsu TC, Wang CL, Tsai WC, Kuo JK, Tang FT. 1998. Comparison of the mechanical properties of the heel pad between young and elderly adults. Arch. Phys. Med. Rehab. 79(8): 1101-1104

Humphrey JD. 2004. An introduction to biomechanics: Solids and Fluids, Analysis and Design. New York: Springer-Verlag.

Jahss MH, Michelson JD, Kummer F. 1992. Investigations into the fat pads of the sole of the foot: heel pressure studies. Foot Ankle Int. 13:233-242.

Jørgensen U, Larsen E, Varmarken JE. 1989. The HPC-device: a method to quantify the heel pad shock absorbency, Foot Ankle. 10(2):93-98.

Ker R. 1996. The time-dependent mechanical properties of the human heel pad in the context of locomotion. J Exp Biol. 199:1501–8.

Kinoshita H, Francis PR, Murase T, Kawai S, Ogawa T. 1996. The mechanical properties of the heel pad in elderly adults. European Journal of applied physiology and occupational physiology. 73(5):404-409.

Klaesner JW, Hastings MK, Zou DQ, Lewis C, Mueller MJ. 2002. Plantar tissue stiffness in patients with diabetes mellitus and peripheral neuropathy. Arch. Phys. Med. Rehabil. 83(12):1796-180.

Ledoux W, Blevins J. 2007. The compressive material properties of the plantar soft tissue. J. Biomech. 40:2975-81

Ledoux WR, Meaney DF, Hillstrom HJ. 2004. A quasi-linear, viscoelastic, structural model of the plantar soft tissue with frequency-sensitive damping properties. J. of Biomechanical Engineering. 126: 831-837.

Miller-Young JE. 2003. Factors affecting human heel pad mechanics: a finite element study. Doctoral Dissertation, Department of Mechanical Engineering, University of Calgary, Canada

Miller-Young JE, Duncan NA, Baroud G. 2002. Material properties of the human calcaneal fat pad in compression: experiment and theory. J. Biomech. 35:1523-1531.

Natali AN, Carniel EL, Pavan PG. 2010. Modelling of mandible bone properties in the numerical analysis of oral implant biomechanics. Computer Methods Biomech Biomed Eng 100(2):158-165.

Natali AN, Fontanella CG, Carniel EL. 2010. Constitutive formulation and analysis of heel pad tissues mechanics. Med. Eng. Phys. 32:516-522.

Natali AN, Fontanella CG, Carniel EL, Miller-Young JE. 2011. Biomechanical behaviour of heel pad tissue. Experimental testing, constitutive formulation, and numerical modelling. Proc IME H: J Eng Med. 225:449–59.

Pai S, Ledoux WR. 2011. The quasi-linear viscoelastic properties of diabetic and non-diabetic plantar soft tissue. Ann. Biomed. Eng. 39(5): 1517-1527.

Robbins SE, Gouw GJ, Hanna AM, 1989. Running-Related Injury Prevention through Innate Impact-Moderating Behavior. Med. Sci. Sports. Exerc. 21(2):130-139.

Spears I.R., Miller-Young J.E. 2006. The effect of heel-pad thickness and loading protocol on measured heel-pad stiffness and a standardized protocol for inter-subject comparability. Clin. Biomech. 21:204-212.

Sopher R, Nixon J, McGinnis E, Gefen A. 2011. The influence of foot posture, support stiffness, heel pad loading and tissue mechanical properties on biomechanical factors associated with a risk of heel ulceration. J Mech Behav Biomed. 4(4):572-582.

Tong J, Lim CS, Goh OL. 2003. Technique to study the biomechanical properties of the human calcaneal heel pad. The Foot 13:83-91.

Tsai WC, Wang CL, Hsu TC, Hsieh FJ, Tang FT. 1999. The mechanical properties of the heel pad in unilateral plantar heel pain syndrome. Foot Ankle Int. 20(10):663-668.

Wang CL, Hsu T.C, Shau YW, Wong MK. 1998. Variations in heel pad mechanical properties variation between children and young adults. J Formos Med Ass. 97: 850-854.

Wearing SC, Smeathers JE, Urry SR, Sullivan PM, Yates B, Dubois P. 2010. Thickening of the enthesis is correlated with energy dissipation of the plantar fat pad during walking. Am. J. Sport Med. 38:2522-2527.

Wearing S.C, Smeathers JE, Yates B, Urry SR, Dubois P. 2009. Bulk compressive properties of the heel fat pad during walking: A pilot investigation in plantar heel pain. Clin. Biomech. 24(4):397-102.

Zhang M, Mak FT. 1999. In vivo friction properties of human skin. Prosthet. Orthot. Int. 23:135-141.

Zheng YP, Choi YKC, Wong K, Chan S, Mak AFT. 2000. Biomechanical assessment of plantar foot tissue in diabetic patients using an ultrasound indentation system. Ultrasound in Med. & Bio. 26(3):451-456.

Table caption

Table 1. Energy Dissipation Ratio calculated from load-displacement curves obtained from both experimental and numerical tests by using all pistons (15, 20 and 40 mm in diameter).

Table 2. Energy Dissipation Ratio calculated from the stress relaxation characteristics obtained from both experimental and numerical tests by using all pistons (15, 20 and 40 mm in diameter).

.

Table 1

Piston diameter (mm)	Energy Dissipation Ratio (%)	
	Experimental method	Numerical method
15	24.1±1.1	21.6±1.0
20	22.5±1.8	23.0±1.0
40	27.1±2.1	26.0±1.0

Table 2

Piston diameter (mm)	Energy Dissipation Ratio (%)	
	Experimental method	Numerical method
15	40.8±3.4	45.6±1.0
20	46.3±3.1	61.0±1.0
40	40.4±4.2	56.4±1.0

Figure captions

Figure 1. (a) The compression device, (b) the different pistons used (from top, diameter of 40 mm, 20 mm and 15 mm).

Figure 2. Position of the fiducial marker placed on the skin of the ankle. The marker is used for ankle translation correction of load-displacement curves and stress relaxation characteristics by video-processing.

Figure 3. Load-displacement curves obtained from the experimental tests with (in black) and without (in grey) ankle translation correction when using the piston of 40 mm in diameter. This sort of correction is used on all subsequent plots.

Figure 4. Compression and stress relaxation tests done with a piston of 40mm diameter. The stress relaxation is obtained with 1.73 mm/s of strain rate and a break of 40 s: (a) force vs. displacement and (b) force vs. time.

Figure 5. Compression and stress relaxation tests done with a piston of 20mm diameter. The stress relaxation is obtained with 1.73 mm/s of strain rate and a break of 40 s: (a) force vs. displacement and (b) force vs. time.

Figure 6. Compression and stress relaxation tests done with a piston of 15mm diameter. The stress relaxation obtained with 1.73 mm/s of strain rate and a break of 40 s: (a) force vs. displacement and (b) force vs. time.

Figure 7. (a) Numerical model of heel region with indication of sagittal section AA. Results from the numerical analysis of compression test at 1.73 mm/s strain rate with a piston of 40 mm diameter. Contours of minimum principal stress in the deformed configuration of heel pad structure after a loading: stress relaxation time $t=t_l+0$ s (b) and $t= t_l+40$ s (c), where t_l is the time of loading. Contours are reported over a transversal section AA of heel pad structure.

Figure 8. Compression tests developed at 1.73 mm/s of strain rate: force vs. displacement (a) done with a piston of diameter (a) 40 mm (b) 20 mm and (c) 10 mm.

Figure 9. Results from the numerical analysis of compression test at 1.73 mm/s strain rate with a piston of 40 mm diameter. Contours of minimum principal stretch in the deformed configuration of heel pad structure after a loading-unloading cycle: viscous recovery time t_r=0 s (a), t_r = 5 s (b) and t_r = 60 s. Contours are reported over a transversal section AA of heel pad structure.

Figures

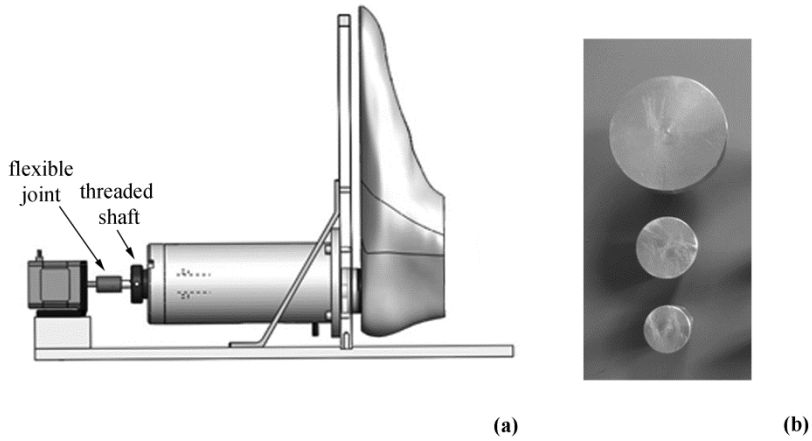

Figure 1

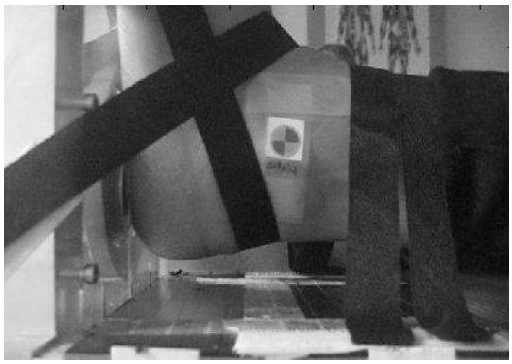

Figure 2

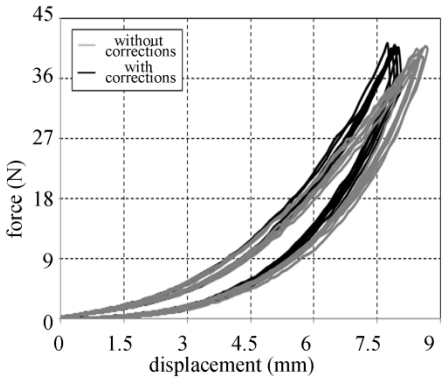

Figure 3

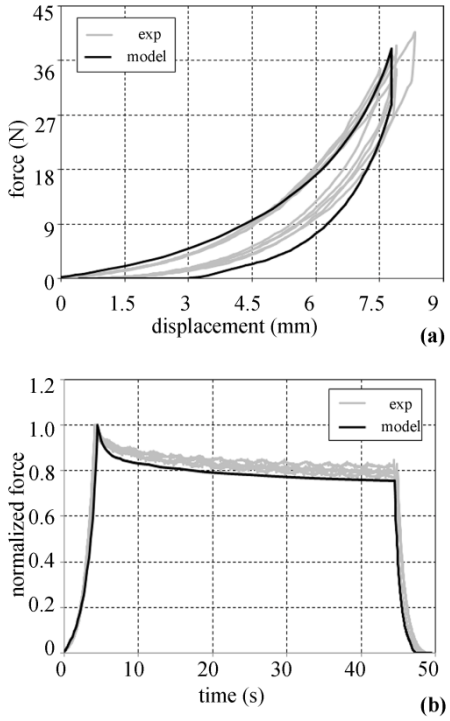

Figure 4

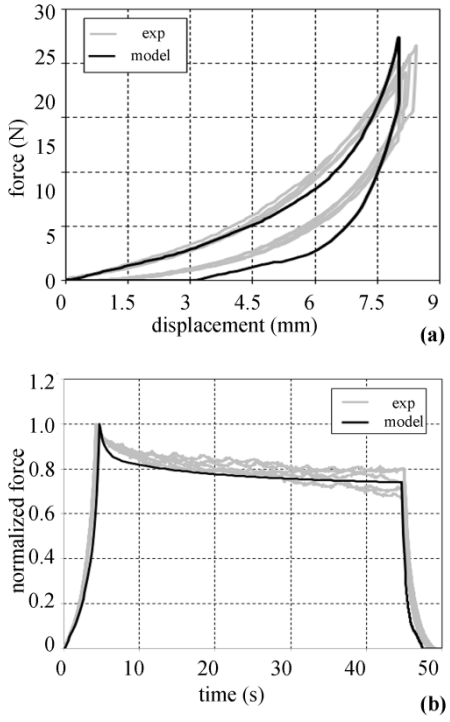

Figure 5

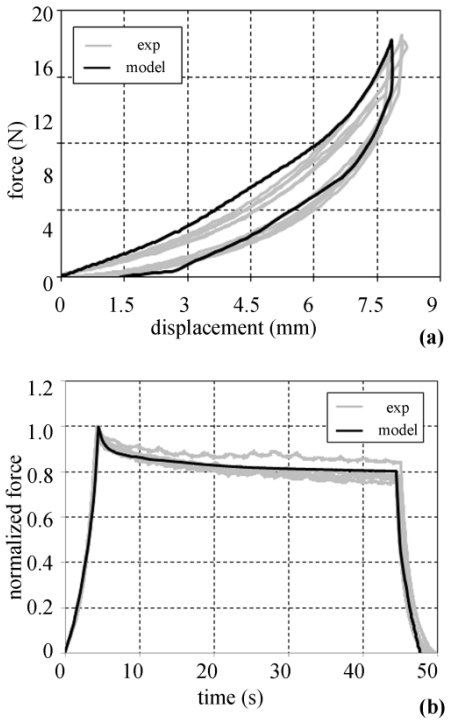
20
16
12
8
4
0
force (N)
exp
model
0
1.5
3
4.5
6
7.5
9
displacement (mm)
(a)
1.2
1.0
0.8
0.6
0.4
0.2
0
normalized force
exp
model
0
10
20
30
40
50
time (s)
(b)

Figure 6

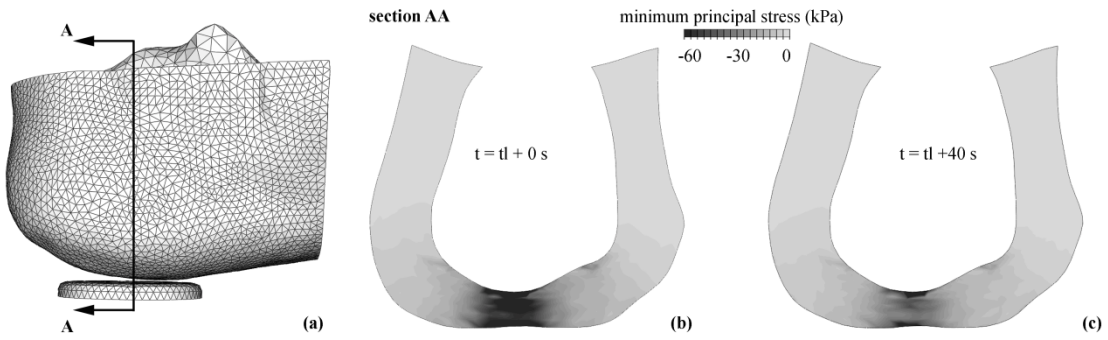

Figure 7

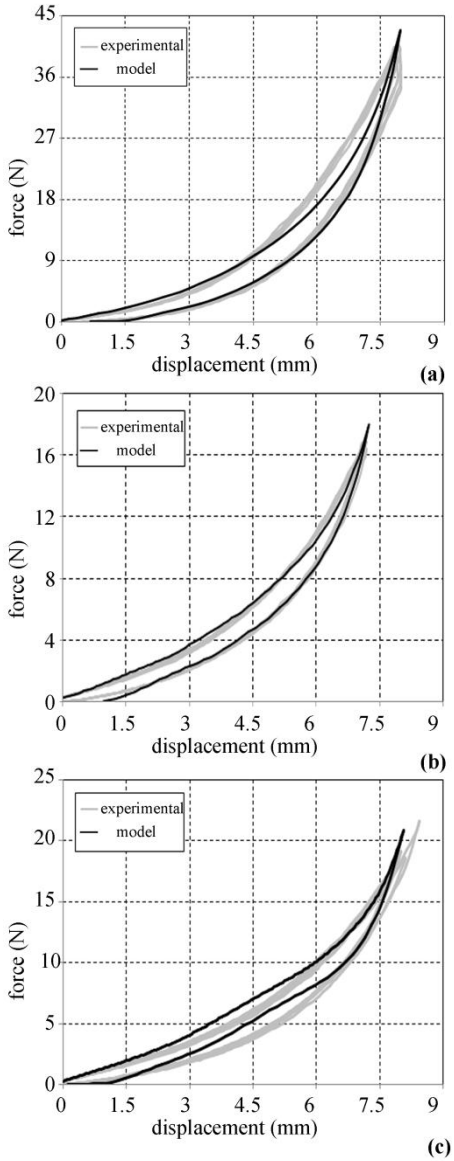

Figure 8

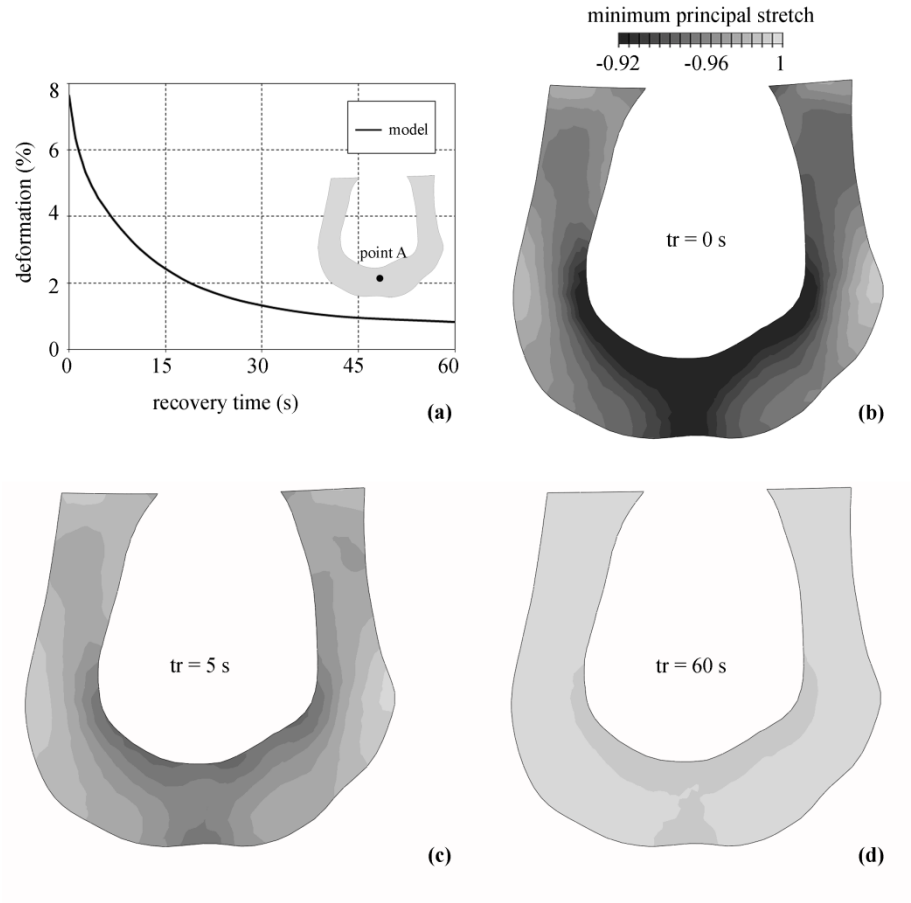
minimum principal stretch
-0.92
-0.96
1
8
6
4
2
0
deformation (%)
0
15
30
45
60
recovery time (s)
model
point A
(a)
tr = 0 s
(b)
tr = 5 s
(c)
tr = 60 s
(d)

Figure 9

IX PAPER

Title: On the comparison between MRI and US imaging for human heel pad thickness measurements.
Authors: Sara Matteoli, Nadège Corbin, Jens E. Wilhjelm, Søren T. Torp-Pedersen.
Conference: Oral contribution at the International Tissue Elasticity Conference, Arlington, Texas, USA.
Submission: Submitted for publication in final form on the Proceedings Book on October 12, 2011.

013 **ON THE COMPARISON BETWEEN MRI AND US IMAGING FOR HUMAN HEEL PAD THICKNESS MEASUREMENTS.**

Sara Matteoli[1], Nadège Corbin[1], Jens E. Wilhjelm[1], Søren T. Torp-Pedersen[2].*

[1]DTU Elektro, Biomedical Engineering, Technical University of Denmark, Ørsteds Plads, Bldg. 348, DK–2800, Kgs. Lyngby, DENMARK; [2]The Parker Institute, Frederiksberg Hospital, University of Copenhagen, Nordre Fasanvej 57, DK–2000 Frederiksberg, DENMARK.

Submitted for publication in final form: October 12, 2011.

Abstract: The human heel pad thickness, defined as the shortest distance between the calcaneus and heel skin, is one of the intrinsic factor which must be taken into account when investigating the biomechanics of the heel pad. US and MRI are the preferable imaging modalities used to measure the heel pad thickness as they are both ionizing-free radiations. The aim of this paper is to measure the bone to skin distance of nine heel pad phantoms from MRI and US images, and to compare the results with a true value (TV) in order to find the errors. Paired sample *t-test* was used to compare the measurements. Results showed a statistically significant difference between MRI and US_{1540} (P-value=0.005), and between TV and US_{1540} (P-value=0.013). Furthermore, results showed no statistically significant difference between US_{1530} or MRI and TV (P-value=0.103 and P-value=0.358, respectively), and between MRI and US_{1530} (P-value=0.402). Results confirm the necessity to investigate on the real speed of sound for the heel pad tissues, in order to have realistic measurements when dealing with human heel pads.

I. Introduction

The human heel pad thickness, defined as the shortest distance between the calcaneus and heel skin, is one of the intrinsic factor which must be taken into account when investigating the biomechanics of the heel pad [1,2]. In fact, heel pad thickness has been reported to be an important factor in determining stresses observed in healthy as well as pathological feet [1,2]. Ultrasound (US), Magnetic Resonance Imaging (MRI), Computer Tomography (CT), and X-ray can be used to measure the heel pad thickness. Among those, US (portable, fast scanning time, ionizing-free radiations, low expense), and MRI (ionizing-free radiations) are preferable choices. For US however, measurement errors may occur due to the operator-dependability, the uncertainty of the speed of sound in heel pad tissues as well as the presence of artifacts and angle- dependence. It is thus, necessary to verify the reliability of the imaging techniques by comparing results with a true value. PVA-cryogel, being a suitable material for mimicking the human soft tissues and compatible to both MRI and US imaging [3], was chosen to build artificial heel pad phantoms in order to investigate the reliability of the measurements. The present study concentrates on measuring the bone to skin distance of nine heel pad phantoms from MRI and US images. The comparison with a true value (TV) allows finding the error.

II. Material and Methods

Nine heel pad phantoms were created. They consisted of a plastic calcaneus (only the part which is facing the load in a human foot in normal standing position) fixed to a Plexiglas support and surrounded by heel pad mimicking tissue. Specifically, the heel pad was modeled by using 10% of polyvinyl alcohol (PVA-C) dissolved in water as based material. In order to obtain ultrasound echoes from within the heel pad mimicking tissue, some silica powder was added to the PVA-C [4].
The elastic modulus (E) of PVA-C was controlled by the number of freeze/thaw cycles each model was exposed to. In the present study, the heel pad phantom underwent to three different number of freeze/thaw cycles. The skin-to-bone distances were controlled by adjusting the height of the Plexiglas support of the plastic calcaneus bone. Thus, the models had three different elasticities (E1 = 64 KPa, E2 = 127 KPa, E3 = 161 KPa) combined with 9 different known skin-to-bone distances.
The true value (TV) of the skin-to-bone distance was calculated from the dimensions of the mould and the phantom. Figure 1 shows a typical mould used to create the heel pad phantom, as well as the typical heel pad phantom.

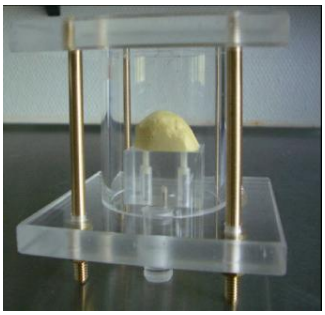

Fig.1 Typical heel pad mould

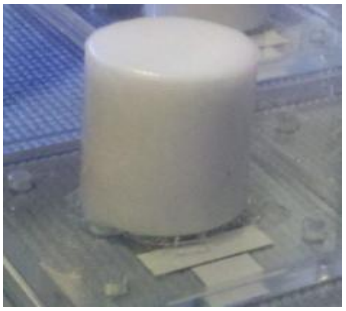

Fig.2 Typical heel pad phantom

All heel pad phantoms underwent both 3D MRI [3T Siemens Magnetom Verio, T1 Vibe isotropic sequence. TE/TR=5.41/12.4 ms, flip angle 10 degrees, TA=5 min, slice thickness=0.60 mm], and 3D US (LOQICE9-GE healthcare, 12MHz). Each phantom was scanned twice from the top with the US transducer in both longitudinal and transversal position by the same experienced doctor, as shown in Figure 3. Figure 4 shows one of the heel pad phantom placed inside the coil in the MRI scanner. All the images were stored in DICOM format.

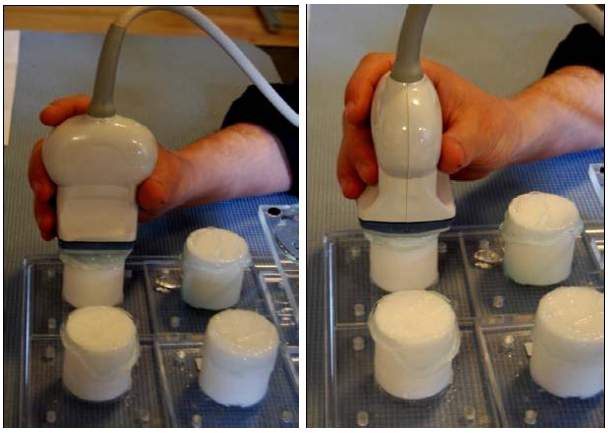

Fig.3 US measurements with the transducer in longitudinal (on the left) and transversal position (on the right)

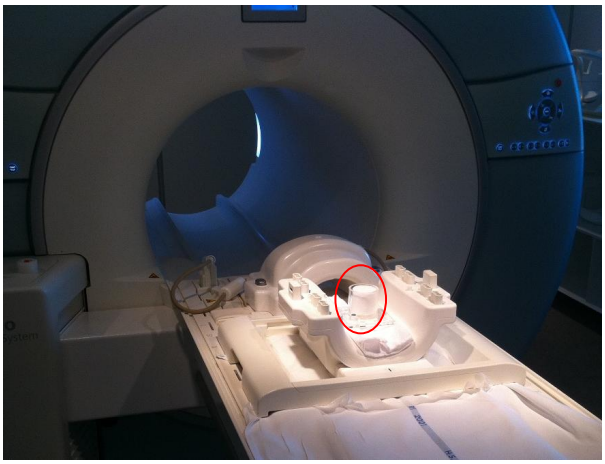

Fig.4 Heel pad phantom (marked by the red circle) placed inside the coil in the MRI scanner

All DICOM images were processed by using MATLAB tools, so that 3D data were extracted. For each heel pad phantom the contours of both the calcaneus and the top of phantom were delineated on each plane with an automatic procedure, as shown in Figure 5. Each image corresponded to a matrix of pixel values from 0 to 1, which determined the contours of calcaneus and the top of phantom. Specifically, for the US images the calcaneus was represented by pixels with values higher than 0.9, whereas the top of the phantom by pixels with values higher than 0.6. Each column of each image was read starting by the top, and the first pixels superior to those thresholds were stored. Then, the coordinates of the highest point of calcaneus were found automatically, and the skin-to-bone distance was found. A 3D visualization was made for each phantom, as shown in Figure 6.

The standard value of the speed of sound used by the ultrasound scanner for human tissue is $1540ms^{-1}$, but for PVA-cryogel it ranges from $1520ms^{-1}$ to $1540\ ms^{-1}$ [3]. Therefore, for each heel pad phantom the thickness was calculated also by using a speed of sound of $1530ms^{-1}$.

Paired sample *t-test* was used to compare the thickness measured by MR or US images with the TV. A P-value less than 0.05 was accepted as significant, thus the difference was not negligible.

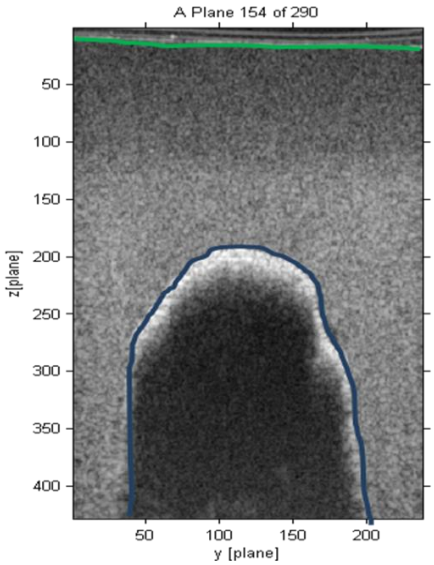

Fig.5 US image of a typical heel pad phantom

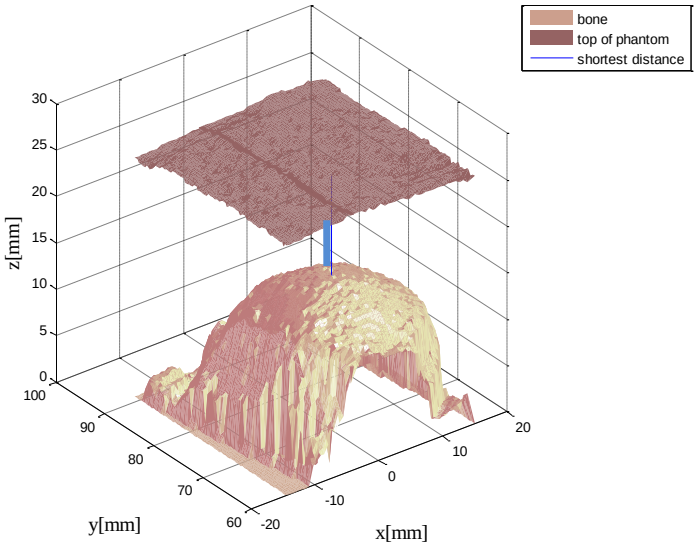

Fig.6 3D reconstruction of a typical heel pad phantom.

III. Results

Table 1 shows the values of the thickness of all 9 heel pad phantoms measured from US_{1530}, US_{1540}, MRI and GR. Figure 7 plots with histograms the values reported in Table 1. Figure 8 shows for each phantom the difference between the true values and the clinical imaging measurements (so called error). It is clearly visible that MRI measurements underestimate the phantoms thickness for five phantoms out of nine, while US_{1540} overestimates for seven phantoms out of 9. Furthermore, the thickness calculated with US_{1530} is always lower than US_{1540}, as is expected. Furthermore, for the phantom number six, the thickness measured with US_{1530} matches the true value.

In order to verify whether there is a linear correlation between the clinical imaging measurements and the true values, the error made by US and MRI is plotted as a function of the true value, as shown in Figure 9.

The statistical analysis showed that there was statistically significant difference between MRI and US_{1540} (P-value=0.005) as well as between TV and US_{1540} (P-value=0.013). Furthermore, results showed that there was no statistically significant difference between US_{1530} or MRI and TV (P-value=0.103 and P-value=0.358,

respectively), and between MRI and US_{1530} (P-value=0.402).

Table 1 Thickness measured for each phantom from all techniques

Heel pad phantom	US_{1540} (mm)	US_{1530} (mm)	MRI (mm)	TV (mm)
1	13.15	13,04	12.45	12.61
2	13.12	13.02	12.60	12.63
3	13.05	12.95	12.60	13.14
4	17.36	17.25	17.29	16.74
5	15.73	15.63	15.23	15.56
6	15.68	15.59	15.09	15.59
7	18.94	18.77	18.89	18.54
8	18.54	18.41	17.72	18.18
9	17.35	17.19	17.43	17.41

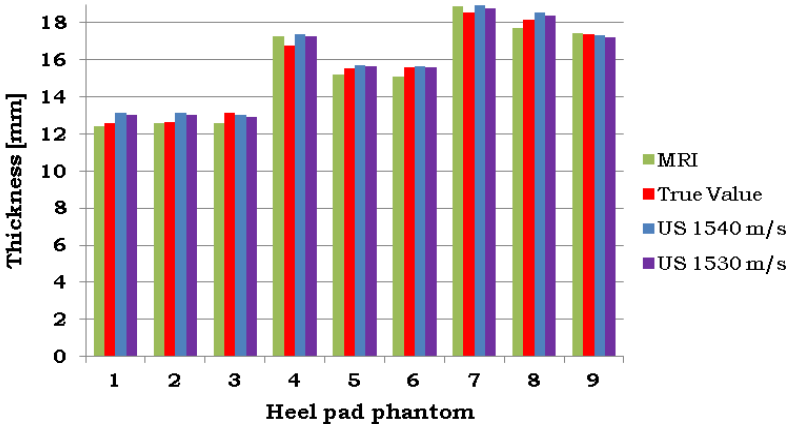

Fig 7 Thickness of all phantoms measured from all techniques

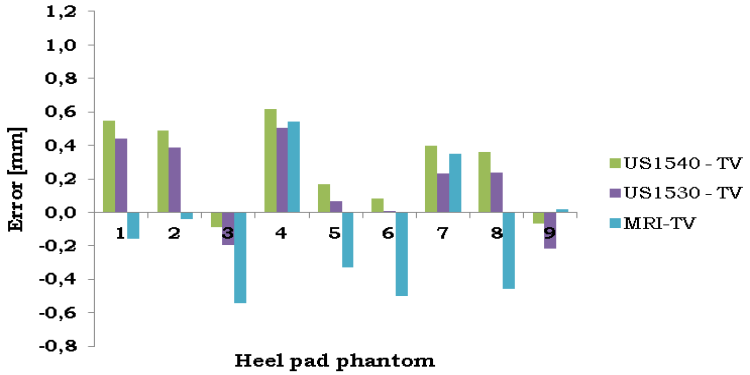

Fig 8 Difference of measurements between US or MRI and the true value (TV)

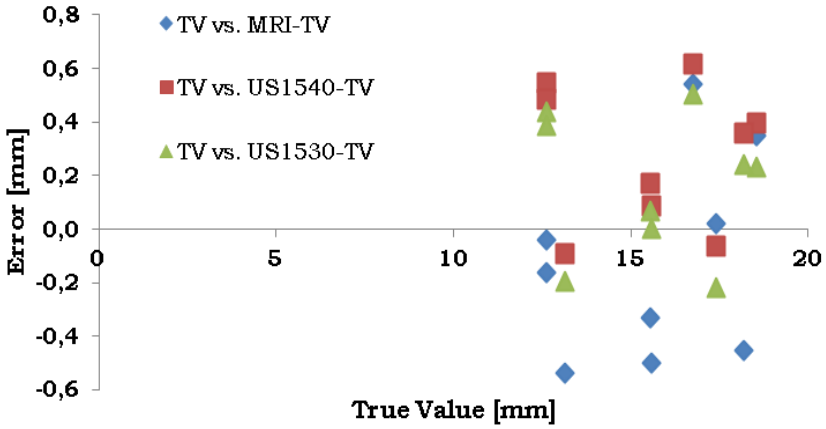

Fig 9 The difference of the measurement between the true value and imaging technique (MRI and US) is plotted as a function of the True Value.

IV. Conclusions

From Figure 9 it is seen that there is no linear correlation between clinical imaging measurements and the true values. However, this does not imply the absence of any systematic errors. For US measurements the main uncertainty is the average speed of sound assumed by the scanner (1540ms^{-1}), but errors might due also to the angle-dependency as well as the operator-dependency. Error measurements for TV might be reduced by using a true value extracted from µ-CT images by applying the same 3D estimation procedure. In this case 3D reconstruction obtained from MRI, US and µ-CT images should be overlapped in order to verify whether the measurements are done at the same place of the calcaneus. Finally, the error measurements for MRI might be due to the sequence applied, and thus the optimization of it might reduce the uncertainty of the measurements.

The present study confirms, once minimized the error measurement before mentioned, the necessity to investigate on the real speed of sound for the heel pad tissues, in order to have realistic measurements when dealing with human heel pad.

Acknowledgment

The authors would like to thank Dr. Rasmus Bouert from Frederiksberg Hospital, Copenhagen, for his efficient contribution to the MRI, as well as PhD Antonio Virga from the Department of Mechanics and Industrial Technologies, University of Florence, for his help in the statistical analysis.

References:

[1] Uzel M., et al. Comparison of ultrasonography and radiography in assessment of the heel pad compressibility index of patients with plantar heel pain syndrome. Joint Bone Spine 73, pp.196-199, 2006.
[2] Rome K., Campbell R., Flint A., Haslock I. Ultrasonic heel pad thickness measurements: a preliminary study. Br J Radiology 71, pp. 1149-1152, 1998.
[3] Surry K J M., Austin H J B., Fenster A., Peters T M. Poly(vinyl alcohol) cryogel phantoms for use in ultrasound and MR imaging. Phys. Med. Biol. 49, pp.5529-5546, 2004.
[4] Torp-Pedersen S., et al. Diagnostic accuracy of heel pad palpation – A phantom study. Journal of Forensic and Legal Medicine 15, pp.437–442, 2008.

www.elektro.dtu.dk

Department of Electrical Engineering
Biomedical Group
Technical University of Denmark
Ørsteds Plads
Building 348
DK-2800 Kgs. Lyngby
Denmark
Tel: (+45) 45 25 38 00
Fax: (+45) 45 93 16 34
Email: info@elektro.dtu.dk

ISBN 978-87-92465-85-6